

DISCLAIMER

This report was prepared as an account of work sponsored by an agency of the United States Government. Neither the United States Government nor any agency thereof, nor any of their employees, makes any warranty, express or implied, or assumes any legal liability or responsibility for the accuracy, completeness, or usefulness of any information, apparatus, product, or process disclosed, or represents that its use would not infringe privately owned rights. Reference herein to any specific commercial product, process, or service by trade name, trademark, manufacturer, or otherwise does not necessarily constitute or imply its endorsement, recommendation, or favoring by the United States Government or any agency thereof. The views and opinions of authors expressed herein do not necessarily state or reflect those of the United States Government or any agency thereof.

This report has been reproduced directly from the best available copy.

Available to DOE and DOE contractors from the Office of Scientific and Technical Information, P.O. Box 62, Oak Ridge, TN 37831; prices available from (615)576-8401, FTS 626-8401.

Available to the public from the National Technical Information Service, U.S. Department of Commerce, 5285 Port Royal Rd., Springfield, VA 22161.

Measuring and Predicting Reservoir Heterogeneity in Complex Deposystems
The Fluvial-Deltaic Big Injun Sandstone in West Virginia

Annual Report for the Period
September 20, 1991--September 20, 1992

By
Douglas G. Patchen
Michael Ed. Hohn
Khashayar Aminian
Alan Donaldson
Robert Shumaker
Thomas Wilson

April 1993

Work Performed Under Contract No. DE-AC22-90BC14657

Prepared for
U.S. Department of Energy
Assistant Secretary for Fossil Energy

Edith Allison, Project Manager
Bartlesville Project Office
P. O. Box 1398
Bartlesville, OK 74005

Prepared by
Appalachian Oil and Natural Gas Research Consortium
West Virginia University
P.O. Box 6064
617 North Spruce Street
Morgantown, WV 26506-6064

LIST OF CONTENTS

List of Figures and Tables

ABSTRACT

EXECUTIVE SUMMARY

 Technical Perspective

 Results

 Approach

INTRODUCTION

 Research Objectives

 Acknowledgements

EVIDENCE OF HETEROGENEITY IN THE BIG INJUN SANDSTONE

 Regional Heterogeneity

 Field Scale Heterogeneity

 Drilling History

 Well-to-Well Communication

 Reservoir Modeling

GEOLOGIC CONTROLS OF REGIONAL HETEROGENEITY

 Structural Controls

 Introduction

 Basement Structure

 Detached Structure

 Fractures

 Production

 Stratigraphic Controls

 Introduction

 Facies

 Sandstone Distribution Patterns

 Heterogeneity Between Oil Fields

GEOLOGIC CONTROLS OF FIELD SCALE HETEROGENEITY

 Introduction

 Spatial Trends in Oil Occurrence

 Initial Potential

 Cumulative Production

 Structural Controls

 Introduction

 Big Injun Structure

 Thief Zones

 Heterogeneity Interpreted from Seismic Studies

 Introduction

 Field Scale Heterogeneity

 Intrafield Heterogeneity

 Basement Faults

 Small-Scale Folds

 Fracture Zones and Faults

Stratigraphic Controls

Subdivisions and Depositional Environments

Petrology of the Pocono Big Injun

Heterogeneity in Gamma-Ray Response

Porosity and Permeability

Geographic Distribution

Estimating Permeability from Porosity

Network Modeling

Heterogeneity Related to Oil Production

Density and Shale Barriers

INTERWELL HETEROGENEITY

VSP Observations

Recommendations

REFERENCES

APPENDICES

Appendix 1: Presentation of Research Results

List of Figures and Tables

1. Regional study area and location of fields
2. Data control in Granny Creek
3. Wells in communication, Granny Creek field
4. Initial open flow map
5. Cumulative production map
6. IP's versus year of completion
7. Injection and production wells in five-spot patterns P1 and P2
8. Injection pressure and rate for injection well I-1
9. Injection pressure and rate for injection well I-2
10. Injection pressure and rate for injection well I-3
11. Injection pressure and rate for injection well I-4
12. Injection pressure and rate for injection well I-5
13. Injection pressure and rate for injection well I-6
14. Cumulative water injection into P1 and P2
15. Cumulative oil and water production, five-spot P1
16. Cumulative oil and water production, five-spot P2
17. Grid patterns used to simulate the water-flooding process in P1 and P2
18. Simulated production versus actual field data, five-spot P1
19. Simulated production versus actual field data, five-spot P2
20. Injection pressure versus time for injection well I-1
21. Injection pressure versus time for injection well I-2
22. Injection pressure versus time for injection well I-3
23. Injection pressure versus time for injection well I-4
24. Injection pressure versus time for injection well I-5
25. Injection pressure versus time for injection well I-6
26. Basement faults and arches
27. Structure on Pittsburgh coal, Rock Creek-Granny Creek area
28. Structure on Greenbrier Limestone, Rock Creek-Granny Creek area
29. Regional map with locations of stratigraphic sections
30. Cross section RJ-RJ' through Rock Creek and Tariff fields
31. Regional sandstone isolith map, Pocono and Maccrady formations
32. Isolith map of Big Injun sandstone in Ohio and West Virginia
33. Stratigraphic section, Cabell County to Clay County
34. Hypotheses for thick belts of Big Injun sandstone
35. Stratigraphic section, Cabell County to Ritchie County
36. Map showing areas where Big Injun thickness patterns were affected by erosion
37. Isolith map with environments interpreted from gamma-ray logs
38. Stratigraphic section, Pleasants County to Ritchie County
39. Omnidirectional variogram for indicative variable I7, I15, and I25
40. Directional variograms (four orientations) for I15
41. Estimated probability (map) that IP in Granny Creek will exceed 15 BOPD
42. Omnidirectional variogram for ten-year oil production
43. Directional variograms of ten-year oil production
44. Kriged estimate of ten-year production, Granny Creek field

45. Structure at the base of the Greenbrier, Granny Creek field
46. Structure on the Greenbrier, Granny Creek field, with faults and thief zones
47. Reflective events along seismic line 2, Granny Creek field
48. Location of seismic lines superposed on map of cumulative production
49. Synthetic seismogram, acoustic impedance and reflectivity in Parker well
50. Synthetic seismogram inserted into seismic traces for line 2
51. Reflection arrival times to the Big Injun along seismic line 1
52. Reflection arrival times to the Big Injun along seismic line 2
53. Reflection arrival times to the Big Injun along seismic line 3
54. Reflection arrival times to the Big Injun along seismic line 4
55. Reflection arrival times to the Big Injun along seismic line 6
56. Shifted travel-time difference along seismic line 6
57. Isotime map, Big Injun
58. Isotime map, basement
59. Thickness of A+B, and C versus arrival times to the top of Big Injun along line 2
60. Thickness of A+B, and C versus arrival times to the top of Big Injun along line 6
61. Original seismic data along line 2
62. Reprocessed seismic data along line 2
63. Close up view of seismic data along line 2
64. Close up view of seismic data along line 2 after reprocessing
65. Depth model and synthetic showing the combined effect of faults
66. Mid-point map with wells and lines of communication
67. Stratigraphic section GB-GB', Clay County
68. Delta front facies model of the C member
69. Map of distributary-mouth bar C2
70. Core description of the Big Injun sandstone, Clay 1130
71. Depositional environments, stratigraphic units, porosity and permeability for Clay 1126
72. Spider plots (a) less than 200 m and (b) less than 1000 m
73. Directional correlogram for gamma-ray logs
74. Porosity superposed on facies along section GB-GB'
75. Permeability superposed on facies along section GB-GB'
76. Quartz cemented B member along GB-GB'
77. Details of the southern water-flood area, Granny Creek
78. Porosity cross plots a and b for southern water-flood area
79. Subsurface porosity map for southern water-flood area
80. Permeability map (core data), Zone A
81. Permeability map (core data), Zone B
82. Permeability map (core data), Zone C
83. Porosity map (core data), Zone A
84. Porosity map (core data), Zone B
85. Porosity map (core data), Zone C
86. Porosity-Permeability plot Clay 735
87. Porosity-Permeability plot Clay 735, Zone A
88. Porosity-Permeability plot Clay 735, Zone B
89. Porosity-Permeability plot Clay 735, Zone C
90. Core porosity versus log porosity, Clay 1109, Zone B

91. Core porosity versus log porosity, Clay 1109, Zone C3
92. Core porosity versus log porosity, Clay 1109, Zone C2
93. Porosity-Permeability plot for four depositional environments
94. Facies diagram P1-P1' with IOP
95. Cross section P4-P4' with IOP
96. Density breaks between sandstone tongues
97. Density breaks due to diagenesis that cut across sandstone tongues
98. Cross Section through Granny Creek with density barriers
99. Map of Granny Creek with extent of shale and siltstone barriers
100. Map of Granny Creek with extent of density barriers
101. Density barriers in section P1-P1' with IOP
102. Density barriers in section P2-2' with ten-year production
103. Location map of three VSP offsets
104. Western offset VSP
105. Northeastern offset VSP
106. Line 2 arrival times versus travel-time difference, Big Injun-Huron
107. Line 6 arrival times versus travel-time difference, Big Injun-Huron
108. Line 3 arrival times versus travel-time difference, Big Injun-Huron
109. Line 4 arrival times versus travel-time difference, Big Injun-Huron
110. Line 1 arrival times versus travel-time difference, Big Injun-Huron

Tables

1. General Trends of Structural Features, Granny Creek Field
2. Petrographic Features in Different Subfacies
3. Porosity and Water Saturation Data
4. Measured Permeability Values
5. Porosity and Water Saturation Data from Logs
6. Reservoir Parameters along Facies Profiles

ABSTRACT

Evidence for heterogeneity in the Big Injun reservoir-forming sandstones on a regional scale is found in the distribution of hydrocarbons into distinct fields across the basin. The easternmost fields traditionally have been considered to be updip unconformity traps; those to the west appear to be regionally downdip from the truncated margin of the reservoir. At the field scale, reservoir heterogeneity is indicated by patterns of initial open flow and cumulative production. Two trends are evident; a north-south trend along the western edge of the field, and a shorter northwest to southeast trend through the central portion of the field. The large contrast in values across the trends is indicative of heterogeneity in the reservoir. An analysis of initial open flows versus year of completion and geographic location provides further evidence of heterogeneity in the reservoir. Infill wells drilled 20 or more years after the offset wells went on production flowed at initial rates comparable to the offset wells. The non-uniform behavior of injection pressures and rates in two adjacent five-spot, water-flood patterns is a further suggestion of heterogeneity in the reservoir. The volumes of water and cumulative rates of injection are similar for both patterns, but one produced oil whereas the second experienced almost immediate water breakthrough.

The regional distribution of hydrocarbons suggests that both basement and detached structures have in part determined the locations of Big Injun oil fields. Primary migration pathways resulted in oil accumulations above basement structures; secondary migration (remigration) occurred later into Alleghanian detached structures. However, stratigraphic controls also are important at the regional scale. Pocono sandstones were deposited in fluvial-deltaic systems that prograded into the study area from both the east and west. As a result, even though the Pocono Big Injun can be subdivided into an upper coarse-grained channel facies and a lower fine-grained distributary mouth bar facies, equivalent facies in the two systems do not connect. Distribution of sandstone facies and thicknesses suggests control by structural features such as the Waverly Arch and Cambridge Arch. These patterns were modified later by pre-Greenbrier erosion associated with growth of the West Virginia Dome. Thus, at the regional scale, there are three causes for stratigraphic discontinuities resulting from pre-Greenbrier and pre-Pottsville erosion: lateral discontinuities resulting from pre-Greenbrier and pre-Pottsville erosion; lateral discontinuities due to facies changes from sandstones to shales at the distal margins of deltaic-river-mouth bars and channels; and vertical discontinuities resulting from shales separating Pocono Big Injun reservoir sandstones from overlying Maccrady reservoirs.

A spatial analysis of trends of oil production in Granny Creek field suggests that initial oil potential is extremely variable from well to well; the presence of heterogeneities in porosity and permeability is one way to explain this behavior. Variograms constructed from initial potential and well distance and direction data show the presence of anisotropies in the north-south and northwest-southeast directions, reflecting kriged maps of initial potential and cumulative production. Cumulative production for wells spaced farther than 0.75 kilometers apart is statistically independent.

Big Injun structure mapped from well data suggests a number of small wave-length, low-relief folds that plunge northeast on the flank of the large syncline in which Granny Creek field is located. Some, but not all, of these folds appear to correlate with folds mapped using seismic data. These minor structural highs on seismic profiles appear to match areas of high initial potential and high cumulative production when these data are plotted along the seismic lines. Shifted travel-time distances for major stratigraphic units recognized in seismic data

indicate areas of thickening in the Big Injun to Huron Shale interval beneath the small folds. Thickening of the shale section is interpreted as evidence that the folds are detached. However, folds located over basement structures appear to be more productive than those which are not.

Although a high degree of structural control for heterogeneity observed in Granny Creek can be demonstrated, stratigraphic and petrographic controls are present, as well. The lower, fine-grained, distributary mouth-bar facies can be subdivided into three subfacies with differing porosity-permeability characteristics. The highest porosity occurs in the marine-influenced proximal bar, and the lowest in the distal mouth bar as well as between prograding tongues of the bar sandstones. Permeable facies correspond to the distribution of porosity facies; thus, porosity and permeability can be related to depositional environments in a predictable manner.

Petrographic analysis of the Big Injun supports core and log porosity analyses. Original porosity in the channel sandstones was low due to poor sorting, and the lack of coatings in the lower fluvial channel sandstones resulted in quartz cementation, further reducing the original low porosity and permeability. In contrast, porosity and permeability were preserved in the lower proximal bar facies due to the presence of well-formed chlorite coatings that restricted quartz cementation. Original sedimentary conditions apparently set the stage for later diagenetic variations in porosity and permeability, again emphasizing the importance of depositional environments in predicting favorable porosity-permeability trends.

Preliminary analysis indicates a positive correlation between high initial oil production and preservation of subfacies of the distributary mouth-bar and channel facies. High production occurs where the upper distal and marine-influenced proximal mouth-bar subfacies pinch out against the overlying channel facies and where at least a few feet of the relatively impermeable channel facies are present. Low production is associated with thin areas of proximal mouth-bar subfacies; a change from marine to fluvial dominance of the mouth-bar subfacies, which is accompanied by reduction of porosity and permeability; and loss of the overlying channel subfacies (possible seal).

Density barriers interpreted from logs, cores and petrographic analysis of thin sections are due to both shale (depositional barriers) and cementation (diagenetic barriers). Shale breaks between sandstone tongues at the base of the distal bar parallel bedding and facies boundaries, whereas diagenetic breaks appear to cut across bedding and sandstone tongues. Thus, these barriers, or high-density zones, form horizontal, inclined and irregular pods of impermeable sandstone that may alter fluid flow paths and divide the reservoir into discrete compartments.

EXECUTIVE SUMMARY

TECHNICAL PERSPECTIVE

Non-uniform composition and permeability of a reservoir, commonly referred to as reservoir heterogeneity, is recognized as a major factor in the efficient recovery of oil during primary production and enhanced recovery operations. Heterogeneities are present at various scales and are caused by various factors, including folding and faulting, fractures, diagenesis and depositional environments. Thus, a reservoir consists of a complex flow system, or series of flow systems, dependent on lithology, sandstone genesis, and structural and thermal history. Ultimately, however, the fundamental flow units are controlled by the distribution and type of depositional environments.

Reservoir heterogeneity is difficult to measure and predict, especially in more complex reservoirs such as fluvial-deltaic sandstones versus wave dominated deltaic rocks. The Appalachian Oil and Natural Gas Research Consortium (AONGRC), a partnership of Appalachian basin state geological surveys and West Virginia University, is currently studying two heterogeneous reservoirs: the Lower Mississippian Big Injun sandstone in West Virginia, and the Upper Cambrian Rose Run sandstone in Ohio and Pennsylvania. A final report on the results of the Rose Run study is being reported separately. The ongoing Big Injun research is multi-disciplinary and has been designed to measure and map heterogeneity at various scales, and to develop tools and techniques to predict heterogeneity in existing fields and undrilled areas. The main goal is to develop an understanding of the reservoir sufficient to predict, in a given reservoir, optimum drilling locations versus high-risk locations for infill, outpost, or deeper-pool tests.

RESULTS

Several lines of evidence substantiate the presence of heterogeneity in the Big Injun reservoir in Granny Creek field, West Virginia. These include the patterns of initial open flow and cumulative production, infill wells that flowed at high rates 20 to 30 years after offset wells had gone on production, and the non-uniform behavior of injection pressures and rates during water-flood operations. An integrated analysis of stratigraphic, structural, seismic, petrographic, and engineering data has led to the conclusion that heterogeneity within the field is due to the interplay of various geologic controls. At the regional scale, geologic controls include the distribution of basement-related and detached structures, the distribution of sandstone facies and thickness patterns, and a pre-Greenbrier erosional event, the Greenbrier unconformity, that modified these patterns of sedimentation.

Within Granny Creek field, areas of high initial potential and cumulative production appear to correlate with small-scale, northeast-plunging folds developed on the flank of the main syncline that controls Granny Creek oil accumulation. Seismic data indicate these folds are detached. However, folds located over basement structures appear to be even more productive. In addition to these structural controls, stratigraphic and petrographic controls also have been documented. The Big Injun reservoir has been divided into two main facies, an upper, coarse-grained channel facies, and a lower, fine-grained distributary mouth-bar facies that forms the

reservoir. Reservoir rocks have further been divided into subfacies with differing porosity-permeability characteristics. Thus, the distribution of porosity and permeability can be related to depositional environments in a predictable manner. Petrographic analysis of thin sections from cores confirmed that a lack of coatings in the lower channel facies led to quartz cementation that reduced porosity and permeability, whereas well-formed chlorite coatings on fine sand grains in the bar facies preserved porosity and permeability by reducing quartz cementation. A high positive correlation was demonstrated between the distribution of subfacies and both initial and cumulative production. High production is related to areas where the upper distal and marine-dominated proximal bar subfacies pinch out against the overlying, less permeable channel facies. The presence of this tighter facies appears to some degree to control production in the bar sandstones below it. Density barriers in the reservoir have been identified on logs and in cores, and can be divided into shale breaks, usually between tongues of distal bar sandstones, and cementation breaks due to diagenesis. These high-density diagenetic barriers often cut across bedding and facies and may subdivide the reservoir into compartments.

APPROACH

During the second year of this three-year project, regional cross-sections of the interval between the Greenbrier Limestone and the Squaw sandstone were completed, and data from correlated logs were used to construct isopach and isolith maps. Sandstones within the study area were divided into genetic types (channel versus bar) using gamma-ray log character. Within Granny Creek field these genetic types were further subdivided using both core and log data. All available cores were cut and described, and thin sections were made and examined. Displays of porosity and permeability, as related to lithofacies, were prepared, and lithofacies distribution was correlated to initial potential and cumulative production trends. Subcrop maps were prepared for both Granny Creek and Rock Creek fields, and surface fracture patterns were mapped over parts of both fields. Additional seismic data were obtained over Granny Creek field, and reprocessing of data was initiated. Maps and interpretations from seismic and vertical seismic profile data obtained during the initial contract year were completed.

Reservoir modeling, network modeling, an analysis of textural transforms, porosity and permeability correlations, and an analysis of water-flood data continued. A Monte Carlo simulator was developed to measure particle entrapment in porous media, and the potential of particles of various sizes to block pore throats was evaluated. In the analysis of textural transforms, three parameters were evaluated: number of pores per unit volume; average coordination number; and size distribution of pores. A three-fold coordination number was chosen as having the greatest potential for success.

Data collection efforts were focused on obtaining production data for both Granny Creek and Rock Creek fields. All data were verified and entered into a common account for the project. Computer programs were written to generate graphs, statistics, panel diagrams and maps. Conditional simulation, an analysis of lithofacies continuity, and a detailed analysis of well performance versus date of completion and well location were performed. Variograms of porosity, permeability and production data were initiated.

Biweekly meetings among all Principal Investigators and key researchers were beneficial in integrating both results and future research directions.

INTRODUCTION

The purpose of this research is to develop techniques to measure and predict heterogeneities in oil reservoirs that are the products of complex deposystems. The unit chosen for study is the Lower Mississippian Big Injun sandstone, a prolific oil producer (nearly 60 fields) in West Virginia. The Big Injun is a drillers' term and generally refers to the first sandstone penetrated below the Greenbrier Limestone (Big Lime of the driller). In most cases, the first sandstone in this stratigraphic portion will be within the Pocono (Price) Formation. However, the pre-Greenbrier unconformity, which represents an erosion event that removed varying amounts of Pocono rocks, is present throughout the productive area, so different Pocono-age sandstones pinch out against the overlying Greenbrier Limestone across the basin. Furthermore, recognition of red beds below the Big Injun reservoir in several fields under study has led to the realization that the sandstones above them may be in the Maccrady Formation, which is stratigraphically above the Pocono Formation and its Big Injun reservoir sandstone. Therefore, within the regional study area (Figure 1) it is important to know which Big Injun sandstone forms the reservoir in the various fields of interest. A stratigraphic cross section through several of these fields suggests that the Pocono Big Injun is the only reservoir in Granny Creek field and the Maccrady Big Injun is the only reservoir in Rock Creek field. Other fields, however, contain reservoir sandstones in both formations. All of these sandstones tend to be discontinuous, due to their fluvial-deltaic origin, so careful correlation, at various scales, is essential to the success of the project.

Because of this, the Big Injun is being studied at various scales, including a 23-county regional scale, and a field scale. Granny Creek field in Clay and Roane counties, West Virginia, and Rock Creek field in Roane County (Figure 1) have been chosen for detailed study. However, to this point in time, Granny Creek field has been the main focus for analyzing the various geologic controls on heterogeneity in an oil producing area. Available data include geophysical logs, cores, seismic data, and a vertical seismic profile run as part of this research (Figure 2). The field has been developed by two companies that have contributed data for this research: Pennzoil (northern part) and Columbia Natural Resources (southern part). Analysis of these and other data has led to the conclusion that heterogeneities in the Big Injun reservoir sandstone are due to the complex interplay of stratigraphic, structural, and diagenetic factors that are present at various scales. In this report, these heterogeneities and their geologic controls will be discussed in order of diminishing scale, from regional to inter-well.

RESEARCH OBJECTIVES

This research effort has been designed and is being implemented as an integrated effort involving stratigraphy, structural geology, petrology, seismic study, petroleum engineering, modeling and geostatistics. Sandstone bodies are being mapped within their regional depositional systems, and then sandstone bodies are being classified in a scheme of relative heterogeneity to determine heterogeneity across depositional systems. Facies changes are being mapped within given reservoirs, and the environments of deposition responsible for each facies are being interpreted to predict the inherent relative heterogeneity of each facies. Structural variations will

be correlated both with production, where the availability of production data will permit, and with variations in geologic and engineering parameters that affect production. A reliable seismic model of the Big Injun reservoirs in Granny Creek field is being developed to help interpret physical heterogeneity in that field. Pore types are being described and related to permeability, fluid flow and diagenesis, and petrographic data are being integrated with facies and depositional environments to develop a technique to use diagenesis as a predictive tool in future reservoir development.

Another objective in the Big Injun study is to determine the effect of heterogeneity on fluid flow and efficient hydrocarbon recovery in order to improve reservoir management. Graphical methods will be applied to Big Injun production data and new geostatistical methods will be developed to detect regional trends in heterogeneity. Geologic and engineering data on Big Injun reservoirs will be used to construct facies maps and compute the probability that new, infill wells will encounter favorable reservoir rock.

ACKNOWLEDGMENTS

The Consortium would like to acknowledge the assistance of scientists and engineers of the Columbia Natural Resources and Pennzoil companies. Specific thanks are due to Richard Beardsley, John Buurman, Joe Lemon, and Mian Ahmad of Columbia and Greg Morrison and Bill Toomey of Pennzoil for their advice and assistance throughout this project, particularly during the beginning phase of the research when they were often bothered on a daily basis for basic data. The cumulative production and initial flow maps used in this report come directly from Pennzoil and Columbia.

The Program Manager and Principal Investigators were responsible for producing this report and wrote much of it. However, significant contributions were made by other members of the integrated research team. These researchers and their area of contribution are: Ron McDowell, Ana Vargo, and David Matchen (Geostatistical Studies); Ilkin Bilgesu and Shahab Mohaghegh (Petroleum Engineering); Milton T. Heald and James Britton (Petrology); Xiangdong Zou (Stratigraphy); and Li Zheng (Structural Geology and Seismic Studies).

EVIDENCE OF HETEROGENEITY IN THE BIG INJUN RESERVOIR

REGIONAL HETEROGENEITY

Evidence for heterogeneity in the Big Injun on a regional scale is shown by the distribution of hydrocarbon production in distinct fields across central West Virginia (Figure 1). The easternmost of these fields traditionally have been considered to be fairly simple updip unconformity traps. Those on the west, like the Blue Creek and Rock Creek fields, have not been studied in detail and little has been published concerning their relationship to those further east prior to our study. However, the western fields appear to be regionally downdip from the truncated margin of the reservoir, and thus it is presumed that the trapping mechanism is different than that for fields to the east.

FIELD SCALE HETEROGENEITY

At the field scale, shallow oil reservoirs, like the Big Injun sandstone, typically have been developed as if they were homogeneous units enclosed by thick lateral and top seals. Well spacing has commonly been based on optimum spacing dictated largely by owned acreage rather than any precise knowledge of reservoir heterogeneity. Most secondary recovery projects in these fields have been undertaken with little more knowledge or foresight other than that used to initially develop the field. In part, this is because secondary recovery projects generally incorporate wells that were drilled on regular spacing for primary production. Such is the case with Granny Creek field. The five-spot pattern (Figure 3) used for secondary recovery is a modification of well spacing utilized during primary recovery. Even though the secondary recovery project has been a commercial success (John Buurman, personal communication), it still has had a number of problems related to reservoir heterogeneities.

Reservoir heterogeneity in Granny Creek field is indicated by patterns of primary production shown by two maps of the field. Specifically, high initial-flows of oil (Figure 4) occur in two trends; one that is slightly east of north on the west edge of the field and another trending slightly west of north through the center of the field. The large contrast in values across these two trends indicates internal heterogeneity within the Big Injun reservoir. The map of cumulative production (Figure 5) has an appearance that is similar, but not identical to, that of initial flows (Figure 4). Reliable data on field pressure are difficult to find in this old (1920's and 1930's) field, but those that are available are being compiled to determine if they can shed more light on reservoir heterogeneity.

Drilling History

Initial potentials (IP) for producing Big Injun wells in Granny Creek field were analyzed according to completion date of a well and its geographic location. Previous work (Patchen, et al, 1991) has shown that oil wells in Granny Creek field were sited and completed in a fashion that indicates clustering in time (six periods of drilling activity: 1920-1930, 1931-1944, 1945-

1965, 1966-1972, 1972-1981, 1982-date) and geographic location. Figure 6 is a plot of IP values versus time for producing wells in Granny Creek. As might be expected, IP's for the discovery period (1920-1930) are relatively high. Notice, however, that during the next two periods of well completion (1931-1944 and 1945-1965) comparable IP's also were encountered. In fact, the highest IP recorded in Granny Creek field (440 BOPD) came during the 1945-1965 period. This appears to go against the idea of a homogeneous reservoir with significant drawdown of pressure and oil-in-place after a 20-30 year period of production. The pattern of both drilling activity and the placement of wells for Granny Creek suggests that the Big Injun is a heterogeneous reservoir in the field. The presence of areas where wells could be drilled with high IP values thirty years after the discovery of the field seems to agree with that suggestion.

Well-to-Well Communication

A map showing the location of "problem" wells that have shown rapid communication of injected fluids during secondary recovery is shown in Figure 3. The solid lines drawn between highlighted wells on this map indicate communication between those wells as indicated by rapid breakthrough, pressure, pumping and tracer tests. This map suggests linear heterogeneity within the field that is distinctly different in its characteristics and trend from that indicated by primary production.

Reservoir Modeling

One focus of this study was on the second stage of production in Granny Creek field. This phase of the study started with a comparison of water injection rates and water injection pressures of six injection wells in two adjacent five-spot, water-flood patterns (Figures 3 and 7). These water-flood patterns are referred to as P1 and P2; the six injection wells are numbered I-1 through I-6. Data on injection rates and injection pressures of each injection well have been plotted versus time (Figures 8 through 13). The non-uniform pressure/rate behavior of these wells suggests the existence of heterogeneity in this formation. As an example, injection wells I-2 and I-4 (Figures 9 and 11) show very different injection pressures. Pressure in I-2 is nearly twice as high as I-4, whereas the injection rates are quite similar. The difference in pressure cannot be attributed to formation permeability because it changes only a few millidarcies between these two wells. Again, injection pressure at wells I-1 and I-5 (Figures 8 and 12) stabilized at around 900 psi whereas the injection rate into I-5 was considerably higher than that of I-1. More of this behavior can be observed when comparing most of the injection wells.

Furthermore, a look at cumulative injection and fluid production in the two patterns reveals more indications of heterogeneity in this formation. The cumulative water injected into each five-spot, water-flood pattern is quite similar (Figure 14) and so is the cumulative rate of injection. However, oil production in P1 is much higher than oil production in P2 (Figures 15 and 16), whereas P2 produced much more water than P1. Water breakthrough took place almost immediately in P2 whereas it did not happen in P1 until much later. Again, all of these characteristics indicate a great deal of heterogeneity in this formation.

After evaluating these data, it was decided that the two five-spot patterns should be studied in detail to identify heterogeneities within and between them. The approach was to simulate the water-flooding process. Five-spot pattern P1 was studied first using a grid system (Figure 17). Core data from nearby wells and completion and log data of the wells involved in the pattern were used to provide input for the simulator. Reports from previous studies on Granny Creek field also were used to generate necessary fluid and rock-fluid data. A three-phase, three-dimensional, black oil simulator (BOAST) was used for simulation.

The results of the simulation were plotted against actual field data for cumulative oil production (Figure 18). This five-spot pattern, as mentioned before, did not produce a considerable amount of water. The good match that was achieved after the model was modified suggests that formation heterogeneity in this part of the field is confined to changes of rock properties (porosity, permeability, and thickness) between wells. Initial simulated injection pressures did not translate to actual injection pressures experienced in the field. Calculated (or simulated) injection pressures were consistently lower than actual field injection pressures. To account for this, several hypotheses were suggested. These suggested hypotheses were implemented in the simulator and one of them provided reasonable results. This hypothesis indicates that localized low-permeability zones in the formation, which coincide with an injection well, will cause high injection pressures. Another way of explaining such phenomena (localized low-permeability zones) could be clay swelling. The hypothesis of clay swelling was not enthusiastically supported among geologists and engineers who worked in Granny Creek field. Further study on the possibility of clay swelling, its effects, and the mechanism around the wellbore is currently being conducted, and the results will be reported as they become available. Regardless of the mechanism by which localized low permeability zones are formed, it seems to be the only explanation at this point.

A grid system also was used to simulate waterflooding in five-spot P2 (Figure 17). Using the rock, fluid, and rock-fluid properties as input data, and calling the simulation the basic run, Figure 19 shows how different the results are from the actual field data. The basic run, which accounts only for the so-called "conventional heterogeneities" (change in the spatial distribution of rock properties), was unable to match actual field data. This suggests that there may be some "unconventional heterogeneity" (major heterogeneity) involved in this system.

During the actual waterflooding process, some communication between wells was observed. According to engineers who have worked with this formation, this communication may or may not have been through the same interval in the well as the producing interval. Tracer tests were run by one operator to identify communication between wells, possibly through natural fractures. Most of the natural fractures that may be responsible for well communication are interpreted to have a southwest to northeast orientation (Figure 3) parallel to the trend of communication between wells. Because of this, the research team became interested in studying the effects of such "unconventional heterogeneities" (natural fractures; channels and sealed faults; obstacles) in waterflooding processes using a numerical approach. The preliminary results on a five-spot, waterflood pattern concluded that the effects of channels and/or obstacles in five-spot patterns are a direct function of their orientation with respect to injection wells. The conclusion can be summarized as follows. If a channel is parallel to the stream lines, sweep efficiency and production are affected. This will result in low sweep efficiency, and thus, low oil production. However, if a channel is placed at an angle to the stream lines, the sweep

efficiency, and thus, oil production, will not be affected significantly. This effect becomes less significant as the angle nears 90°. An obstacle parallel to the stream lines has no effect on production, and an obstacle placed at an angle to the stream lines does not alter production significantly.

In light of these conclusions, a natural fracture (channel) was simulated between two injection wells, parallel to the stream lines which pass through the production well. The result of this run, called modified simulation, is shown (Figure 19) in comparison with the basic and actual field data. It is obvious that the production well in the P2 pattern is in communication with some injection wells. Whether this communication is between wells within this five-spot cannot be accurately judged at this point.

As mentioned before, assuming localized low permeability zones can justify the high injection pressures observed. Actual field injection pressures versus time compare favorably to simulated injection pressures after the introduction of localized low-permeability zones (Figures 20 through 25). Localized low-permeability zones and their possible formation during drilling and/or injection are currently under investigation.

The discussions that follow summarize progress made during the past two years in understanding the geologic controls for the heterogeneities indicated on the three maps (Figures 3, 4, and 5). This report also includes discussions of progress made in designing methods of identifying and predicting heterogeneities in reservoirs deposited and deformed under conditions similar to those found at Granny Creek and Rock Creek fields.

GEOLOGIC CONTROLS OF REGIONAL HETEROGENEITY

STRUCTURAL CONTROLS

Introduction

The regional distribution of both detached and basement structures has directly and indirectly influenced the regional distribution of oil production from Big Injun reservoirs. Basement structure will be discussed first inasmuch as the configuration and movement of basement blocks influenced the deposition of sands that have become the Big Injun reservoir. Detached structure of the region was formed later by the late Paleozoic Alleghanian orogeny, probably well after these sands were lithified.

Most basement structure formed as the result of two deforming events. The older of the two, called the Grenville orogeny, formed the continental crust, or basement, under the Appalachian foreland (Beardsley and Cable, 1983). Radiometric dates of samples taken from the basement date at approximately one billion years before present (bp). The second deforming event relates to the post-Grenville breakup of the North American continent that was part of a supercontinent called Pangea II. This second deformation, dated at approximately 550-600 million years bp (Shumaker, 1986a), formed the Interior Graben System that includes normal and strike-slip faults of the Rome trough in the study area. Most basement faults and arches (Figure 26) that were active during the Paleozoic to affect sedimentation in the outer foreland appear largely to be the result of reactivation of basement structures formed by these two deformations. Lack of precise data concerning structure of the Precambrian basement forces one to simplify what must have been a more complex history, and likewise, it forces one to speculate on the time of formation of many of the basement structures which have been mapped. The assignment of an age and origin to a particular basement structure largely rests on the physical relationships between basement and adjacent Paleozoic sediments and the dip of intra-basement seismic reflections. Basement structure can be considered to have been formed by extensional deformation associated with formation of the Interior System, if bedded sediments lie adjacent to vertically offset basement, whereas low-angle, east-dipping seismic events within the basement are considered to be thrusts formed by the Grenville orogeny (Beardsley and Cable, 1983). It is likely, however, that many normal faults which are considered to be part of the Interior Graben System are, in reality, Grenville structures that were reactivated or modified during Cambrian extension.

Basement Structure

The regional distribution of Paleozoic lithofacies and thicknesses (Donaldson and Shumaker, 1981; Shumaker, 1986a) indicates the distribution of those large basement blocks that differentially subsided during the Paleozoic (Figure 26). Some block boundaries are arches which coincide with axes of sedimentary thinning. Such is the case along the Cambridge arch

and its faulted southward extension into West Virginia under the Burning Springs anticline (Shumaker, 1986b). Other block boundaries occur along large faults identified as basement faults, such as along the eastern edge of the Rome trough and along the east and northeasterly striking faults that cross the trough (Figure 26). The regional study area largely lies within the Ohio-West Virginia block, the Rome Graben, and the horst block along the east margin of the trough (Figure 26) which Kulander and others (1980) called the Central West Virginia arch (Figure 26). This study shows that Granny Creek field lies on a cross-fault zone at the eastern margin of the Rome Graben. The absence of deep drilling and seismic data in the Rock Creek area does not permit definition of basement structure there.

The West Virginia dome (Figure 26), also called the Pocono dome or the Beverly uplift, is another regional feature that was important in the sedimentary and structural development of the study area. That the dome was high-standing during the mid-Mississippian is indicated by pre-Greenbrier erosion of sediments as old as the Upper Devonian Hampshire (Catskill) red beds near the center of the dome east of the study area. That it was a structure, at least a west-plunging nose, is indicated by low-angle dip of subcropping (pre-Greenbrier) units away from the dome on its north, west, and south flanks. The origin of the dome is uncertain, but it is presumed to have been a basement feature that grew during Mississippian time to influence the extent and depth of erosion that occurred prior to deposition of carbonates and sands of the Greenbrier Group. The eastern extent of Big Injun reservoirs and hydrocarbon production associated with them are limited by erosion that occurred during this time interval. Details of how structural growth and sub-crop patterns associated with this uplift affected Granny Creek field will be discussed in more detail in the sections under field and intrafield scale heterogeneities.

Detached Structure

The study area is located at the outer margin of detached deformation in the Appalachian foreland. These structures were formed by the Alleghany Orogeny of Permian age, and as such, they are considered not to have affected Paleozoic sedimentation. A number of authors have proposed early (mid-Paleozoic) growth of certain detached structures in the Appalachian foreland, but a strong interrelationship between the position and trend of basement structure and overlying detached structure (Shumaker, 1986b) suggests that any reported growth may relate to underlying basement structure rather than pre-Alleghanian growth of detached structure. Unless clearly documented, it is assumed that all of the detached structures are Alleghanian (Permian) in age.

Several horizons were zones of detachment within the study region, including the Cambrian Rome Formation, the Ordovician Martinsburg Formation, Silurian salt beds, Devonian shales, the Mississippian Mauch Chunk Formation, and Pennsylvanian coals. Even though these units are recognized as the principal intervals of regional detachment, any incompetent interval or stratigraphic zone that has a large contrast in ductility could serve as a candidate for differential movement. As such, it might be more intensely fractured than the surrounding rocks. One need only to look at the difference in the structural configuration between the Pittsburgh coal (Figure 27) and the Greenbrier Group (Figure 28), that lies directly above the

Big Injun reservoir, to recognize the presence of structural disharmony in the Granny Creek-Rock Creek area. This contrast is greatest at the southeastern margin of these regional maps (Figures 27 and 28). Evidence of disharmonic deformation is occasionally seen at outcrop scale in the field and in cores from wells within this area. These observations indicate that detached structures of various scales occur throughout the Granny Creek-Rock Creek area and that detached deformation is more intense on the eastern (hinterland) side of the area.

The contrast in the configuration of structure between that of the Pittsburgh coal and the Greenbrier Limestone indicates the presence of either a major or many minor horizons of detachment above the Big Injun reservoir. This work suggests that the Upper Devonian Huron Shale is the major detachment horizon below the Big Injun reservoir within the Granny Creek-Rock Creek study area.

Fractures

Joints within surface rocks of the study area have not been studied in detail, but our preliminary analysis of joints in Granny Creek and Rock Creek fields indicates that they are vertical to high dipping and have complex strike patterns (Table 1). The trend of face cleats in surface coals (Kulander et al. 1980) has been mapped throughout the region. The cleat trend is approximately east-west in the Rock Creek-Granny Creek area, but there is an abrupt change in strike to west-northwest along the western margin of the study area in Kanawha County.

Small thrust faults, mapped at the surface and also in the Devonian shale section (Gas Research Institute, 1991) and in the Greenbrier Group (Dowell Schlumberger, 1986), strike southwest-northeast parallel to the trend of surface folds. The importance of these faults in creating permeability within the otherwise tight Devonian shale (Gas Research Institute, 1991) suggests that they and their attendant cross faults (tears), may be an important source of secondary porosity in other reservoirs such as the Big Injun. The occurrence of small thrusts in areas that traditionally have been considered to be beyond the margin of detachment in the Appalachian foreland suggests the necessity of reassessing the role of small thrusts in creating fracture porosity at the periphery of other forelands.

Oriented cores from three wells within the Rock Creek-Granny Creek area have been analyzed for induced fractures that reflect the trend of regional in situ stress. All three cores, two of which were in limestones of the Greenbrier Group in Granny Creek field whereas the third was in the Devonian shale at the northeastern margin of Figure 3, indicate that principle stress direction for the region is north 75 east to east (Table 1).

Production

As noted in last year's annual report (Donaldson, et al, 1991), Big Injun oil fields are found in the synclines between anticlines of the region (Figure 28). The synclinal nature of the oil traps in the Big Injun sandstone is apparent on the map of Greenbrier structure as compared with the map of the Pittsburgh coal because of the disharmony between structure on these two units. These accumulations occur at the northern end of the basement-cored Warfield anticline,

but the synclines in which the oil occurs may, in part, be detached at the Devonian shale level. Analysis of the distribution of hydrocarbons and the time of growth of structures in the Rock Creek-Granny Creek area during the upcoming year should lead to a better understanding of pathways and timing of hydrocarbon migration in this part of the basin. Because this report suggests that basement structures grew throughout the Paleozoic, primary migration of hydrocarbons being generated in the basin may have been into a large field or several fields above basement structures. Secondary (re)migration may have occurred during the Alleghany orogeny into current detached structures formed by that terminal event.

STRATIGRAPHIC CONTROLS

Introduction

A regional stratigraphic framework of the Pocono (Price) Formation is being established in order to determine the correct correlation and continuity of Big Injun sandstones on a regional scale. This framework is based on 24 stratigraphic cross sections utilizing approximately 500 of the 2000 wells with geophysical log data in the study area. These cross sections traverse 23 counties in West Virginia (Figure 29). The study initially referred to the reservoir sandstones of both Granny Creek and Rock Creek fields as lower Big Injun, but noted that they had different source areas and times of deposition. Recognition of red beds below the oil reservoir rock in Rock Creek field confirmed the younger age of this sandstone, and indicated it to be the Maccrady Big Injun as compared to the Pocono Big Injun in Granny Creek field. Both Big Injun sandstones, i.e. Maccrady and Pocono, consist of multiple sandstones that were deposited in a variety of fluvial-deltaic depositional environments. Their multiple sandstones became amalgamated and now appear as widespread blanket sandstones as a result of ancient cut and fill processes associated with river channel sedimentation.

Facies

The regional study determined the continuity of the two main facies of the Pocono and Maccrady Big Injun sandstones in their respective oil reservoirs, finding:(1) the lower fine-grained sandstone to be of interpreted river-mouth bar origin; and (2) the coarse-grained sandstone/conglomerate fill to be of bedload deltaic streams. The analysis correlated the different Big Injun sandstones and their facies for Granny Creek (Clay County), Rock Creek (Roane County), Tariff (Roane County), Clendenin (Clay County), Blue Creek (Kanawha County), and the Pond Fork (Kanawha County) fields in particular (Figure 1), and also extended to 19 surrounding counties in western West Virginia to include other Big Injun fields as well. The Big Injun sandstones are truncated not only by the pre-Greenbrier unconformity, but also by the pre-Pottsville unconformity.

Regional stratigraphic cross section RJ-RJ' (Figure 30) is an east-west profile that traverses the Tariff and Rock Creek fields of Roane County. Stratigraphy in Tariff field is

similar to Granny Creek field, with tongues of the C sandstone of the Pocono Big Injun interfingering with shales to the west. Importantly, the fine-grained, C sandstone in the Tariff field does not continue to Rock Creek field, and the A and B sandstones in Granny Creek have been replaced by the pre-Greenbrier unconformity in the Tariff field. On the other hand, the Maccrady Big Injun of Rock Creek field, particularly in the eastern part of the field, consists of fine-grained sandstone, similar to the C sandstone in the Tariff field, but does not connect with it. The shale that separates the Big Injun sandstones of the two fields widens southward into Kanawha County. Red beds underlie the Big Injun sandstones in Rock Creek field and define its oil reservoir as Maccrady rather than Pocono. Apparently, the fine-grained sandstones in both fields represent deposits of similar depositional environments, namely river-mouth bars or the delta front, that were fed by different river systems which prograded into the same general area at slightly different times. Sandstones of the Tariff (also Granny Creek) field are interpreted to have been derived from a source area east of Clay County, whereas sandstones of the Rock Creek field seem to have come from a different drainage basin located west of Roane County. The stratigraphic cross section (Figure 30) shows upper Weir and multiple Big Injun sandstones of interpreted fluvial-deltaic mouth bars and channels that prograded eastward into the area of Rock Creek field. Widely separated fluvial-deltaic systems prograded toward each other from upper Weir time to Maccrady Big Injun time within the study area.

Sandstone Distribution Patterns

A regional-scale sandstone isolith map of the combined Pocono and Maccrady Big Injun sandstones (Figure 31) indicates the maximum thickness of sandstones occurs in Mason County along a southeast-northwest trend that continues into adjacent Gallia County, Ohio. This trend aligns with a north-south trend farther north in Ohio (Figure 32) in the equivalent Black Hand Sandstone Member of the Cuyahoga Formation, according to an isopach by Ver Steeg (1947). A stratigraphic cross section (Figure 33) extending from Cabell and Mason counties eastward to Clay County shows that the Big Injun consists of vertically stacked sandstones in excess of 200 feet thick in Mason County that thin eastward as they prograde toward the present location of Blue Creek and Pond Fork fields. The thickness maps (Figures 31 and 32) reveal multiple sandstones exceeding 200 feet in thickness along a depoaxis trending southeast-northwest across Gallia County (Ohio) into Mason County (WV), where the sandstone belt bifurcates into a southward lobe into Cabell County, an east-northeastward lobe into Jackson County and an eastward lobe into Putnam and Roane counties (Rock Creek field).

Initially, this thick belt of Big Injun sandstones was interpreted to be a barrier island (Figure 34; hypothesis B) with fluvial feeder channels oriented southwestward toward it. This hypothesis would suggest that sandstones of Rock Creek field are continuous with a southwesterly trending sandstone belt in Ritchie and Wirt counties (Figure 31). Another stratigraphic cross section (Figure 35) extending from Cabell County northwestward to Ritchie County was constructed to verify this hypothesis. The cross section indicates that the Pocono Big Injun sandstones in Wirt and Ritchie counties are ancient river-mouth bar deposits that prograded southwestward but terminated before reaching the Rock Creek field area. On the other hand, the uppermost coarse-grained facies of river channels coalesce. The 24 regional

stratigraphic cross sections indicate that erosion during post-Big Injun time must have affected the thicknesses shown on the sandstone isolith maps (Figures 31 and 32). Another map (Figure 36) shows areas where Big Injun sandstones are totally missing or partially eroded by either the pre-Greenbrier unconformity or the pre-Pottsville unconformity. This map sorts out the changes in thickness of the Big Injun sandstones that are the result of post-depositional erosion.

The sandstone isolith map was modified (Figure 37) to show regional changes in gamma-ray signatures for the Big Injun sandstones. The gamma-ray signatures can be grouped into: (1) vase type, texturally coarsening upward; (2) vase with blocky cap, texturally coarsening upward with additional coarse-grained deposits on top; and (3) thick blocky type, coarse-grained deposits from bottom to top, and vertically stacked where very thick. The map shows that the thickest sandstones occur in the core of sandstone belts and show blocky gamma-ray signatures. In the southern part of the region, the patterns show a consistent pattern across the sandstone belts as well as toward the lobe margins; blocky in the center, then vase with blocky cap, to vase type at the outer part of the belts. In the thinner belt situated in the northern part of West Virginia (Wirt and Ritchie counties), the blocky type again occurs along the axis of the belt (its core or center) and changes to the vase type in the outer part of the belt. A final stratigraphic cross section (Figure 38) that cuts across the sandstone belt of Ritchie County was interpreted as having log signatures that suggest shifting bedload channel fill (blocky pattern) and progradation of river-mouth bars of the delta front (vase type) and crevasse splays and levees of the delta plain/alluvial plain.

The Big Injun sandstones of Figure 37 are not differentiated into Pocono and Maccrady units, and appear laterally extensive regionally. However, there are stratigraphic discontinuities in the otherwise blanket-style geometry and extent of the Big Injun sandstones. These discontinuities establish stratigraphic heterogeneity at the regional scale for the following three reasons:

1. lateral discontinuities resulting from total or partial erosion of the Big Injun sandstones by the pre-Greenbrier unconformity and/or the pre-Pottsville unconformity (see Figures 30, 31, 32, 33, 35, 36, 37, and 38);
2. lateral discontinuities resulting from facies changes of the sandstones to shales at the distal margins of the deltaic river-mouth bars and/or fluvial channels (see Figures 30, 33, 35, and 38);
3. vertical discontinuities resulting from shales separating the Pocono Big Injun sandstone from the younger (overlying where both present) Maccrady Big Injun sandstone (see Figures 30, 33, and 35).

Heterogeneity Between Oil Fields

The stratigraphic heterogeneities between oil fields seems to be related to the control of basement structures on sedimentation of the Big Injun sandstone, or conversely, its erosion as a result of uplift of the West Virginia dome. A comparison of the distribution of large basement blocks (Figure 26) that differentially subsided during the Paleozoic with the sandstone isolith maps (Figures 31, 32, 36, and 37) shows thinning or absence where the Cambridge arch and its faulted southward extension occur in West Virginia under the Burning Springs anticline. The

West Virginia dome caused the extrabasinal rivers that emanated from the orogenic mountain belt to the east to flow around it during Early Mississippian time. The bedload-type stream that deposited the sandstones and conglomerates in Granny Creek field probably was intrabasinal, with its headwaters within the dome area. This braid delta and its feeder braided stream flowed from the ancient dome westward across the eastern edge of the Rome trough. The confirmation of the minor size of the drainage basin traversing the Granny Creek area is reflected in the relatively small extent of the braid delta (Figure 37, where the western limit is shown by the supposed dividing line between eastern and northern depositional systems) from the center of the West Virginia dome. The extrabasinal river flowing around the northern periphery, paralleled the northwestern edge of the dome in Ritchie and Wirt counties and occupied the axis of the Rome trough. The resulting thick southwest trend of the Pocono Big Injun thins and ends in the area of the Pottsville unconformity (Figure 37) west of the Burning Springs structure. Multistory (vertically stacked) Mississippian sandstone reservoirs identified as Weir and Big Injun occur along the axis of the Rome trough in West Virginia, as well as along a parallel sag in Ohio between the Waverly arch and the Cambridge arch (Figure 26). Where the Cambridge arch turns toward West Virginia and the Burning Springs anticline, this thick trend of Big Injun extends southward along the western flank of these positive structures into Mason, Cabell, Putnam and Kanawha counties. This thickness trend also is approximately parallel to the pinch-out trend of the Big Injun, which occurs along the south-oriented margin of the pre-Greenbrier unconformity. Both Pocono and Maccrady Big Injun sandstones are recognized in the thick sandstone trend of southeastern Ohio that extends into southwest West Virginia south of the Burning Springs anticline. These Big Injun sandstones are interpreted to represent fluvial deltaic deposits of a very large river system that developed with the merging of orogenically derived rivers from the east with cratonic-derived rivers from the north and northwest. The large drainage basin was structurally controlled (Zou and Donaldson, 1992).

Basement structures apparently controlled the paleoflow directions of Big Injun rivers as well as the distribution patterns of erosion associated with the West Virginia dome. This relationship is evident at the regional scale between oil fields, and the local scale within fields, such as Granny Creek field. Lateral disconformities are located where basement structures were active during Early Mississippian sedimentation and erosion.

GEOLOGIC CONTROLS OF FIELD-SCALE HETEROGENEITY

INTRODUCTION

This part of the report describes reservoir heterogeneity within Granny Creek field. Cumulative production and initial potential show a number of trends and small-scale features on maps. Heterogeneities in structure, petrology, porosity, and permeability are present and can be related to spatial patterns in initial potential and production.

Specifically, the section on structural geology describes northeast-trending, low-relief folds of small areal extent, and presence of thief zones oriented in the same direction. Seismic work confirms the existence of these small-scale structural features, and suggests that areas of above-average production arise from folded Big Injun reservoir rock that lies over basement faults.

Within this field, the Big Injun includes a channel facies comprising coarse sandstones, and an underlying mouth-bar facies of finer sandstone. Important variations in sorting, clay composition, and cementation led to heterogeneities in porosity and permeability.

Estimates of permeability from porosity improve when facies or depositional environment are taken into account. The geometry of these facies and presence of high-density zones apparently affect initial potential and cumulative production of oil.

SPATIAL TRENDS IN OIL OCCURRENCE

Initial Potential

Initial potential data were available for 301 wells in the Granny Creek field. These data were converted to three indicator variables through the simple transform:

1. $I_7(x) = \begin{cases} 1 & \text{if } z(x) \leq 7 \text{ BOPD} \\ 0 & \text{if } z(x) > 7 \end{cases}$
2. $I_{15}(x) = \begin{cases} 1 & \text{if } z(x) \leq 15 \text{ BOPD} \\ 0 & \text{if } z(x) > 15 \end{cases}$
3. $I_{25}(x) = \begin{cases} 1 & \text{if } z(x) \leq 25 \text{ BOPD} \\ & z(x) > 25 \text{ BOPD} \end{cases}$

The median of the 301 values of initial potential is 15 BOPD. The 25th and 75th percentiles equal 7 and 25 BOPD. Hence, the three new variables indicate whether initial potential $z(x)$ at location x is greater than the 25th, 50th, and 75th percentiles, respectively.

For each indicator variable, a variogram was computed:

$$\gamma(h) = \sum_{i=j}^{n_p} [I(x_i) - I(x_i + h)]^2 / 2n_p$$

where I is an indicator variable; h is the distance between pairs of wells at locations x_i and $x_i + h$; and n_p is the number of pairs. $\gamma(h)$ is computed for several values of $h \pm h_t$, where h_t is a distance tolerance. For all indicator variables, both omnidirectional variogram and directional variograms were inspected. Directional variograms are made by finding the direction of the vector separating wells in each pair. The variogram in the east-west direction represents pairs situated $0^\circ \pm 22.5^\circ$, (assume angles to be measured counterclockwise from east). The three additional directions are northeast-southwest ($45^\circ \pm 22.5^\circ$), north-south ($90^\circ \pm 22.5^\circ$), and northwest-southeast ($135^\circ \pm 22.5^\circ$). By this means, we observed directional anisotropies.

The omnidirectional variogram for all indicator variables was fitted by inspection with a nested spherical model with nugget effect:

$$\begin{aligned} \gamma(h) &= C_o + C [3h/2a - h^3/2a^3] & C \leq a \\ &= C_o + C & C > a \end{aligned}$$

where C_o , C and a are constants. C_o is usually called the nugget effect, C is the constant associated with the spherical model, and a is the range, beyond which data are essentially spatially independent. The nugget effect represents very small-scale variability, including measurement error (see Hohn, 1988, p. 29).

The following constants were fitted to the omnidirectional variograms (Figure 39):

I7:	$C_o = 0.11$	$C = 0.14$	$a = 6000\text{m}$
I15:	$C_o = 0.20$	$C = 0.06$	$a = 2000\text{m}$
I25:	$C_o = 0.15$	$C = 0.05$	$a = 2000\text{m}$

All of these variograms show a large degree of variation in initial potential at the well-to-well scale. Gradual changes in initial potential would result in a variogram that approached zero at small distances. That is not the case here. Thus, initial potential behaves very erratically from one well to the next.

This observation can be explained in several ways: (1) measurement error; (2) pressure decline during the history of the field; and (3) heterogeneities in porosity and permeability. Certainly, there is a degree of error in measuring initial potential. No single, standard method exists for measuring this parameter; results are dependent upon the method used to complete each well; and results are not always reported accurately, or unambiguously. However, most of the wells—drilled before 1960—were shot. Although no absolute criteria exist for judging whether variograms reflect measurement error or actual heterogeneity, the nugget effect in these variograms is usually high, tending to rule out error as the sole cause.

Much of this variation is probably explained by interwell-scale variation in porosity and permeability. Initial potential should be expected to be particularly affected by local variation in permeability.

All of the variograms showed some degree of directional anisotropy. For example, the

following model of simple, geometric anisotropy was fitted by inspection to the I15 indicator variable (Figure 40):

$$C_0 = 0.20 \quad C = 0.06$$

0° (east-west):	a = 1372m
45°	a = 1000m
90°	a = 1372m
135°	a = 4000m

This model shows excellent fit with all but the north-south (90°) variogram, showing the presence of an anisotropy in the north-south direction in addition to major anisotropy in the northwest-southeast direction.

These anisotropies become obvious in kriged maps of the indicator variables. Maps for I7 and I15 are very similar, so only that for I15 is shown (Figure 41). Kriged estimates of an indicator variable when subtracted from one show local frequencies of wells having an initial potential greater than the particular threshold value, i.e. 15 BOPD in Figure 41. These may be interpreted as the estimated probability that a newly drilled well will have an initial potential exceeding 15 BOPD, in this case. The map makes obvious the two principal directions of anisotropy: the north-south trend in the southern part of the field; and the northwest to southeast trend in the northern half. The north-south trend is very well defined, and can be carried up into the northern part of the field. The other trend is less well defined, and a number of sub-trends oblique to the major directionality can be picked out. Unfortunately, the eye always wants to pick out trends in spatial data, so some caution in delineating and interpreting these smaller trends is in order.

Cumulative Production

At the time of this writing, cumulative production data on individual wells were available for the northern half of Granny Creek field. For each well with information on hand, a ten-year cumulative production figure was computed. The data provided to us were missing information for some years on many wells; in these cases, available data were used to estimate values from graphs of the log of annual production versus year.

Standard variography and variogram model-fitting resulted in the following constants for an omnidirectional spherical model with nugget effect (Figure 42):

$$C_0 = 8 \times 10^7 \text{BO}^2 \quad C = 6 \times 10^7 \text{BO}^2 \quad a = 750\text{m}$$

Like initial potential, oil cumulative production displays a large nugget effect. Also, there is a strong north-south anisotropy (Figure 43). A map of kriged estimates for cumulative production shows a north-south trend as expected, roughly parallel with the western margin of the field. Within this trend are several locally high values of cumulative production (Figure 44).

Variograms for cumulative production show a smaller nugget effect than those for initial potential, in spite of the fact that some annual volumes used to calculate cumulative production were estimated. This smaller contribution to overall variance by small-scale spatial variation is probably the result of several factors: (1) cumulative production is measured more accurately than initial potential; (2) computing ten-year cumulative totals averages out some of the variations over time, whereas initial potential is a snapshot measure of flow; (3) cumulative production is very much more porosity dependent than initial potential which is highly dependent on permeability. The Big Injun sandstone might be much less heterogeneous with regard to porosity than permeability on the interwell scale. Nevertheless, this sandstone has a large degree of heterogeneity over even small well spacings; from the variograms, we can conclude that on the average, cumulative production for wells farther than 0.75 kilometer apart is statistically independent.

STRUCTURAL CONTROLS OF FIELD SCALE HETEROGENEITY

Introduction

This section of the text centers on surface and near surface structure interpreted primarily from log data and surface investigations.

The structure of Granny Creek oil field (Figure 45) was mapped on the Big Injun reservoir based solely on geophysical logs. The structure on top of the Greenbrier Group directly above the reservoir (Figure 46) was defined by logs from 642 wells that include both driller's logs and geophysical logs. As noted in our first annual report (Patchen et al., 1991), the quality of well data in West Virginia always is suspect and requires checking well locations and datum elevations for accuracy. This was accomplished in Granny Creek field by carefully comparing data printed on geophysical logs with the original driller's logs, company documents, and a large-scale topographic map provided by Columbia Natural Resources, Inc. Well locations were cross checked using topographic and company field maps. The datums of 20 logs were corrected and used in the study. A few logs were dropped from consideration because of a missing well number, no log datum, or poor log quality. Logs in the northern and central parts of the field generally are of good quality and have reliable datums because these wells were completed in the 1960's and later. Data from older wells were found to be less reliable and commonly more difficult to check. The original data for these wells commonly had been lost. While there still are questions concerning the quality of the subsurface data, it is certain that the general shape of the structure (Figure 45) is correct based on comparisons with structure mapped using seismic data and as mapped on surface coals (Figure 27).

Big Injun Structure

The configuration of the structure on top of the reservoir (Figure 5) suggests that a number of small-wave-length, low-relief folds, which appear as northeast-trending noses, are

present in the northern part of the field. Uncertainties in regard to precise elevations of well datums leave the precise trend of certain of these folds open to question, but there is little question that some of the more prominent folds are present.

Some, but not all, of these folds appear to correlate with folds mapped using seismic data. Analysis and integration of structure based on well data versus seismic data await analysis of additional data from the seismic program scheduled for this upcoming year.

Thief Zones

Data provided by Columbia Natural Resources and Pennzoil indicate that communication between wells in "thief zones" during injection of water is a serious problem to the efficient recovery of hydrocarbons in their secondary recovery programs. Plotting of these problem wells, as shown on the structure map (Figure 46), indicates that they usually have a northeast trend, which is the same trend as the low-relief folds. Plotting breaks on the seismic records, interpreted as fractures, in relation to the low folds, suggests that folds, fracture zones, and thief zones may all be interrelated. Evidence favoring the occurrence of faults and fracture zones in the reservoir include: (1) pumping tests from wells adjacent to mapped breaks in seismic continuity; (2) minor stratigraphic repetition noted on several logs within the field that may indicate the presence of small reverse faults; (3) the presence of slickensided, inclined fractures in the Greenbrier Limestone of two oriented cores taken in the heart of the field (Dowell Schlumberger, 1986); (4) the presence of a northeast-trending small detached fold and reverse fault within Pennsylvanian surface sediments; and (5) the presence of several linear thief zones that have been identified by pumping tests during water-flood operations in the field. A preliminary interpretation that interrelates folds, minor faults as mapped by breaks in seismic continuity and thief zones is presented in Figure 46. Establishing a firm correlation between the breaks in seismic reflection continuity, minor faults, low-relief folds and specific thief zones awaits additional analysis and data such as that which will be obtained from the seismic program scheduled for the upcoming year.

A compilation of structural trends (Table 1) in the northern part of the Granny Creek field is given below. Structural trends in the southern part of the field are less defined and are not included in Table 1. This change in the structural style of deformation between the northern and southern parts of the field (Figure 45) is discussed in more detail later in the text.

HETEROGENEITY INTERPRETED FROM SEISMIC STUDIES

Introduction

The main objective of this portion of the study is to determine whether production-related heterogeneity in the geometrical framework of the reservoir can be identified seismically. Six seismic lines representing a total of approximately 28 miles of common midpoint coverage have been collected over Granny Creek field. Fold of the data is, on the average, about 30, but exceeds 60 in places. Two of these lines (lines 5 and 6), representing a total of 14 miles of data, were provided for this study by Columbia Natural Resources Inc.

Seismic line 2 (Figure 47) illustrates the general characteristics of the seismic data collected over Granny Creek. This line cuts through the middle of the field as defined by primary production data (Figure 48) roughly along the dividing line between Columbia Natural Resources and Pennzoil acreage. The line begins on the east end of the field and trends north-south a short distance before cutting across the field. Prominent reflection events along the line have been identified on the basis of synthetic seismograms compiled from density and sonic logs from the field and surrounding area. Sonic and density control from surface to basement are not available within the field. However, prominent reflective intervals such as the organic-rich Huron Shale, the Onondaga Limestone, the Newburg and Keefer sandstones, and the Trenton Limestone are regionally extensive and the general sequence of reflection events associated with these intervals is useful for approximate correlation.

Sonic and density logs, along with their vertical seismic profile (VSP), were run in the Clay 2509 well close to common mid point (CMP) no. 300. This well extends several feet below the Big Injun. A synthetic seismogram (Figure 49) was calculated using an average wavelet extracted from the downgoing wavefield measured in the vicinity of the Big Injun sandstone from the borehole VSP. The tie (Figure 50) is good and provides a reliable match between seismic response and subsurface stratigraphic intervals.

A good match also was obtained between the synthetic seismogram and seismic data near the well, and forms the basis for relating individual reflection events in the zone of interest to subsurface stratigraphic intervals. The Big Injun sandstone is marked by a large amplitude negative cycle at 0.31 seconds (Figures 49 and 50) produced by the large negative impedance contrast between the overlying Greenbrier Limestone and Big Injun Sandstone. This reflection event is easily followed across the line and throughout the field.

Regionally the field lies in the Appalachian Plateau province of the central Appalachians. The Mississippian-aged reservoir interval lies above the eastern margin of an Early Cambrian-aged, failed-rift complex known as the Rome Trough. A slight drop of the pre-Cambrian basement reflector into the trough is noticeable on Line 2 (Figure 47). Structural heterogeneity observed within the reservoir is in general controlled by syn- and post-depositional reactivation of deeper fault zones, and also to subsequent detached deformation that occurred during Alleghanian orogenesis.

Seismic evaluations of the Granny Creek field reveal significant interrelationships between heterogeneity within the structural framework of the reservoir and the distribution of oil production in the reservoir.

Field-Scale Heterogeneity

Brief inspection of the cumulative (primary) production map (Figure 48) reveals that cumulative production is quite variable over short distances within the field, falling from more than 500,000 barrels of oil to zero over distances of less than a mile. Variations of initial, cumulative, and (in some cases) ten-year cumulative production data along each seismic line are shown in Figures 51 through 55. The ten-year cumulative production figures were recently compiled and include wells not used to construct the earlier cumulative map (Figure 44). In general, cumulative production drops off rapidly up the limbs of the syncline as defined by arrival time variations to the reservoir interval (Figures 51 through 55).

An erosional unconformity truncates the Big Injun along the eastern and northeastern margins of the field - the result of differential uplift and erosional truncation, believed to be associated with the rise of the West Virginia Dome further to the east (Donaldson and Shumaker, 1981). As described by Wilson et al. (in prep.) the southeastern basement block (SEB of Figure 47) beneath the field actively subsided or rotated into the Rome Trough along a hinge or high area east of the field. Subsidence and rotation are consistently into the Trough, but occurred at different rates from Early Cambrian through Mississippian time, as revealed from an analysis of traveltimes differences through successive stratigraphic intervals such as those shown in Figure 56. The southeastern basement block remained structurally high throughout the Paleozoic and defines the southeastern margin of the field.

The western margin of the field also was controlled by periodic reactivation of a deeper basement fault (basement fault B of Figure 48), but the displacements have not always been downward (relative to the eastern margin of the field) into the Rome Trough. Critical to the formation of a reservoir is that significant inversion or relative uplift of the northwestern basement block along fault B occurred during the Paleozoic, resulting in the present day structural high along the western margin of the field.

Basement Faults. Evaluation of isotime contour and isochron maps from various stratigraphic intervals reveals additional interrelationships that are relevant to understanding the distribution of oil production within the field. One of the most noticeable characteristics of oil production within the field is its division into a highly productive northern part and a less productive southern part.

Correlation of basement fault patterns observed on the seismic lines over the field reveals the presence of a basement fault (basement fault A in Figures 47 and 48) that cuts across the field, dividing it into the productive northern and less productive southern halves (Figure 48). This fault trends generally to the northeast, but takes a "right-lateral" bend between the northern and southern halves of the field. This right-lateral bend is observed in all traveltimes and isochron maps. Whether variation in the trend of the fault is simply due to an irregularity in shape occurring during normal fault offset or associated with actual strike-slip offset, is not known.

Across the northern half of the field, patterns of growth from the overlying Lower Cambrian through Mississippian intervals consistently reveal an imprint of basement fault A, indicating active growth of this structure during Paleozoic sedimentation. To the south, the basement fault extends beneath the western margin of the field, but is poorly defined because

it lies at the edge of data coverage. Isochron maps indicate that thickening to the west across this fault along its southern extension is much less than that observed across the center of the field. This suggests that the fault rotated downwards to the northeast as it dropped to the west. There also is a change in the location of the axis of greatest thickening observed in the various isochron maps. During the Middle and Early Devonian and Late Ordovician-to-Early Silurian time areas of greatest thickening lie much closer to the basement fault in the southern part of the field than they do in the northern part. These are the same periods of time that we see thinning or relative inverse motion along fault B in the northwestern corner of the field. These time periods bracket the Acadian and Taconic orogenies.

The syncline revealed in the isotime map of the Big Injun oil reservoir (Figure 57) does not overlie the downthrown side of basement fault A (Figure 58), but crosses the fault. The structural low lies on the low side of the basement fault in the northern part of the field and crosses onto the high-side of this fault in the middle of the field. Big Injun traveltime contours become disharmonious above the basement fault, and the shape of the syncline possesses the right-lateral bend observed in the basement isotime map (Figure 58) as well as in isochron maps of other intervals (Wilson et al., in prep.).

A brief mention is made here of the possibility that the time structures observed in the seismic data, and that arrival-time and arrival-time difference plots may have their origins in velocity anomalies. Simulation of the time structures using only velocity variations would require a very unusual distribution of vertical and lateral velocity variations. The possibility that the time structures in the Big Injun, for instance, have their origins with velocity reduction in the overlying Greenbrier Limestone sequence would require significant changes of reflectivity within the Greenbrier interval above these structures. Such changes were not observed. One also would expect that the highs in the Big Injun, if velocity related, would show up as structural highs in succeeding layers. However, no such relationship was observed. In places there are time "lows" beneath the time "highs" of the Big Injun, which might suggest that the underlying lows are related to thickening of the relatively lower-velocity Big Injun sandstone. However, stratigraphic thickness variations along the line do not support this hypothesis (Figure 60, for example). While it is true that arrival time variations in a seismic section can be simulated by changes of interval velocity only, there is no geological support for taking this approach.

Intrafield Heterogeneity

Small-Scale Folds. Individual profiles (Figures 51 through 55) reveal that the reservoir interval is disrupted internally by small-scale folds and that total cumulative oil production is highest in these folded areas.

These folds are believed to be detached (Wilson et al., in prep.) based on the disharmony between the traveltimes to the Big Injun and lower Huron. Through the heart of the field along line 6 (Figures 55 and 56), small folds are clearly defined and correlate with thickening of the Big Injun-to-Huron interval. Interval thickening is in some cases greater than the structural relief along the Big Injun reflector and suggests that some of the disharmony between the configuration of the Big Injun and the Huron reflectors is, in part, the result of basement growth.

Although shallow detachment of the section appears to be the major source of disharmony between the Big Injun and the organic-rich Huron Shale, lack of reflection continuity in this interval makes it difficult to locate a specific decollement zone(s). Weak continuity of reflectors within the Huron-to-Big Injun interval, when visible, suggests that detachment begins at intermediate depths. Vertical disharmony between these "noisy" reflectors also is observed, indicating that these folds may be the result of incremental growth of detached structures at various levels above the lower Huron.

Folds located over basement structures appear to be more productive. Fracture intensity may be greater over deeper structures that were repeatedly active during the early and middle Paleozoic. Hence, the section overlying these basement faults may be mechanically weakened and therefore, more likely to be deformed during post-Mississippian deformation. Late-stage fluid migration and cementation could also alter the mechanical properties of these fractured regions and complicate the affects of later deformation. The role of fracture porosity associated with detached structures is reminiscent of the interrelationships suggested for the deeper Devonian shale reservoirs (Shumaker, 1980). Examination of oriented Devonian shale cores revealed numerous slickensided surfaces oriented normal to the regional trend of the central Appalachians, suggestive of detached origins.

The possibility that folds observed in Granny Creek field are simply due to relief on the unconformity is ruled out (Wilson et al., in prep.) because of a general lack of correlation between seismic travelttime to the unconformity and the thickness of Big Injun intervals exposed on the unconformity (Figure 59). Additional illustration of this disagreement is shown along line 6 (Figure 60). This conclusion also is consistent with the observation that arrival time variations are observed above and below the Big Injun/ Greenbrier reflector rather than only along the interface. Although the net relief along this reflector must be the result of both post-unconformity deformation and erosion, the contribution of erosional relief to arrival time variation is thought to be relatively minor.

Fracture Zones and Faults. Line 2 (Figure 61) is a reprocessed version of the data shown in Figure 62. The data are presented for comparison at an expanded time scale in Figures 63 and 64. Significant aspects of the reprocessing of the line are discussed by Zheng and Wilson (1992). The majority of the improvements in the data can be attributed to use of Berkhout's (1977) zero phase deconvolution approach. Examination of reprocessed Line 2 (Figures 62 and 64) reveals some improvement of temporal resolution and the presence of local disruptions in the reflections from the Big Injun and surrounding intervals.

Based on the half-cycle width of the composite "Big Injun" reflection event near the VSP well at CMP 300 the peak frequency of the event in the reprocessed data (Figure 64) is about 62 Hz compared to 50 Hz in the original processing of the data by Lauren Geophysical Inc. Resolution of isolated interfaces separated by approximately 46 feet could be resolved in the reprocessed data compared to about 58 feet in the original, assuming an interval velocity of 11,500 fps.

The small folds discussed in the previous section are observable in both the original and reprocessed versions of the data; however, local disruptions of the interval are enhanced by reprocessing (Figure 64). The disruptions are particularly noticeable in the positive (black) cycle immediately above the Big Injun event. Weak patterns of disruption also can be followed into

the intervals above and below the Big Injun along with the small time structures.

Computer simulations such as that shown in Figure 65 (generated using a Kirchoff approximation of the wave equation) suggest that these zones are not simple faults, but are the result of significant impedance reduction over horizontal distances of more than several hundred feet. In this preliminary model (Figure 65), several low-velocity zones were scattered through the lower 25 feet of the Greenbrier Limestone interval. The synthetic seismogram indicates that isolated low relief faults (30 foot offsets or less) such as those associated with the time reliefs shown in Figures 52 and 59 do not affect reflection amplitude unless velocity reductions across the fault are introduced. Additional simulations planned for the coming year will address this issue more thoroughly.

Disrupted zones identified on the reprocessed data (Figures 63 and 65) are located across the bottom of the expanded scale plot (Figure 65). The disruption in the vicinity of the VSP well near midpoint 300 is supported by interpretations of the offset VSP's recorded in the well (see Interwell Heterogeneity below). This disruption occurs along the southeast flank of a small fold and takes the form of abrupt time-offsets with little amplitude variation. The location of problem wells in this area suggests that the time-offsets may be fault related; however, abrupt offsets of 2 ms are expected along a dipping reflection event when the sample rate is two milliseconds. Taken by themselves, these abrupt time offsets may represent nothing more than a digital sampling problem.

Direct communication between wells identified during waterflooding also was observed near reflector disruptions at midpoints 395 and 417. These interwell connections are referred to as thief zones. A local map of the area along this part of the line (Figure 66) shows the locations of the wells between which direct communication has been identified by Pennzoil and Columbia Natural Resources. The coincidence of "problem" wells with the seismic disruptions lends credence to the interpretation that these seismic features may be associated with fault and/or fracture zones.

An interpretation of the distribution of these wells that are in communication was presented under the structural discussion above. The interpretation is based on the locations of wells between which communication problems have been identified. The possibility of identifying thief zones seismically would be important to the economical and effective design of secondary recovery operations, since direct well communication usually results in significant reduction of sweep efficiency during waterflooding. Prior information about the location of these zones would allow operators to avoid potential problem areas and increase the recovery of oil from the formation.

STRATIGRAPHIC CONTROLS

Subdivisions and Depositional Environments

The Pocono Big Injun sandstone has been subdivided into informal members, tongues, and subfacies in stratigraphic cross section GB-GB' (Figure 67) extending west to east across Granny Creek field, which was constructed using data from cores and geophysical logs, with the underlying Squaw sandstone as the datum. Three informal members of the Big Injun sandstone

were recognized using signatures on gamma-ray logs that correspond to grain-size distribution and deflections in the bulk density log that relate to high and low density: (1) a basal fine-grained sandstone of the C member (low density); (2) an overlying coarse-grained sandstone and conglomerate of the B member, (high density); and (3) the uppermost coarse-grained sandstone and conglomerate of the A member (low density). The cross section illustrates that pre-Greenbrier erosion removed increasing amounts of Big Injun sandstone toward the east. A sharp erosional contact separates the fine-grained sandstone of the C member from the overlying coarse-grained B and A members, whereas the basal contact of the C member is gradational into shales. Laterally, the C member consists of westward-prograding tongues, numbered from oldest to youngest, respectively, as C1, C2, and C3 (Figure 67) within Granny Creek field. Subfacies of the tongues of the C member also are indicated. These subfacies are characterized by composition, texture, fossils, sedimentary structures, porosity and permeability (where available), geophysical log signatures (caliper, gamma ray, density) and nature of contacts. The subfacies are named according to the depositional environment that they suggest. Therefore, the C member and its tongues represent a facies deposited in a deltaic river-mouth bar environment and the subfacies are the distal and proximal parts of the bar, further distinguished by whether dominated by marine or fluvial processes. Importantly, the distal river-mouth bar subfacies (Figure 67) intertongues with shale, which also is a permeability barrier to fluid flow. The textures, fossils, and sedimentary structures are similar between the B and A members, but the pore-plugging composition (due to diagenesis) is sufficiently different to affect the porosity and permeability of the units, and thereby warrant their separate distinction.

In general, the fine-grained sandstone of the C member is a texturally coarsening upward facies with shale drapes bounding the tongues. Interbedding of basal sandstone and shale beds probably is due to supply shifts (autocyclic sedimentation) that caused local transgression of the sea, periodically interrupting an otherwise steady westward progradation of a deltaic shoreline. The subfacies of the C member along GB-GB' are emphasized in Figure 68 and keyed to three cored wells (permits Clay #1126, 1108, and 1134). In Figure 69, an isopach map of the C2 tongue is shown for the Granny Creek field (note the location of the cored wells #1126, 1108, and 1134) with the interpreted environments of the distal and proximal bar, as well as speculated river-mouth orifice, superimposed. The C2 mouth bar shows a thick trend oriented north-south (depositional strike trend locally), although regionally the reservoir sandstone of the Big Injun mouth-bar sandstone facies exhibits a depositional dip trend (classified as DS2 sandstone reservoir according to Donaldson and Boswell, 1990). In Granny Creek field, paleoflow direction seems to have changed from mostly westward during Pocono C member time, to southwest paleoflow during Pocono B and A member time, probably reflecting the emergence of the West Virginia dome.

Detailed examination of the Big Injun A and B members in a Clay County core allowed the interpretation of minor channel and bar fill of a bedload paleostream (Figure 70). Probably, the initial porosity and permeability of this river-channel fill was high, based on petrographic data, but cementation of the B member during burial produced a diagenetic facies, which is discussed in the next section.

Petrology of the Pocono Big Injun Sandstone

The Big Injun sandstone in Granny Creek field is mainly a sublitharenite, with grain components having been contributed from a variety of source rocks. A plutonic igneous source is indicated by K-feldspar, a metamorphic source by quartzite and schist grains, and a sedimentary source by grains of chert and shale.

The upper A member of the channel facies is a well-sorted, largely medium-grained sandstone with generally good porosity and permeability. Typically the grains are well coated with illite. These coatings may have resulted from redistribution of some of the illite which had accumulated along laminae or from early infiltration of muddy waters. Downward flow is definitely indicated in some places by geopetal features. Alternately some illite could have come from possible soils related to the unconformity at the top of the Big Injun, but the illite laminae seem to have been an adequate source. These illite coatings had important effects on diagenetic processes in that the coatings were instrumental in preserving porosity by preventing detrital quartz grains from serving as suitable seed crystals for quartz cement.

Calcite is particularly abundant in the upper few feet of the Big Injun. Its occurrence there is related to the availability of carbonate in the Greenbrier sea that produced the overlying Greenbrier Limestone. The calcite partially replaced illite in the sandstone and filled pores, particularly in the coarse sandstone producing tight zones which otherwise would have retained high permeability.

The lower part of the channel facies, the B member, is markedly different from the upper A member. Original porosity was only fair in some layers because of poor sorting resulting from strong fluctuations in flow, whereas original porosity in the A member was good.

Quartz cementation was a major factor in porosity and permeability reduction in the lower part of the fluvial channel sandstone (B member). The cement apparently formed there because, in almost every core, coatings on grains were either absent or poorly developed in this interval. Although some workers now question the importance of coatings in determining whether or not quartz cementation occurs, other research has documented the relationships between coatings and high porosity versus lack of coatings and quartz cementation (Pittman, et al, 1992). It is true that in a few places in the Big Injun argillaceous dust rings occur in the quartz, suggesting that coatings were ineffective and were largely replaced by secondary quartz. However, the scarcity of this type of dust ring and general habit of the quartz overgrowths indicate that the lack of well-formed coatings was the main reason for the localization of quartz cement in this interval.

Illite also was instrumental in reducing porosity in the lower fluvial channel. During periods of slack water, illite laminae formed which later caused formation of microstylolite seams. Sandstones adjacent to these laminae contained illite which promoted pressure solution that reduced or eliminated intergranular porosity.

Pressure solution along microstylolites and between quartz grains in the illitic areas yielded much silica in solution. This may have been the source of the relatively high quartz cement in the B member of the channel facies although other sources cannot be ruled out.

The porosity and permeability of the fluvial channel sandstone are particularly variable for a number of reasons. Fluctuation in stream flow resulted in marked differences in sorting and in the distribution of illite which aided porosity preservation in some places, but promoted

pressure solution in other places. Erratic distribution of calcite near the overlying Greenbrier Limestone contributed to diagenetic heterogeneity. Lack of coatings in the lower fluvial channel sandstone resulted in quartz cementation and low porosity and permeability.

Core analyses and geophysical log data indicate that the best porosity and permeability in Granny Creek field occur more consistently in the proximal mouth-bar facies of the Big Injun. Well-sorted, fine- to very fine-grained, high quartz sand was deposited in this interval. The main factor in porosity preservation was the development of well-formed chlorite coatings. These restricted quartz cementation, unlike the heavily cemented, uncoated sandstone above. Chlorite flakes in the coatings are loosely packed so the coatings have a microporosity of perhaps 75%-90%. Thus, the overall porosity is little reduced by the coatings, and they are not thick enough to seriously reduce pore throat size in this interval, ensuring that good permeability was maintained.

The origin of the chlorite coatings is important because of their role in porosity preservation, but unfortunately their origin is difficult to determine. Feldspars do not seem to be the local source because their alteration occurred after chlorite formation. Volcanic materials would be a good source but only in a few samples is there any hint of a volcanic contribution. The fact that the boundary between the coated and uncoated zones seems to follow stratigraphic layers suggests more of a control by sedimentary conditions. Studies in other areas (Fuchbauer, 1974) have led to the idea that mixing of fresh and saline waters produces conditions favorable for later diagenetic development of chlorite. A certain amount of mixing of fresh and saline waters would have been expected in the environment where the distributary mouth bar formed in Granny Creek field whereas predominantly fresh water would be involved in the development of the overlying fluvial channel sandstone. This could have accounted for the observed differences in distribution of chlorite coatings.

Although some of the distal mouth-bar facies is a suitable reservoir sandstone, much of it is unsatisfactory for a number of reasons. Some of the sandstone has an above average content of argillaceous ductile grains which compacted and were squeezed into adjacent pores, thereby reducing porosity and permeability. Some of the sandstone is very fine grained, with corresponding small throat cross sections, so coatings of normal thickness block the pore throats, leading to very low permeability, even though porosity (including microporosity in the coatings) is still high. In other cases the sandstones are not unusually fine, but the coatings are thicker so that throats are blocked with attending loss of permeability. In addition, several percent siderite occurs as a pore filling in this facies. Commonly a combination of these factors came into play to lower porosity to some extent and drastically reduce permeability.

In all of the sandstone units secondary porosity generally ranging from 1-5%, has resulted from partial to complete dissolution of both K-feldspar and plagioclase. In most cases the resulting voids are connected to the pore system so that effective porosity is increased.

Calcite patches occur erratically in the Big Injun and are generally spaced far enough apart that they do not greatly reduce permeability but do reduce porosity to a small extent. Taken together, the intertonguing of basal sandstone and shale beds, the presence of illite coating, and the distribution of calcite and siderite have created barriers to fluid flow within the reservoir.

An example of important relationships between petrophysical features is given in Table 2 for the core from well 1126. The facies of the Big Injun sandstone referred to in Table 2 for

well 1126 are equivalent to the depositional environment shown in Figure 71. Figure 71 indicates the textures and sedimentary structures recognized in the core for the various stratigraphic units of the Big Injun sandstone, and compares them with porosity and permeability values.

It is apparent that diagenesis played an especially important role in contributing to the heterogeneity of the Big Injun reservoir in Granny Creek field, particularly in terms of porosity and permeability. Original sedimentary conditions, in some way, apparently set the stage for later diagenetic variations in porosity and permeability. This emphasizes the importance of considering the environment of deposition in prospecting for favorable porosity trends.

Heterogeneity in Gamma-Ray Response

A suite of 279, digitized gamma-ray logs was selected from Granny Creek field and all possible cross-correlations between well logs were performed by computer. Each correlation was "scored" by recording the value of correlation coefficient, r , (where $r = 1$ indicates a perfect correlation and $r = 0$ indicates no correlation) associated with the correlation. All correlation coefficients were then collected into a correlation matrix. This exercise was repeated for the entire Big Injun sandstone, the coarse-grained Big Injun, the fine-grained Big Injun, and the Squaw sandstone.

In an attempt to represent the results of correlation analysis over the entire Granny Creek field, a series of "spider" plots (Poelchau, 1987) was created and examined for each correlated stratigraphic interval. Poelchau's spider plots show the geographic distribution and "quality" of well-to-well correlations as a pair of vectors, with length proportional to the correlation coefficient, between each pair of correlated wells. The numbers of poor ($r < 0.80$) correlations at each well were extracted from the spider plots and used to produce Figure 72a and 72b. Figure 72a displays the locations of poor well-to-well correlations for wells 656 feet (200 meters) or closer to each other. Examination of Figure 72a shows a few poor correlations centered in the north-central and south-central portions of the field. Figure 72b displays poor correlation locations for wells 3280 feet (1000 meters) or closer to each other. In this figure, the numbers of poor correlations have increased dramatically but essentially have remained centered around the two areas observed in Figure 72a.

These two figures represent "near"- and "far"-neighborhood well correlations and indicate that for correlation of gamma-ray logs of the entire Big Injun interval, closer wells correlate better than distant wells. Examination of directional correlograms (Figure 73) of correlation coefficient versus distance between wells, shows that beyond a distance of 6500' (2000 meters) correlation of gamma-ray logs may be difficult because computed correlation coefficients begin to fall sharply. Furthermore, in certain portions of Granny Creek field (north-central and south-central), difficulty may be encountered even in correlating wells spaced 600' or closer. Similar results were obtained during separate analysis of the coarse- and fine-grained members of the Big Injun in Granny Creek. Interestingly, correlation analysis for the Squaw sandstone in Granny Creek showed proportionally more poor correlations than the Big Injun between both near and distant wells, with poor correlations distributed fairly uniformly throughout the field (strongest concentration in the extreme north end of the field).

Geographically localized, poor correlation of gamma-ray logs in Granny Creek may be due to heterogeneity in the gamma-ray response of the Big Injun throughout the field. It has been discovered, however, that a relatively large proportion (30% to 70% depending on maximum distance between correlated wells) of poorly correlated gamma-ray logs are associated with a single geophysical logging company. This company was active throughout the field, and research is currently underway to differentiate between the sedimentological (inter-well scale heterogeneity) and the logging company components of poor gamma-ray correlations in Granny Creek.

Porosity and Permeability

Geographic Distribution. Porosity of the Pocono Big Injun was determined from core analyses and from density logs. The members, tongues, and subfacies of the Big Injun sandstone have been shown in a stratigraphic cross section along profile GB-GB' (Figure 67). Porosity determined from either log density or analyses of cores has been grouped in categories of 5 percent and superimposed on the stratigraphy previously depicted (Figure 74). Within the fine-grained C member, the highest porosity occurs in the marine-influenced proximal bar, and the lowest porosity in the distal mouth-bar subfacies as well as the imbricated margins between the tongues of C1, C2, and C3. In the coarse-grained sandstones and conglomerates of the B and A members, log porosities are erratic, although generally poorer in the B member.

Permeability facies (Figure 75) from core analyses also have been superimposed on the same stratigraphic cross section (GB-GB') as shown previously in Figures 67 and 73. In general, the permeability facies correspond to the porosity values; low porosity-low permeability, high porosity-high permeability. The porosity and permeability facies can be related to the depositional environments in a predictable manner. Although diagenesis has modified the original porosity and permeability of the sandstone deposits, its changes are influenced by the characteristics associated with the subfacies and their depositional environments. Importantly, the diagenetic facies can be correlated between wells in the field. For example, the increased secondary quartz cement associated with the B member of the coarse-grained fluvial channel fill created a laterally persistent layer above the C and below the A members (Figure 76).

An investigation of well-to-well porosity was undertaken in one of several waterflood injection areas in Granny Creek field (see Figure 77). Gamma-ray logs for fifteen wells in and around the waterflood area were cross-correlated by a computer program written for the project using algorithms from Davis (1973). Density logs for each well were converted to porosity values and a series of porosity-depth cross-sections were generated for each of the section lines shown in Figure 77.

In this preliminary stage, modeling for each cross-section was done using simple, distance-weighted gridding techniques. Figures 78a and 78b show examples of porosity cross-sections for the waterflood area. Lines of section and the associated cross-sections were chosen to produce an intersecting network of subsurface porosity information for the waterflood area. Examination of cross-sections indicates that the Big Injun interval in the waterflood area is uniformly underlain by an extremely low porosity interval (< 5% log porosity) within the shale separating the Big Injun and Squaw sandstones. The second feature common to all cross-sections is an interval of sharply decreasing porosity associated with the Big Injun coarse-fine

boundary.

Production and injection in the waterflood area are restricted to the fine-grained Big Injun. Heterogeneity in well-to-well porosity is observed in the cross-sections of the fine-grained Big Injun as several zones of relatively high and low porosity--both isolated and apparently connected high and low porosity zones are suggested. These zones may be 2' to 10' in thickness and may occur in only a single well or connect several wells. Figure 79 is a subsurface porosity map based on the porosity cross-sections for the waterflood area that illustrates both isolated and connected porosity at a single stratigraphic horizon (50% of the Big Injun fine-grained interval).

The most porous and permeable interval corresponds to the proximal mouth-bar subfacies of the C member, which is sandwiched between the relatively impermeable lower distal mouth-bar subfacies of the C member and the overlying tightly cemented B member. The marine-influenced proximal bar subfacies is considered to be the primary pay zone, whereas the cemented B member may serve as a seal.

Statistical analysis of the porosity-permeability relationships in the various subfacies seems to substantiate these conclusions based on stratigraphic and petrographic analyses.

In the stratigraphic phase of this study, the gamma-ray log was used to divide the Big Injun into three units: the A, B, and C. Further examination of cores indicated that A and B comprise an upper, coarser-grained lithofacies whereas C represents a lower finer-grained facies. Log data from cored wells were used to select clean sandstone intervals A, B, and C. The zone selection criteria were based on the density porosity value of 2.6 as the cut-off for the clean sandstone selection. Average permeability and porosity values from cored wells and log analyses were used to plot the iso-porosity and iso-permeability variations for zones A, B, and C within the Big Injun Formation. Plots prepared from the core analysis based on 21 wells are shown in Figures 80, 81, and 82 for permeability variations at 5 mD intervals and in Figures 83, 84, and 85 for porosity variations at 2% intervals. The iso-porosity and iso-permeability plots for zones A and B indicated zero permeability and porosity on the eastern boundary with a northeast-southwest trend. A similar change was not observed for the C zone.

These maps also show that using porosity and permeability in reservoir modeling will require inference from geophysical logs. Porosity can be computed from available density logs, but estimation of permeability requires a more extensive suite of logs, or establishment of empirical relationships. The next section reports observed relations between porosity and permeability by stratigraphic unit within the Big Injun, and by depositional environment.

Estimating Permeability from Porosity. Porosity values were determined from density log readings at each well, whereas induction logs were used for water saturation determinations. The average values of porosity and water saturation from the initial study are listed in Table 3. Separate porosity-permeability correlations were prepared for each zone. The selection of three zones and the elimination of points outside the tool range resulted in a fewer number of data points for the correlation of each zone. The permeability-porosity correlation from well number 735 from Granny Creek field, is shown in Figure 86. Similar correlations also are presented for the same well after separating the data for zones A, B, and C (Figures 87, 88, and 89).

Permeability measurements were performed on plugs cut from cores taken in wells 1110, 1133, and 1134 (Table 4). Permeability values measured in a vertical direction showed smaller values than permeability values measured in the horizontal direction.

Additional wells were selected for log analysis, and digitized log data for these wells were obtained from West Virginia Geologic and Economic Survey. Based on the zone information received from the Department of Geology, log analyses were conducted for intervals A, B, C1, C2, and C3 within the Big Injun. The average porosity and water saturation values determined from log analyses are shown in Table 5. Core versus log porosity cross-plots prepared for the B, C3, and C2 units of the Big Injun are shown in Figures 90, 91, and 92 for well permit number 1109 at Granny Creek. The data points on Figures 90, 91, and 92 indicated some grouping for zones B, C2, and C3. However, the data points on Figure 92 for zone C3 showed a more scattered pattern when compared with zones B and C2, that may indicate an increased heterogeneity. A more detailed study to develop the correlation between porosity, permeability, water saturation, pore type, and depositional environment is currently being pursued by the research team.

Sedimentary facies were partitioned among four depositional environments for further statistical analysis: minor bed load channels; fluviially influenced proximal mouth bar; marine-influenced proximal mouth bar; and distal mouth bar. Plotting porosity and permeability (Figure 93) shows that these two parameters are linearly related for each of the depositional environments. An analysis of covariance with porosity and depositional environment as independent variables, and permeability as the dependent variables was highly significant; both porosity and environment were significant contributors.

Simple linear regression was used to fit the model:

$$\text{permeability} = A \times \text{porosity} + B \text{ for each depositional environment.}$$

The results were:

	A	B	r ²	F	Prob > F
Minor Bed Load Channels	.136	-1.379	.47	25.7	0.0001
Distal Mouth Bar	.172	-3.133	.52	28.0	0.0001
Marine-influenced Proximal Mouth Bar	.111	-1.525	.22	4.88	0.0413

The fluviially influenced proximal mouth-bar environment was not represented by enough samples for analysis.

Network Modeling. To improve oil recovery from a reservoir, it is necessary to develop a better understanding of fluid flow in porous media. The most critical parameter that influences fluid flow in a porous media is permeability. Therefore, it is necessary to develop a relationship between the structure of porous media (on a microscopic level) and permeability (which is a macroscopic coefficient). Then one is in a position to relate changes in the microstructure to changes at the macroscopic level.

The complexity of porous rock makes an exact model of it impossible. Previous studies have revealed that porous rock often exhibits a network of large pores that are

connected through long, narrow passageways called ostioles. In this phase of the study, a network model has been developed to study and describe permeability reduction (formation damage) resulting from particle entrapment in porous media by size exclusion.

The work in Textural Transforms has led to the development of pore networks with three-, four-, five- and six-fold coordination numbers. This work originally was done as a prelude to the use of numerical methods to evaluate the behavior of said textural transforms. Serendipity has led to a possibility that this textural transform structural regularization of the pore structure, i.e. representing porous media by a regularized array of interconnected pores, will lead to closed form solutions.

Working with the simplest of these textural transform structural regularization, the structure with a coordination number of three, appears to be amenable to analysis. The regularized structure of the pores means that the pores are in a regular array in three space. One can treat the pores in one level as a sheet of pores wherein each pore in the sheet is connected to one or more pores in the sheet above by ostioles and to one or more pores in the sheet below by ostioles. This means that the flow in and out of the individual pores in the sheet can be treated as an independent event. For a given sheet the flow of fluid can be treated as the sum of flow to the individual pores within the sheet.

Once the flow to and from one sheet is developed, then the flow from one sheet to the next can be developed. From this the flow through a block of sheets can be used to simulate flow through porous media. This means, at least in theory, that it may be possible to treat in closed form, porous media with millions of pores. While this is an optimistic approach, there are many areas where this approach could fail. However, because of its promise, the sheet approach is being pursued.

These studies using a simple, regularized model, have led to the conclusion that flow is sensitive to the presence of small-diameter ostioles (pore connections). Moreover, flow through a reservoir seldom is straight; rather it follows a complex path. Therefore, tortuous flow from pore to pore via small-diameter ostioles is easily blocked if the fluid carries any type of small particles or emulsions whose diameter exceeds that of the pore throats.

Heterogeneity Related to Oil Production

The main intent of this section is to consider the relationship of primary oil production in Granny Creek field to stratigraphic characteristics. Two types of primary oil production are displayed on maps to show heterogeneity of the Granny Creek reservoir in the Pocono Big Injun sandstone: 1) initial oil production (Figure 4); and 2) 10-year cumulative oil production (Figure 5). At this time, rock pressure and well treatment data have not been collected, and a quantitative comparison of primary and secondary oil production has not been made. However, production data clearly associated with primary production show trends that suggest a combined influence of stratigraphy and sedimentation, diagenesis and structure.

Secondary (waterflooding) oil production in Granny Creek field, on the other hand, has occurred for many years and two five-spot areas (Figure 7) have been analyzed. In preliminary findings, secondary oil production seems to be strongly influenced by structural

controls activated by over-stimulation of wells during hydrofrac treatment.

Initial oil production for Granny Creek field is shown in Figure 4. Pods of relatively high initial oil production (IOP) appear to align in a northwest direction in the northern 60 percent of the field approximately parallel to the pre-Greenbrier unconformity.

Preliminary analysis indicates that a positive correlation exists between high initial oil potential and those areas where the upper distal and marine-influenced proximal mouth-bar subfacies of the C member "pinch out" against the base of the B member and where the C member is capped by at least a few feet of the relatively impermeable B member (diagenetic facies). These stratigraphic relationships are compared with initial oil production on two different cross sections. P1-P1' (Figure 94) oriented SW-NE across the field nearly normal to the erosional margin of the coarse-grained B member (possible seal) of the Big Injun; and P4-P4' (Figure 95) oriented parallel and near this same erosional margin where the upper part of the Big Injun reservoir is truncated by the pre-Greenbrier unconformity. The cross sections show the relationship of Big Injun members and tongues to the unconformity. Initial oil production, in barrels per day, is plotted above the cross sections as smooth curves along profiles that traverse areas of both low and high values. The smooth curves were established mostly from wells used in the cross sections, but were supplemented by projecting values from nearby wells (moving average) into the lines of section. Mouth-bar subfacies of the C member are shown in Figure 94 but not in Figure 96. However, subfacies along profile P4-P4' probably occur approximately like their distribution in Figures 67 and 94.

Some important relationships displayed in Figures 94 and 95 are summarized in Table 5. Initial oil production averages about 46 barrels per day where the marine proximal river-mouth-bar subfacies is thick and pinches out against the overlying well-cemented, coarse-grained B member (possible seal). Where the marine proximal river-mouth bar is thick but is some distance from its pinch out against the B member, the average initial oil production drops to about 24 barrels per day. Relatively low initial oil production (11 to 15 barrels per day) occurs where: 1) the permeable/porous marine proximal mouth-bar subfacies is thin near its pinch out; 2) the mouth-bar subfacies changes from marine to fluvial dominated and is less porous and permeable, although it pinches out against the B member; and 3) the B member is absent and presumably the oil may have leaked out (one needs rock pressure data to verify this interpretation).

Where the A and B members are absent and the Big Lime (Greenbrier Limestone) directly overlies the C member, oil possibly was lost into the "thief" Big Lime during lateral migration, or was blocked by a postulated gas cap prior to the Allegheny orogeny for these wells northeastward of the eroded B member (possible seal), or some other cause. Apparently, the B member does not need to be very thick to serve as a possible seal, according to this preliminary hypothesis.

Cross section P4-P4' is constructed NW-SE through the generally high initial oil production trend in the "pinch-out" belt affected by the pre-Greenbrier unconformity. The cross section also shows wells with relatively low initial oil production along this trend, suggesting compartments within the oil reservoir. The zero isopach contour for the B member indicates "embayments" oriented southwestward for approximately 2000 feet, and these areas of thin to absent B member occur where the low initial oil production wells are located. These localized southwest trends probably developed where ancient rivers eroded

and reduced the thickness of the possible seal above the pay zone in the C member of the Big Injun. The interpreted southwest trend of paleoflow of ancient rivers is based on thickness maps of these members, and portends emergence of the West Virginia dome (or Pocono dome, Donaldson and Shumaker, 1981), which apparently influenced the erosional patterns of the pre-Greenbrier unconformity for this combination oil trap. Compartments of oil production, therefore, can be attributed to the occurrence of high permeability/porosity facies (marine-dominant proximal mouth-bar subfacies) of different C member tongues capped by a less permeable B member, which exhibits discontinuities because of either the pattern of pre-Greenbrier erosion near the "pinch-out" margin, or because of facies changes as a result of diagenetic conditions. These examples suggest that there are stratigraphic controls on heterogeneity within the reservoir in Granny Creek field.

Density and Shale Barriers. Density barriers were interpreted from bulk density logs at intervals where the log shows a relatively higher density (an abrupt change in slope). High-density zones without a corresponding high gamma-ray kick probably result from cementation (Figure 96). Where a high gamma-ray kick and high bulk density occur at the same interval, this zone is interpreted as a shale (Figure 97).

Shale in the fine-grained sandstone creates interfingering of lithofacies which cause pinchout of porosity at the bottom of the reservoir (Figure 98). This causes the contact at the bottom of the reservoir to be "ragged", whereas the upper portion of the fine-grained sandstone may be in communication. The shales and siltstones form north-south linear belts in the eastern and western portion of the field (Figure 99).

The upper, coarse-grained sandstone within the Big Injun includes zero to three density barriers. Core and thin-section analysis from wells with one density barrier in the coarse-grained sandstone suggests this density barrier is due to an increase in quartz cement and a decrease in porosity. Cores and thin section analysis show that high density zones in the fine-grained sandstone are associated with an increase in calcite and siderite cement and a decrease in porosity.

To determine the lateral extent of the density barriers in the fine-grained sandstone all wells with a density barrier interpreted from bulk density logs were marked on a map of Granny Creek. This map shows that density barriers range in size from less than 400' to \approx 2500', and may be circular, linear, or irregular in plan view (Figure 100). Some wells may contain up to three density barriers. In the fine-grained sandstone, these high bulk density zones form horizontal, inclined, and irregular pods of impermeable sandstone (Figure 98). At a 400' well spacing, pods may be confined to a single well or encompass as many as 25 wells creating linear and irregular barriers to migration. These pods increase the length of fluid flow path and may divide the reservoir into discrete compartments.

The distribution of these "diagenetic density breaks" in two stratigraphic cross sections (P1-P1', Figure 101 and P2-P2', Figure 102) indicates further compartmentalization of the reservoir and isolated areas that correlate well with initial oil production and cumulative oil production. High initial oil production appears to occur within the proximal subfacies where it is bounded by relatively impermeable, thin intervals separating tongues of the C member; the "diagenetic high density zone"; and the B member (possible seal) capping the high permeability pod. The combination of a permeable subfacies enclosed by lower

permeability barriers in the vicinity of the "pinch out" zone of the B member shows a positive correlation with both initial oil production and cumulative oil production. Rock pressure data across these compartments or cells is presently unavailable, yet critical for substantiation of this hypothesis.

Elongate pods of high initial oil production at least one mile wide, aligned in a belt parallel to the northwest-southeast trend of the B member pinch-out margin, suggest stratigraphic controls on reservoir heterogeneity associated with the pre-Greenbrier unconformity. This mile-wide belt also has a grid-like pattern of oil production that suggests compartments, which probably reflect the influence of basement structures of the West Virginia dome on erosion of the Big Injun. The truncations influenced the configuration of the pay zone and possible seal facies. The proximal mouth-bar subfacies, which contain the thickest high porosity/high permeability intervals within the various westward prograding tongues of the C member, strike approximately north to northeast in the field. In the southern part of the field, where the B member has not been eliminated by erosional or diagenetic conditions, initial and cumulative oil production mainly follows the trend of the fold axis. More numerical spatial analyses are necessary in that area to determine whether depositional patterns represent a subordinate influence on the compartmental distribution of both initial and cumulative oil production.

In the section of this report dealing with the structural interpretations, the northern part of the field was described as occurring on a sub-block, which was tilted sufficiently during Early Mississippian time to initiate erosion that developed the pre-Greenbrier unconformity. It is the relationship of the pay zone to the possible sealing facies that has influenced oil production so greatly in this part of the field. Minor detached folds combined with stratigraphic heterogeneity have created compartments of permeability resulting in definitive patterns of initial and cumulative oil production in the northern sub-block. The sub-block in the southern part of the field provides evidence for less influence from the pre-Greenbrier unconformity and detached folds, and consequently, lower yields of oil production in that part of the field.

INTERWELL HETEROGENEITY

VSP OBSERVATIONS

Three VSP's were run in the CNR's Parker no. 21981 well (Figure 103). Source locations for each VSP included one near-well offset, 390 ft to the southwest (S52W) of the well, and two long offsets, one at 1395 ft southwest (S82W) of the well, and a third 1600 ft to the northeast (N48.5E) of the well. Displays of the 1395 ft offset and the 1600 ft offset are shown in Figures 104 and 105, respectively. The displays were prepared after normal moveout correction and waveshape deconvolution of the upgoing waves. Contour lines crossing the data represents lines of constant reflection point offset from the well. A vertical fault for instance would actually lie along one of these contours. On the other hand, a vertical line on these displays would represent a feature that dips into the northwest or southwest quadrants on the west offset, and a feature dipping into the north or east quadrants for the northeast offset. Migration eliminates this distortion but introduces additional ones including frequency reduction and smearing.

Near vertical interruptions of reflection patterns are observed in the 1395 and 1600 ft offset VSP's. These features are of interest because of their proximity to the small time structure in this area (Figure 59) and because of the indications of possible structural disruption observed in the reprocessed version of the data (Figure 64). These features are located on a detailed map of the area surrounding the VSP. Thief zones encountered in this area during waterflooding mentioned above lend additional weight to a possible fault/fracture zone origin for these features, and to an association of faults and fracture zones with the small scale folds observed elsewhere along this and other lines throughout the field.

Because disruptions of reflection events are enhanced if they dip away from the borehole toward the location of the source, the VSP's to the northeast and west reveal the presence of disruptions dipping in both directions away from the well. Calculated dips indicate that in most cases these features have dips that are less than 12 degrees from the vertical. Their significance will have to be examined more carefully in the coming year, but their presence on a small fold, in an area marked by well communication problems, suggests they have tectonic origins.

The VSP projects onto the southeast-dipping flank of the small fold noted above near CMP 300. The moveout corrected reflection events in the VSP on the other hand appear to dip slightly to the west. An eastward dip, however, is confirmed by well-log-derived structure in this area (Figure 45). A low moveout-correction velocity could produce the anomalous reflector dip observed in the VSP. Moveout corrections were made assuming a flat velocity model, which will contribute error to the result since the layers are actually dipping.

FIELD DEVELOPMENT RECOMMENDATIONS

The seismic time-structural relationships to oil production within the Granny Creek field suggest the following exploration rationale.

1. Concentrate exploration efforts in major synclines: The traditional view that oil production in a field occurs within a synclinal reservoir is supported by the seismic evaluations. The tectonic development of a syncline and others like it is complicated and involves an interplay between basement and detached styles of deformation. These synclinal areas are identifiable on regional structure maps compiled from driller's log data (see Figure 28). Given the great number of wells and the long period of time during which exploration efforts have been conducted in the Plateau area of the central Appalachians, most of these structures have probably been identified.

2. Evaluate internal structures using Big Injun arrival time and Big Injun-to-Huron travelttime-difference data: Along the axis of the syncline, the reservoir is subdivided by low relief folds. These folds are interpreted to be detached above decollements in the Upper Devonian shale section. These folds are not readily visible using standard reflection arrival time contouring and isochroning. In the initial preparation of isotime and isochron maps these structures were missed entirely. Although in hindsight these structures can be observed on a standard seismic display, they are, in general, only about 4 milliseconds in relief, and are therefore difficult to see.

Identification can be aided simply by displaying the seismic data at an expanded time scale such as that shown for line 2 (Figure 63 and 64). Such a display could be requested from the processing contractor or generated in house. In the study, a computer was used to pick and store peak or trough arrival times for given reflection events. Trace-to-trace fluctuations were removed using a lowpass wavenumber domain filter. The filtered arrival times then were transferred into Lotus files for calculating and plotting shifted travelttime and travelttime difference plots.

In an exploration and development environment, data evaluation could be restricted to the identification of detailed structures in the expanded-time-scale Big Injun arrival-time plots and thickened areas in the Big Injun-to-Huron travelttime-distance plots. These plots are shown for lines 2 and 6 which cross through the heart of the field (Figures 106 and 107, respectively). Detached structures (marked D) are suspected to be the cause of thickening or increased time difference through the Big Injun-Huron interval, particularly if they correlate with structures in the Big Injun arrival-time plot.

Although there does not appear to be any relationship between the relief of these small folds and the amount of cumulative oil production across them, the folds are generally associated with local increases of oil production (Figures 106 and 107).

The coincidence of increased cumulative oil production with smaller folds structures within the syncline is not always as well defined as shown on lines 2 and 6. Line 3 (Figures 48 and 108) cuts across the southern part of the field. The syncline is clearly defined, and oil production is confined to it. Internal structures are not evident on the travelttime plot. Evidence for detachment is suggested by thickening and thinning of the Big Injun-to-Huron travelttime differences; however, a clear relationship with variations in cumulative production is lacking.

Line 4 (Figure 109) trends parallel to strike into the field from a structural high bounding the southern part of the field. The Big Injun-to-Huron interval thickens slightly

into the field, and is interrupted by smaller-scale fluctuations, which do, for the most part correlate with shoulders or peaks in the cumulative production data along the line.

For completeness, these recommendations also are compared along line 1 (Figure 110). Although the line lies along the eastern flank of the field, it swings down into the syncline and back out again across the marginally producing periphery of the field. The syncline and detached structures within it are defined by the two curves. The larger detached structure coincides with high cumulative production.

3. Identify interplay between detached and basement structures: As discussed above under **Field Scale Heterogeneity**, a basement fault (fault A) coincides with a subdivision of the field into more productive northern and less productive southern parts. Analysis of traveltimes and traveltime-difference data reveal the active role this fault (and also fault B) played during the Paleozoic development of the area.

Only one line (line 6) crosses the highly productive northern part of the field (Figure 51). Lines 2, 3 and 4 (Figure 106, 108 and 109) cross fault A, but do so along the western margin of the field where the flank of the syncline is relatively high. Based on the first recommendation above, we expect lower production in these areas, and production is, in fact, nearly absent. Along line 6, however, fault A lies roughly along the axis of the syncline. Traveltime differences between various intervals along line 6 suggest that the highly productive detached structure northwest of fault A is in part controlled by the basement fault (see **Intrafield heterogeneity Small-Scale Folds**). A continuous history of growth is recorded in the traveltime difference data, and the thickening of the Big Injun-to-Huron interval is greater than the structural relief of the fold at the level of the Big Injun, suggesting that thickening is in part related to syndepositional subsidence of fault A.

A detailed analysis of time differences is probably not possible within the time frame and economics of exploration and field development efforts. Nonetheless, from an exploration and development viewpoint, it is critical to locate and determine the distribution of basement faults within a field. Detached structures above basement faults within the low areas of a syncline may be the most highly productive areas of the reservoir.

4. Identify reflector disruptions (small time offsets and amplitude anomalies): Problem wells in a waterflood sweeping operation reduce recovery efficiency. Seismic data near problem wells in the Granny Creek field often reveal disruptions of seismic reflections from the reservoir and surrounding intervals. These disruptions are represented by small and abrupt reflection-time offsets, local amplitude reductions, and combinations of both.

Anomalous time offsets are often no greater than the sample rate (2ms), and could occur sporadically along a slightly dipping surface. Hence, their significance needs to be viewed cautiously during data interpretation. Abrupt reflection-time offsets can be ranked according to their interrelationships with other features in the seismic data. Small folds (see **Interfield Heterogeneity Small-Scale Folds**) are usually not considered significant unless their time relief spans at least two sample values, and unless they have wavelengths extending across several adjacent traces. The time offsets observed along the flanks of folds

may simply be related to sampling as noted above. However, the presence of amplitude anomalies associated with these small offsets suggests that changes of acoustic impedance also may be present and extend over distances of a few hundred feet.

If amplitude disruptions are not present, then this may imply one of two possibilities: 1) the time offsets are related only to sampling; or 2) fracturing of the interval is less pervasive, producing only minor changes in acoustic impedance. This may be the case for the thief zone identified in the vicinity of the VSP well. The VSP suggests that the interval may be faulted; however, the intensity of fracturing associated with these faults may be much less than those near midpoints 395 and 417.

Different approaches to processing also can affect reflection amplitude. Note that in the original processing of the data, significant changes in the amplitude of the positive cycle just above the "Big Injun" positive (Figure 63) are observed in the vicinity of the VSP well, whereas in the reprocessed data (Figure 64) these amplitude variations are absent. Hence, the effects of processing, as in other applications, should always be considered, and if possible two or three different approaches should be compared.

These observations indicate that during the integration of seismic interpretations for the purpose of locating of waterflood well locations, areas where amplitude anomalies, small folds, and abrupt offsets in reflection arrival time are all present should be given the highest probability of being associated with highly fractured areas which might serve as thief zones during waterflooding of the reservoir.

REFERENCES

- Ahmad, Mian, 1992, personal communication: Petroleum Engineer, Columbia Natural Resources, Charleston, WV.
- Beardsley, R. W., and D. S. Cable, 1983, Overview of the evolution of the Appalachian basin; *Northeastern Geology*, v. 5, pp. 137-145.
- Buurman, J., 1992, personal communication: Geologist, Columbia Natural Resources, Charleston, WV.
- Berkhout, A. J., 1977, Least squares inverse filtering and wavelet deconvolution: *Geophysics*, v. 42, pp. 1369-1383.
- Davies, J. C., 1973, *Statistics and Data Analysis in Geology*, John Wiley and Sons, New York, 550 p.
- Donaldson, Alan C., and Ray Boswell, 1990, Regional stratigraphy of Upper Devonian and Lower Mississippian sandstones of the Appalachians and their classification as hydrocarbon reservoirs using basin analysis: Twenty-first Annual Appalachian Petroleum Geology Symposium, West Virginia Geological Survey, pp. 10-21.
- _____ and R. C. Shumaker, 1981, Late Paleozoic molasse of the central Appalachians: in *Sedimentation and Tectonics*, edited by A.D. Meall, Geol. Assoc. of Canada, Spec. Paper no. 23, pp. 99-124.
- _____, R. Shumaker, C. Laughrey, K. Aminian, and M. Hohn, 1991, Measuring and predicting reservoir heterogeneity in complex deposystems; Annual Report for Fiscal Year 1991, DOE/BC/14657-7, U.S. Department of Energy.
- Dowell Schlumberger, 1986, Formation evaluation of the J. B. Casto 133 and J. B. Casto 134 wells; Dowell Schlumberger Formation Analysis Laboratory (report to Pennzoil), pp. 1-8,64-65,85-88.
- Fuchbauer, H., 1974, Diagenesis of fluvial sandstones, "Geologische Rundschau, v. 63, p. 404-925.
- Gas Research Institute, 1991, Devonian (Ohio) gas shales workshop; Workshop handout, Gas Research Institute, p. unnumbered, figs. 59.
- Heald, Milton T., and James B. Britton, 1992, May monthly report of D.O.E. Heterogeneity of Reservoir Project, WVU-Geology.

Heller, Paul L., Charles L. Angevine, and Nancy S. Winslow, 1988, Two-phase Stratigraphic model of foreland-basin sequences: *Geology*, v. 16, pp. 501- 504.

Hohn, M. E., 1992, written communication, Unpublished 10 year cumulative production map of the northern part of Granny Creek field.

_____, 1988, *Geostatistics and petroleum geology*, Van Nostrand Reinhold, New York, 264 p.

Kulander, B. R., S. L. Dean and R. E. Williams, 1980, Fracture trends in the Alleghany Plateau of West Virginia; West Virginia Geological and Economic Survey, map WV-11, scale 1:250,000.

Lemon, J., 1990, personal communication: Geophysicist, Columbia Natural Resources, Charleston, WV.

_____, 1992, personal communication: Geophysicist, Columbia Natural Resources, Charleston, WV.

Pittman, E.D., Larese, R.E. and Heald, M.T., 1992, Clay coats; occurrence and relevance to preservation of porosity in sandstones, *SEPM*, special publication no. 47, pp. 241-255.

Poelchau, H. S., 1987, Coherence mapping - an automated approach to display goodness-of-correlation between wells in a field, *Mathematical Geology*, v. 129, No. 8, pp. 833-850.

Ruley, E. E., 1970, "Big Injun" oil and gas production in north-central West Virginia: *American Association of Petroleum Geologists, Bull.*, v. 54, pp. 758-782.

Shumaker, R. C., 1980, The importance of regional and local structure to the Devonian shale gas production from the Appalachian basin: 26th International Congress, Fossil Fuels volume, Editions Technic, Paris France, pp. 147-174.

_____, 1986a, Structural development of paleozoic continental basins of eastern North America; Sixth International Conference on Basement Tectonics, proceedings vol., pp. 82-95.

_____, 1986b, The effect of basement structure on sedimentation and detached structural trends within the Appalachian basin: in the Lowrey Volume; *Studies in Appalachian Geology*, Virginia Polytechnical Institute and State University, Dept. of Geology, Blacksburg, VA., pp. 67-81.

- Ver Steeg, Karl, 1947, Black Hand sandstone and conglomerate in Ohio, Geological Society of America, Bulletin, v. 48, pp. 703-727.
- Wilson, T. H., and D. E. Swimm, 1987, 2D and 3D seismic studies of fractured Devonian shale reservoirs: West Virginia: Final Report (Gas Research Institute) Contract No. 5085-213-1146, NTIS Accession No. GRI-87/262 pp. 1-77.
- _____, 1990, Nonstationarity in seismic data: A VSP case study: in proceedings volume of the 58th annual international meeting of the Society of Exploration Geophysicists, pp. 1681-1686.
- _____, Li Zheng, G. He, and R. C. Shumaker, 1992, Seismic Studies in the Granny Creek oil field, West Virginia: A Annual Appalachian Petroleum Geology Symposium.
- _____, Li Zheng, G. He, R. C. Shumaker, J. Lemon, in prep., Sequential basin development and its influence on heterogeneity in a sandstone oil reservoir: A seismic evaluation.
- Zheng, L., and T. H. Wilson, 1991, Seismic evaluation of the Devonian Ohio Shale in the big Ugly Area, Southwestern West Virginia: Amer. Assoc. Petr. Geol. Bull. 11686.
- _____ and T. H. Wilson, 1992, Vibroseis deconvolution: A case study in the Granny Creek oil field, West Virginia: In proceedings volume of the International Meeting of the Society of Exploration Geophysicists, 4 p.
- _____, T. H. Wilson, G. He, and R. C. Shumaker, 1992, Seismic data reprocessing in the Granny Creek oil field, West Virginia: In the proceedings volume of the Twenty Third Annual Appalachian Petroleum Geology Symposium.
- Zou, X., T. H. Wilson, and A. Donaldson, 1991a, Analysis of some seismic expressions of Big Injun Sandstone and its adjacent intervals: In Abstracts and Program from the 22nd Annual Appalachian Geology Symposium.
- _____, T. H. Wilson, and A. Donaldson, 1991b, Analysis of some seismic expressions of Big Injun Sandstone and its adjacent intervals. Amer. Assoc. Petr. Geol. Bull. pp. 11691-11692.
- _____ and A. Donaldson, 1992, Regional Big Injun (Price/Pocono) subsurface stratigraphy of West Virginia: Twenty-third Annual Appalachian Petroleum Geology Symposium, West Virginia Geological Survey.
- _____ and A. Donaldson, 1992, Reservoir sedimentology of the Big Injun sandstone in Granny Creek field, West Virginia: Twenty-third annual Appalachian Petroleum Geology Symposium, West Virginia Geological Survey.

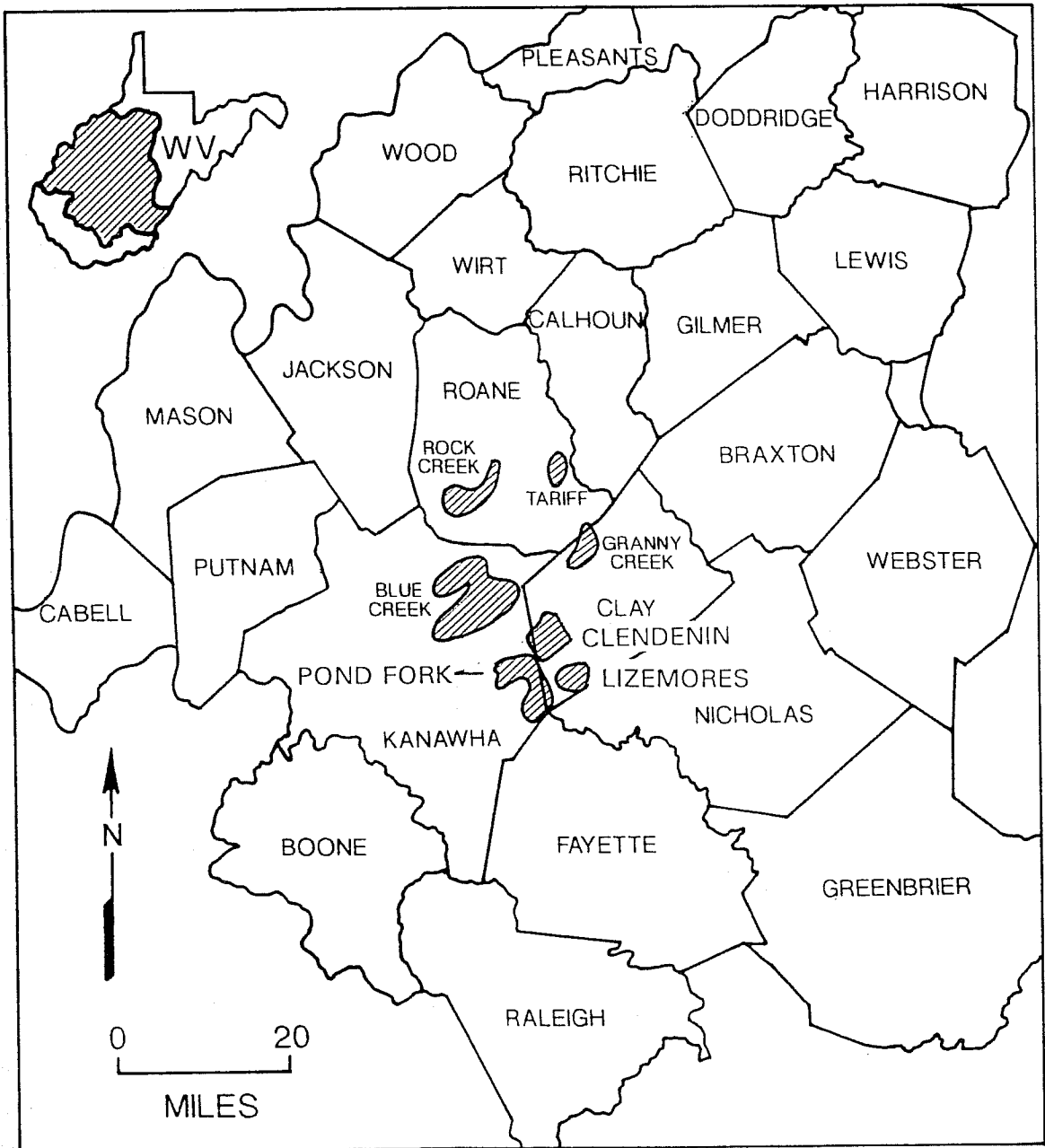


Figure 1. Location of Big Injun oil and gas fields studied in this project. The insert map shows the regional study area.

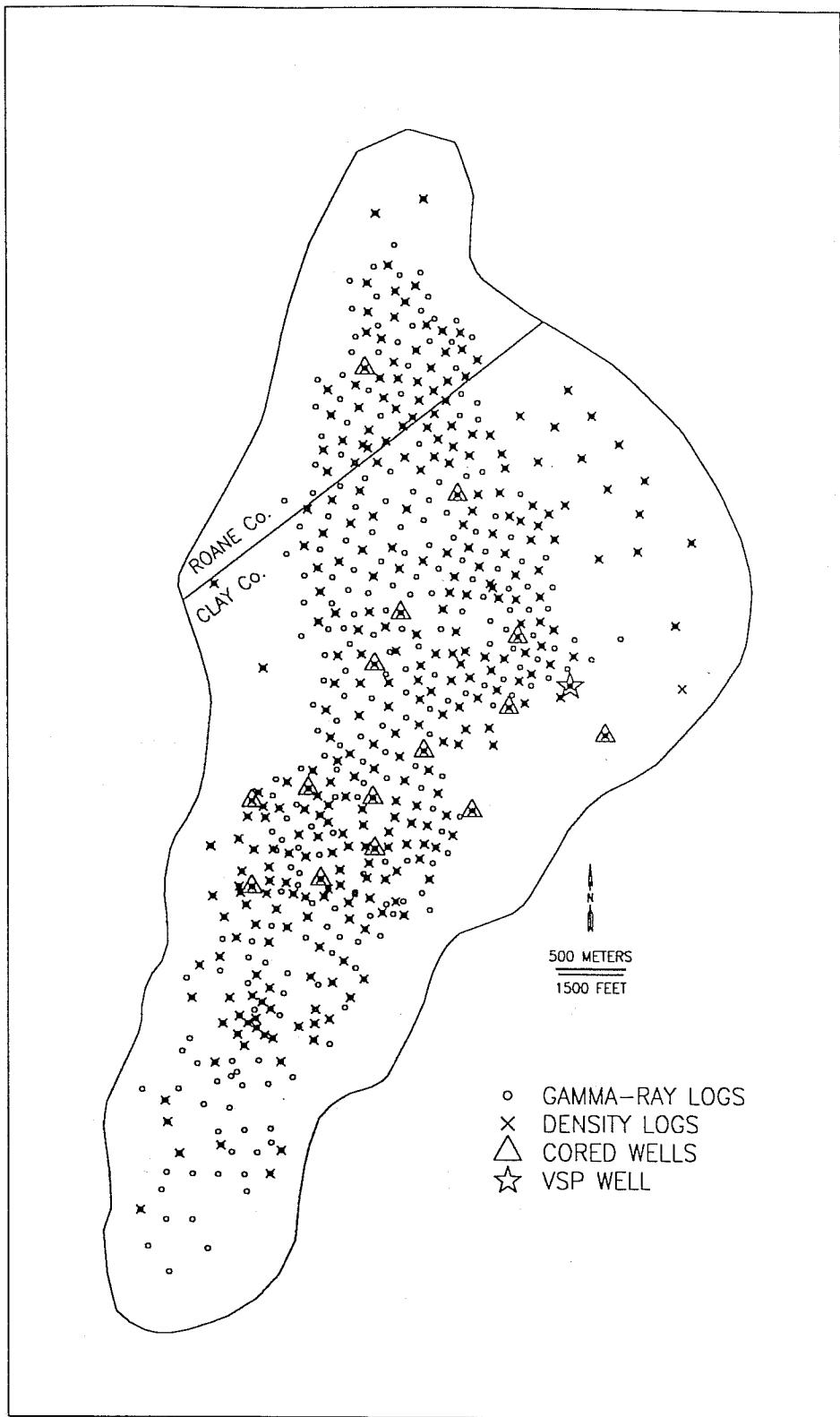


Figure 2. Control points and types of available data in Granny Creek field.

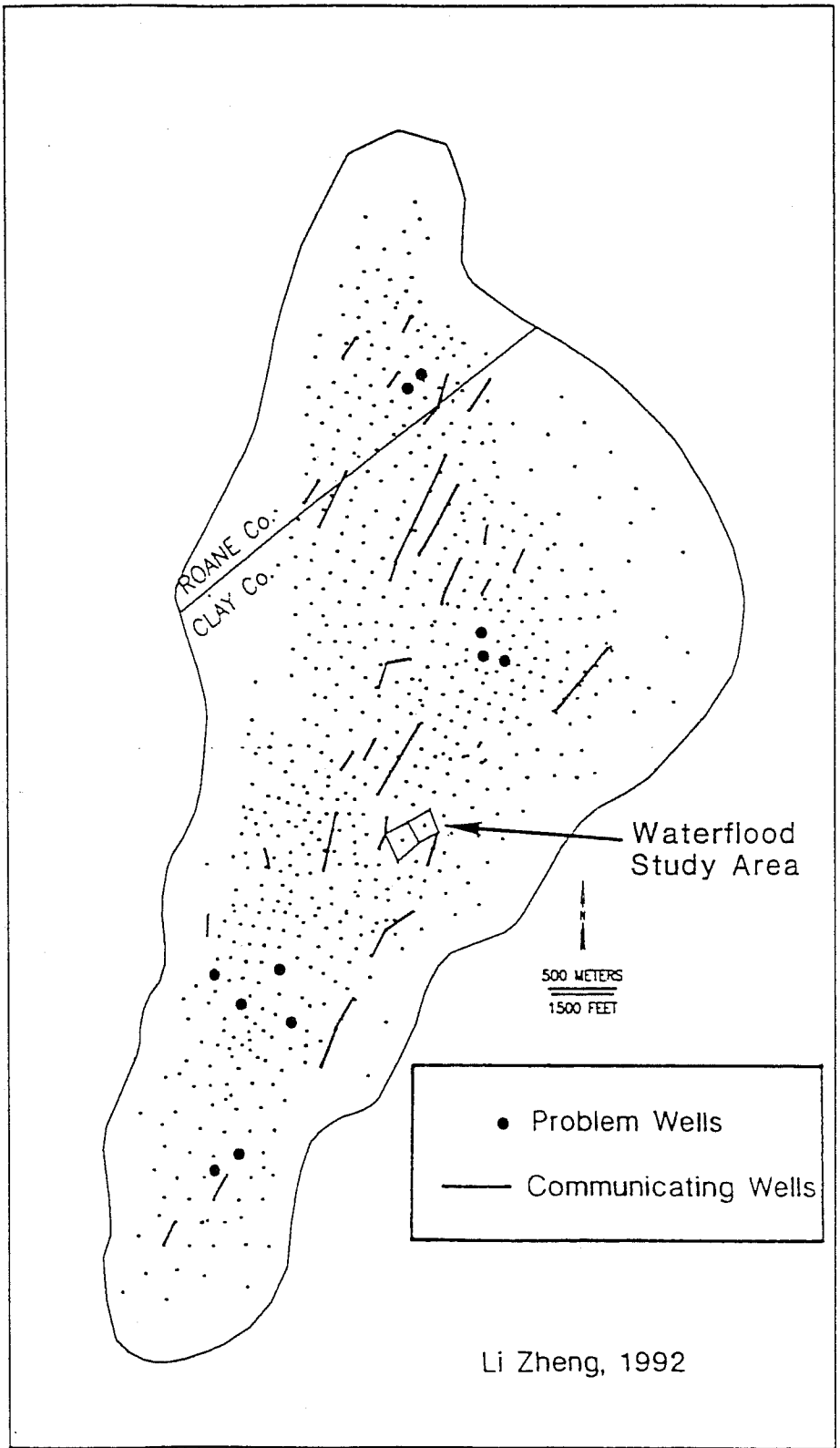


Figure 3. Solid lines join wells that are in communication in Granny Creek field.

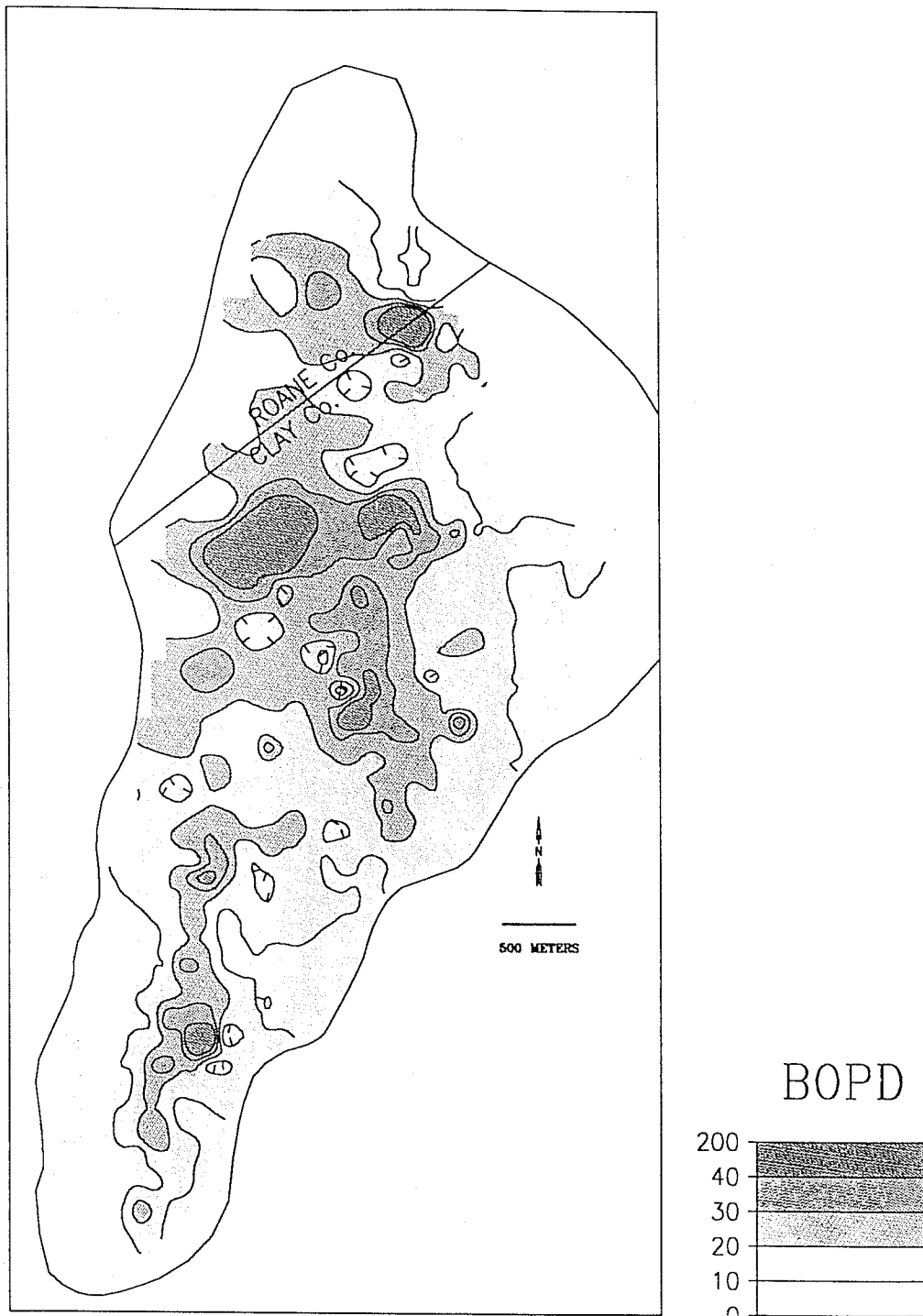


Figure 4. Map of initial open flows, Granny Creek field.

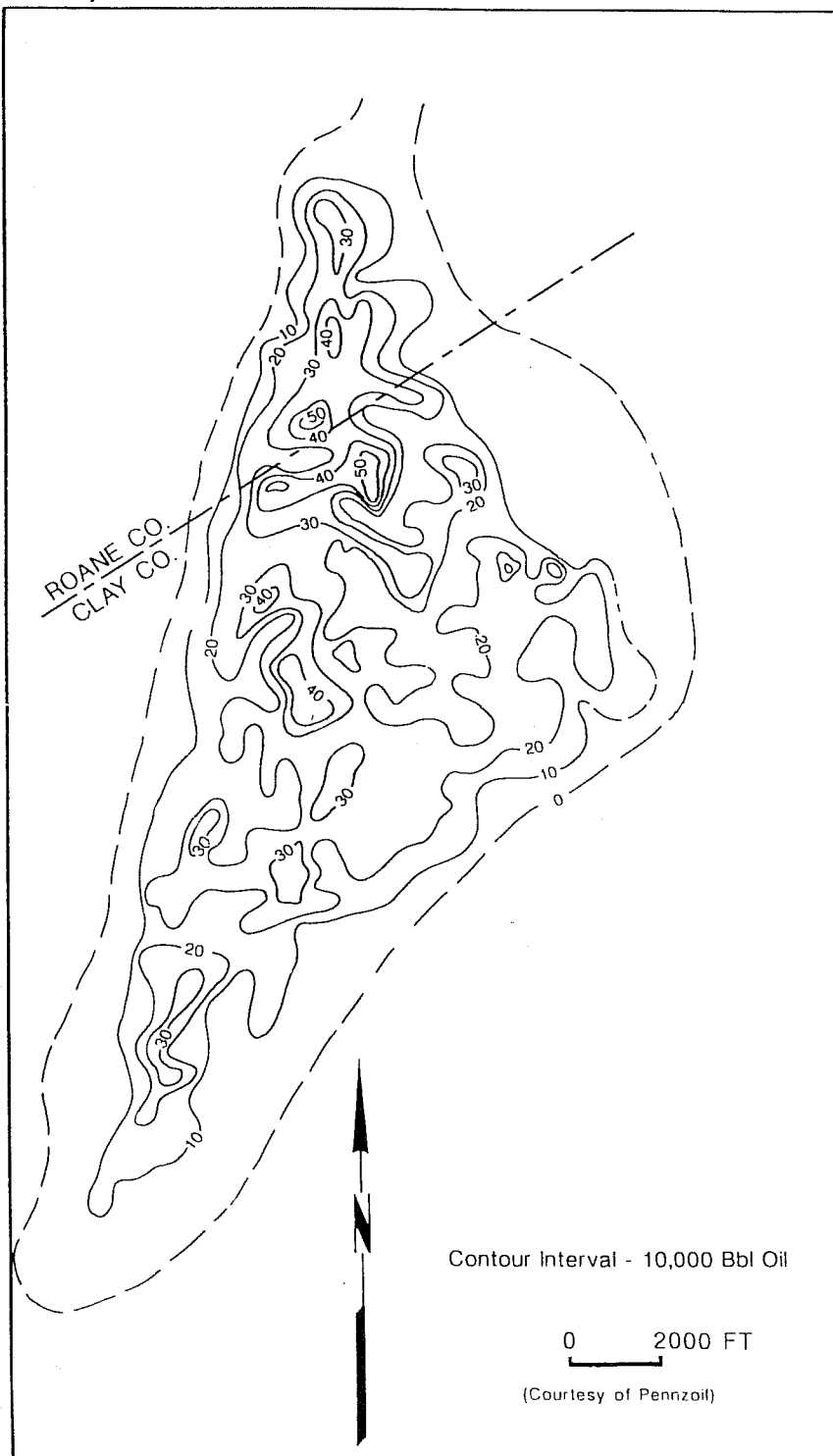


Figure 5. Map of cumulative oil production, Granny Creek field, during first 10 years of primary production.

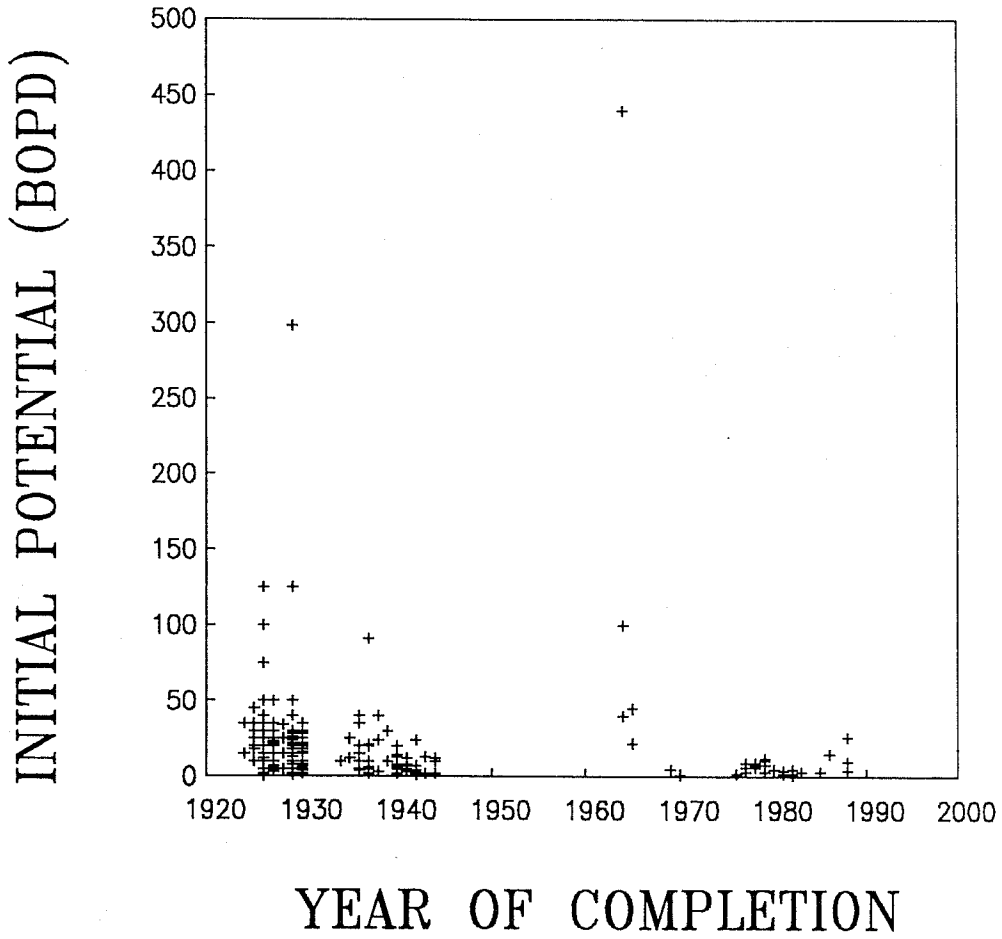


Figure 6. Initial Potential (IP) versus year of completion for producing Big Injun oil wells in Granny Creek field.

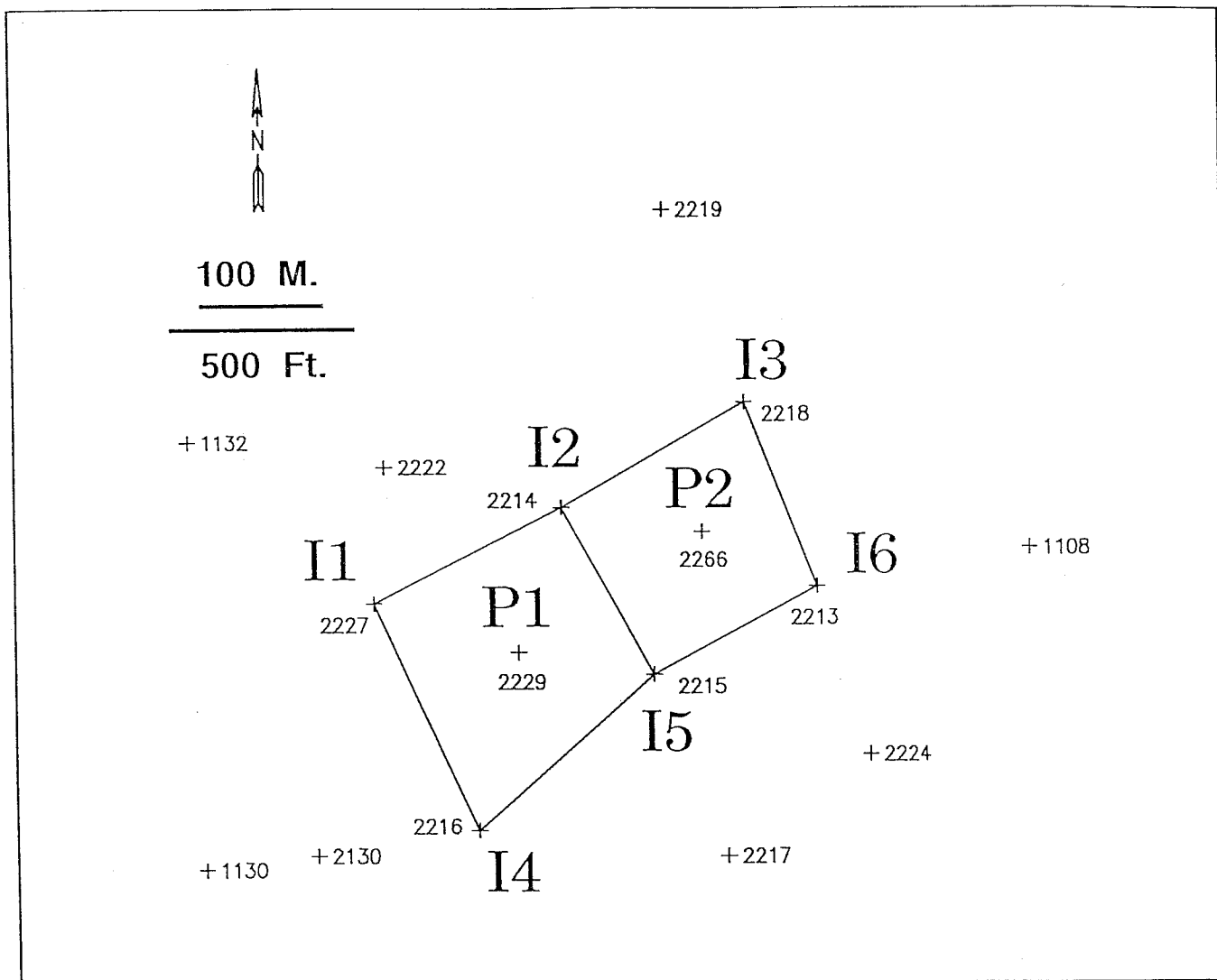


Figure 7. Location of five-spot patterns P1 and P2, Granny Creek field.

Granny Creek - Columbia Lease
5 Spot P1 (I - 1)

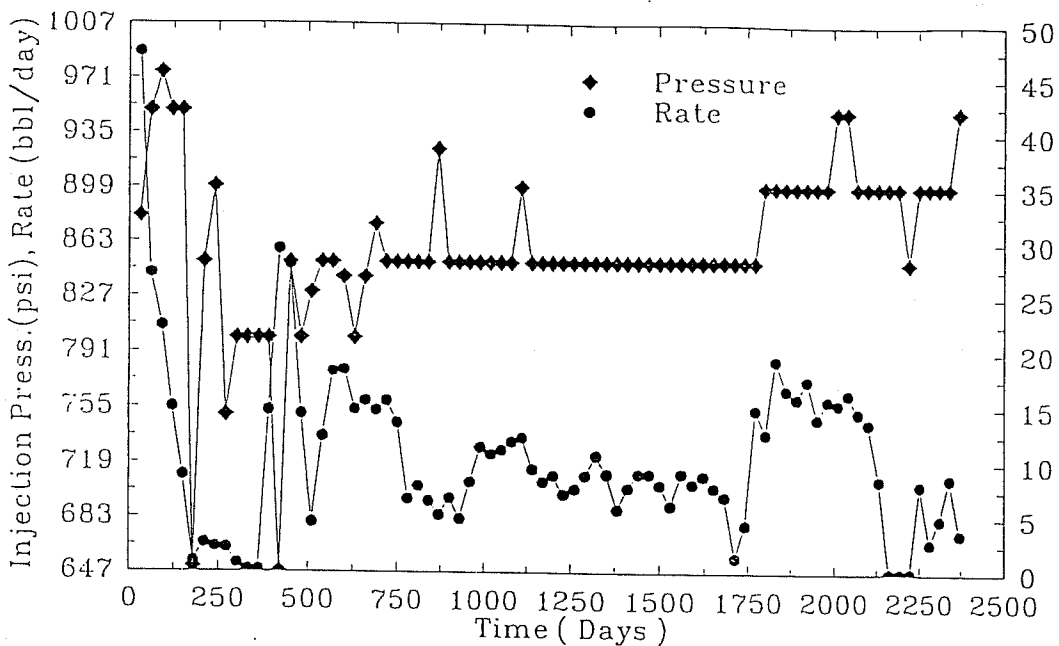


Figure 8. Water injection rate and injection pressure versus time for injection well I-1.

Granny Creek - Columbia Lease
5 Spot P2 (I - 2)

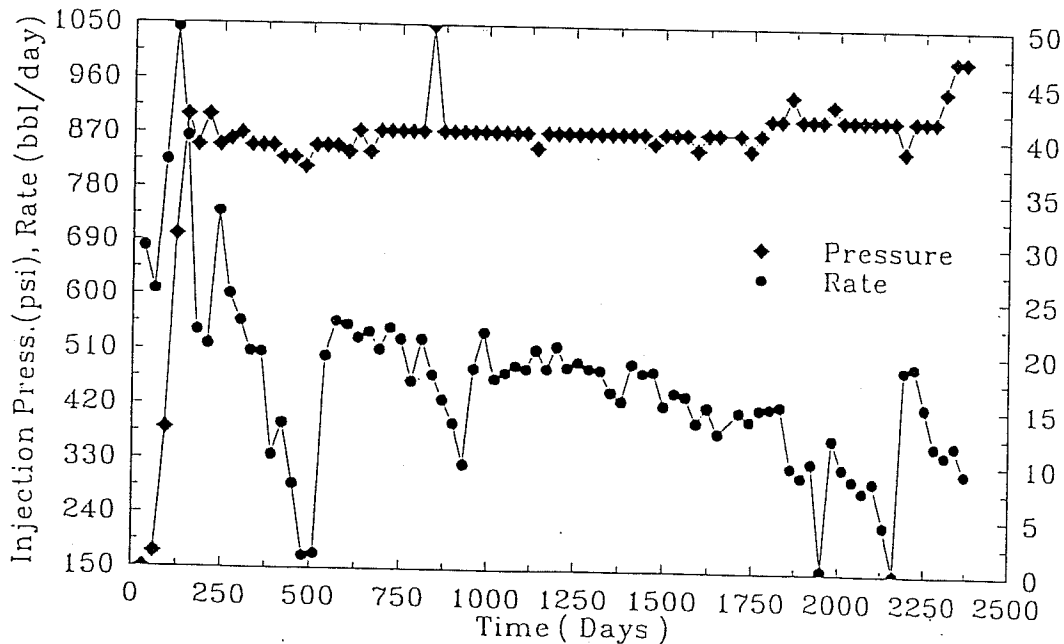


Figure 9. Water injection rate and injection pressure versus time for injection well I-2.

Granny Creek – Columbia Lease
5 Spot P2 (I - 3)

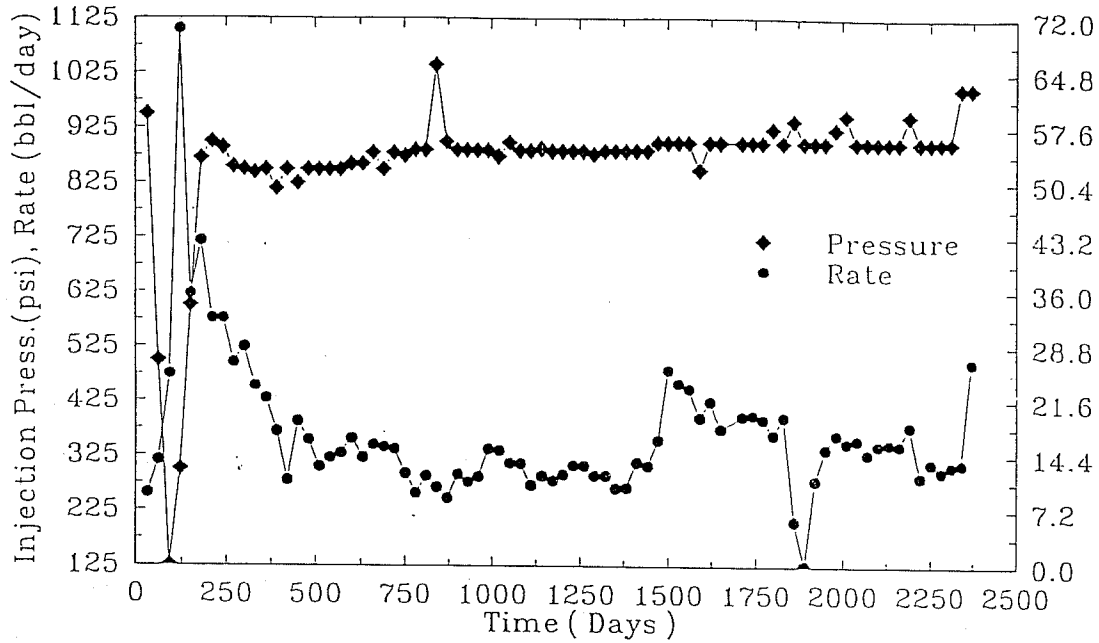


Figure 10. Water injection rate and injection pressure versus time for injection well I-3.

Granny Creek – Columbia Lease
5 Spot P1 (I - 4)

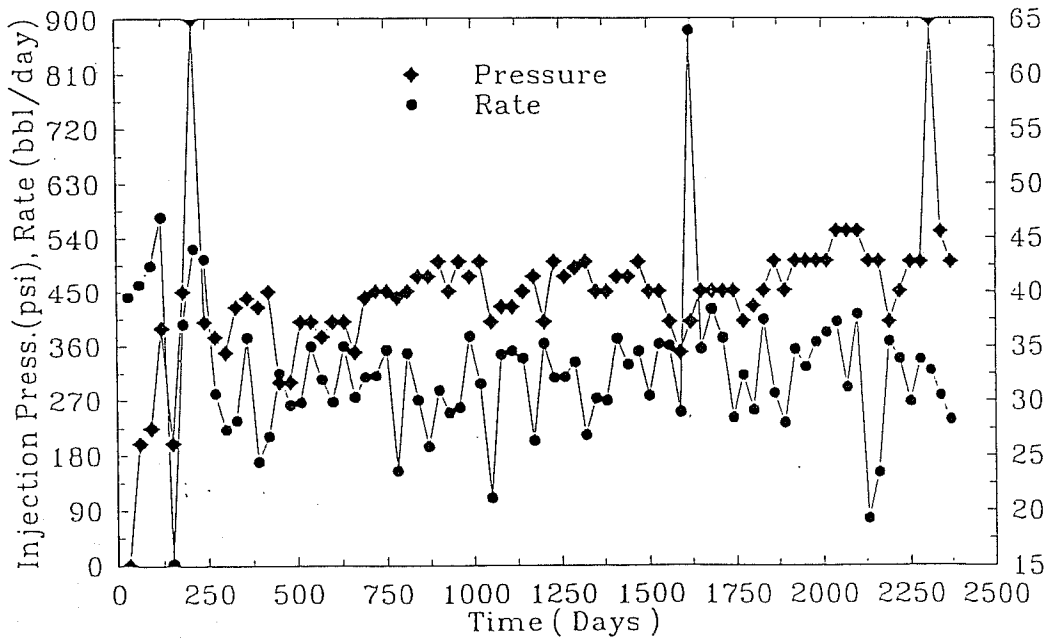


Figure 11. Water injection rate and injection pressure versus time for injection well I-4.

Granny Creek – Columbia Lease
5 Spot P2 (I – 5)

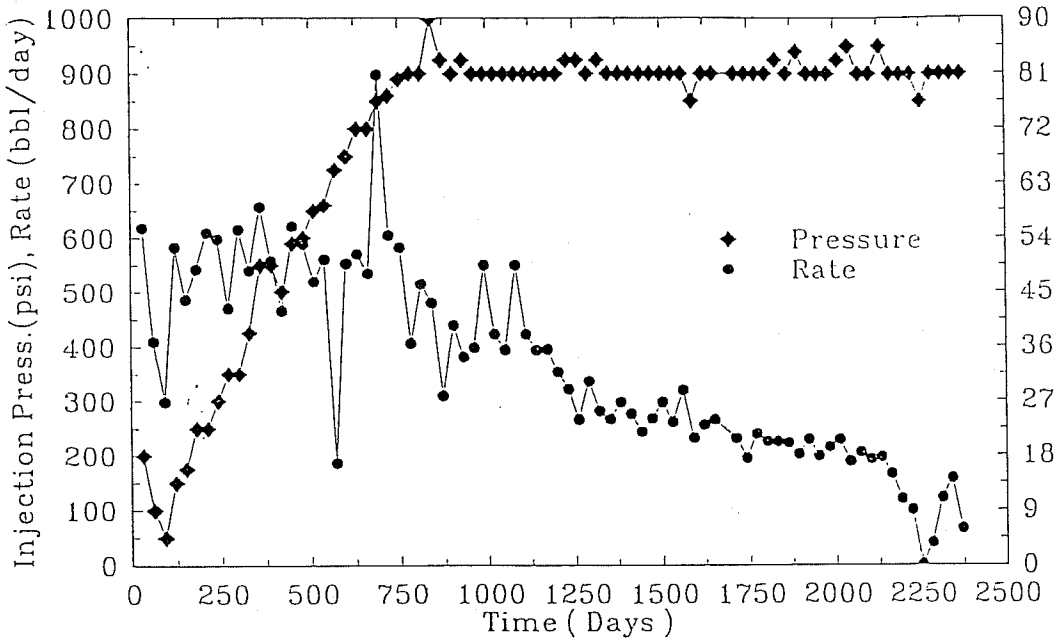


Figure 12. Water injection rate and injection pressure versus time for injection well I-5.

Granny Creek – Columbia Lease
5 Spot P2 (I – 6)

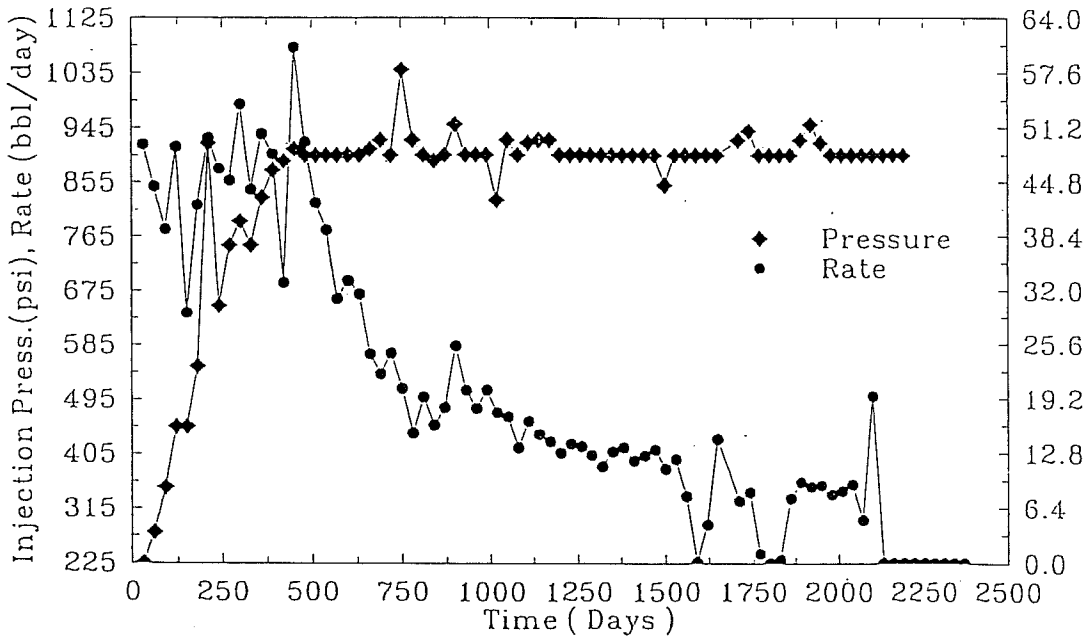


Figure 13. Water injection rate and injection pressure versus time for injection well I-6.

Granny Creek – Columbia Lease
 Cumulative Injection for 5 Spots (P1 & P2)

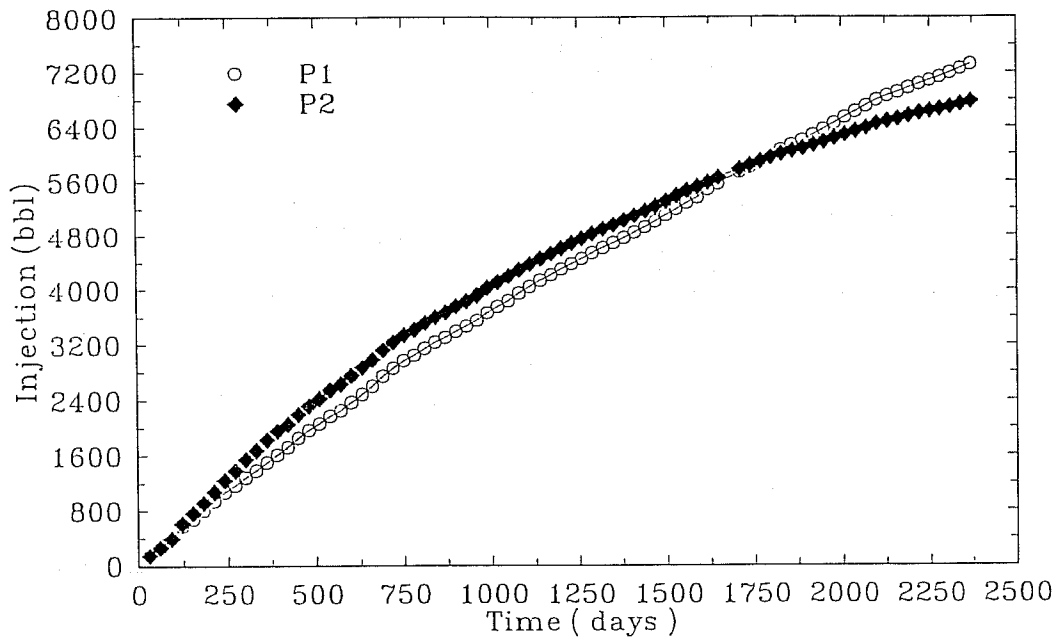


Figure 14. Cumulative water injection rates in P1 and P2 patterns.

Granny Creek – Columbia Lease
 5 Spot P1 (Production)

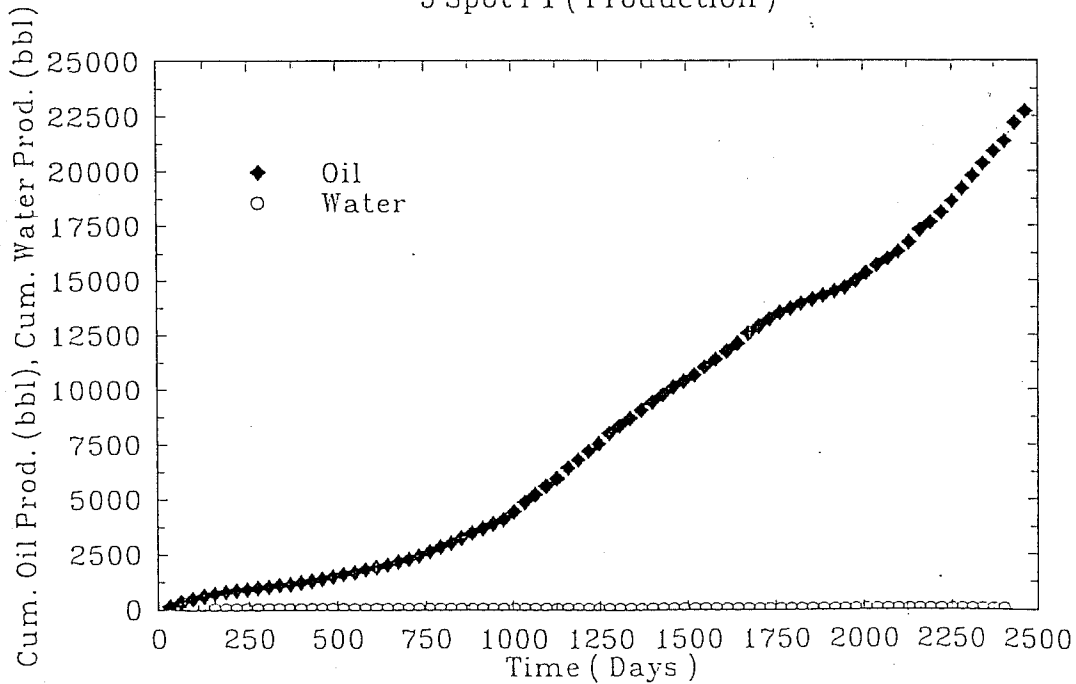


Figure 15. Oil and water productions from P1 flood pattern (actual field data).

Granny Creek – Columbia Lease
5 Spot P2 (Production)

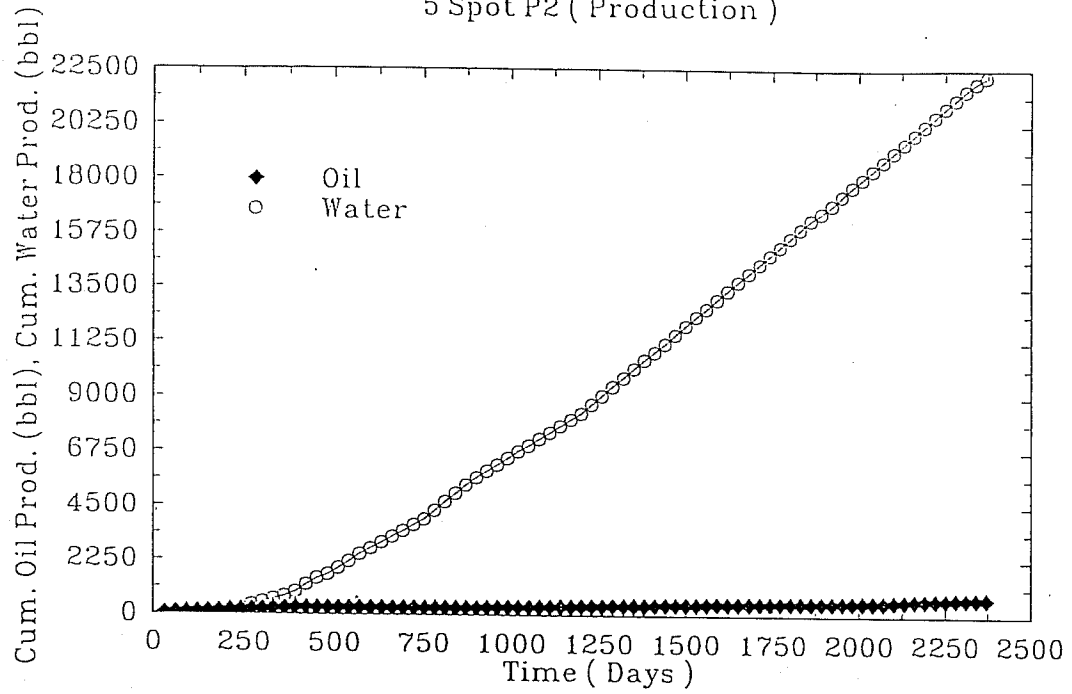


Figure 16. Oil and water productions from P2 flood pattern (actual field data).

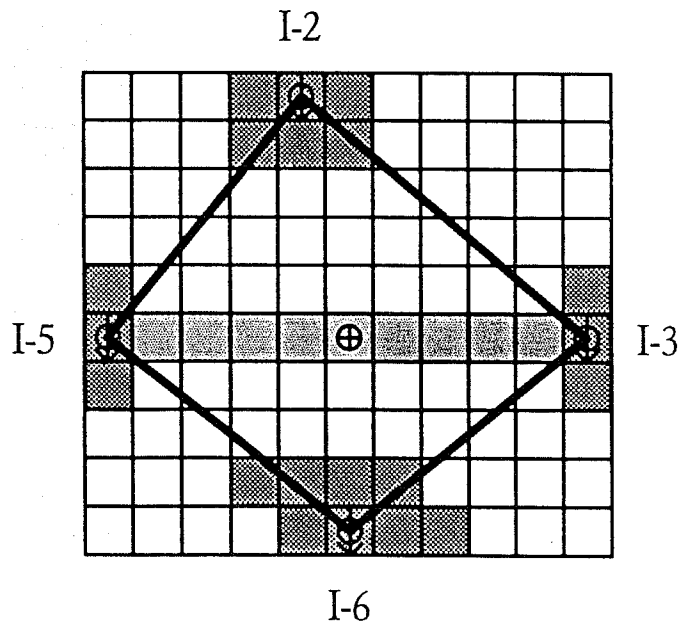
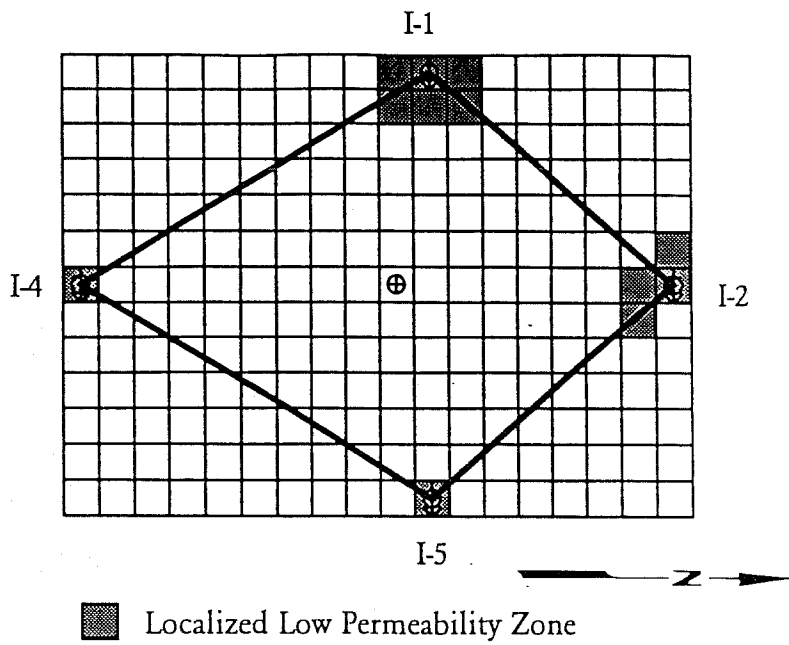


Figure 17. Grid system used for simulation of P1 (top) and P2 (bottom) flood patterns.

Granny Creek – Columbia Lease
5 spot P1

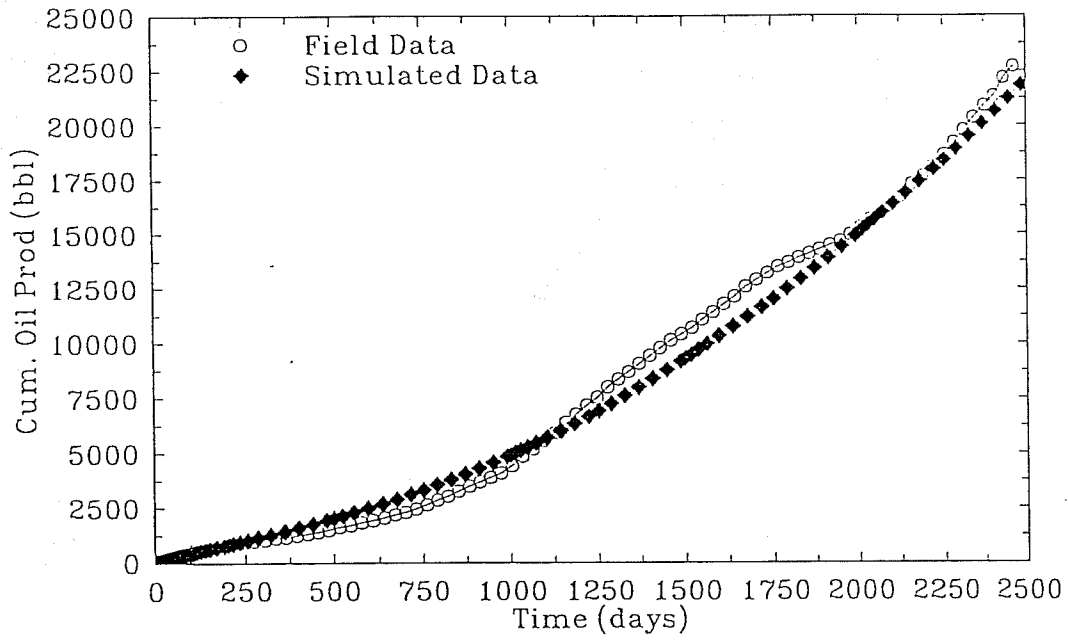


Figure 18. Actual and simulated cumulative oil production from P1 flood pattern.

Granny Creek – Columbia Lease
5 Spot P2

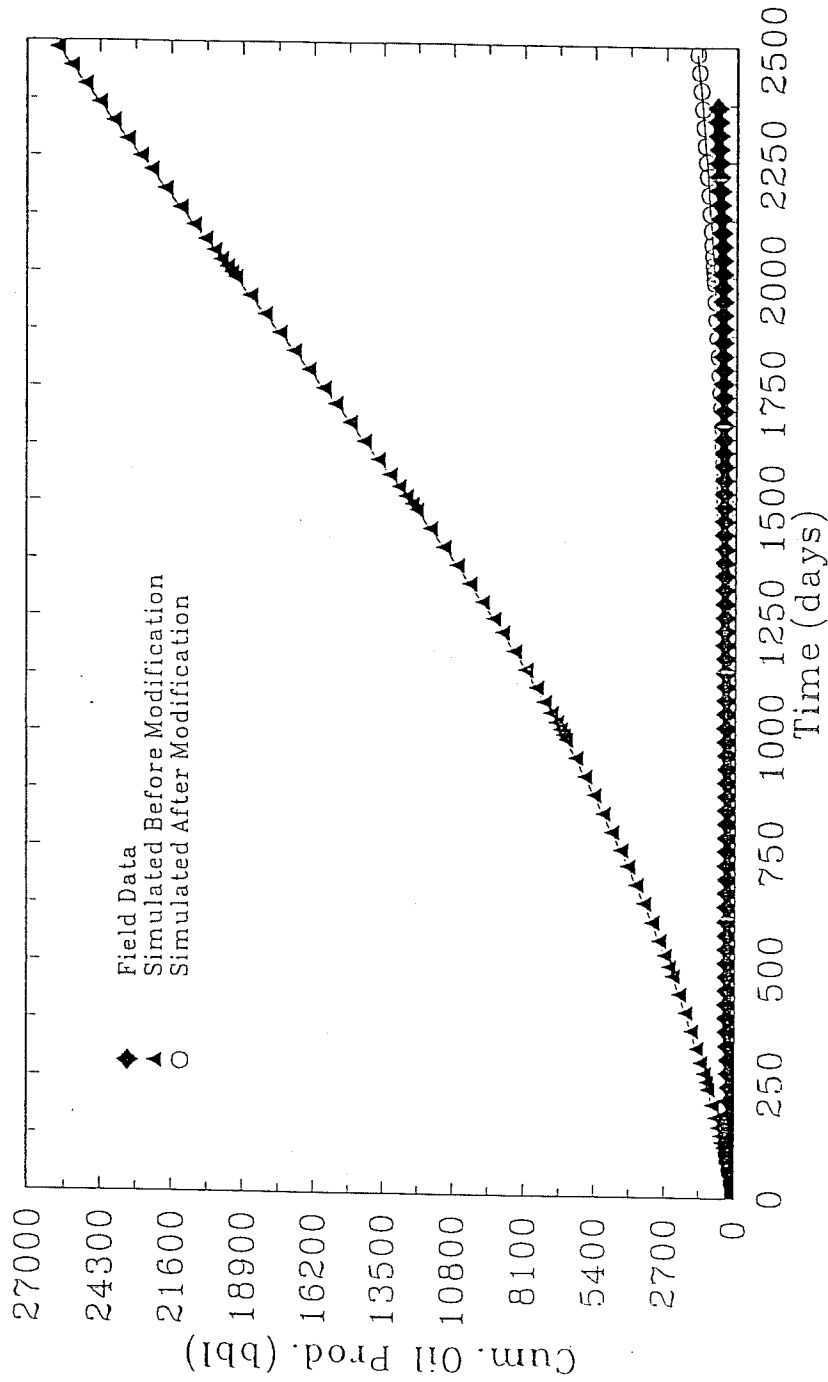


Figure 19. Actual field data and simulated cumulative oil production for P2 flood pattern before and after introduction of natural fracture.

Granny Creek - Columbia Lease
 Inj. Press. VS Time for 5 Spot P1 (I - 1)

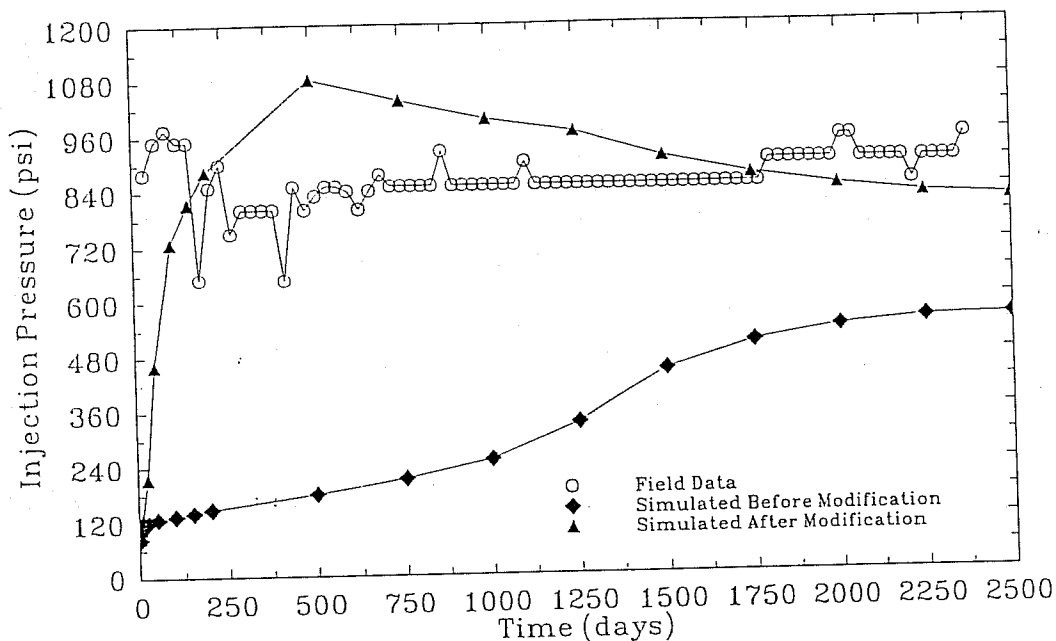


Figure 20. Actual field data and simulated injection pressure, before and after introduction of localized low-permeability zones, for injection well I-1.

Granny Creek - Columbia Lease
 Inj. Press. VS Time for 5 Spot P1 (I - 2)

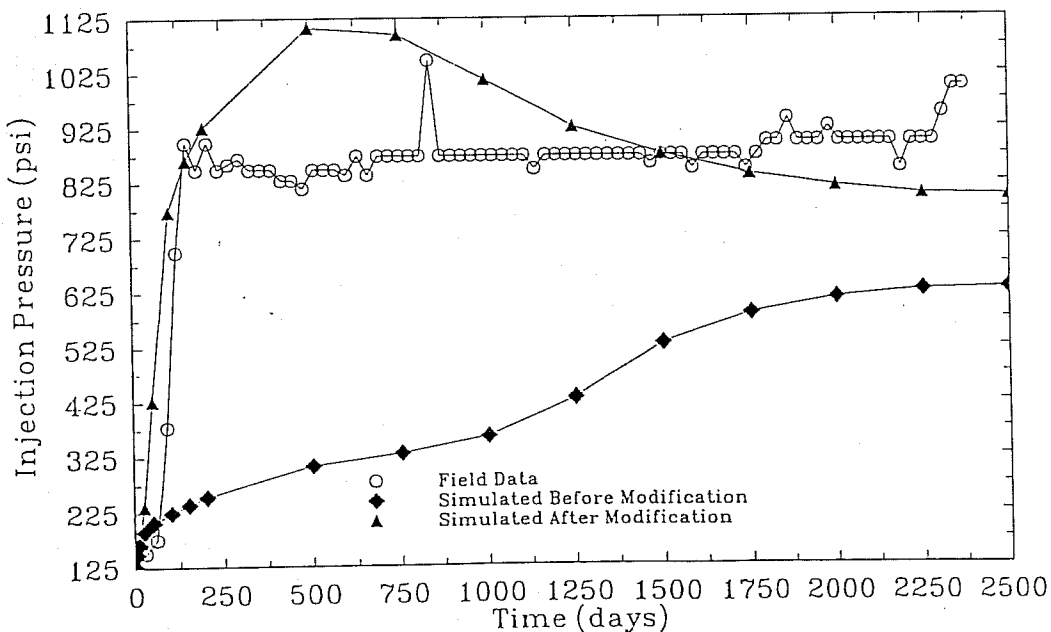


Figure 21. Actual field data and simulated injection pressure, before and after introduction of localized low-permeability zones, for injection well I-2.

Granny Creek - Columbia Lease
 Inj. Press. VS Time for 5 Spot P2 (I - 3)

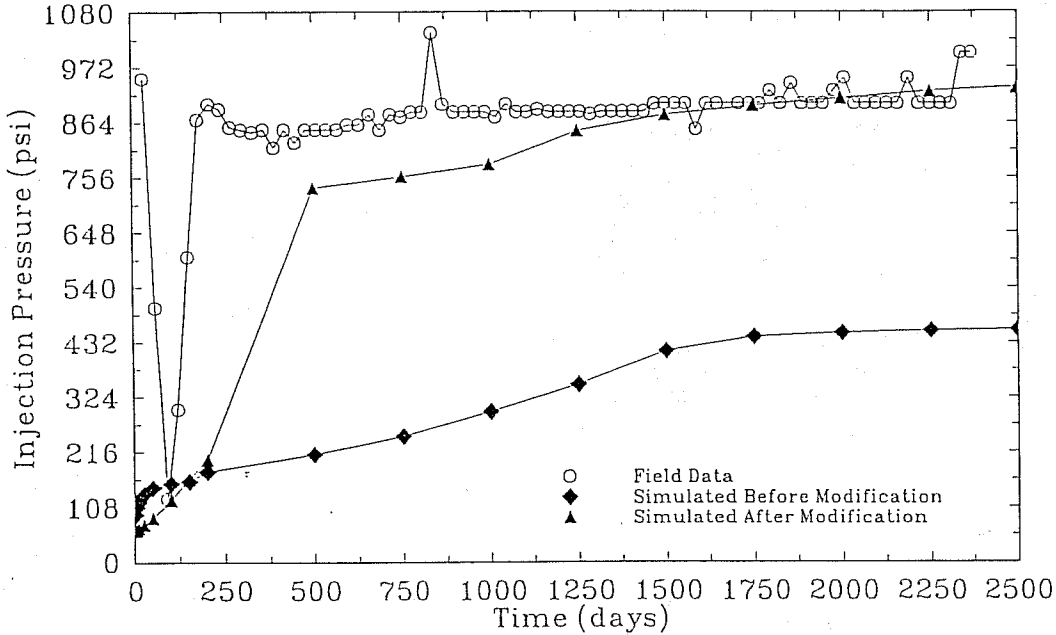


Figure 22. Actual field data and simulated injection pressure, before and after introduction of localized low-permeability zones, for injection well I-3.

Granny Creek - Columbia Lease
 Inj. Press. VS Time for 5 Spot P1 (I - 4)

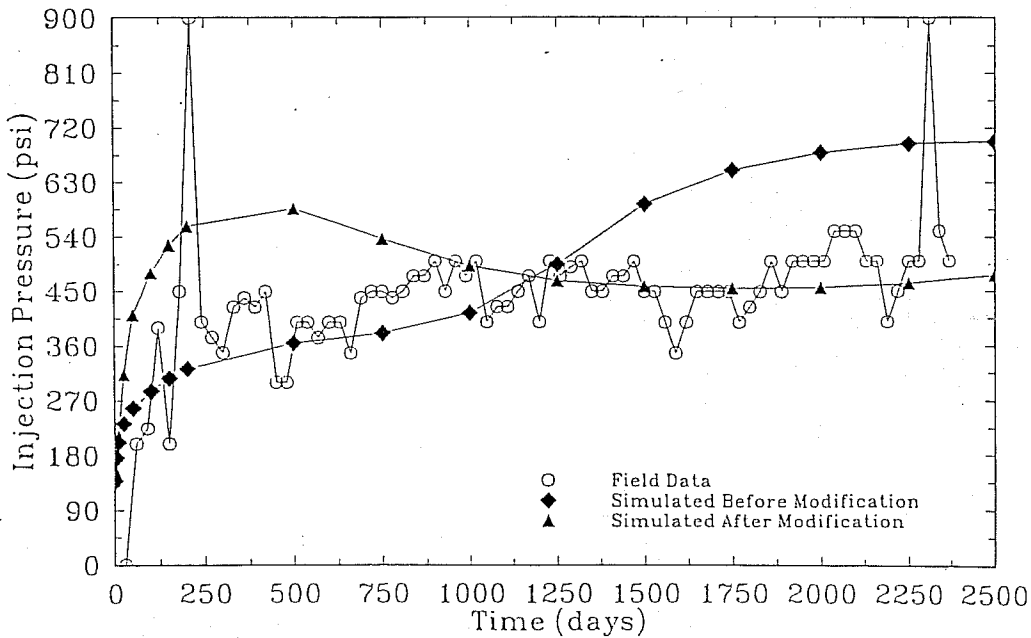


Figure 23. Actual field data and simulated injection pressure, before and after introduction of localized low-permeability zones, for injection well I-4.

Granny Creek – Columbia Lease
Inj. Press. VS Time for 5 Spot P2 (I – 5)

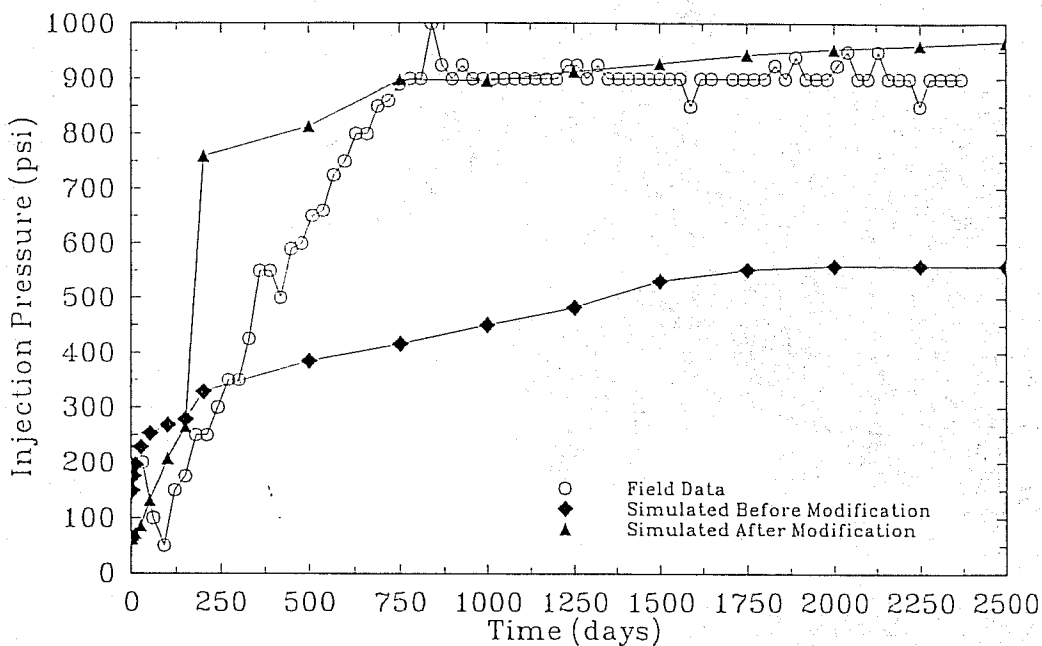


Figure 24. Actual field data and simulated injection pressure, before and after introduction of localized low-permeability zones, for injection well I-5.

Granny Creek – Columbia Lease
Inj. Press. VS Time for 5 Spot P2 (I – 6)

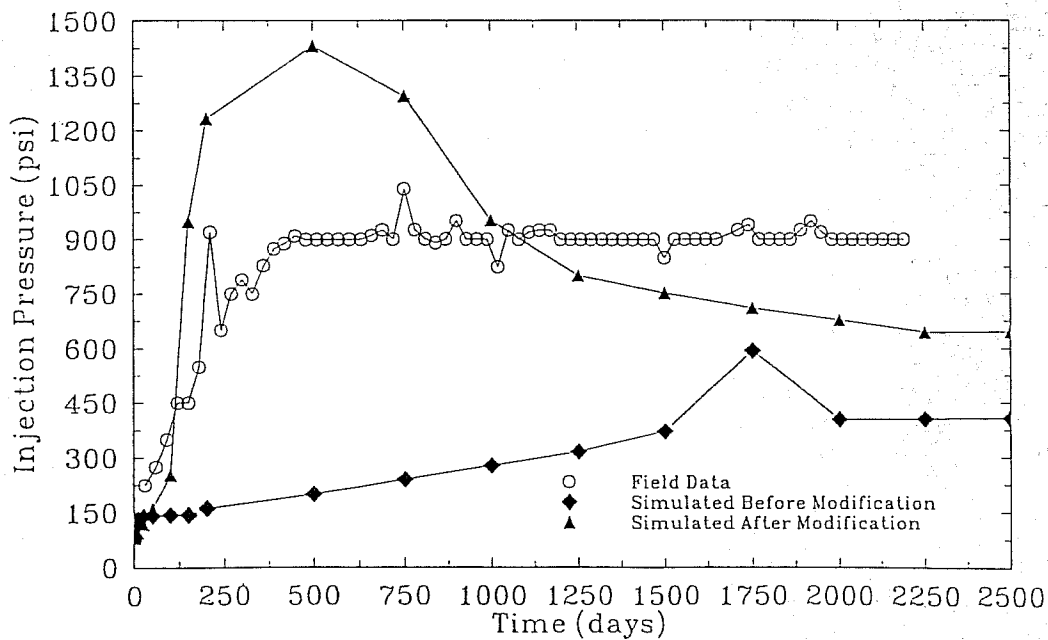


Figure 25. Actual field data and simulated injection pressure, before and after introduction of localized low-permeability zones, for injection well I-6.

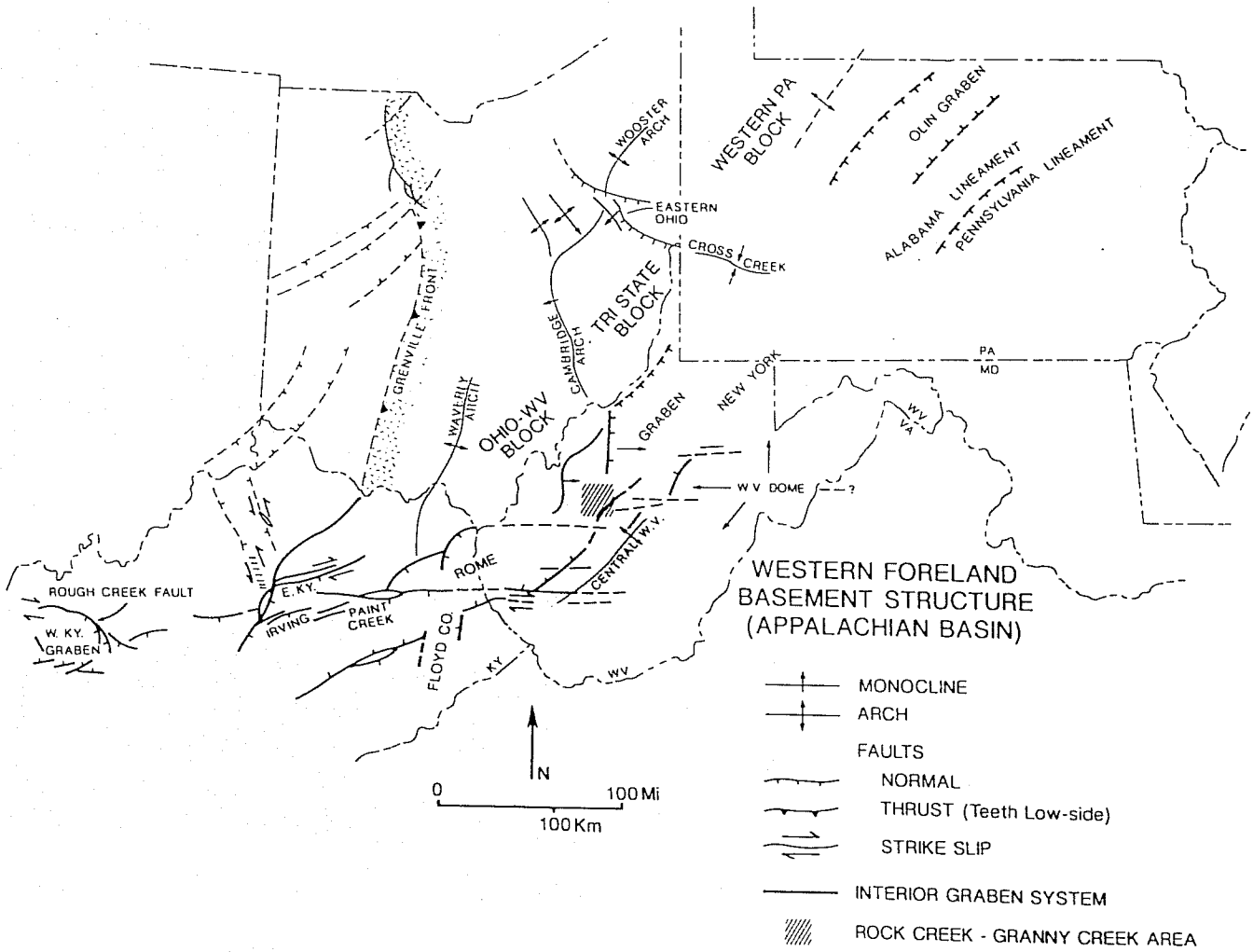


Figure 26. Basement blocks of the Appalachian basin.

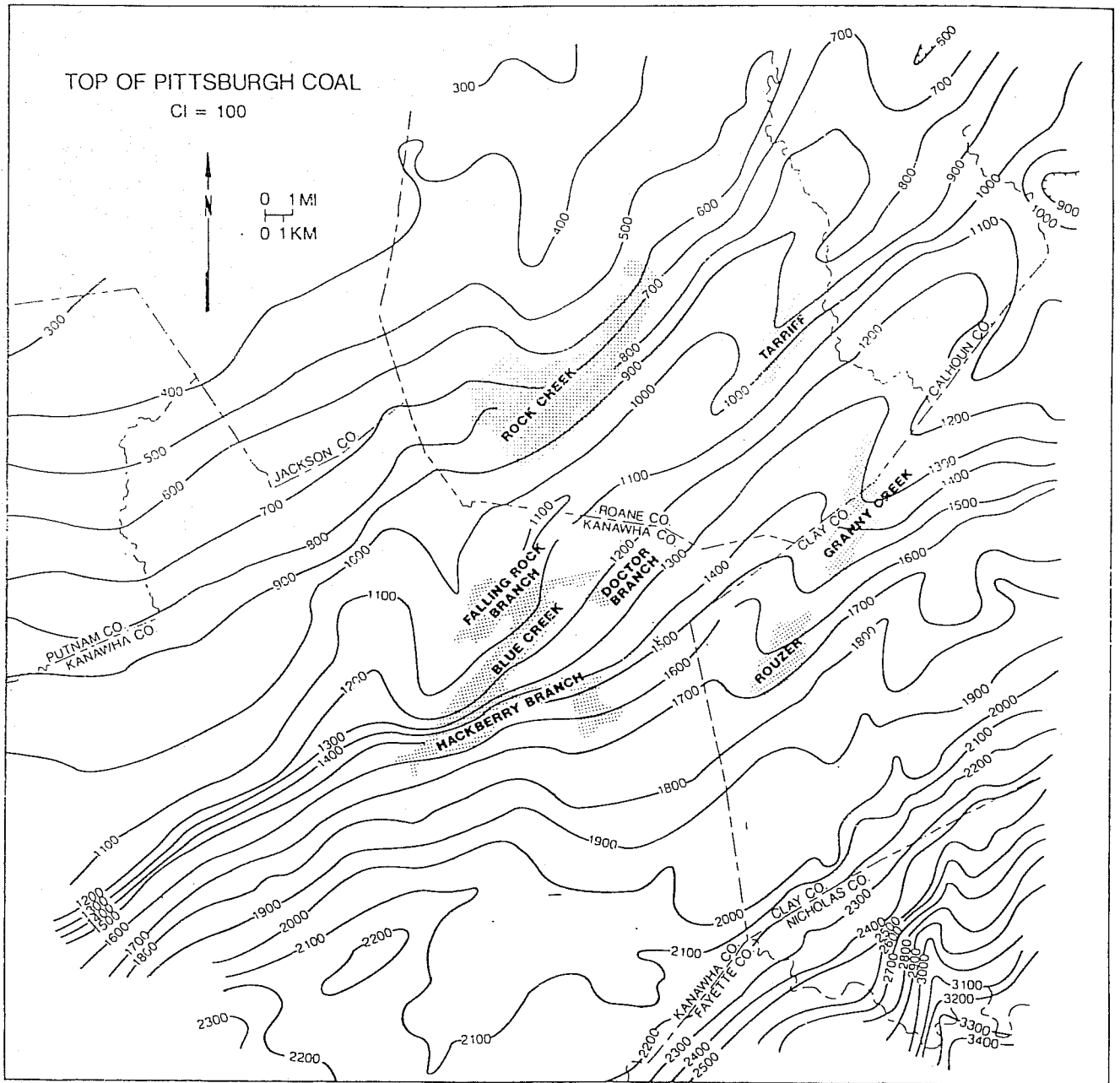


Figure 27. Structure on top of the Pennsylvanian Pittsburgh coal in the Rock Creek-Granny Creek area.

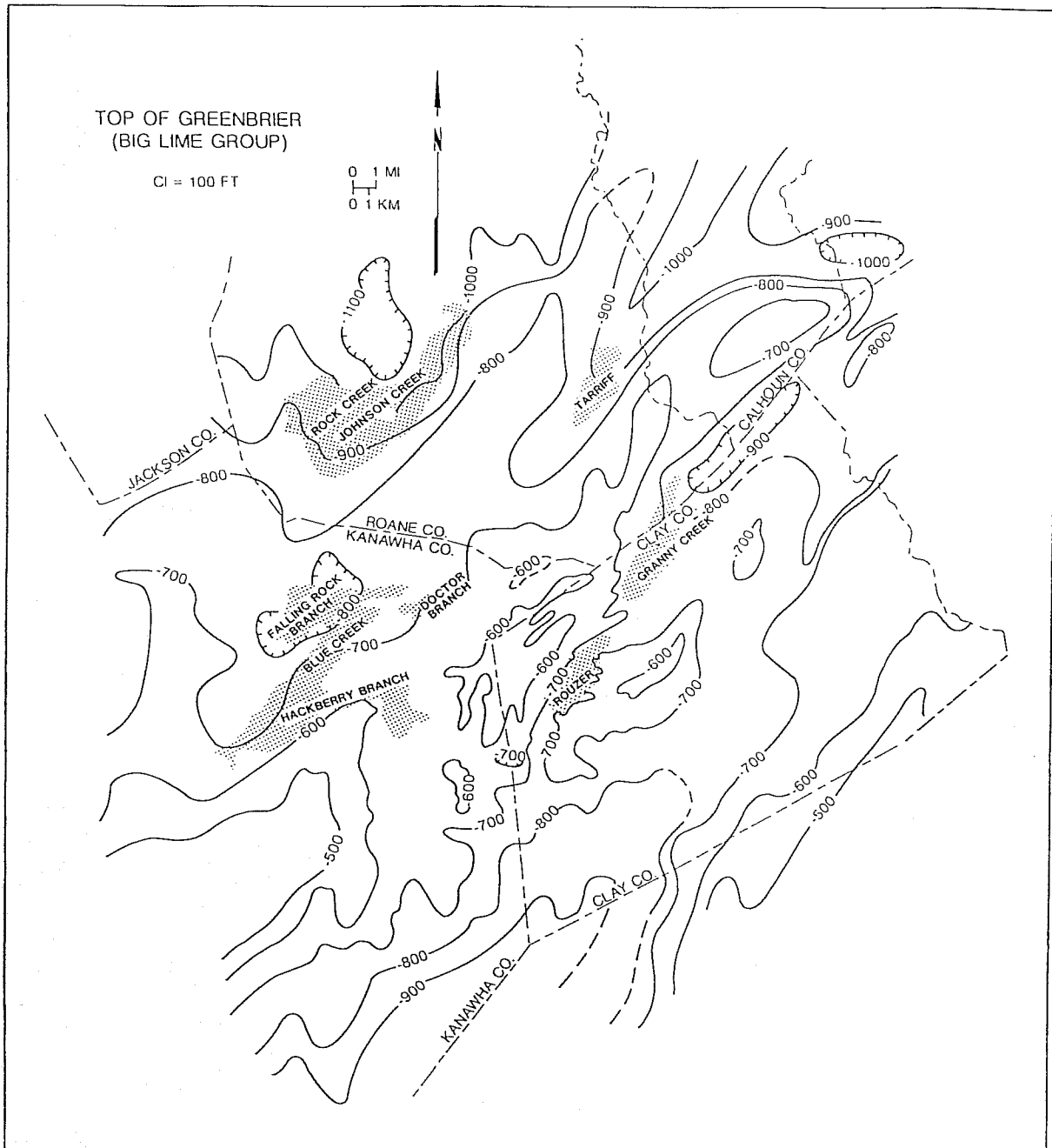


Figure 28. Structure on top of the Mississippian Greenbrier Group (Big Lime) in the Rock Creek-Granny Creek area.

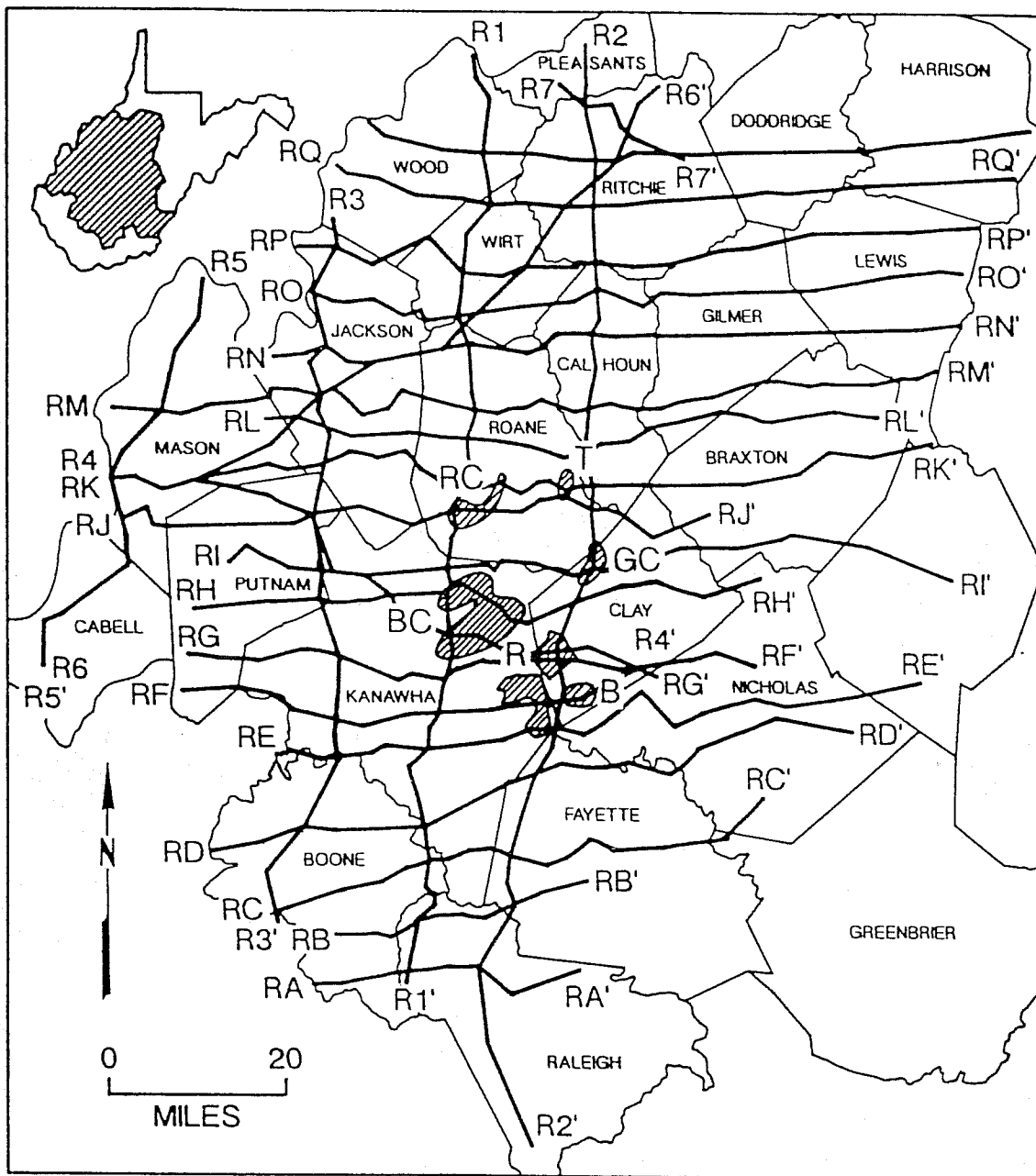


Figure 29. Location map of regional stratigraphic study of the Big Injun sandstone. The profiles of the numerous stratigraphic cross sections are located as well as the Granny Creek (GC), Rock Creek (RC), Tariff (T), Blue Creek (BC), and other fields.

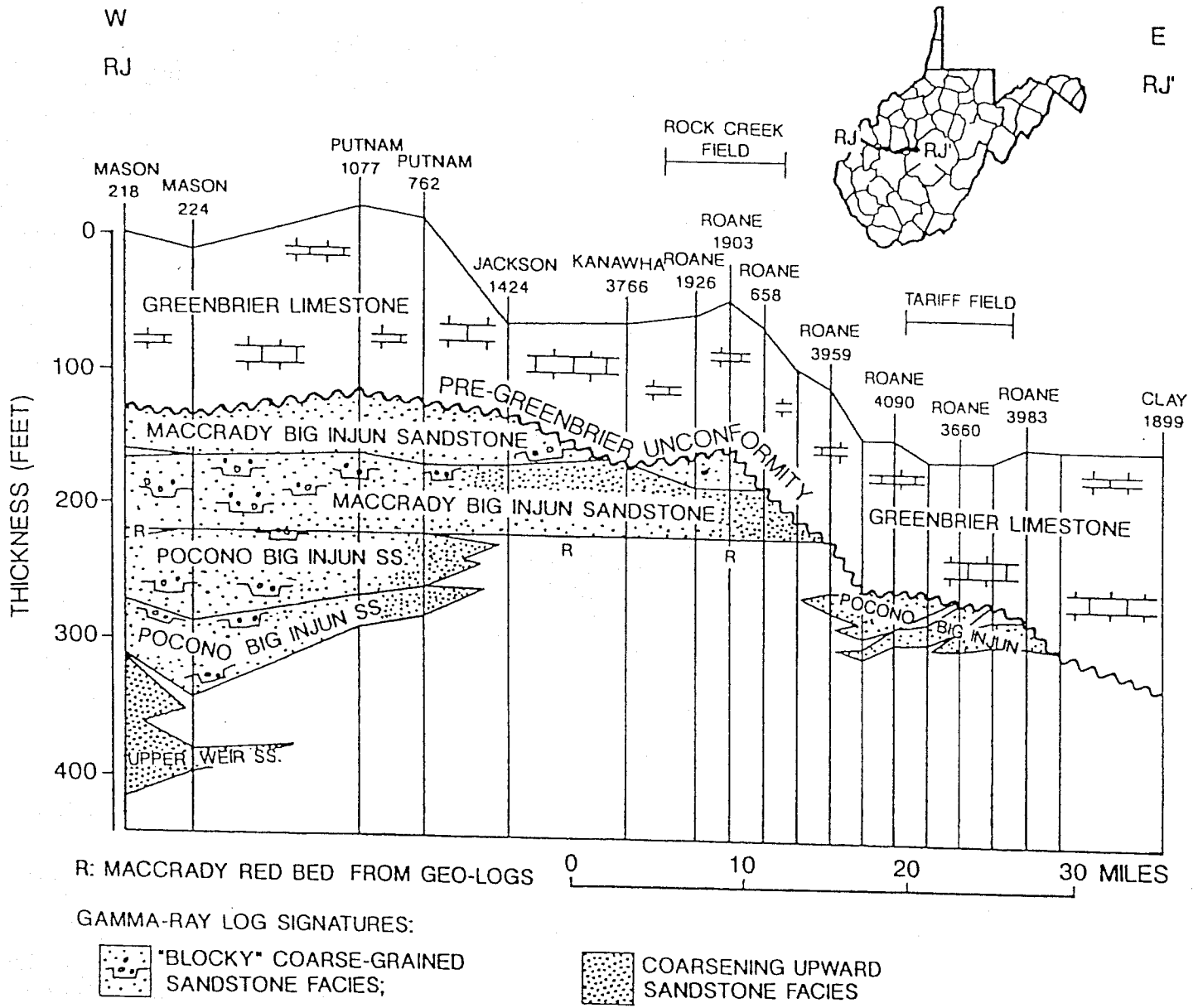


Figure 30. Regional stratigraphic cross section RJ-RJ' (west to east) showing the reservoir rock to be Pocono Big Injun sandstone in the Tariff (also Granny Creek) field and Maccrady Big Injun in Rock Creek field. Datums are the redbed separating the Maccrady from the Pocono Big Injun (west end) and the Sunbury Shale (east end).

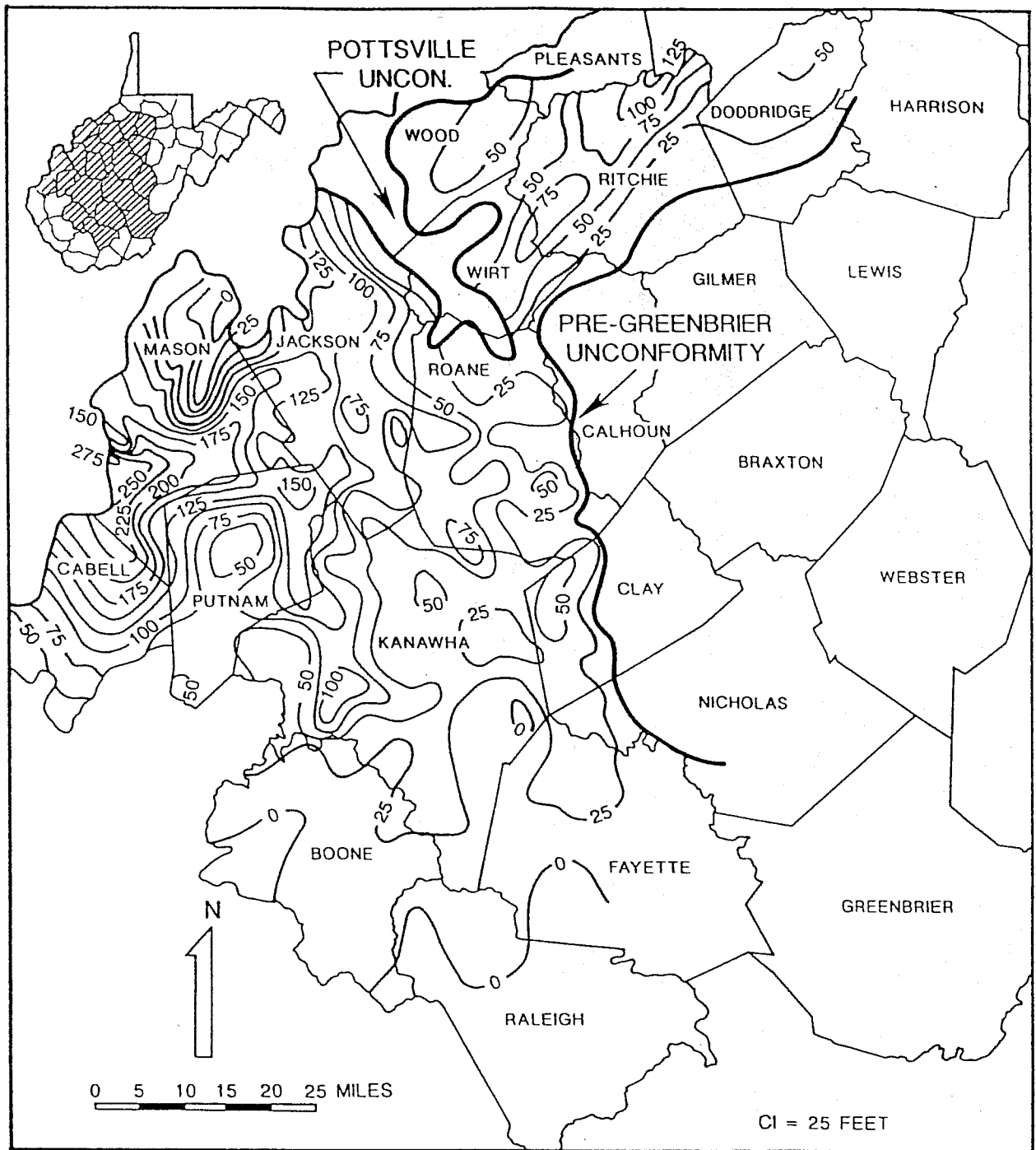


Figure 31. Isolith map of the Pocono and Maccrady Big Injun sandstones in western West Virginia.

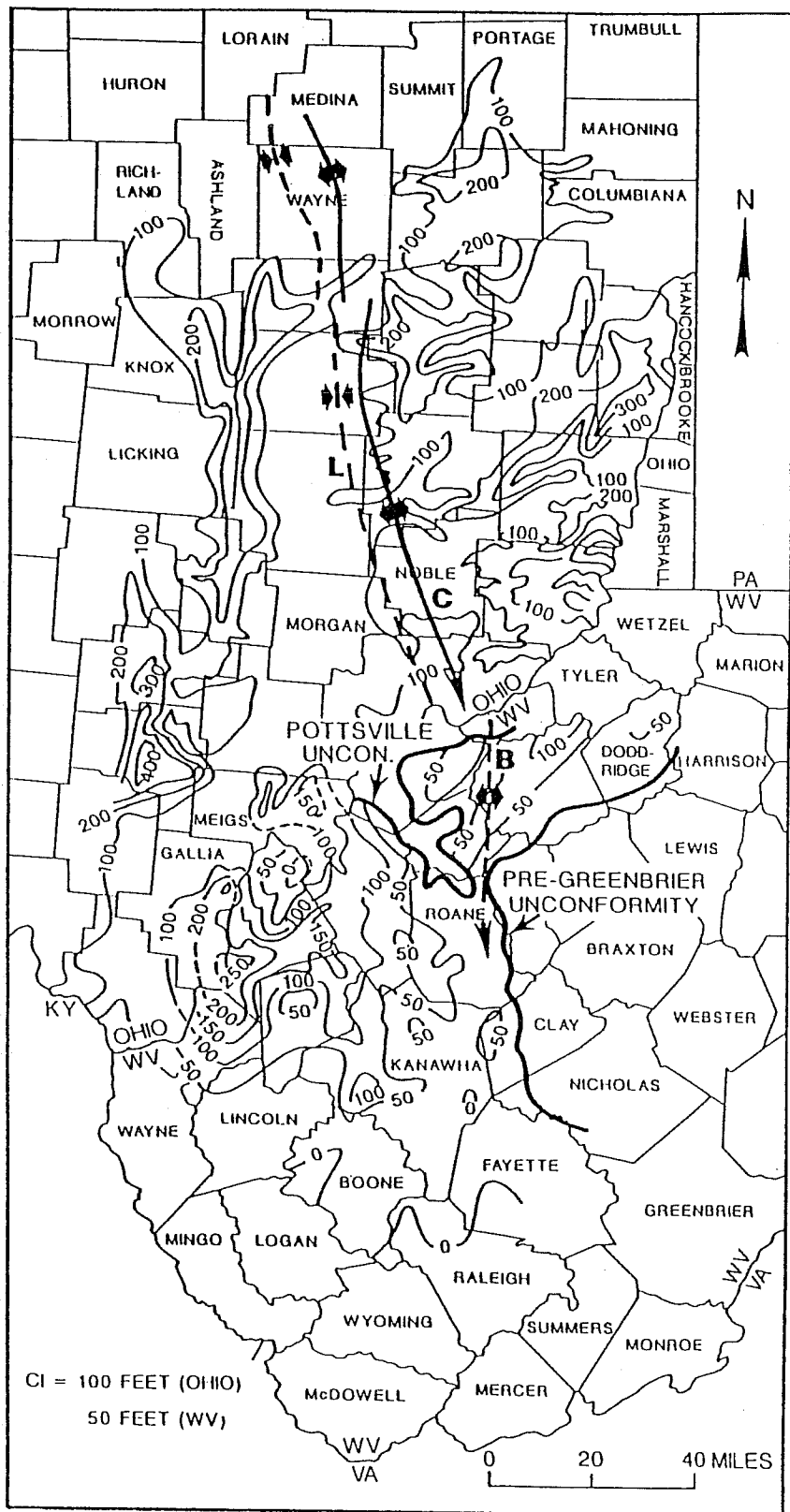


Figure 32. Isolith map of the Big Injun sandstones in West Virginia and Ohio (Ohio part is from Ver Steeg's isopach map of the Black Hand member of the Cuyahoga Formation, 1947, Fig. 5). Structural axes are labelled C, Cambridge arch; L, Lorain (Parkersburg) syncline; B, Burning Springs anticline.

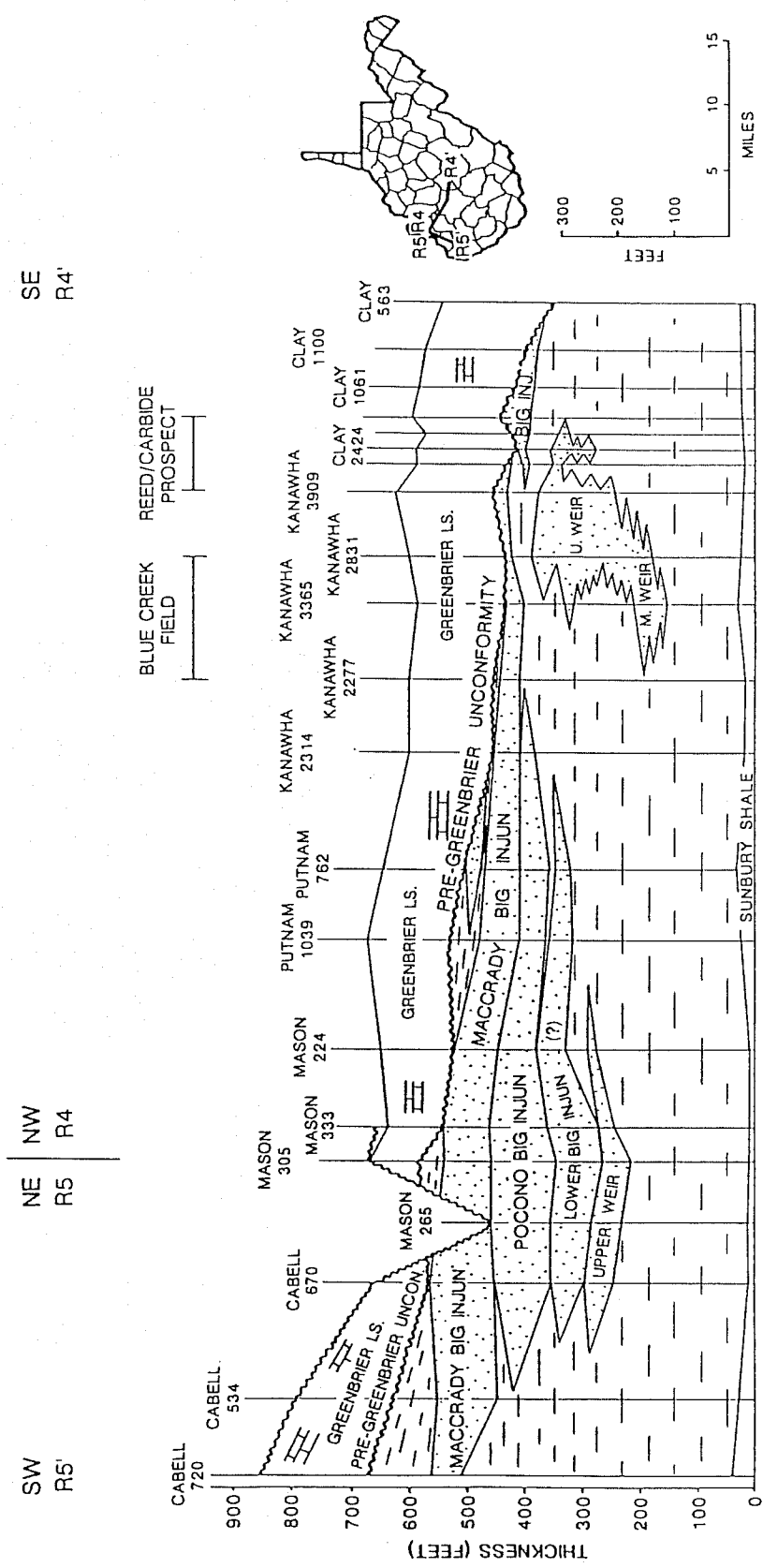


Figure 33. Regional cross section R5'-R4' from Cabell to Clay County indicates that the Big Injun reservoir sandstone is Maccrady in Blue Creek field, but Pocono in fields to the east. Sunbury Shale is datum. Redbeds occur between Pocono and Maccrady Big Injun sandstones.

THICK BELTS OF BIG INJUN SANDSTONES

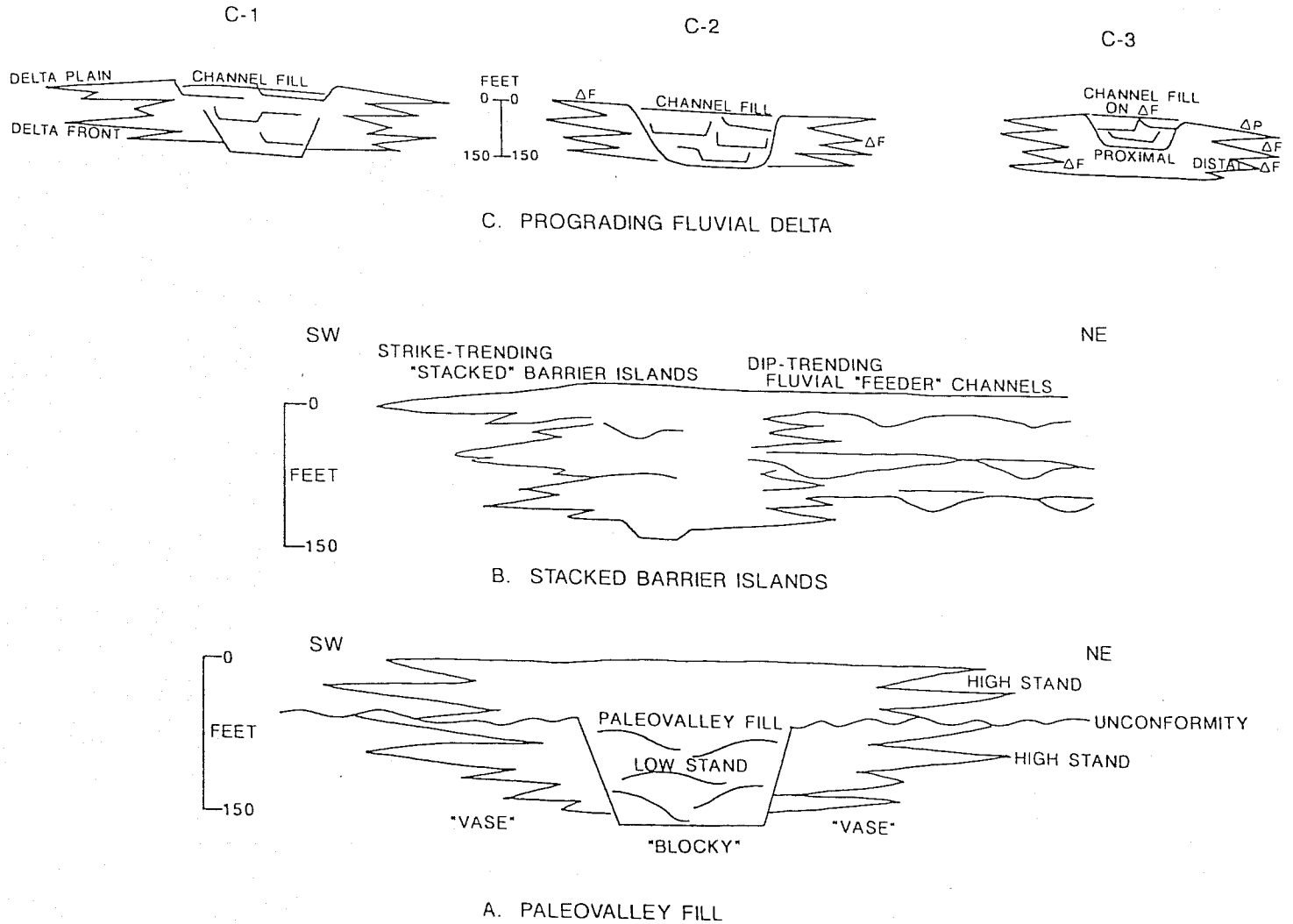


Figure 34. Hypotheses suggested to explain the origin of thick belts of Big Injun sandstone of Cabell, Mason, and Putnam counties (Zou and Donaldson, 1992) also are relevant for the thick belts of Upper Weir of the Blue Creek field and vicinity.

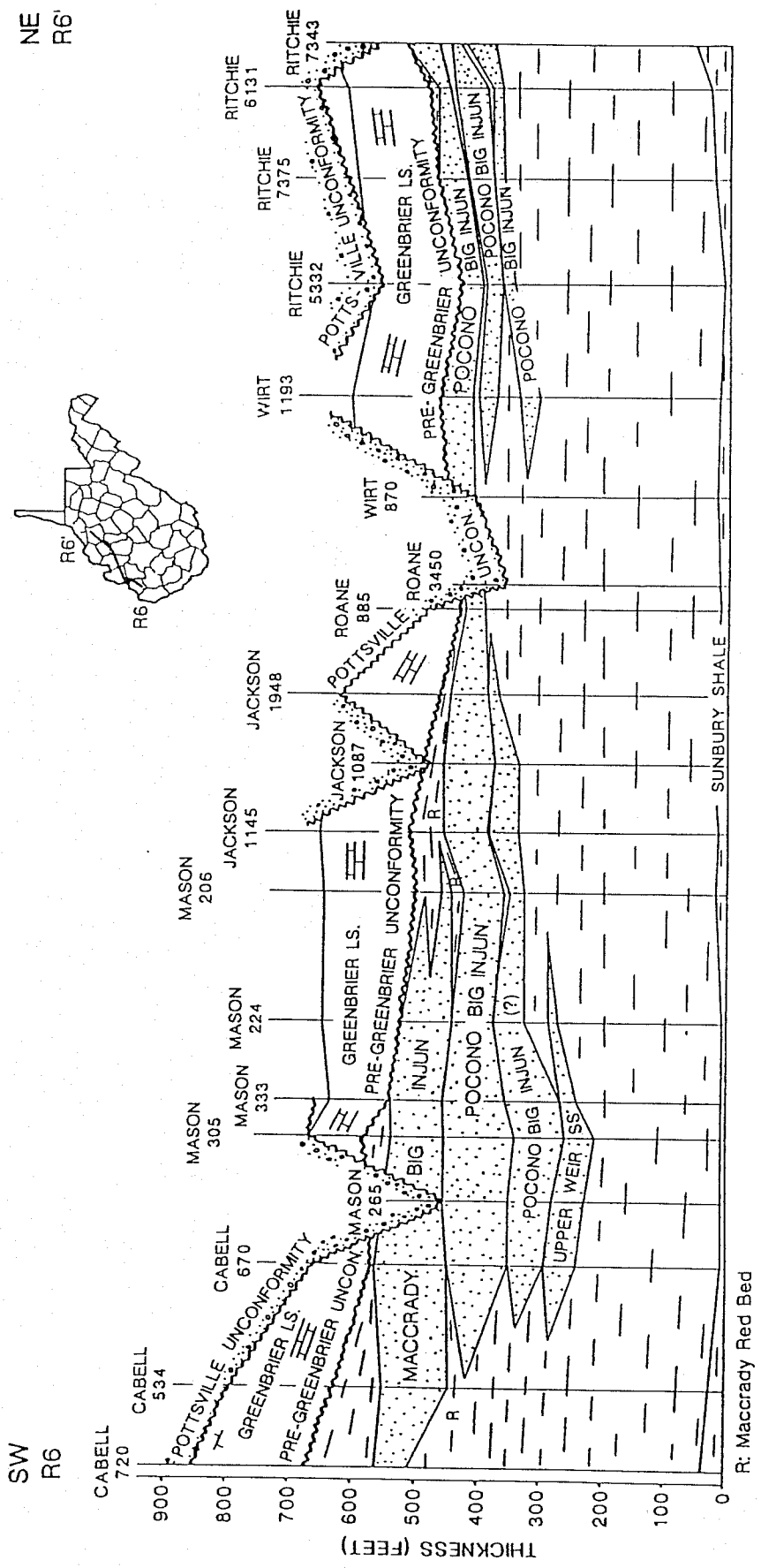
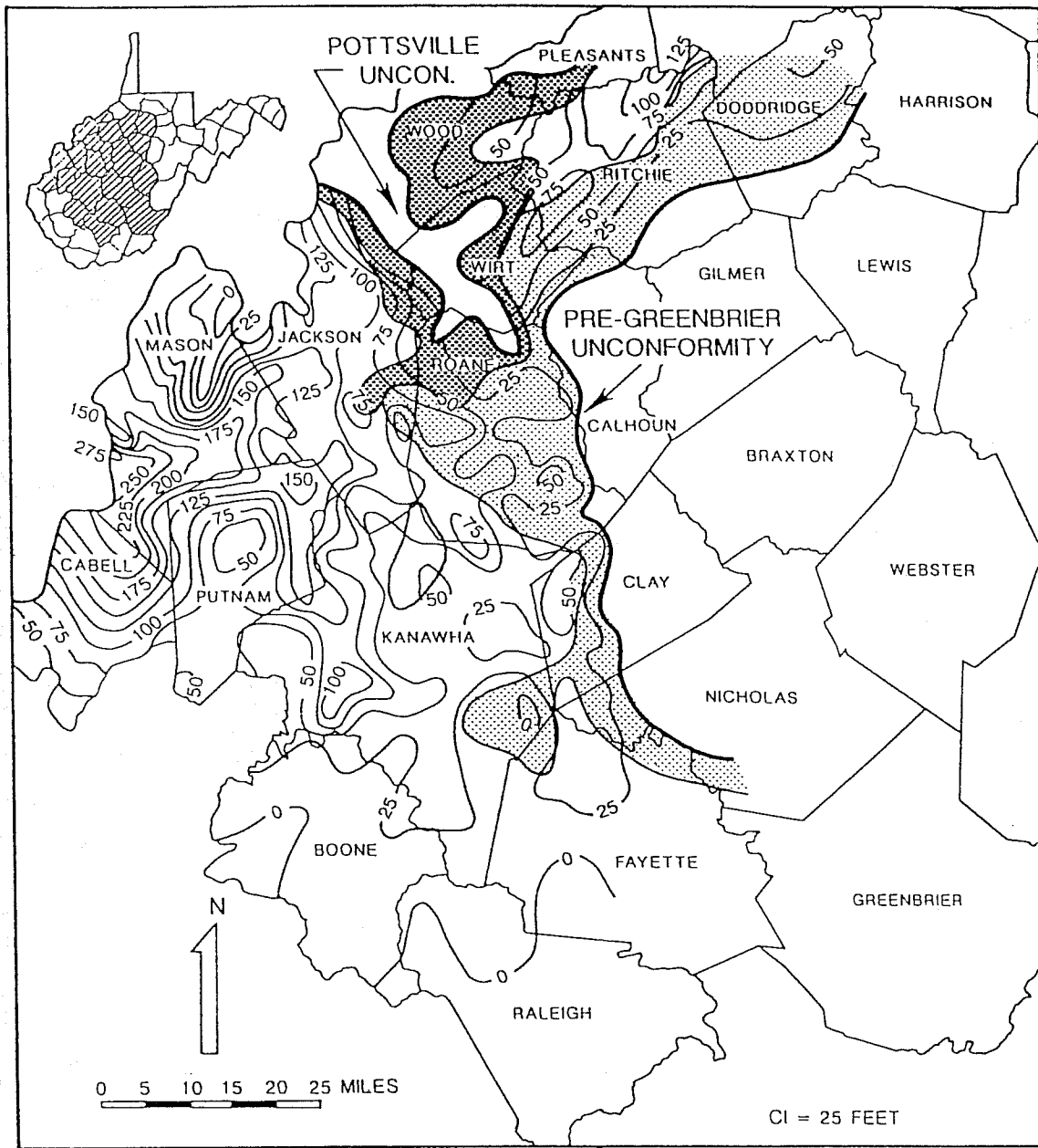


Figure 35. Regional stratigraphic cross section from Cabell to Ritchie County across the Burning Springs anticline showing both pre-Greenbrier and pre-Pottsville unconformities. Along profile, only Pocono Big Injun sandstone occurs north of Burning Springs anticline (Ritchie and Wirt counties), whereas both Pocono and Maccrady Big Injun sandstones are vertically stacked to the south. Sunbury Shale is datum. Maccrady Big Injun sandstone overlies redbeds.



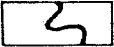
-  Area Big Injun Sandstones Totally Removed
-  Big Injun Sandstones Partially Removed by Pottsville Erosion
-  Big Injun Sandstones Partially Removed by Pre-Greenbrier Erosion

Figure 36. Map showing partial and total removal of Big Injun sandstones by pre-Greenbrier and Pottsville unconformities.

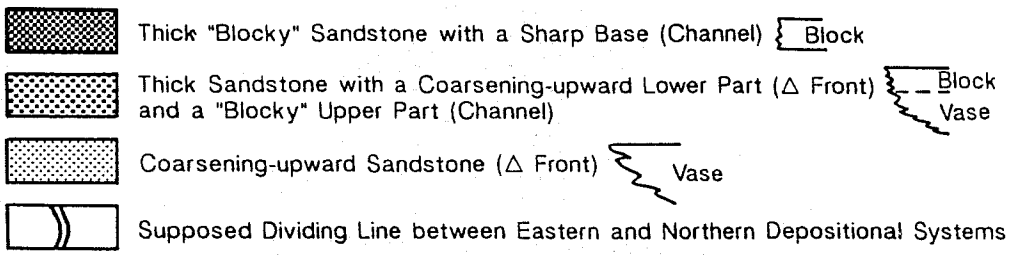
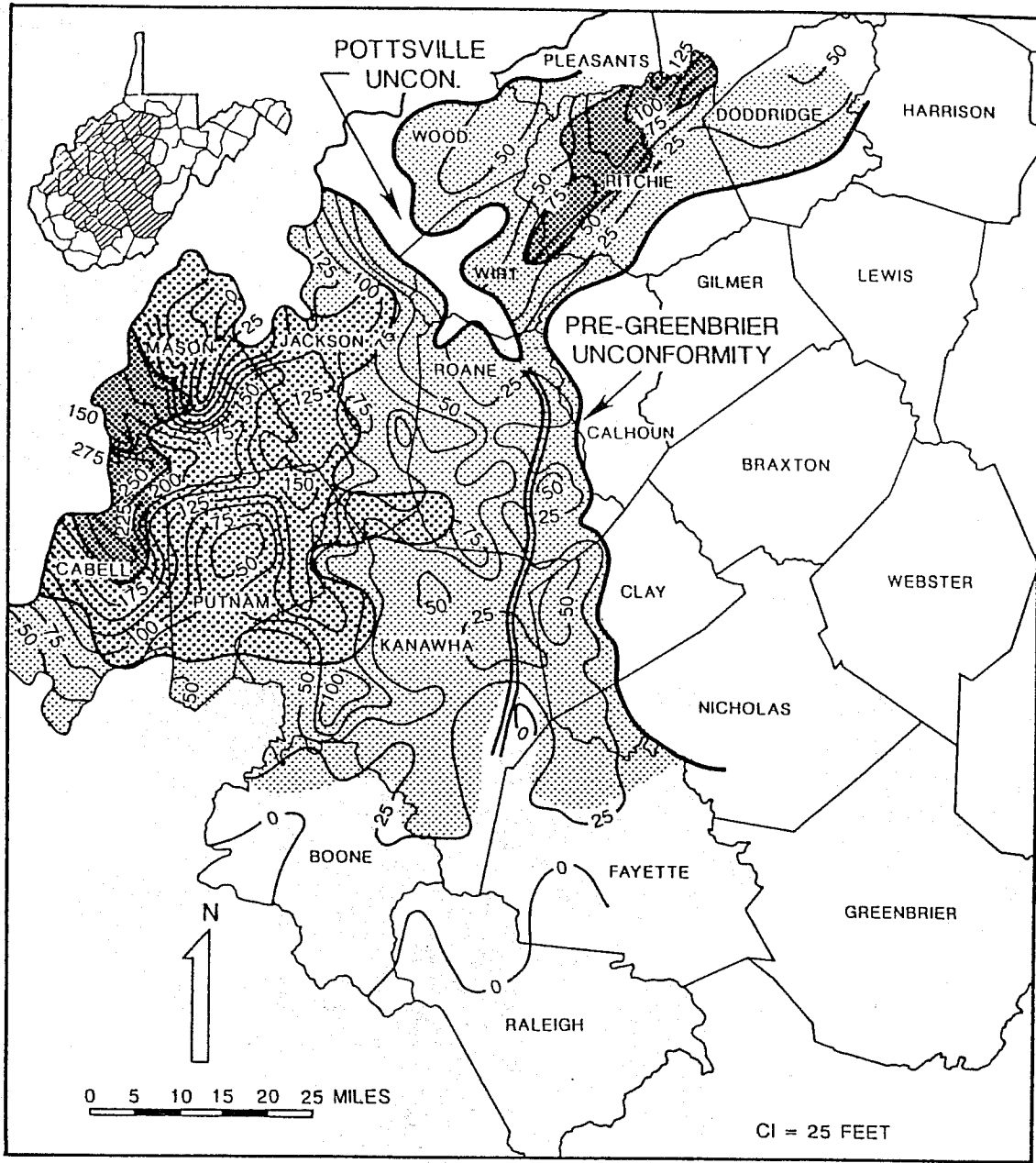


Figure 37. Log signature facies and undifferentiated Pocono and Maccrady Big Injun sandstones in western West Virginia.

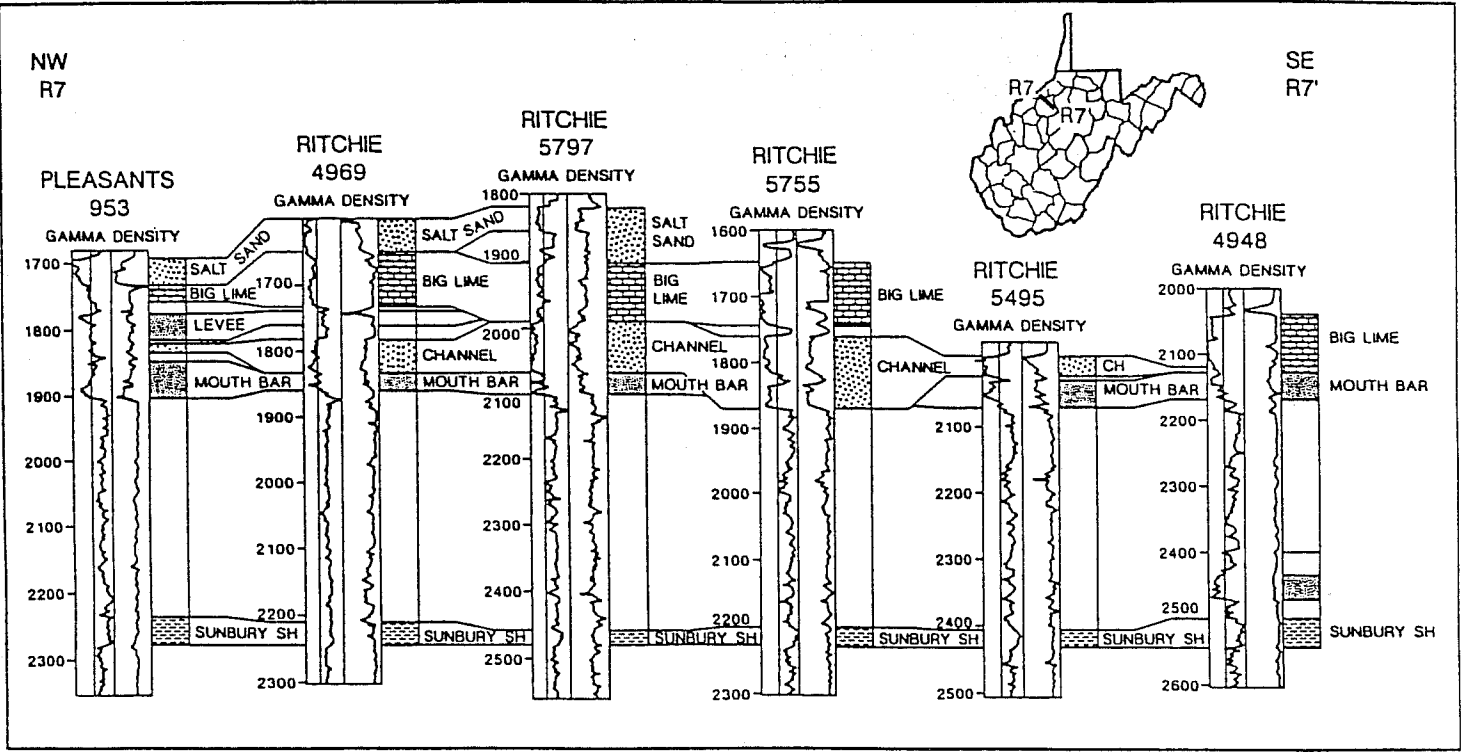


Figure 38. Regional stratigraphic cross section R7-R7' showing levee, channel, and mouth-bar facies in the Pocono Big Injun sandstones, along profile extending from Pleasants southeast across Ritchie County, West Virginia.

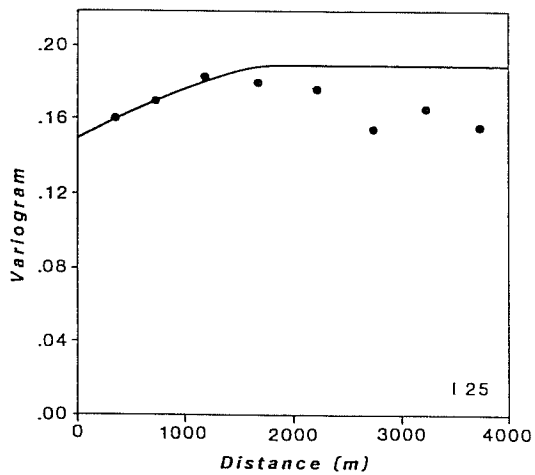
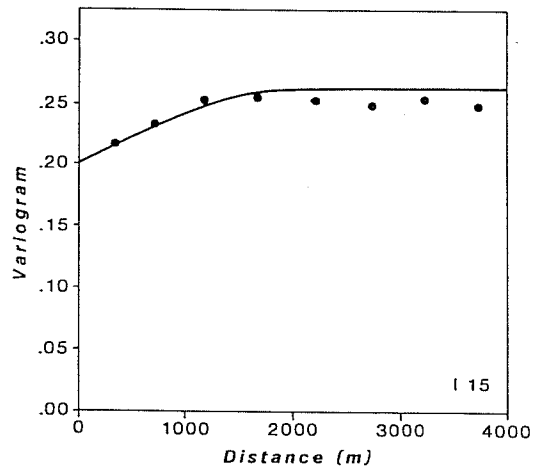
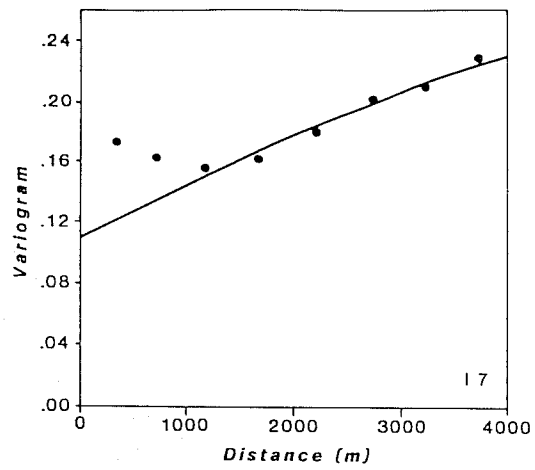


Figure 39. Omnidirectional variogram for the indicator variables I7, I15, and I25. Observed variogram values are symbols, fitted model is solid line. I7 is the indicator transform variable of oil initial potential for wells in Granny Creek such that $I7=1$ if the initial potential is less than 7 BOPD, and $I7=0$ if greater than 7 BOPD. I15 and I25 are created in the same way.

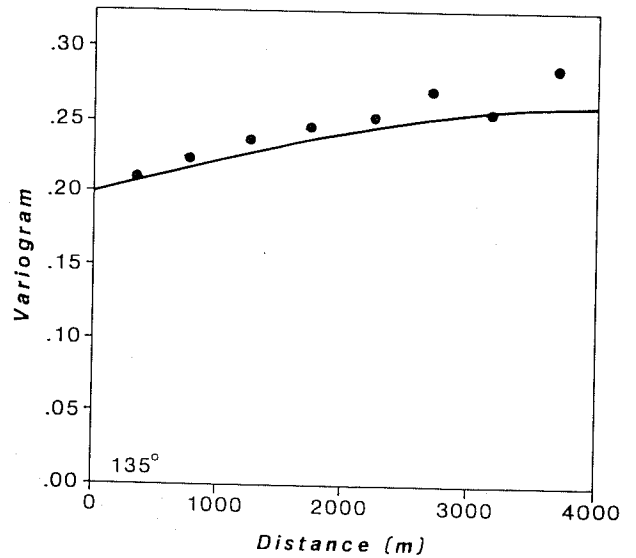
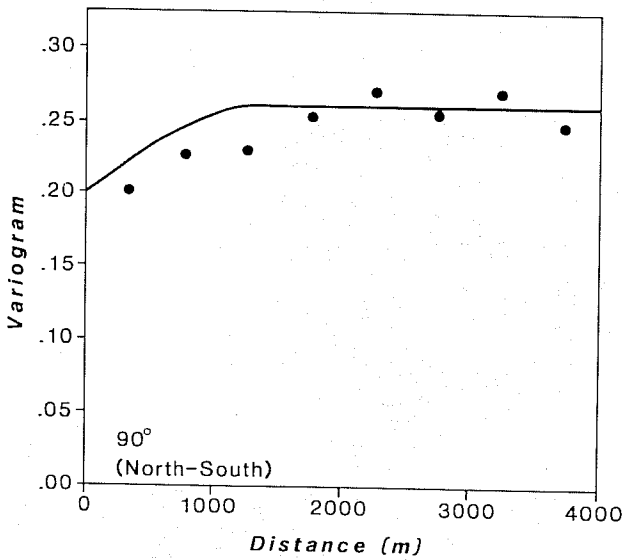
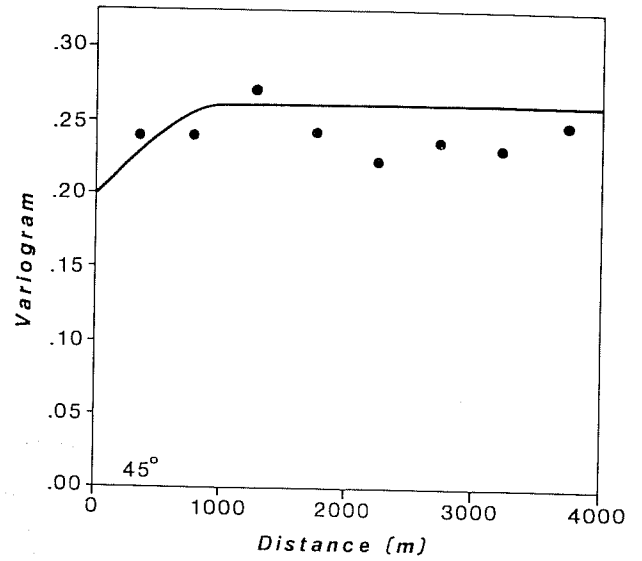
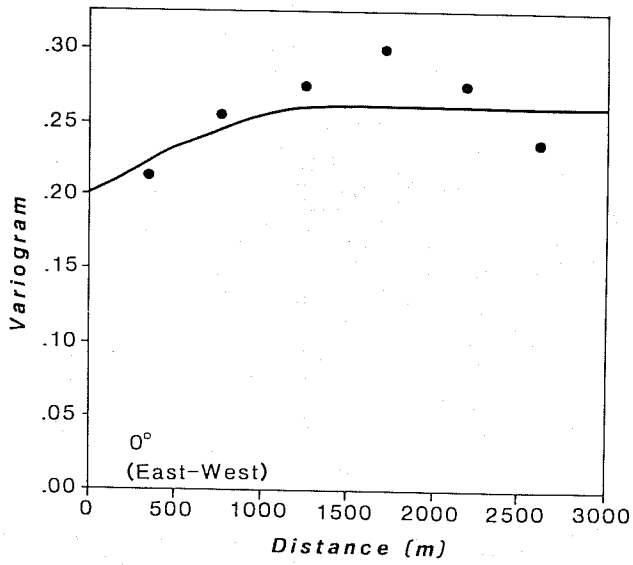


Figure 40. Directional variograms for indicator variable I15 in Granny Creek field. I15=1 if oil initial potential is less than 15 BOPD, I15=0 if greater than 15 BOPD.

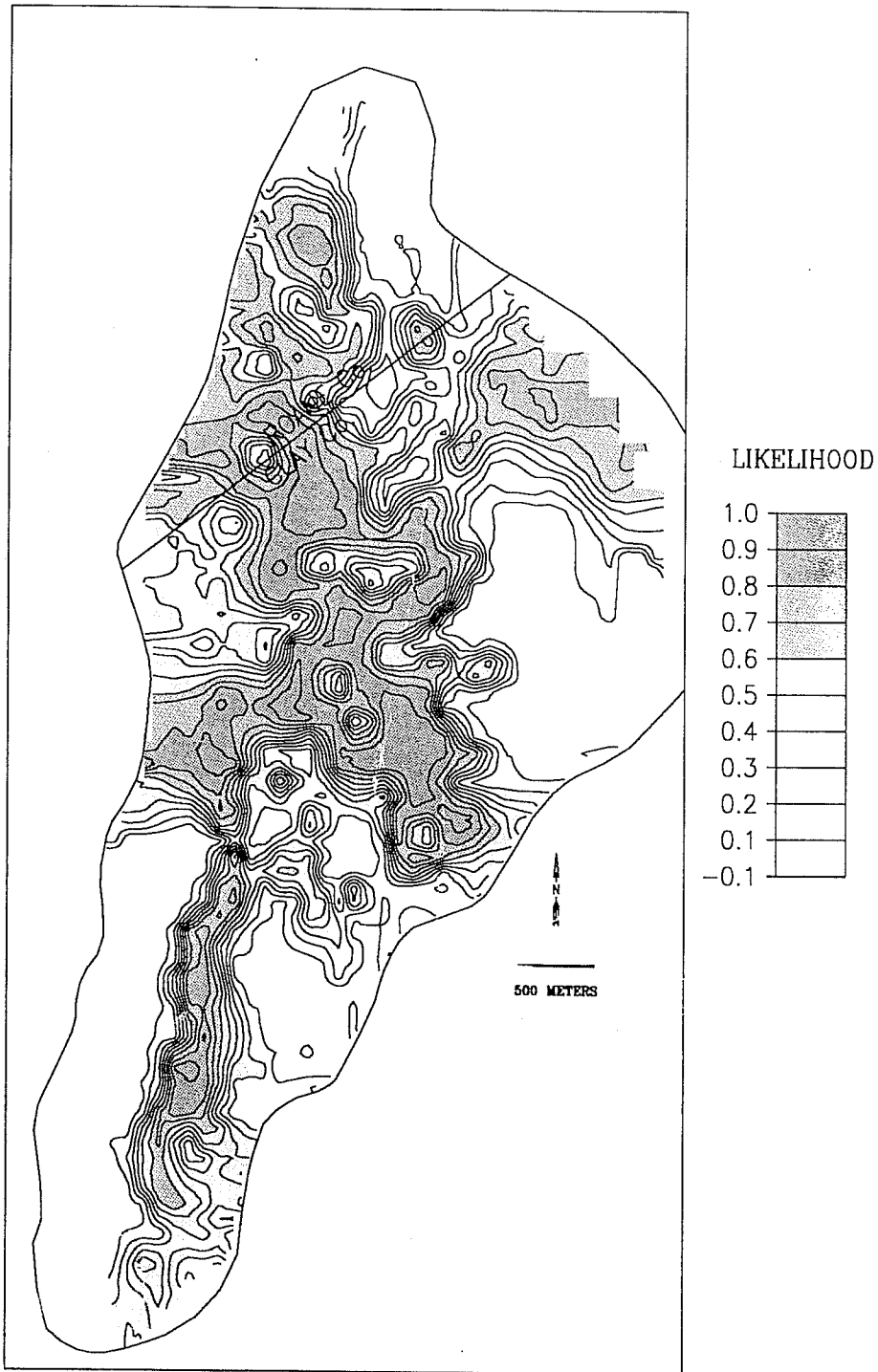


Figure 41. Estimated probability that initial potential in Granny Creek field exceeds 15 BOPD. Computed as the kriged estimate of 1-I15, where I15 is calculated as given in the text.

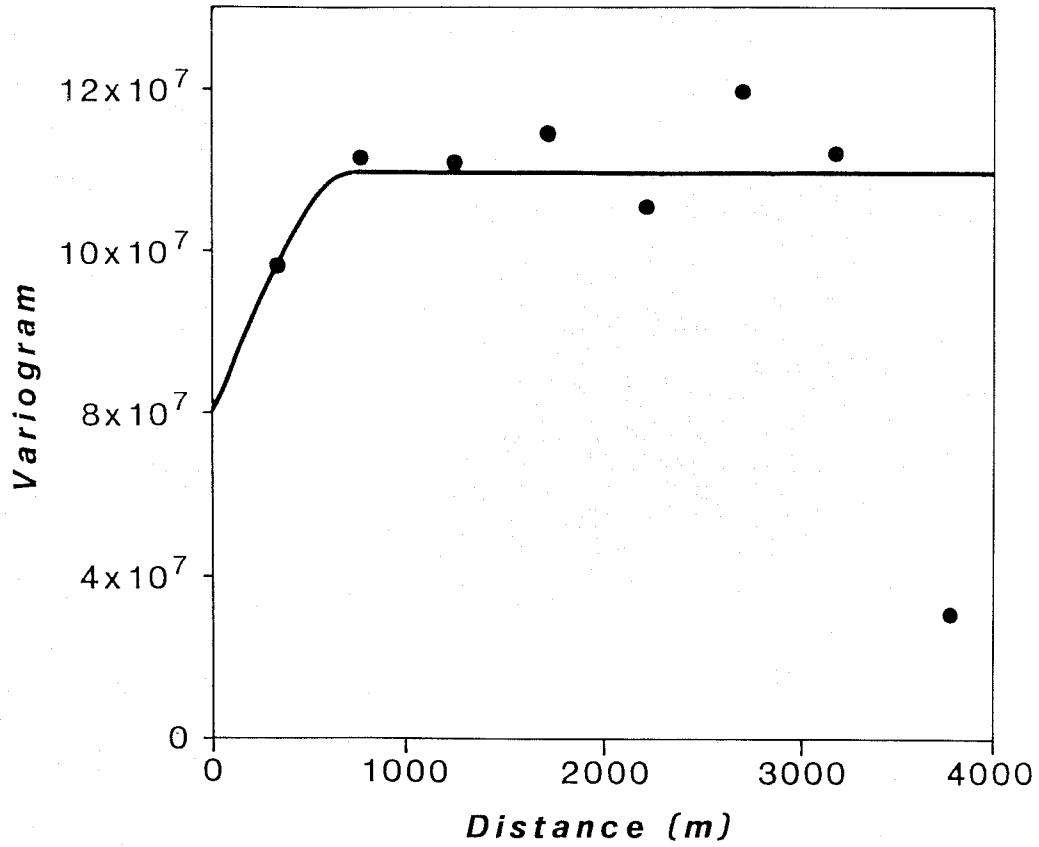


Figure 42. Omnidirectional variogram of cumulative ten-year oil production for wells in Granny Creek field. Observed variogram values are symbols, fitted model is solid line.

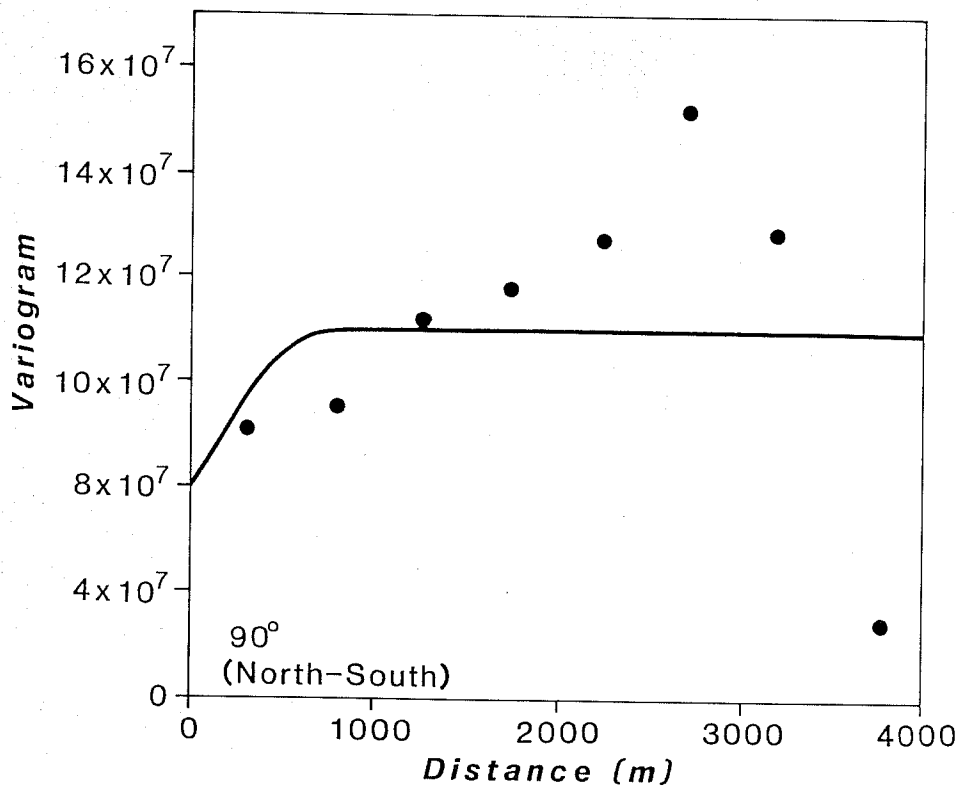
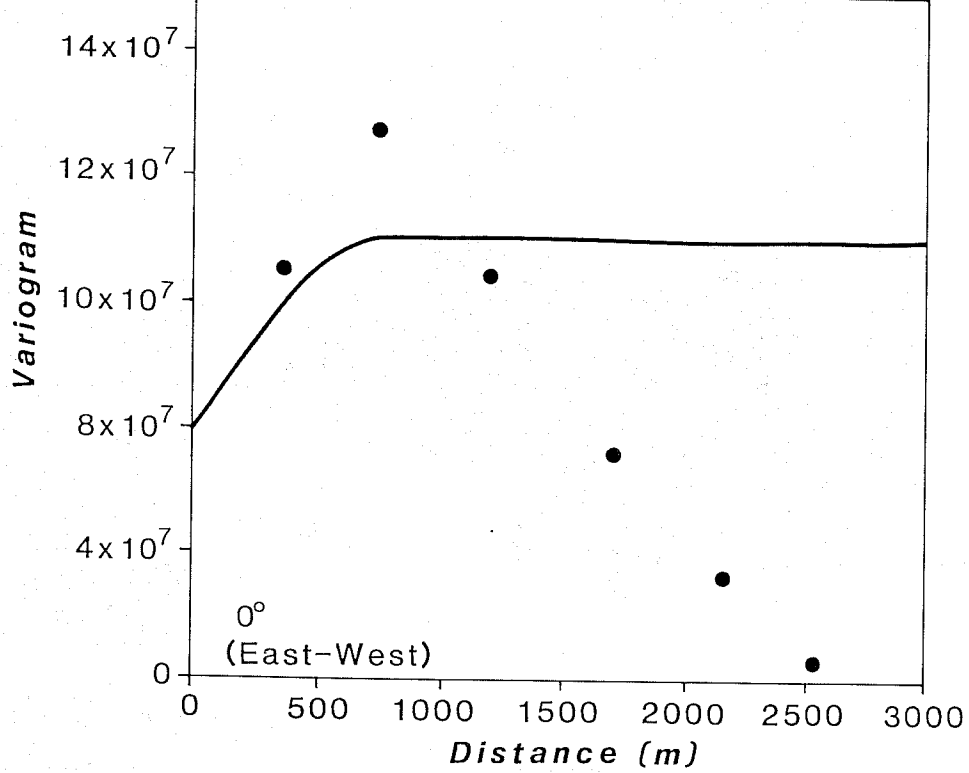


Figure 43. Directional variograms of cumulative ten-year oil production for wells in Granny Creek field. Observed variogram values are symbols; model fitted to omnidirectional variogram is shown as a solid line for contrast.

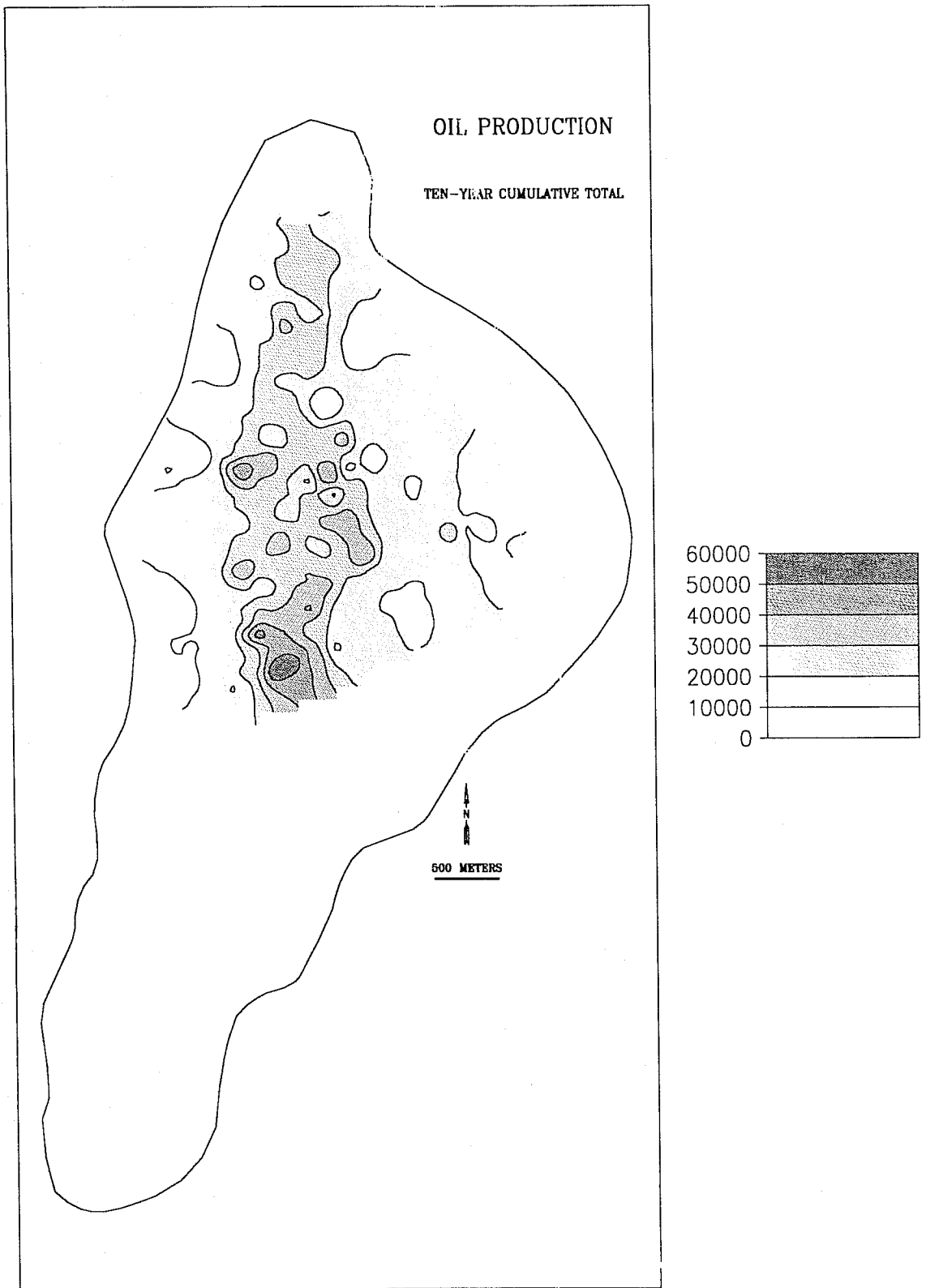


Figure 44. Kriged estimates of cumulative ten-year oil production in Granny Creek field, showing north-south trend.

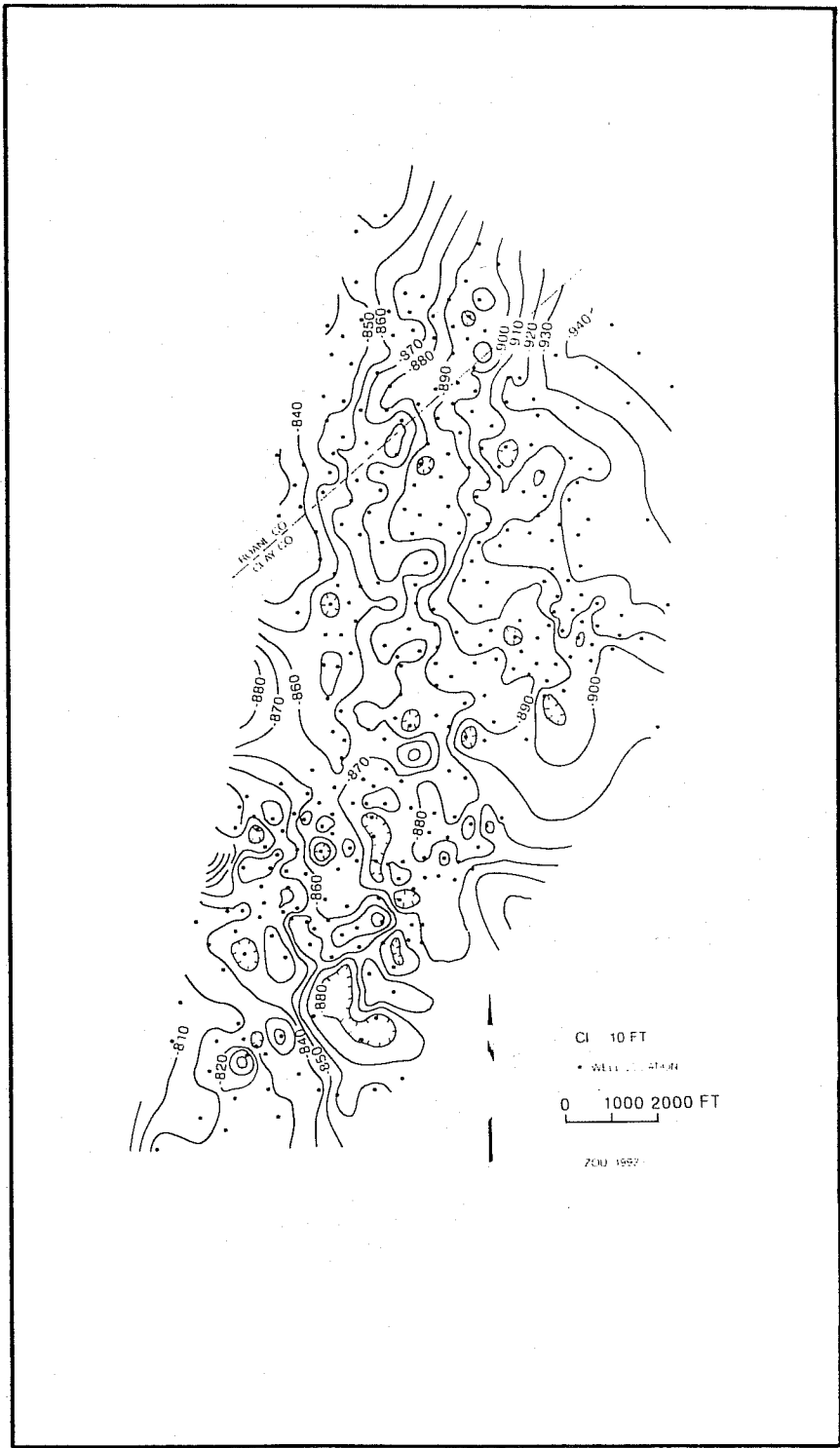


Figure 45. Structure of the unconformity at the base of the Greenbrier Group in Granny Creek field. This map is based on geophysical logs and contoured using the Map Contouring System software.

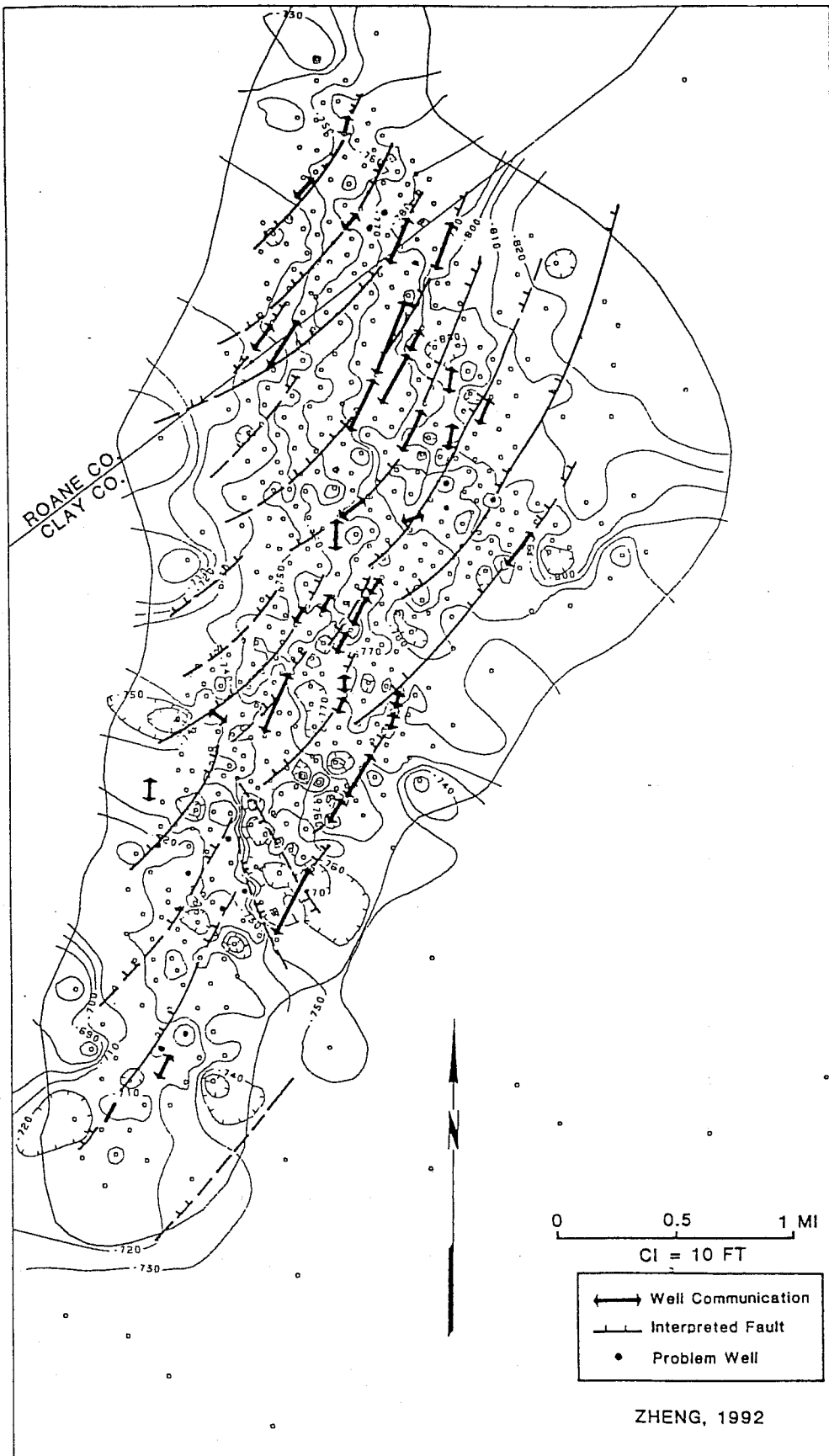


Figure 46. Preliminary interpretation showing possible relationships among geologic structure on top of the Greenbrier Group (Big Lime), possible faults and thief zones in the Granny Creek field. Structure is based on geophysical logs and drillers' logs, and contoured using Surface III software.

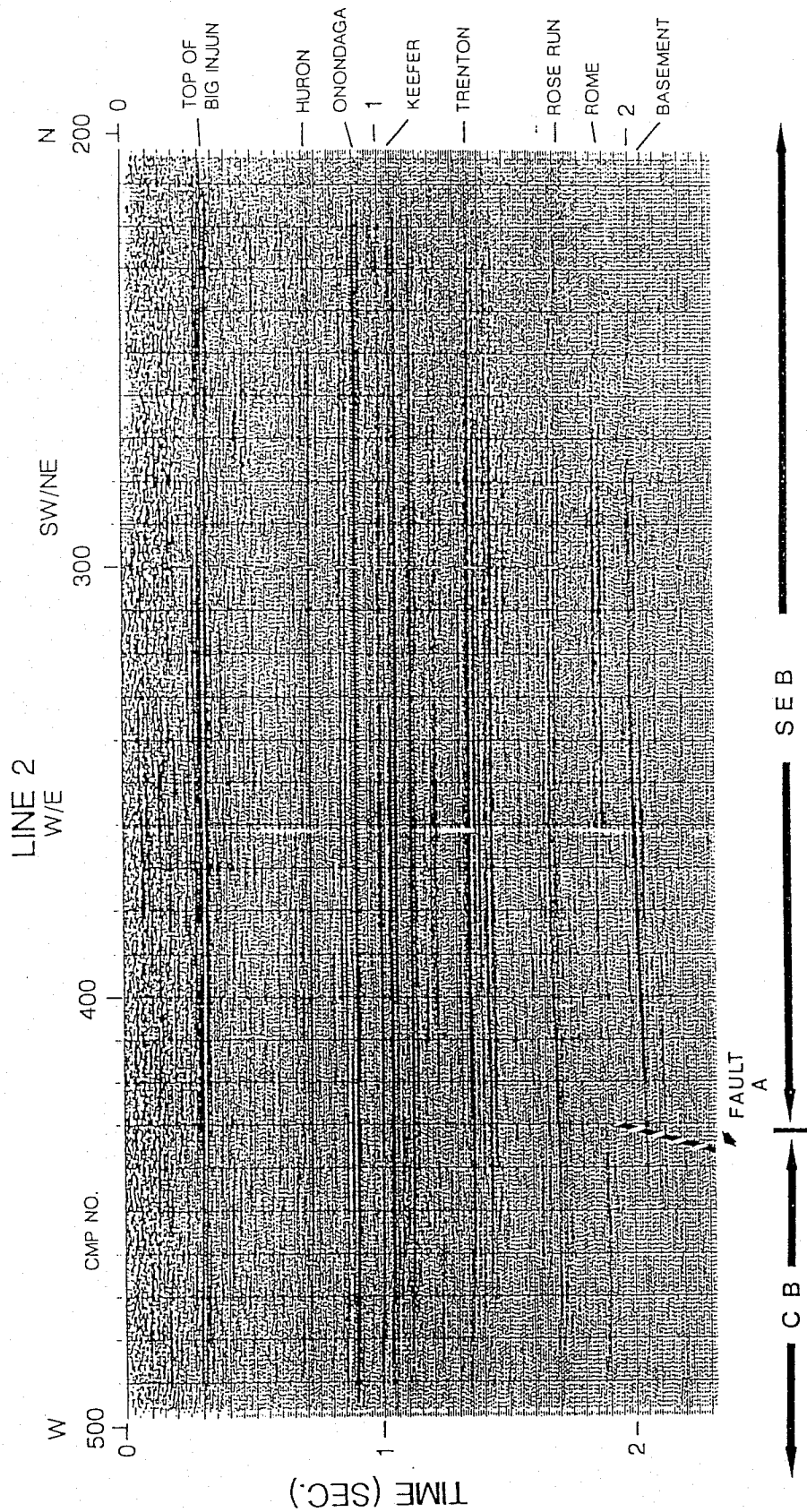


Figure 47. Reflection events, basement blocks and a major basement fault (A) interpreted on seismic line 2 over Granny Creek field.

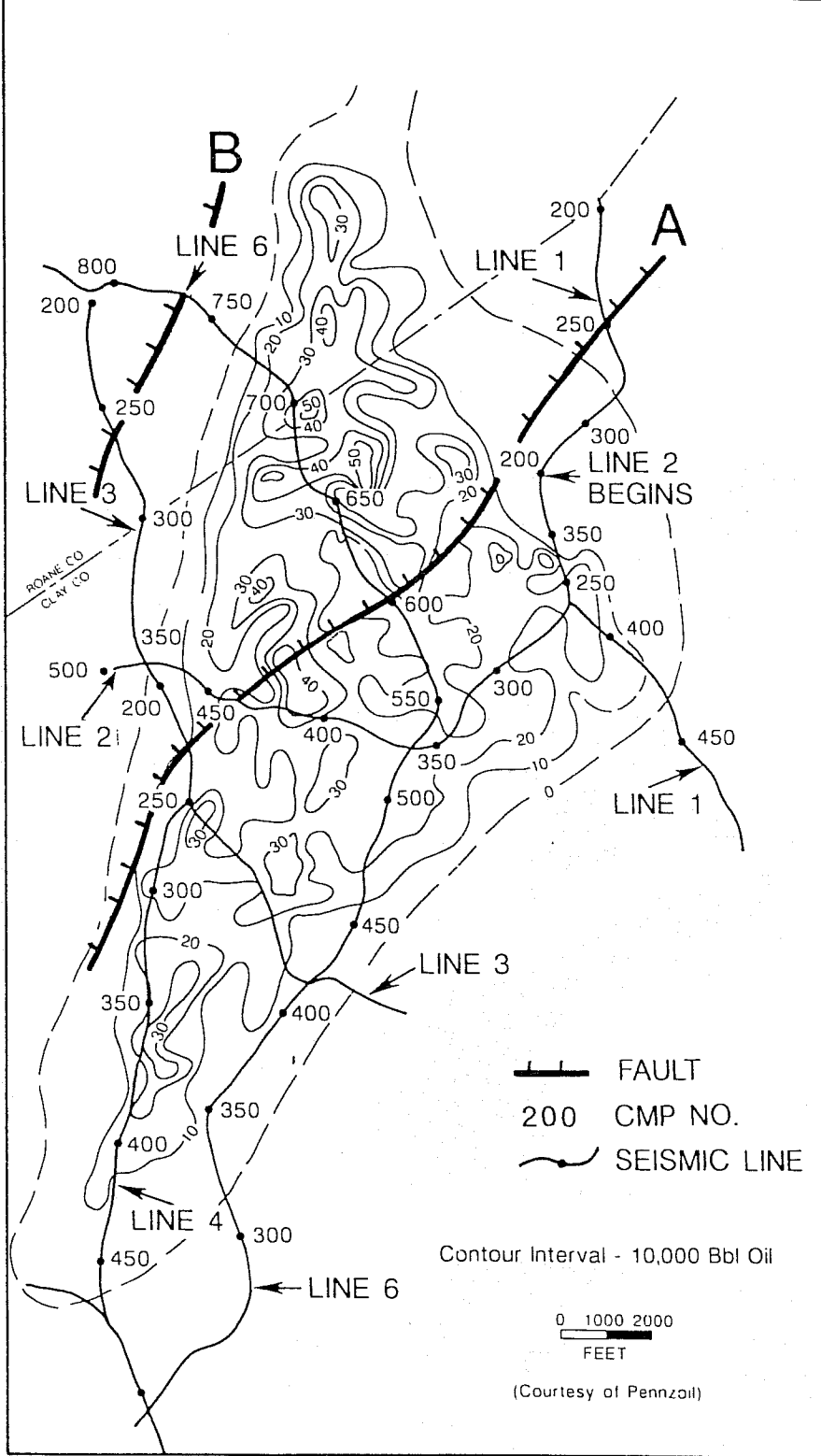


Figure 48. Locations of seismic lines superposed on map of cumulative production, Granny Creek field.

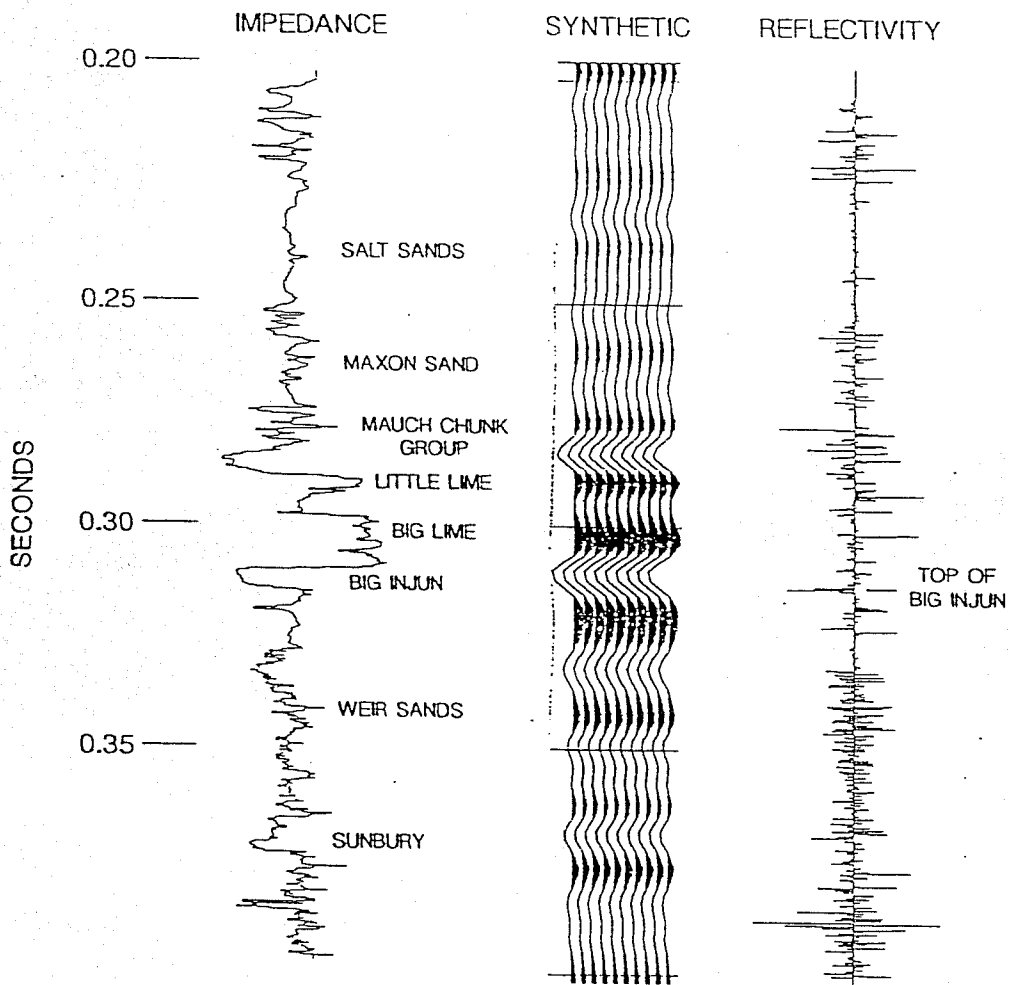


Figure 49. A synthetic seismogram from the Parker no. 21981 well is shown in the middle along with acoustic impedance (left) and reflectivity (right). Major stratigraphic intervals have been labeled.

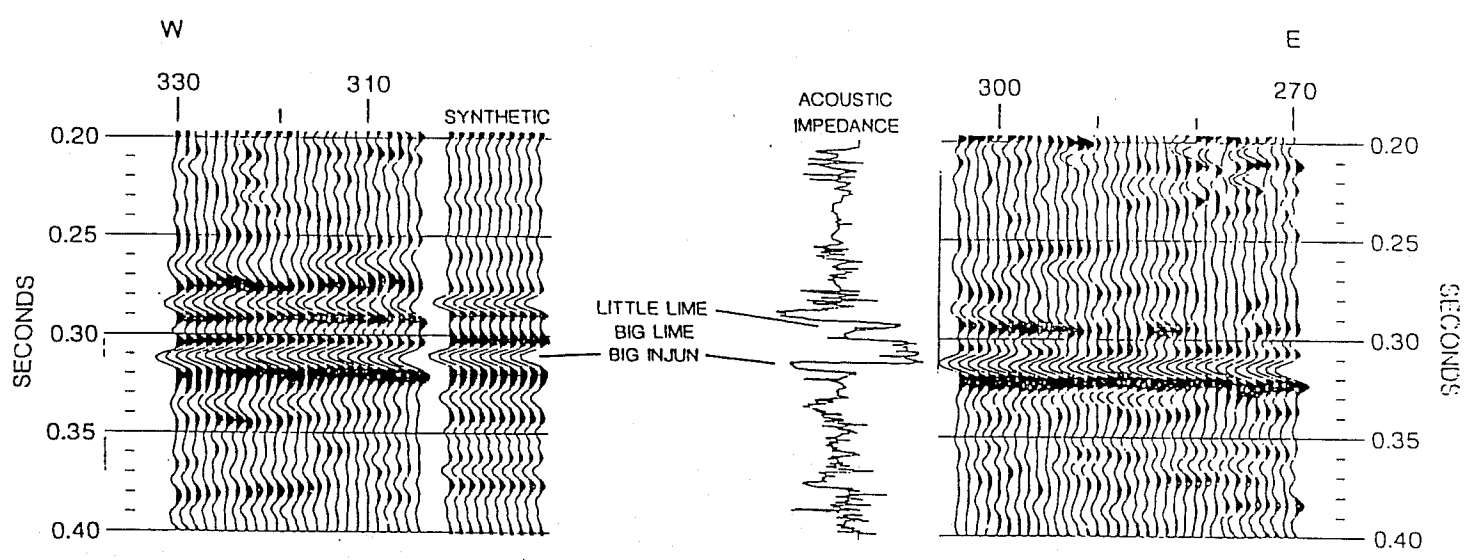


Figure 50. The synthetic seismogram of Figure 49 has been inserted into seismic traces from line 2 near the Parker no. 21981 well. Acoustic impedance log also has been inserted into the display.

LINE 1

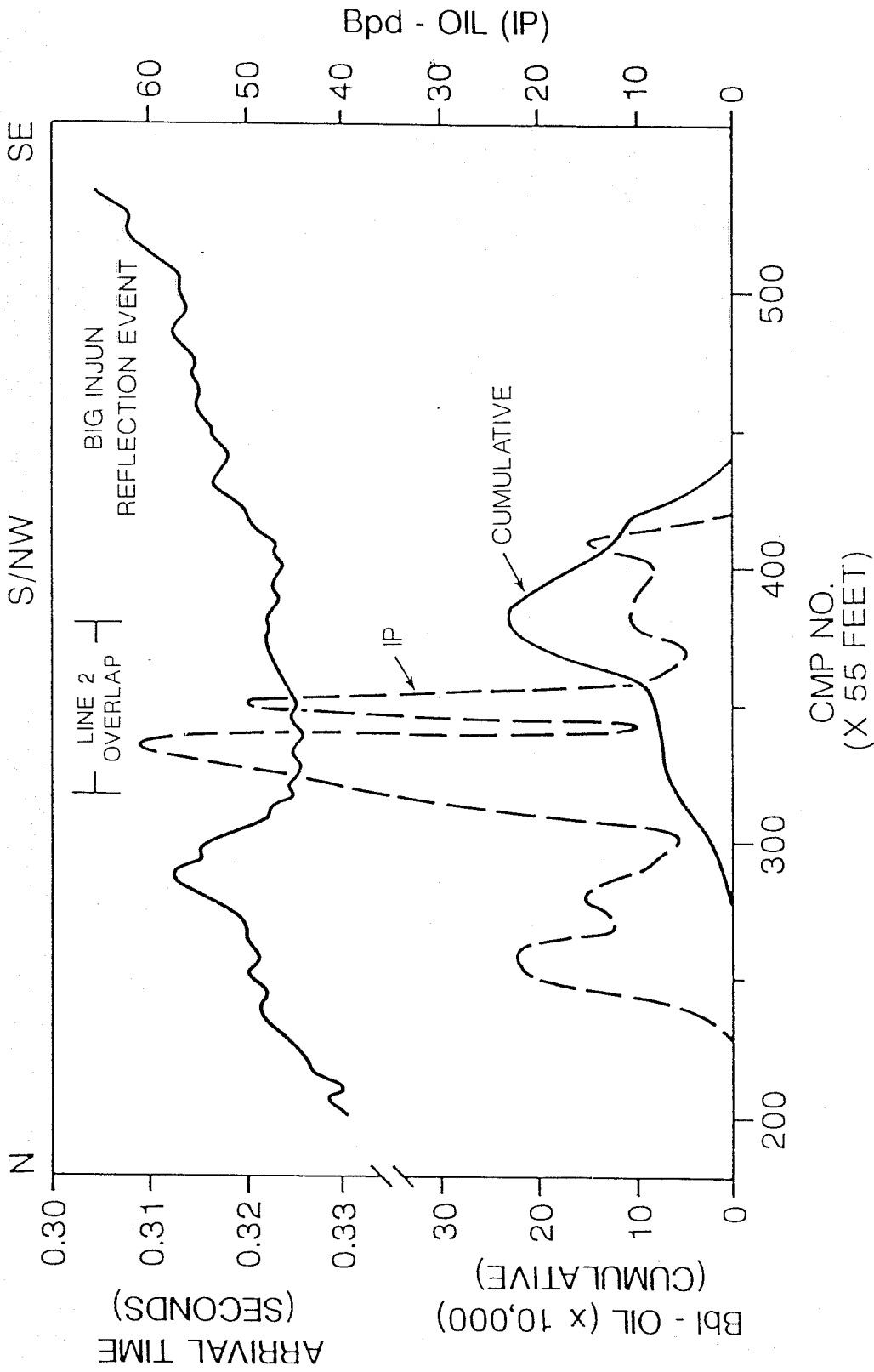


Figure 51. Reflection arrival times to the top of the Big Injun reflection event have been plotted along line 1 for comparison with cumulative and initial production data along the line.

LINE 2

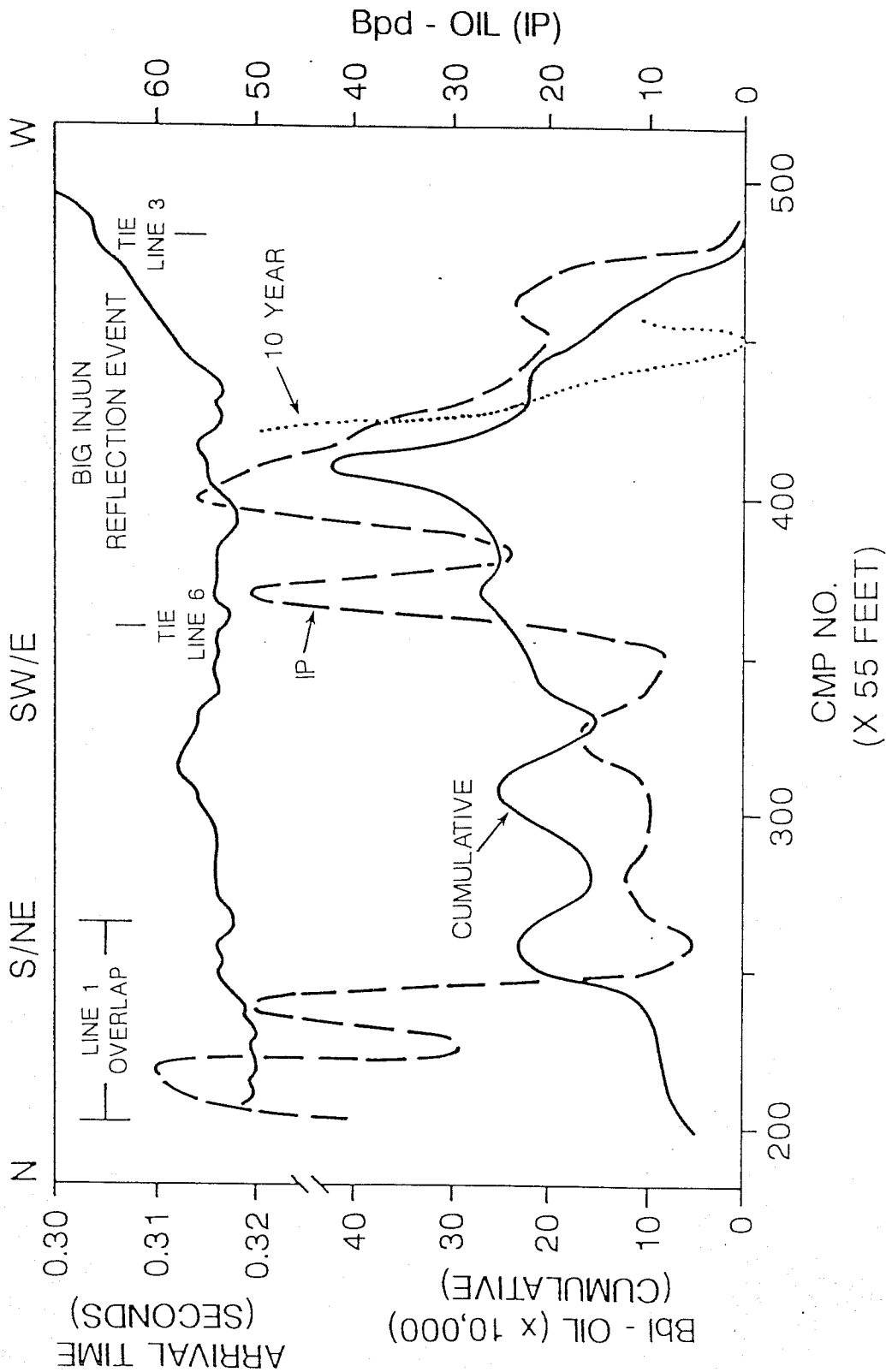


Figure 52. Reflection arrival times to the top of the Big Injun reflection event have been plotted along line 2 for comparison with cumulative and initial production data along the line. Ten year cumulative production data were available along the west end of the line.

LINE 3

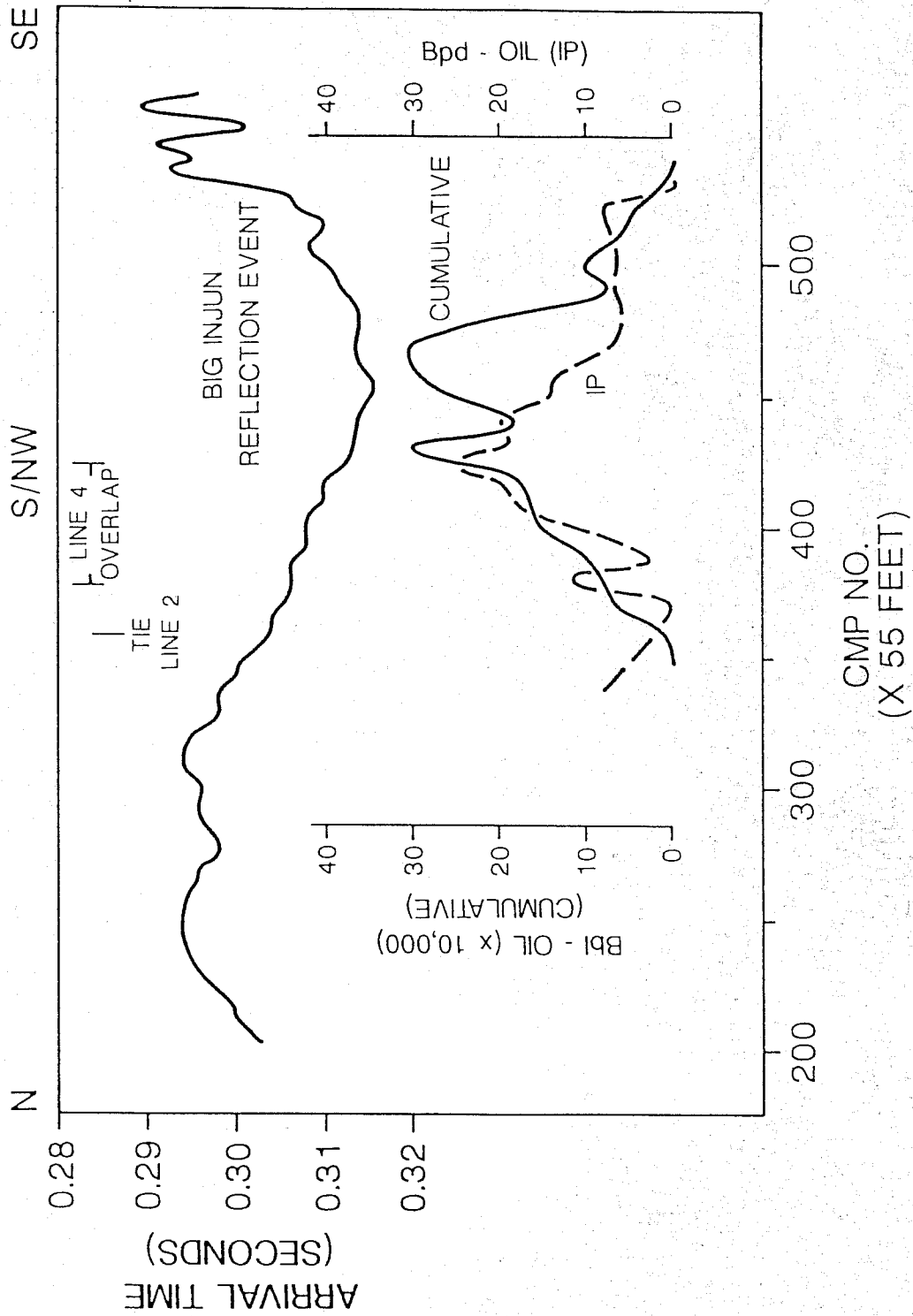


Figure 53. Reflection arrival times to the top of the Big Injun reflection event have been plotted along line 3 for comparison with cumulative and initial production data along the line.

LINE 4

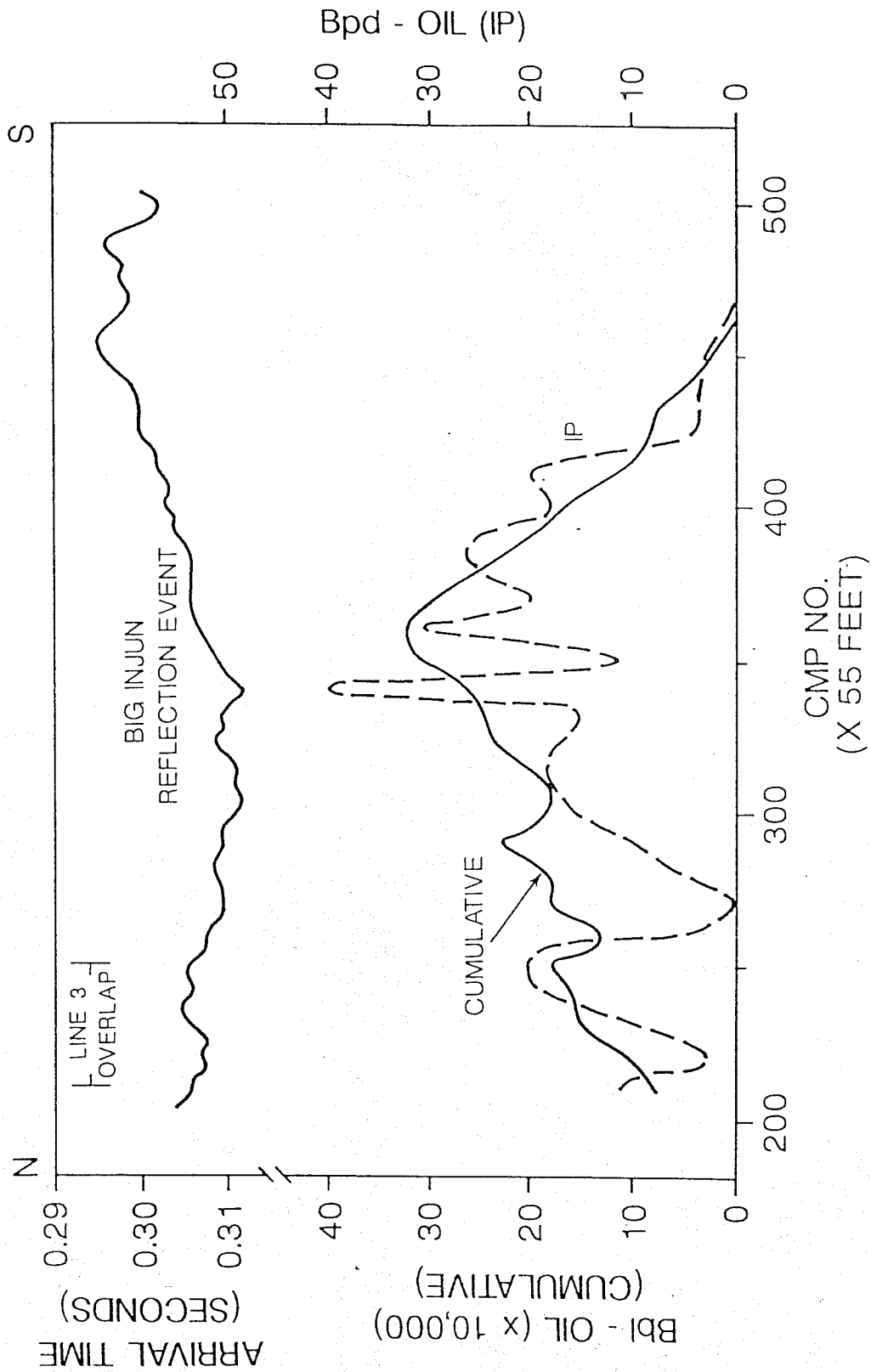


Figure 54. Reflection arrival times to the top of the Big Injun reflection event have been plotted along line 4 for comparison with cumulative and initial production data along the line.

LINE 6

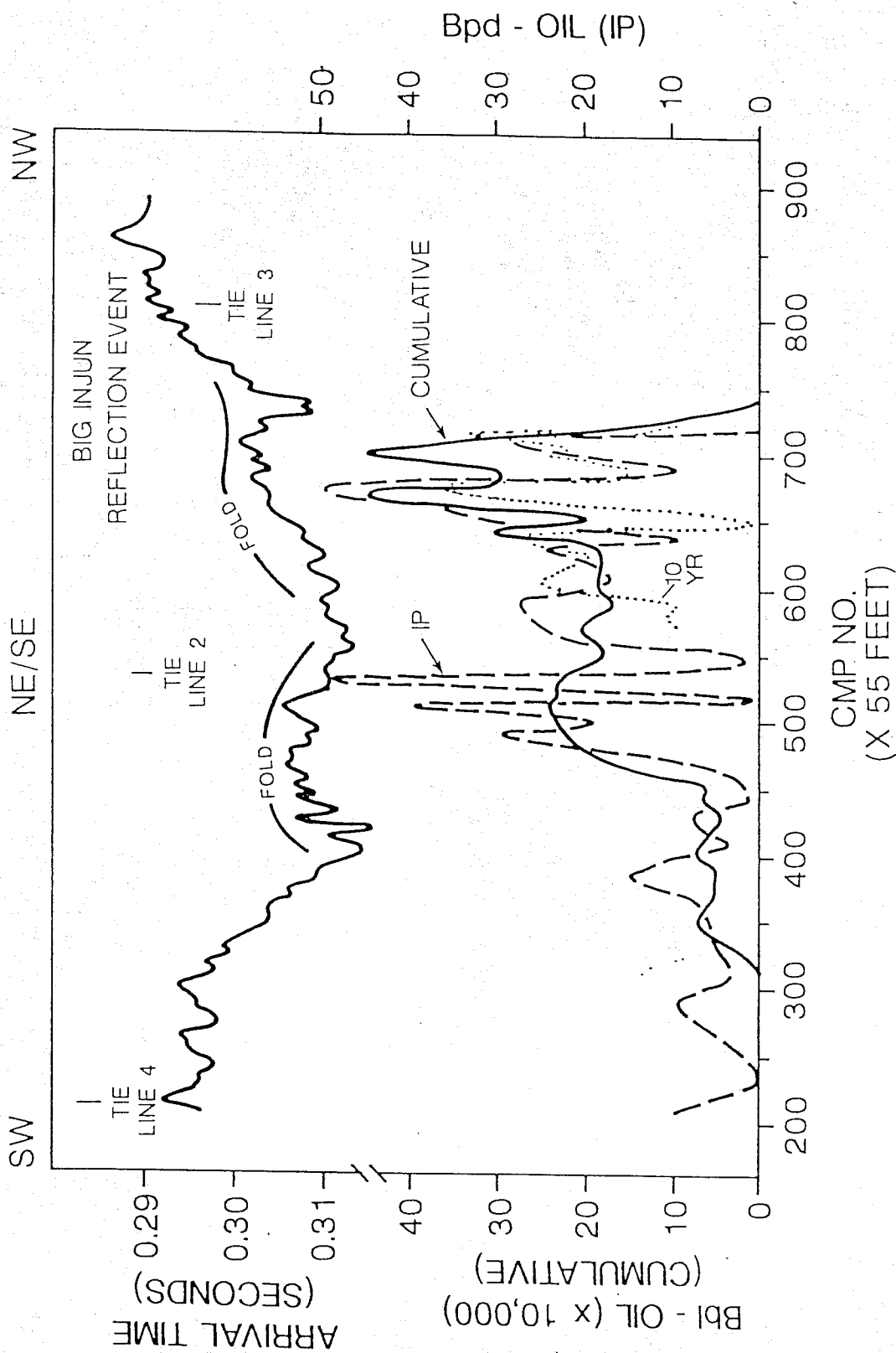


Figure 55. Reflection arrival times to the top of the Big Injun reflection event have been plotted along line 6 for comparison with cumulative and initial production data along the line. Ten year cumulative production data were available along the northwestern end of the line.

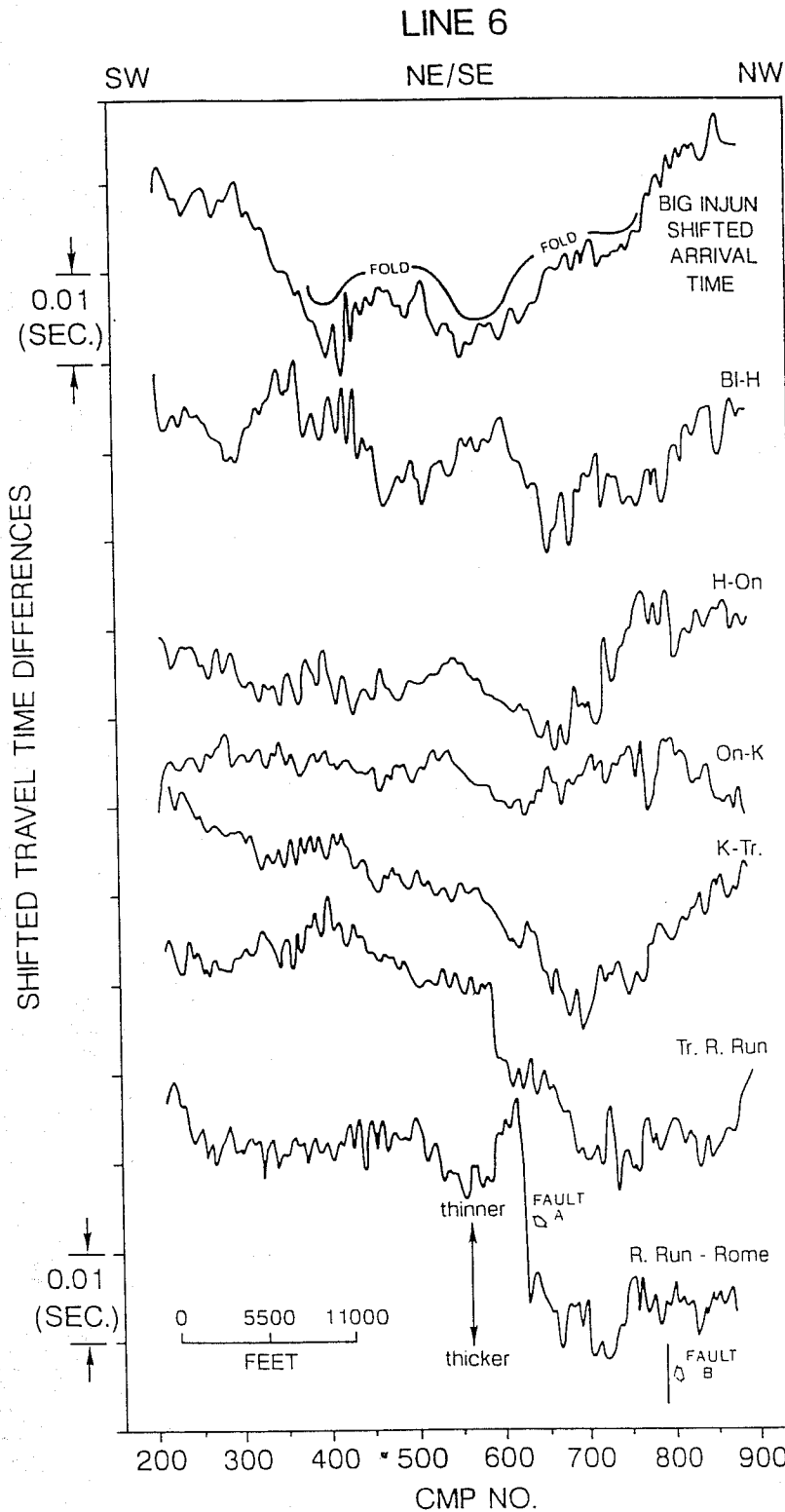


Figure 56. Shifted traveltimes are shown for major stratigraphic subdivisions observed in the seismic section along line 6. Arrival time of the Big Injun event is plotted across the top for comparison. Time scale is not continuous. BI-H = Big Injun-to-Huron. H-On = Huron-to-Onondaga. On-K = Onondaga-to-Keefer. K-Tr = Keefer-to-Trenton. Tr-R.Run = Trenton-Rose Run. R.Run-Rome = Rose Run-to-Rome. Relative traveltimes increase downward.

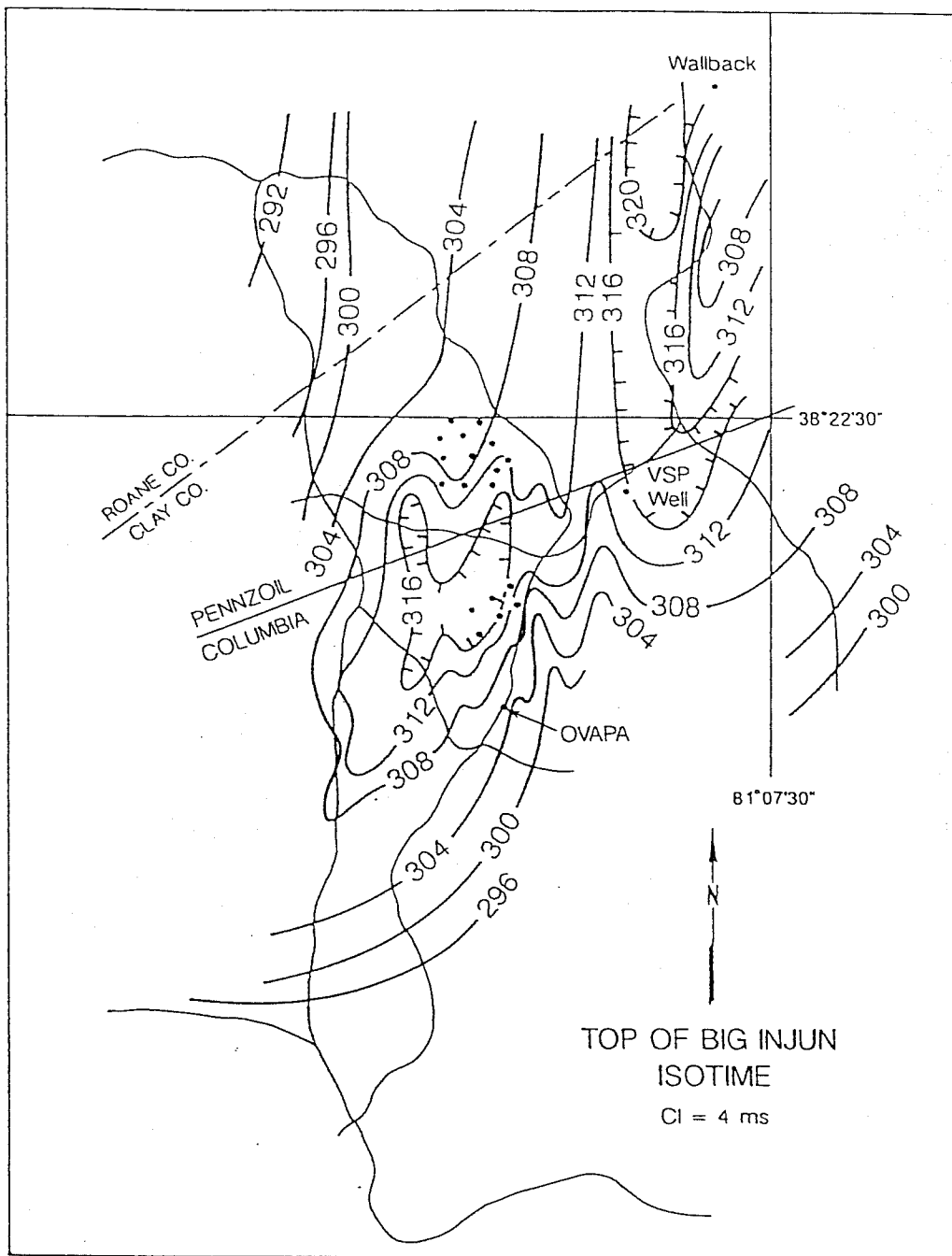


Figure 57. Isotime map for the peak of the negative reflection event associated with the top of the Big Injun sandstone.

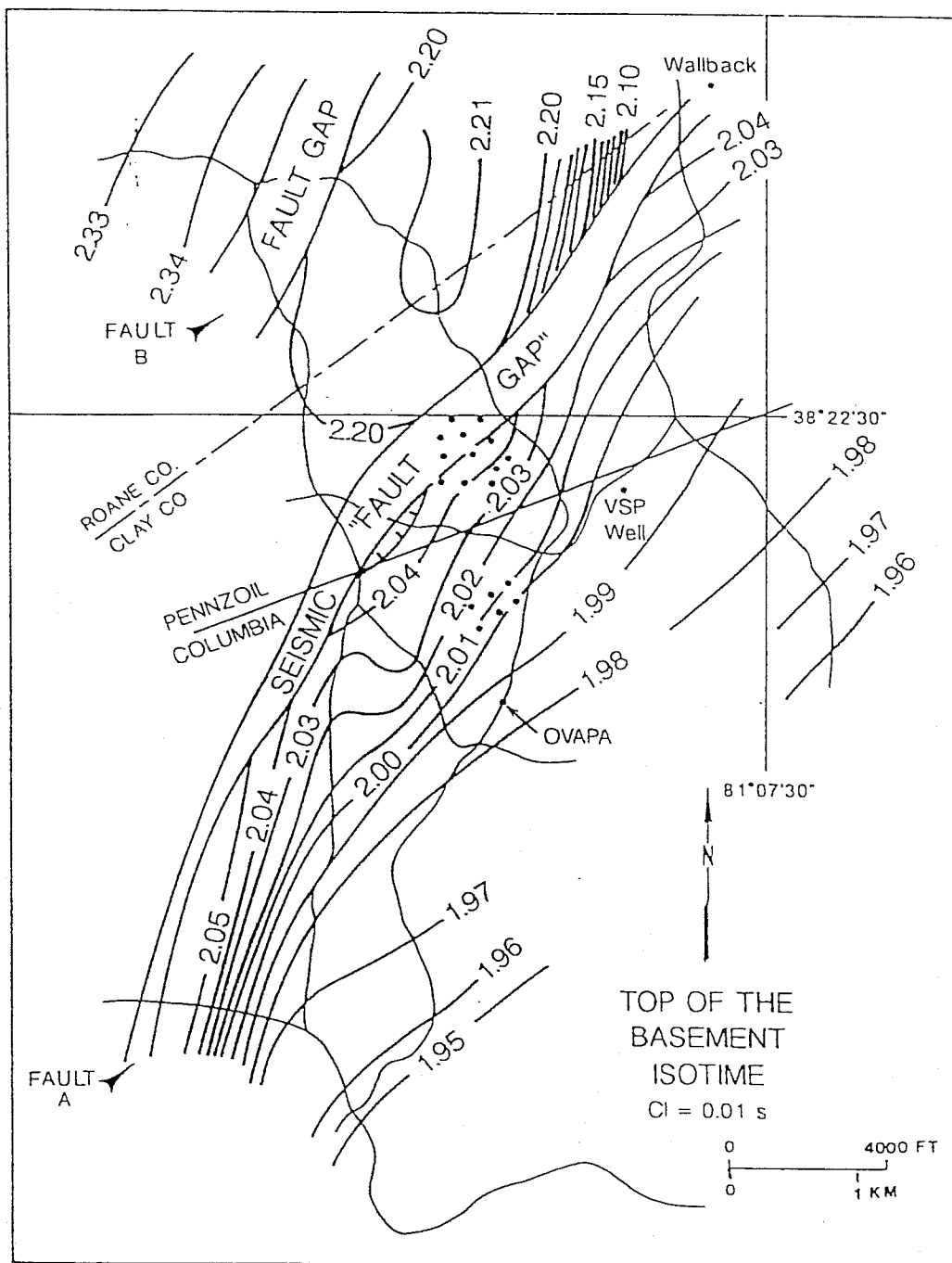


Figure 58. Isotime map for the reflection event associated with acoustic basement.

LINE 2

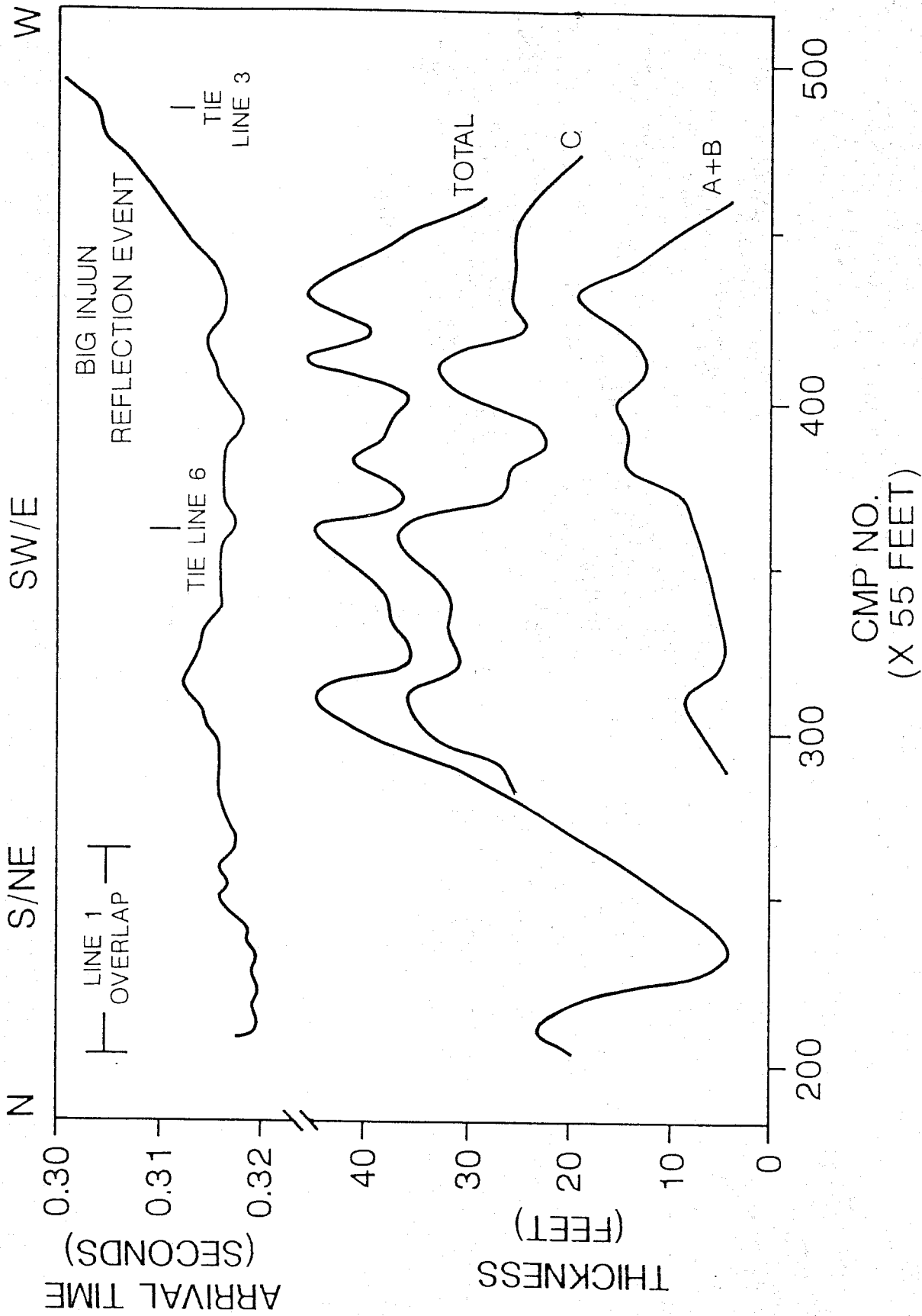


Figure 59. Thickness of the A plus B, and C subdivisions of the Big Injun sandstone along with their total thickness are plotted for comparison to reflection arrival time variations for the Top-of-the-Big Injun event along line 2.

LINE 6

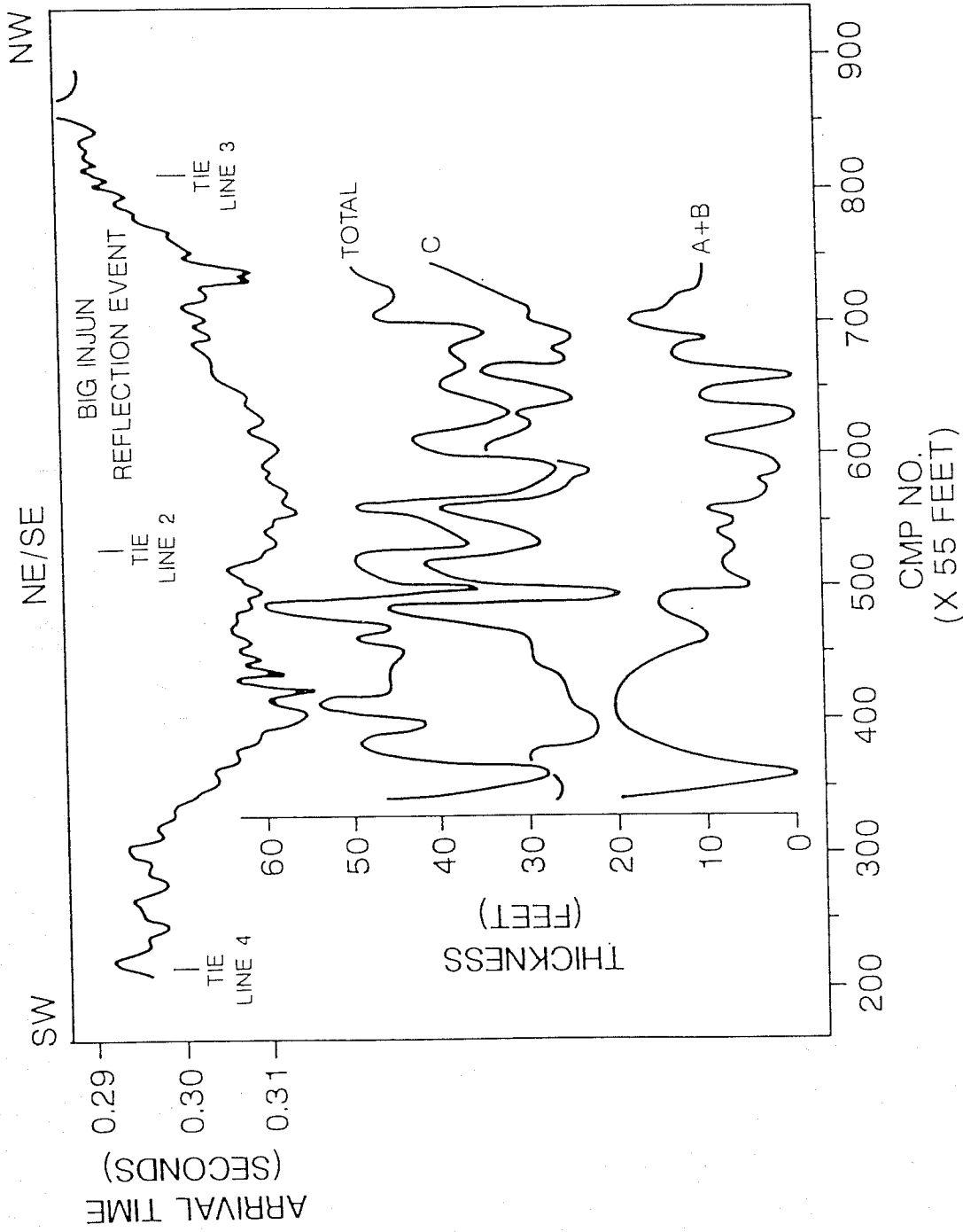


Figure 60. Thickness of the A and B, and C subdivisions of the Big Injun sandstone along with their total thickness are plotted for comparison to reflection-arrival-time variations for the Top-of-the-Big Injun event along line 6.

ORIGINAL LINE 2

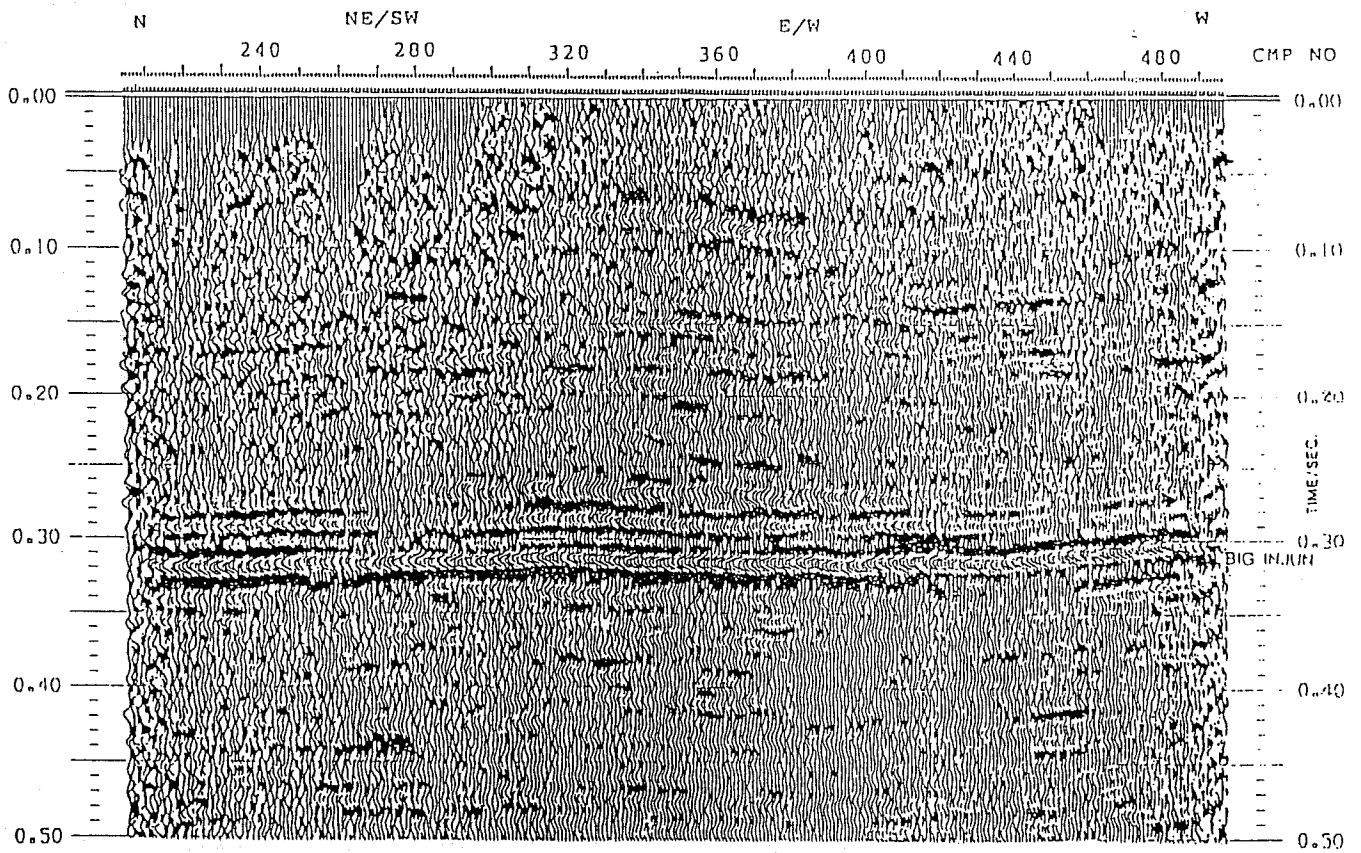


Figure 61. The upper half second of data along line 2 including the Big Injun reflection event at approximately 0.31 seconds was processed by Lauren Geophysical Inc.

REPROCESSED LINE 2

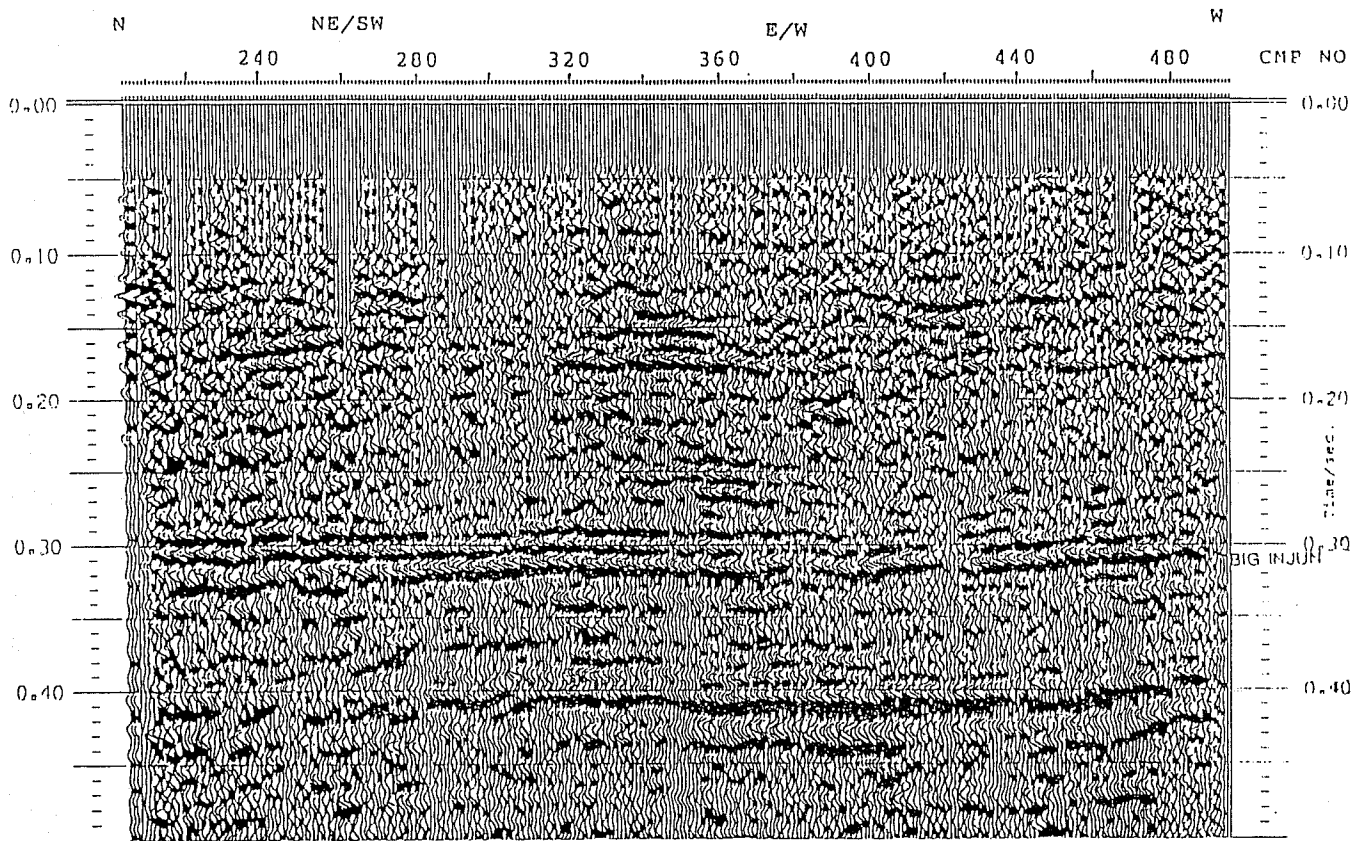


Figure 62. The upper half second of data along line 2 including the Big Injun reflection event at approximately 0.31 seconds after reprocessing (Zheng and Wilson, 1992).

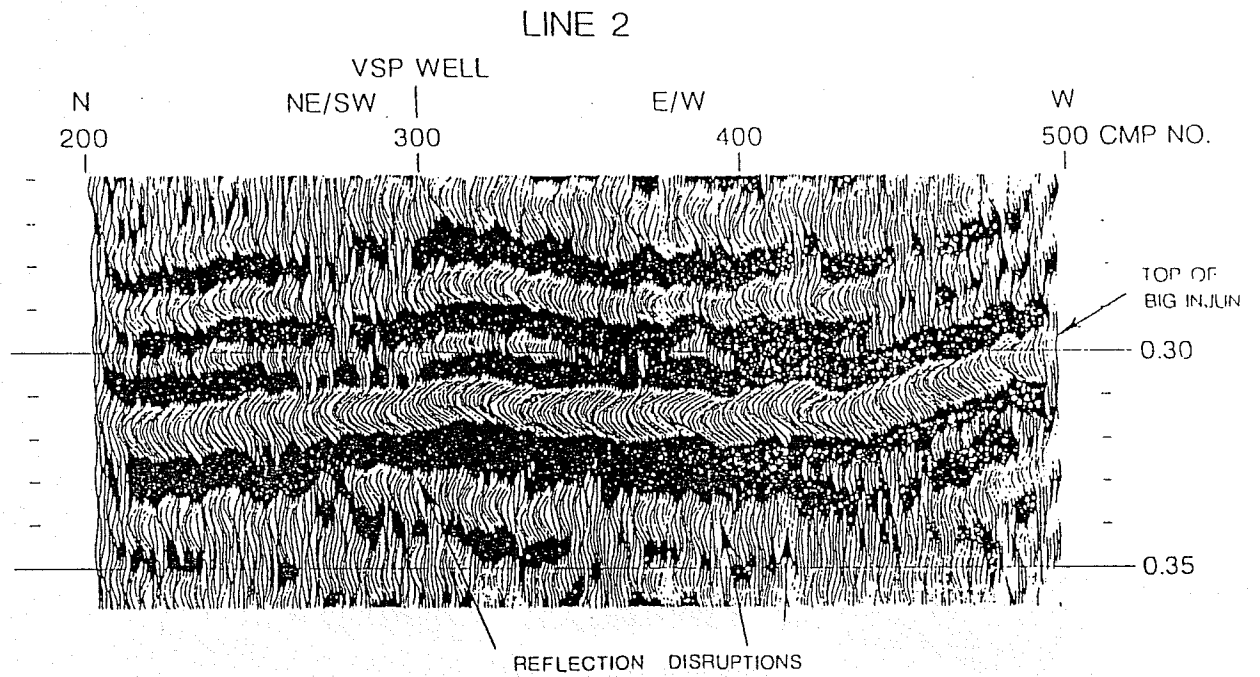


Figure 63. Close-up view of the seismic data along line 2 shown in Figure 60 in the vicinity of the Big Injun reflection processed by Lauren Geophysical Inc.

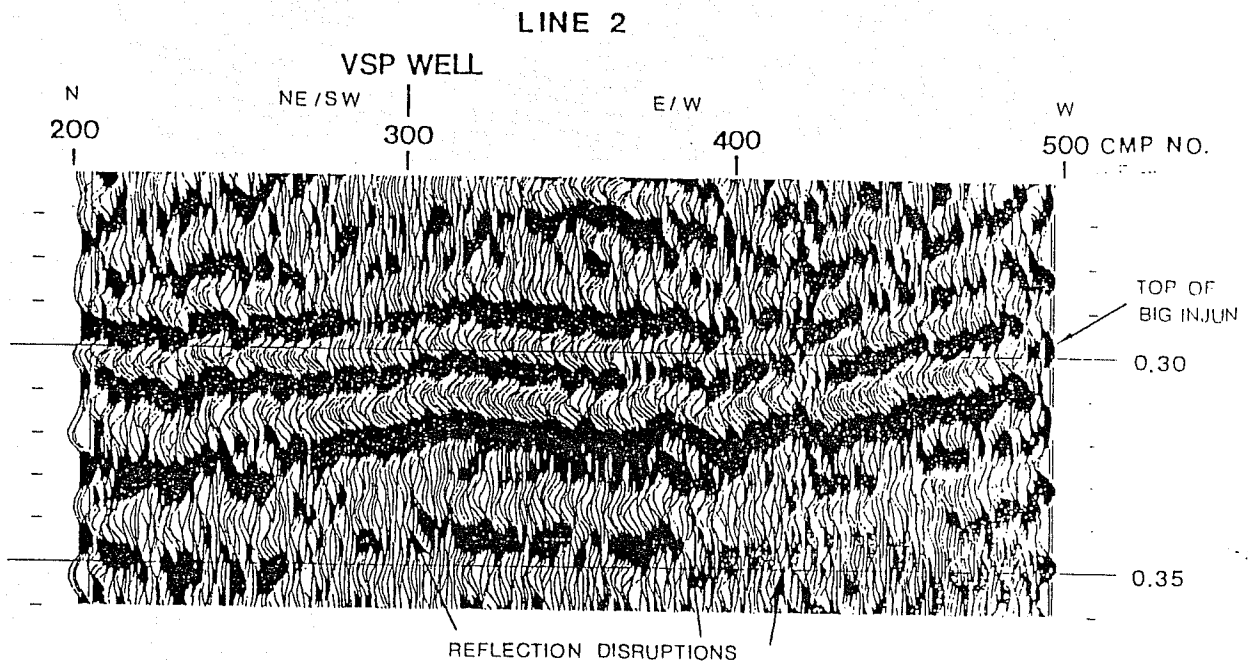


Figure 64. Close-up view of the seismic data along line 2 shown in Figure 61 in the vicinity of the Big Injun reflection event after processing (Zheng and Wilson, 1992).

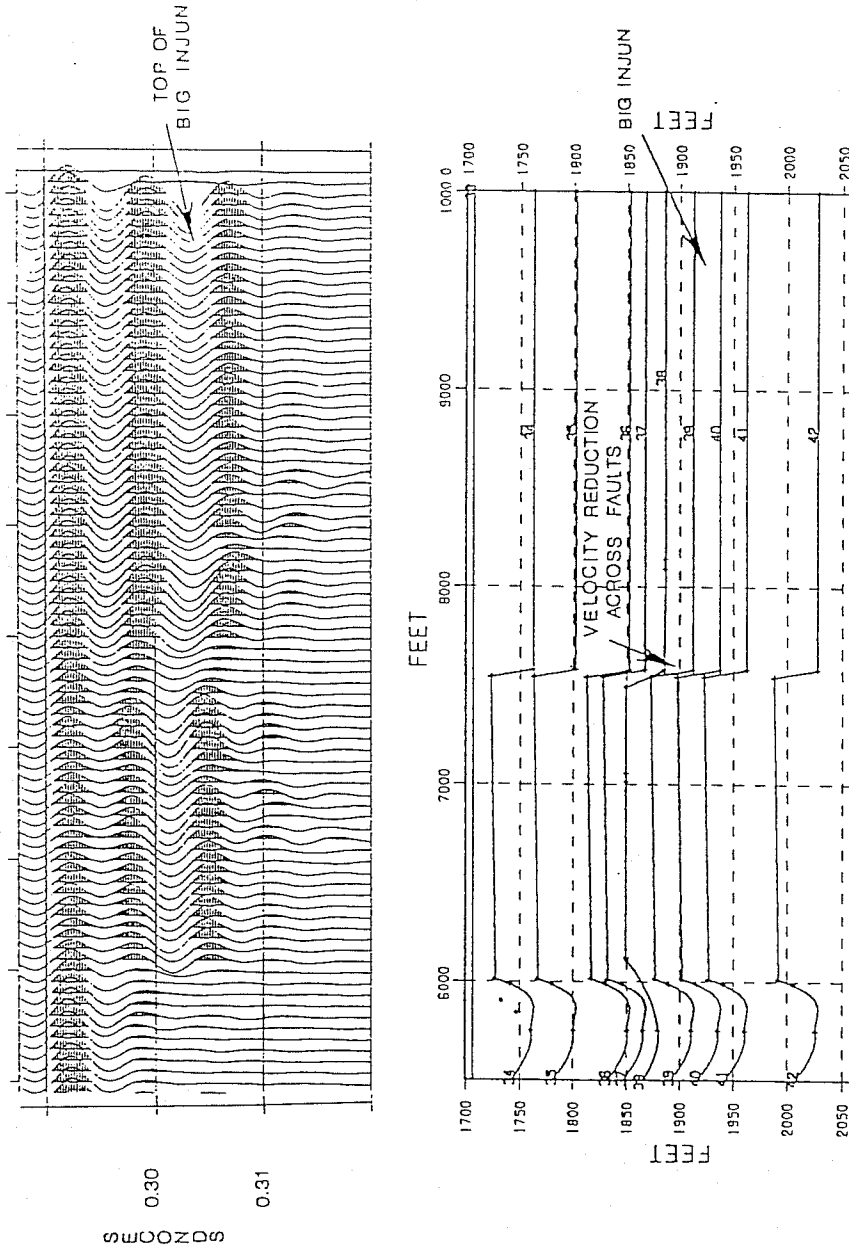


Figure 65. Depth model (bottom) and synthetic (top) showing the combined effect of faults with acoustic impedance reductions across them.

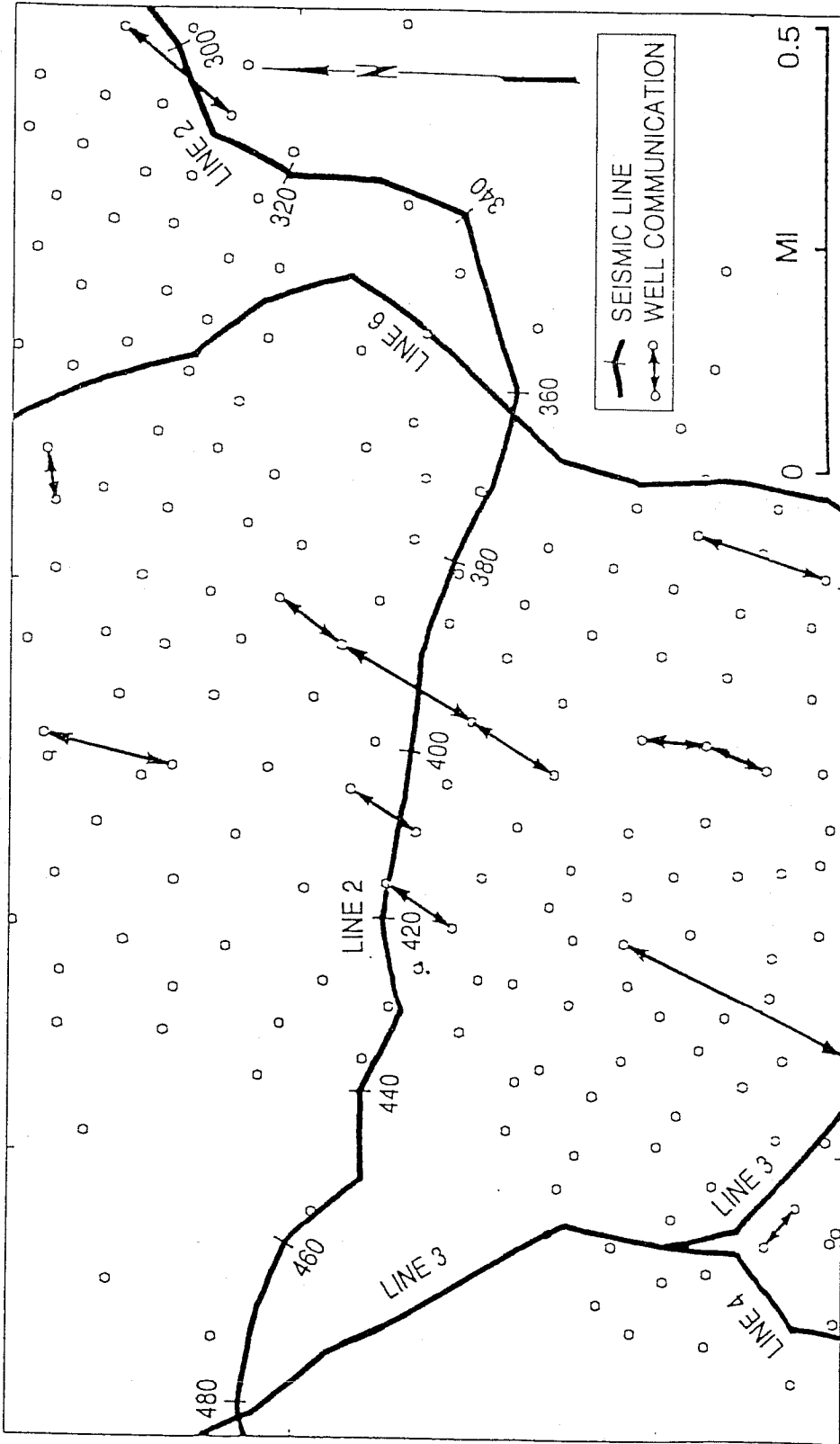


Figure 66. Midpoint map for line 2 along its western end shows the locations of wells where communication problems were encountered. Communication problems encountered along line 2 near midpoints 395 and 417 coincide closely with reflection disruptions and a small fold in the composite Big Injun reflection event.

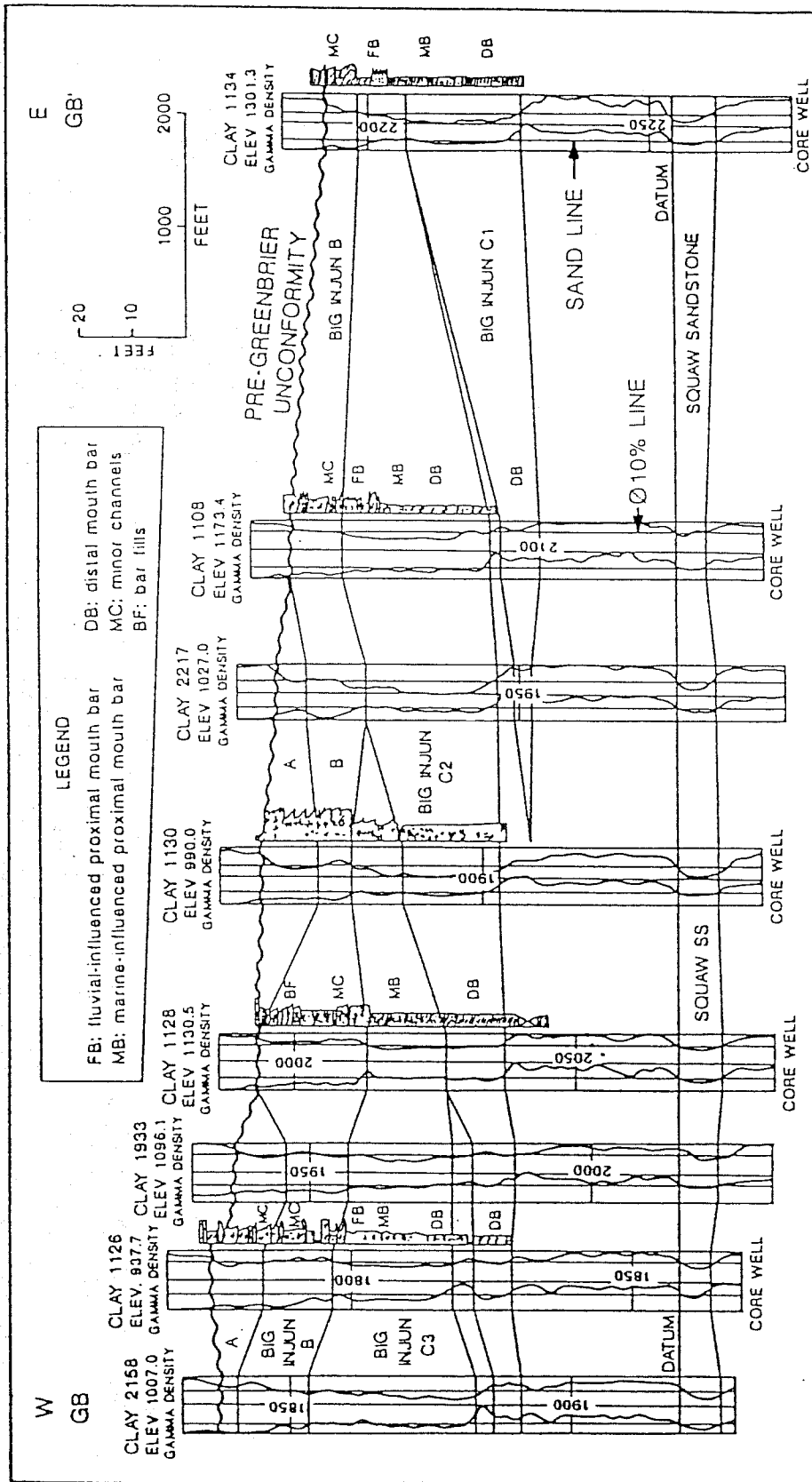


Figure 67. Stratigraphic cross section GB-GB' illustrates members, tongues, and subfacies of Pocono Big Injun sandstone. Squaw is datum; pre-Greenbrier unconformity caps the section. Cored wells display columnar sections alongside gamma-ray bulk-density log signatures. Members A, B, and C are recognized from logs as well as tongues C1, C2, and C3. Subfacies of distal and proximal river-mouth bars, and overlying bedload channel deposits of A and B members are recognized in cores.

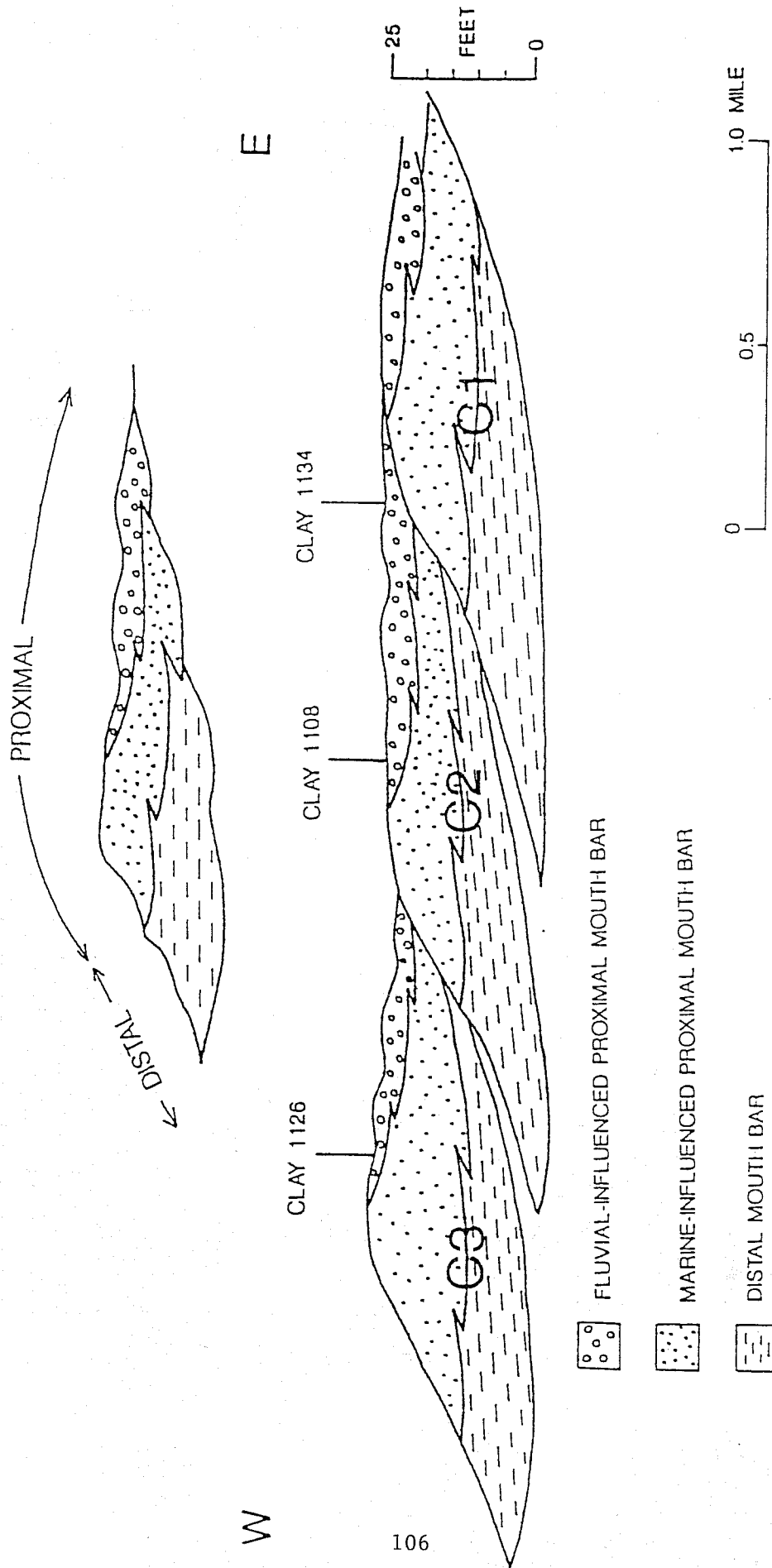


Figure 68. Delta-front facies of the C member of the Pocono Big Injun sandstone along profile GB-GB'.

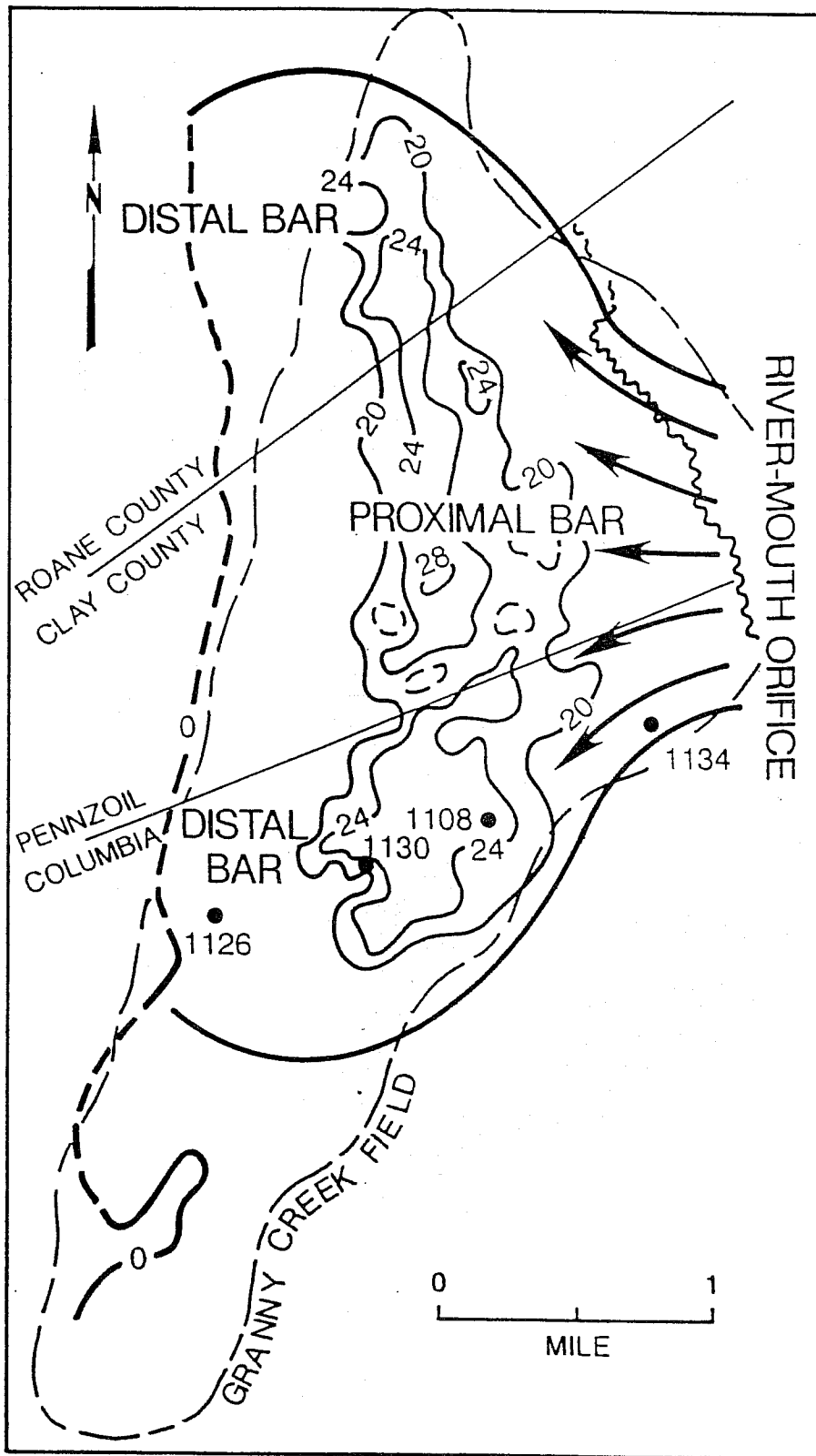


Figure 69. Isopach map of the C2 tongue with the subfacies of an interpreted river-mouth bar labeled. Cored wells of profile GB-GB' are located. Outline of Granny Creek field provides scale for depositional environments.

CLAY 1130

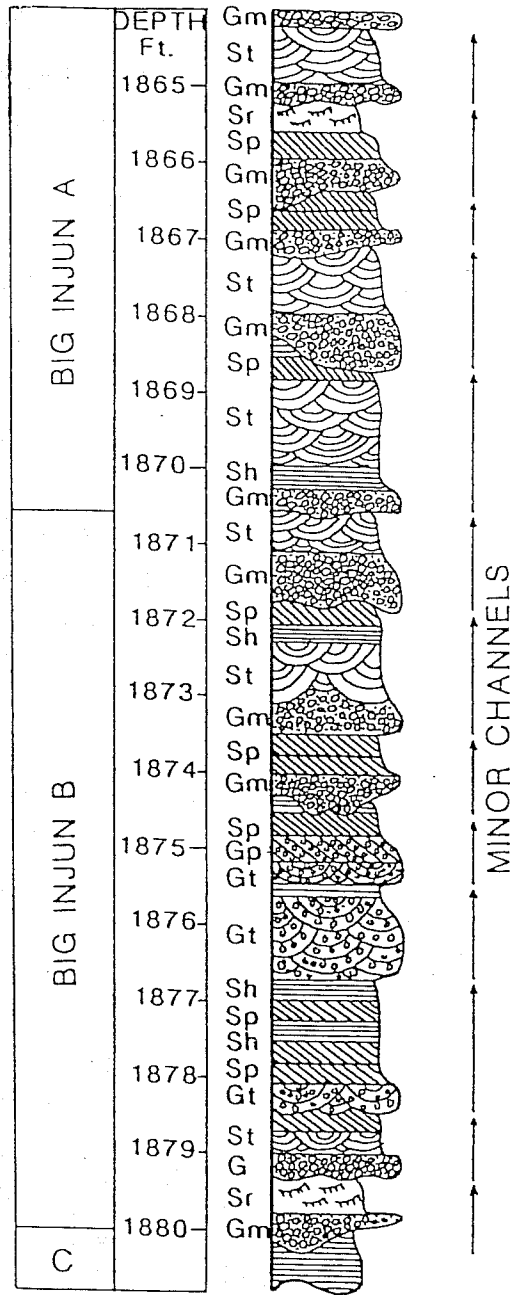


Figure 70. Lithologic description of the Pocono Big Injun sandstone from core of well 1130 (located on Figures 68 and 69) from Granny Creek field. The sequence suggests a bedload channel fill deposit.

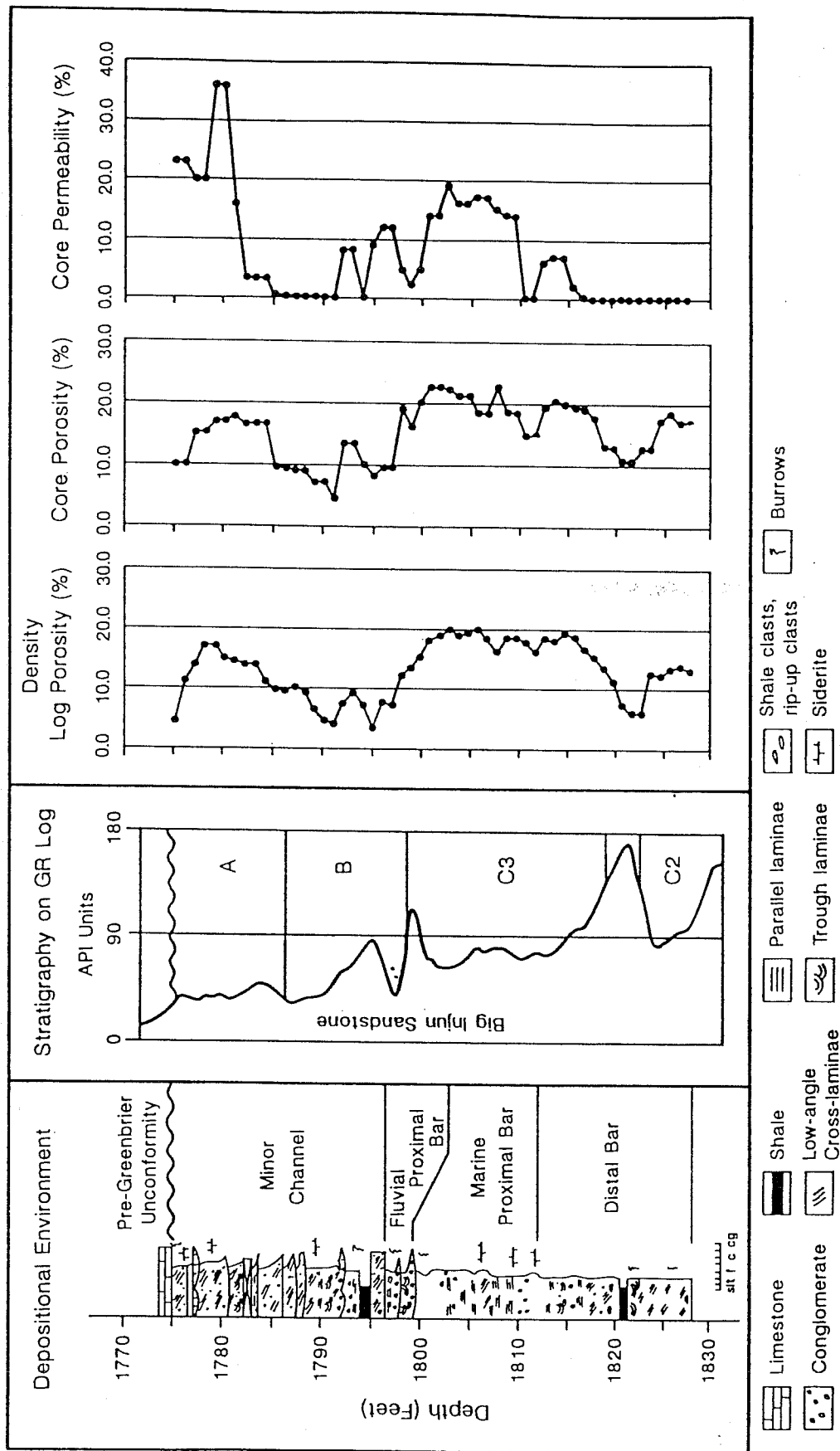


Figure 71. Depositional environments (subfacies) are interpreted from textures, sedimentary structures and fossils of core from well 1126 and related to the stratigraphic units of the Big Injun sandstone and their porosity and permeability values. Refer also to figures 67, 68, 69, 74, and 75 for additional information involving data from well 1126.

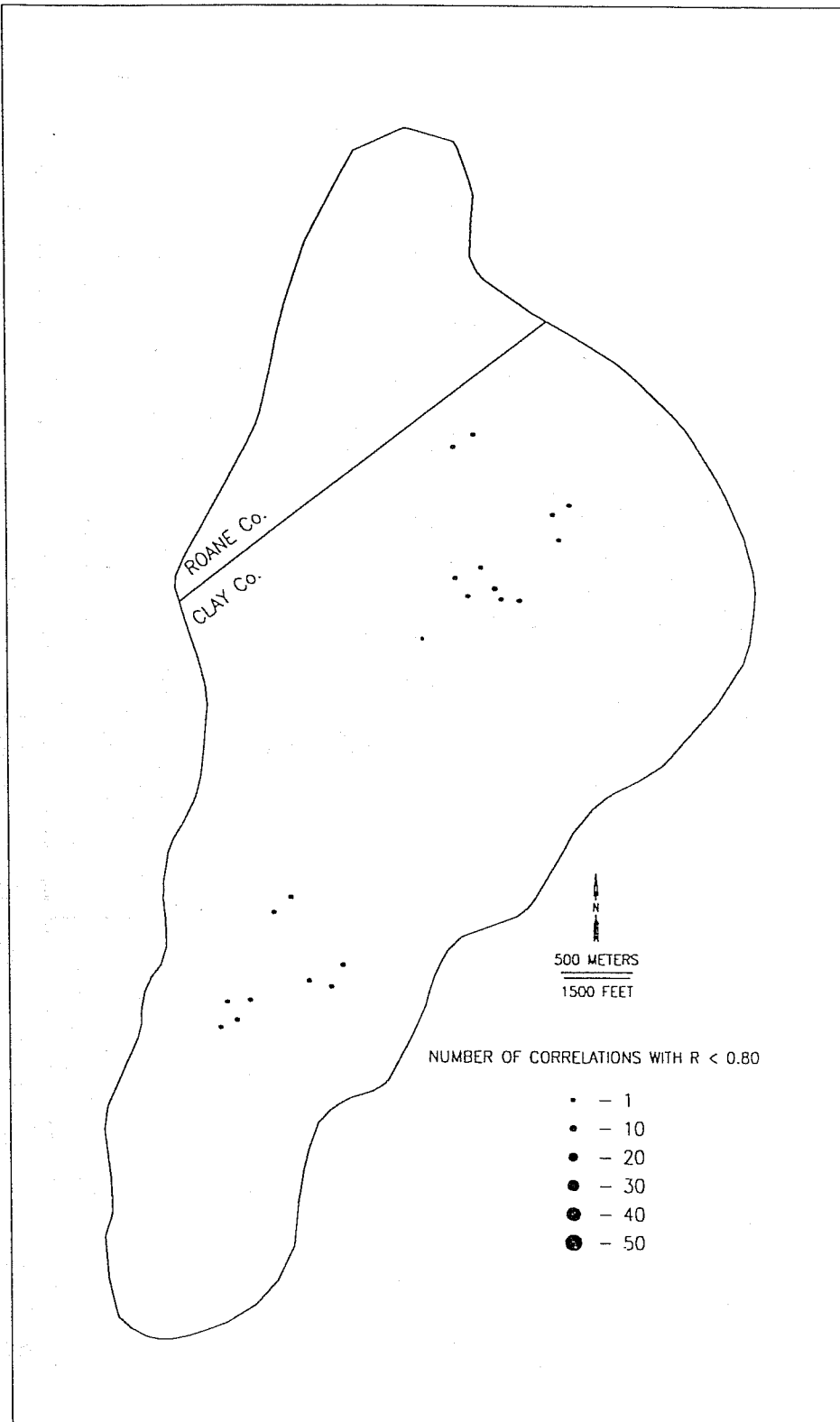


Figure 72a. "Near"-neighborhood (distance between correlated wells ≤ 200 meters) correlation plot for Granny Creek. Only the locations of wells with well-to-well correlations correlation coefficients (r) less than 0.80 are shown. The size of the symbol is proportional to the number of "poor" correlations at each well location. Two centers of poor correlation are indicated - one in the north-central portion of the field and a second in the south-central portion of the field.

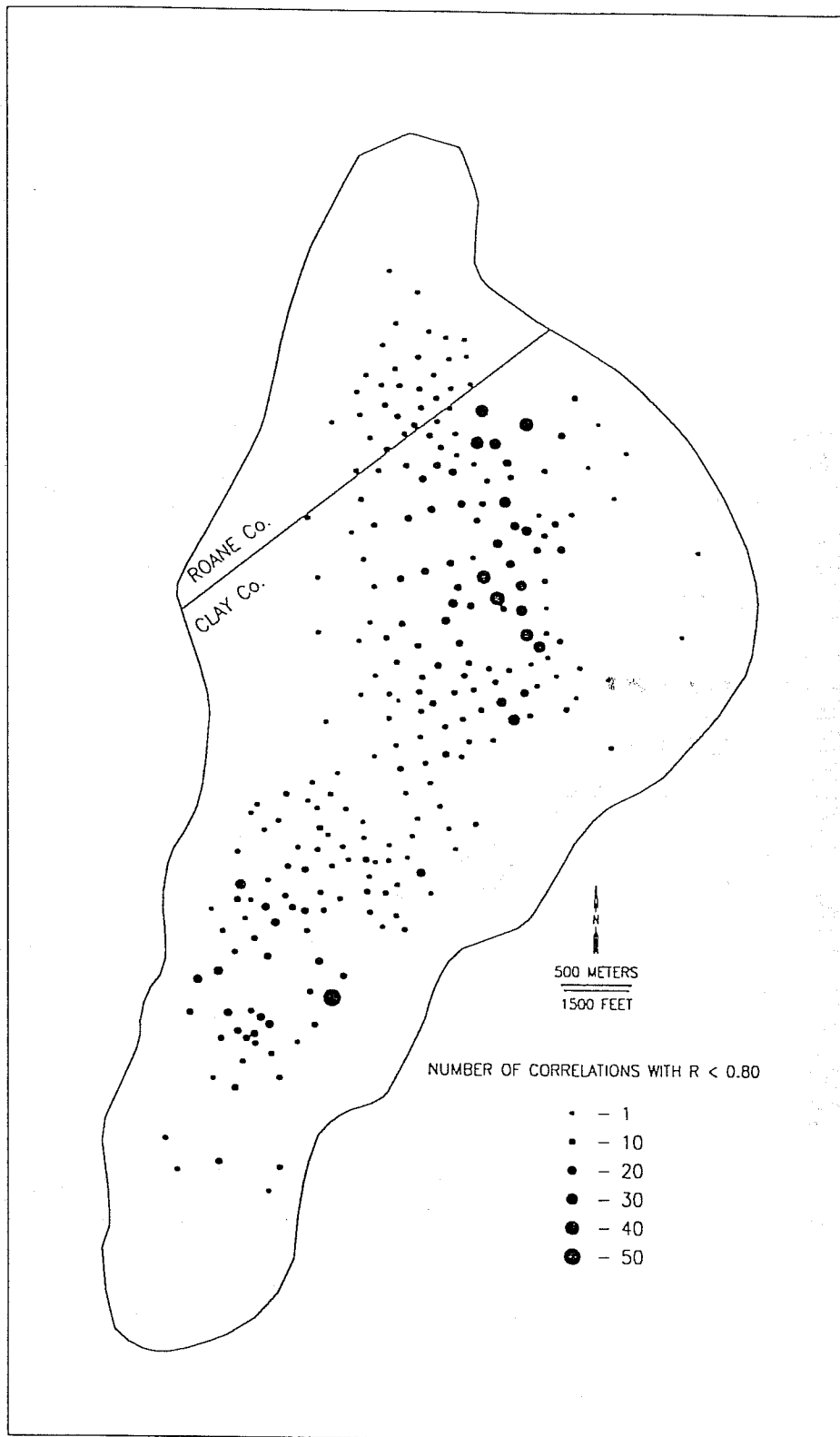


Figure 72b. "Far"-neighborhood (distance between correlated wells ≤ 1000 meters) correlation plot for Granny Creek. Only the locations of wells with well-to-well correlation coefficients (r) less than 0.80 are shown. The size of the symbol is proportional to the number of "poor" correlations at each well location. The number of poor correlations has increased dramatically compared to Figure 72a. The two centers of poor correlation indicated in Figure 72a are now well delineated.

CORRELATION COEFFICIENT (r)

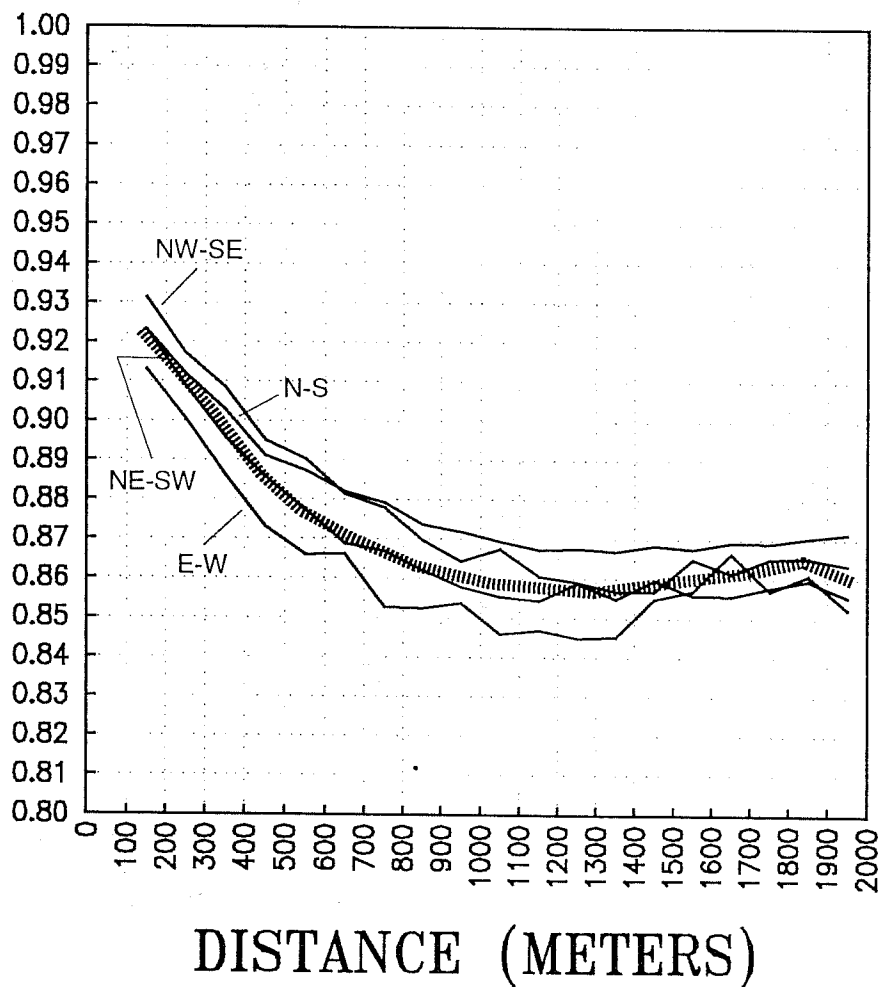


Figure 73. Directional correlograms for gamma ray log correlations in the Granny Creek field. Values of correlation coefficient fall until well separation reaches a distance (range) of approximately 3000' (900 meters) and then remains constant until 7000' (2000 meters) when it starts to fall again. The dashed line represents the approximate average of all correlograms.

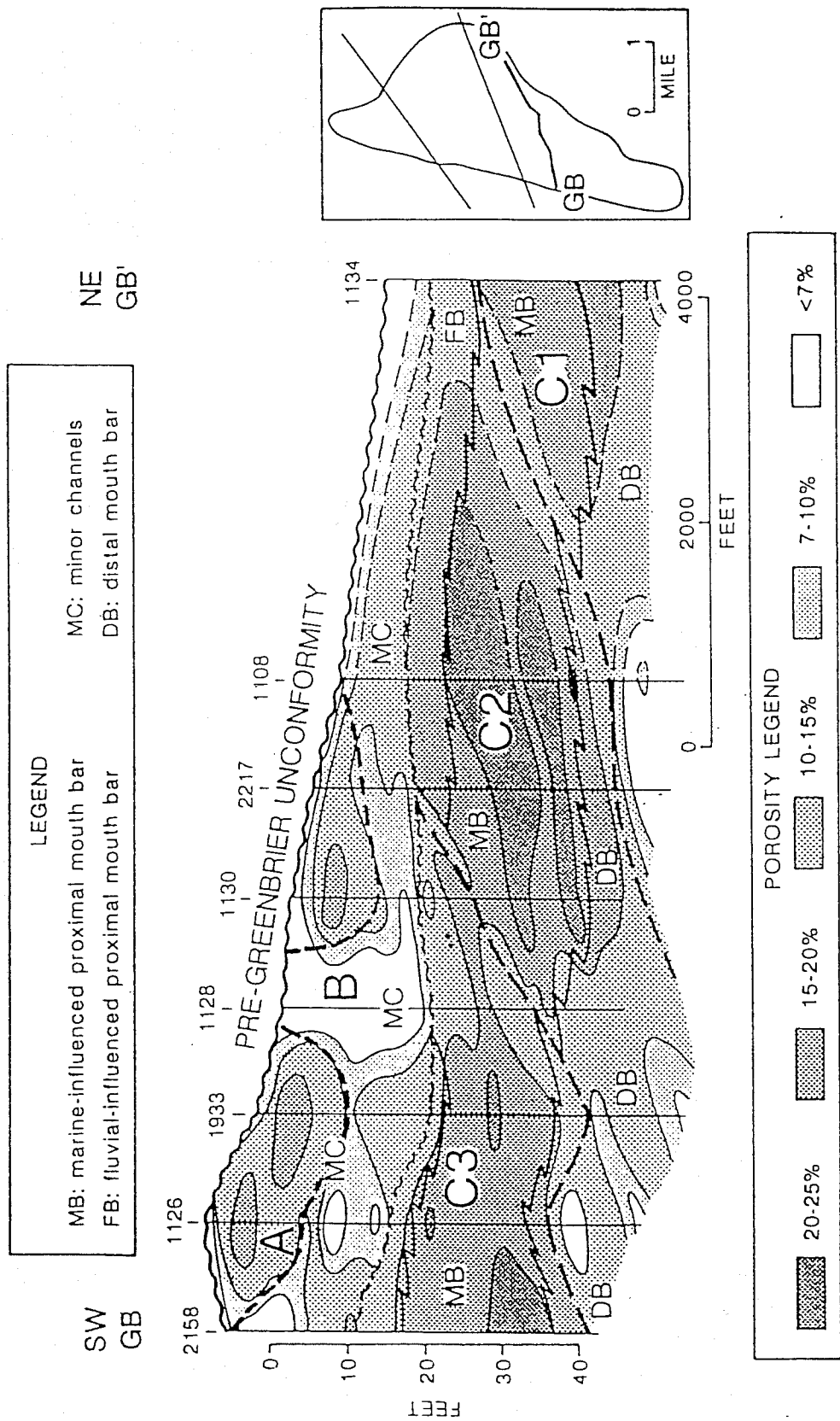


Figure 74. Log porosity facies for stratigraphic cross section GB-GB' superimposed on members, tongues, and subfacies of Pocono Big Injun sandstone, Granny Creek field.

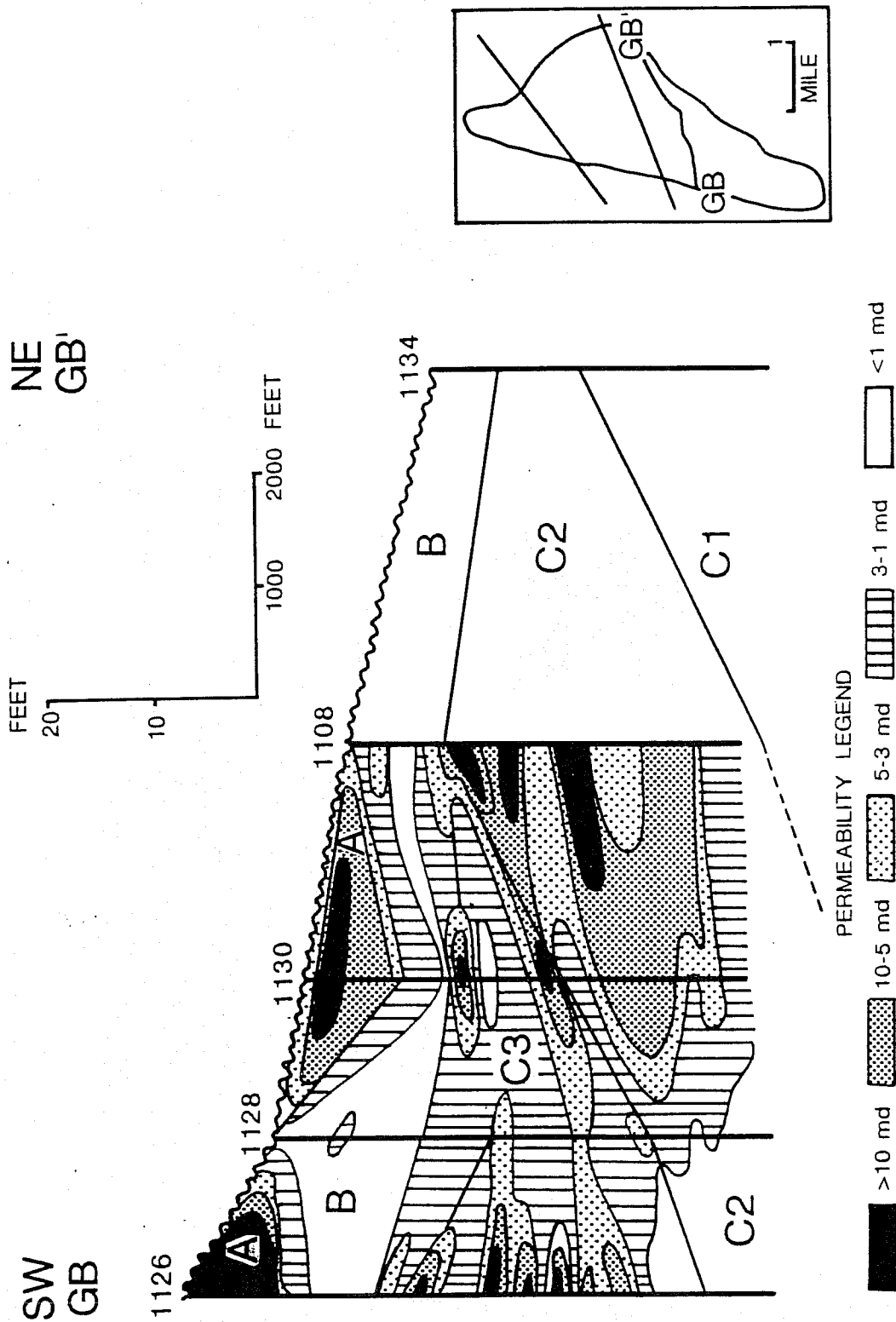


Figure 75. Permeability facies for stratigraphic cross-section GB-GB' from core analyses superposed on members and tongues of the Pocono Big Injun sandstone.

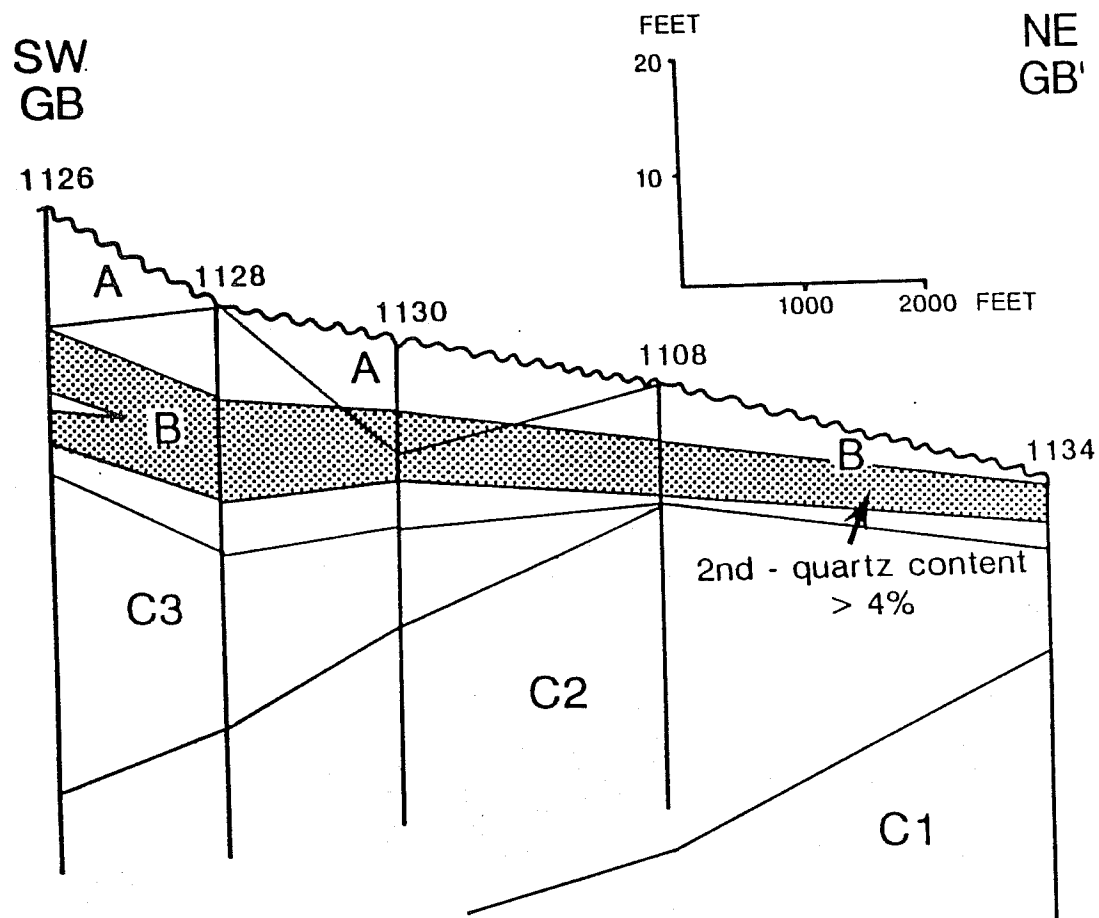
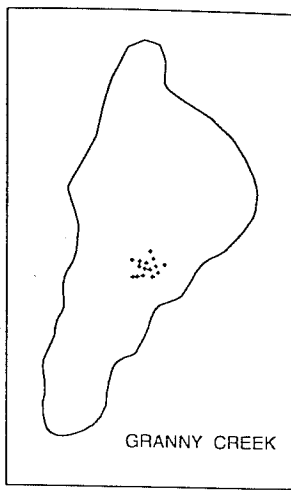


Figure 76. Diagenetic facies due to quartz cement plugging pores in the B member along stratigraphic cross-section GB-GB'.



INDEX MAP

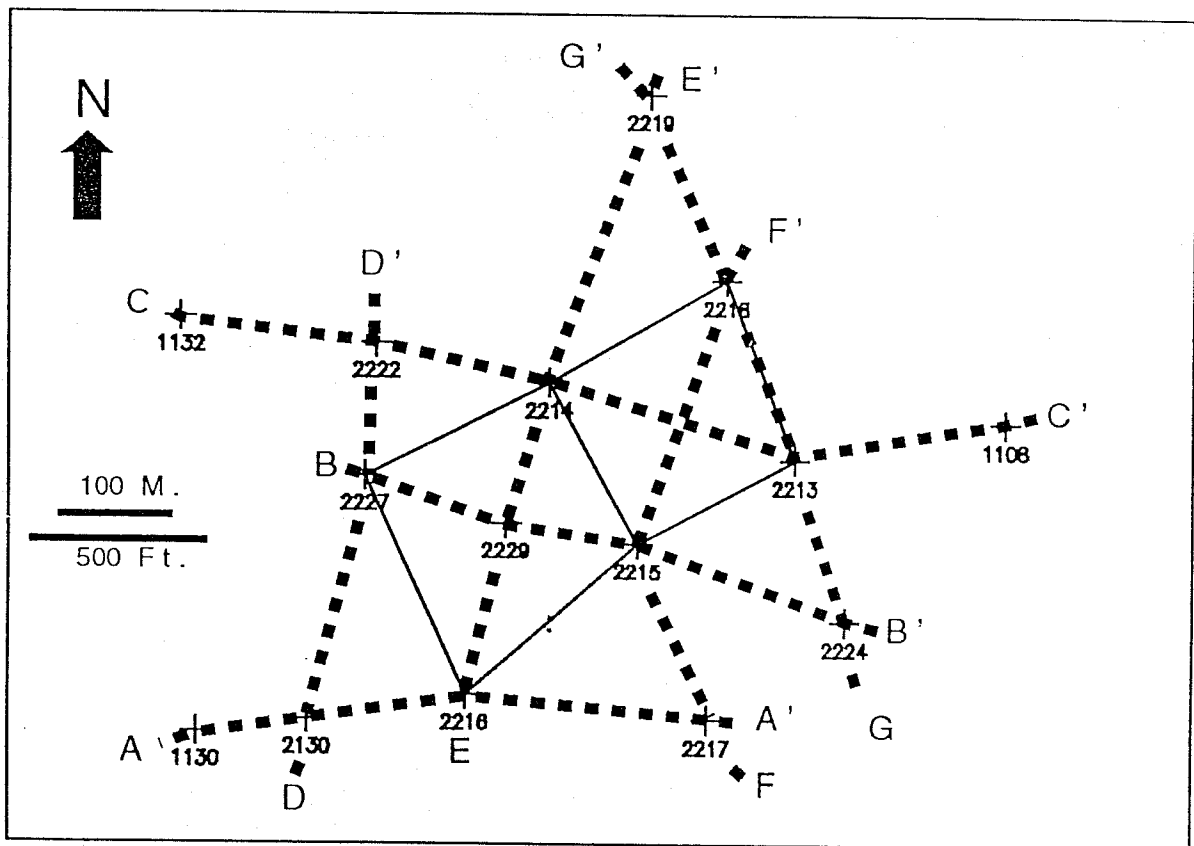


Figure 77. Details of the southern waterflood study area in Granny Creek field showing well locations with permit numbers and lines of sections used to create porosity cross-sections.

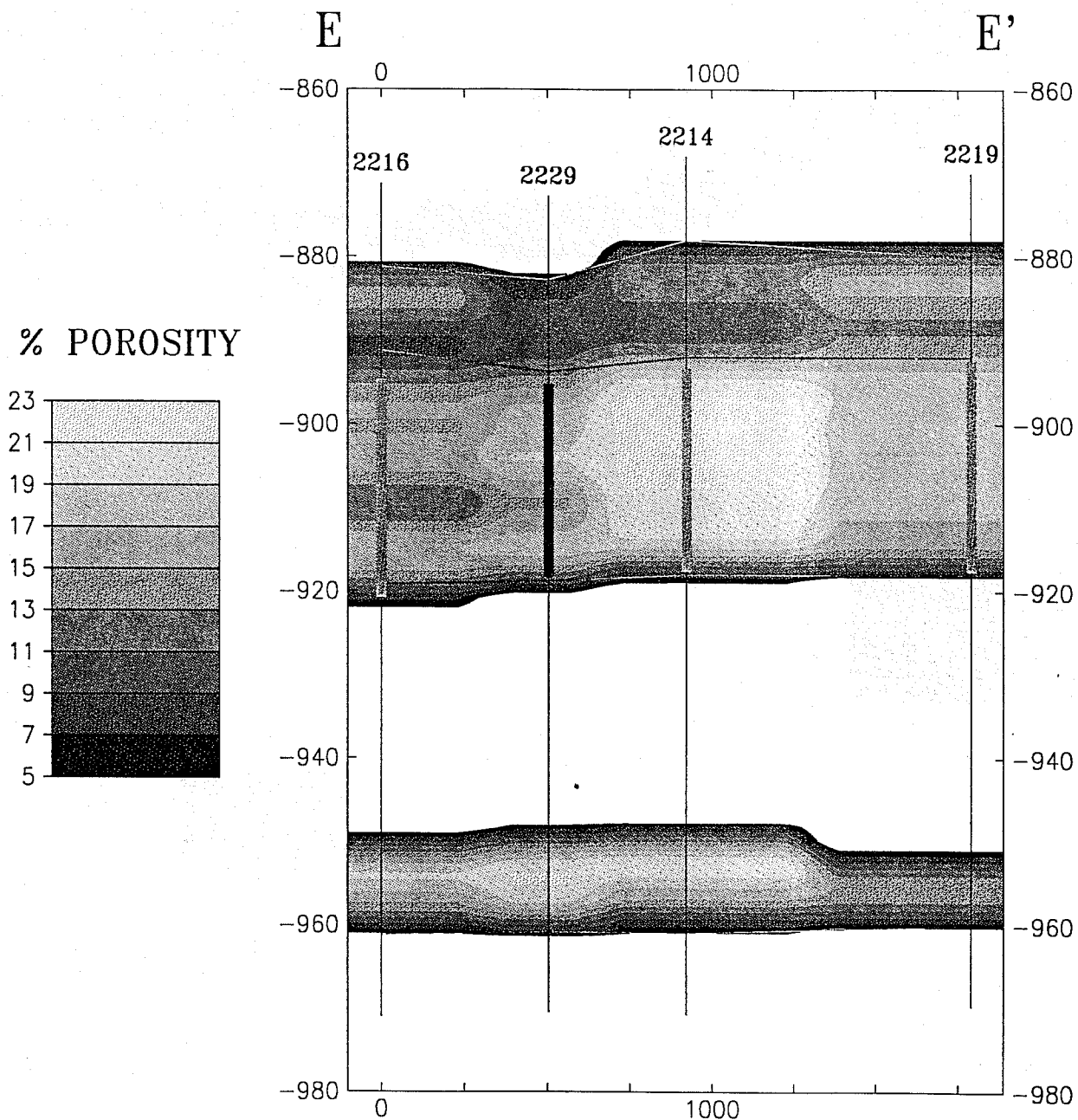


Figure 78a. Porosity cross-section E-E', southern waterflood study area, Granny Creek field. Contour interval = 2%. Horizontal scale = 1:20540; vertical scale = 1:256. White area between -920 and -950 is an interval of shale between the Big Injun (above) and Squaw (below) sandstones.

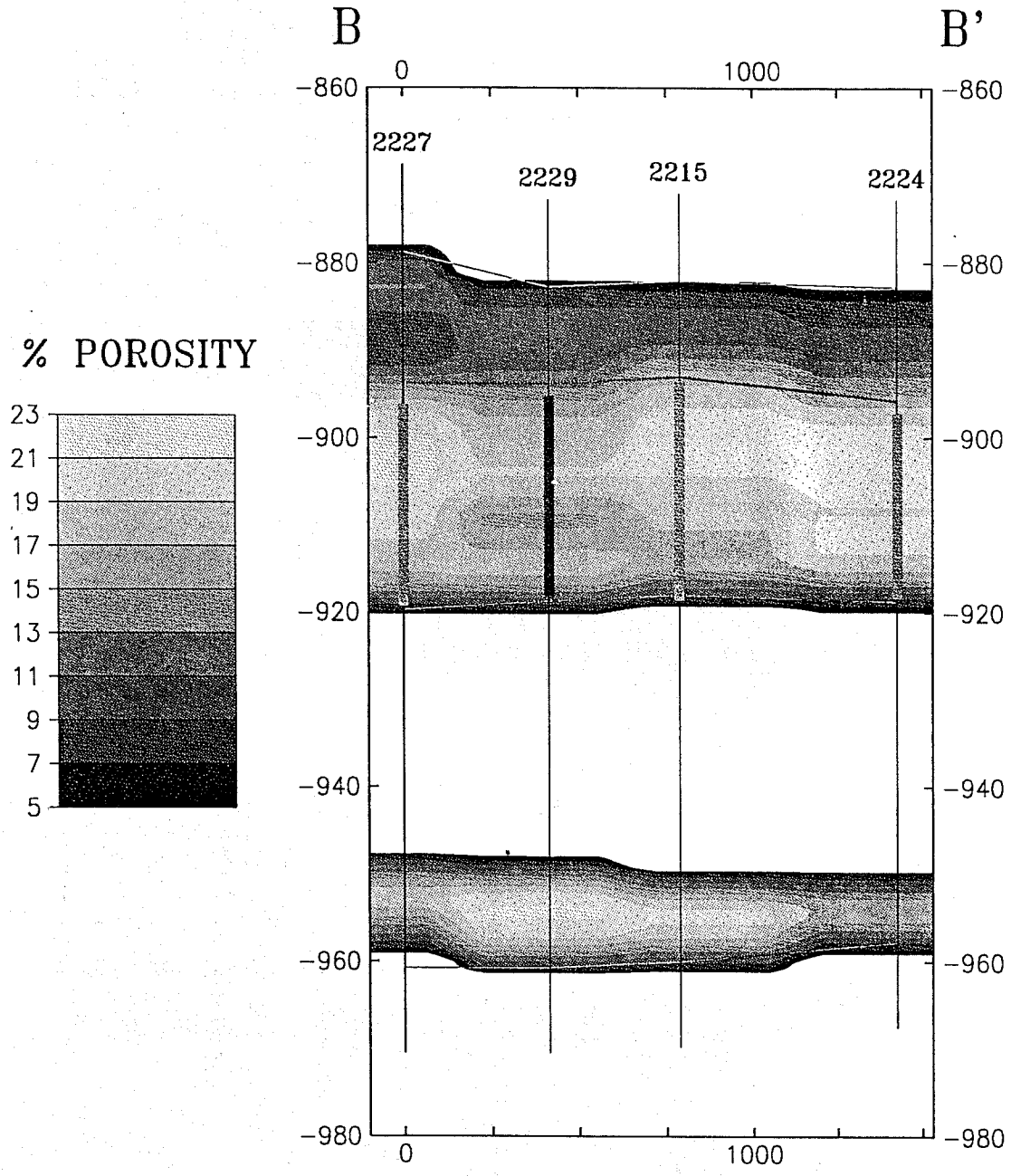


Figure 78b. Porosity cross-section B-B', southern waterflood study area, Granny Creek field. Contour interval = 2%. Horizontal scale = 1:20540; vertical scale = 1:256. White area between -920 and -950 is an interval of shale between the Big Injun (above) and Squaw (below) sandstones.

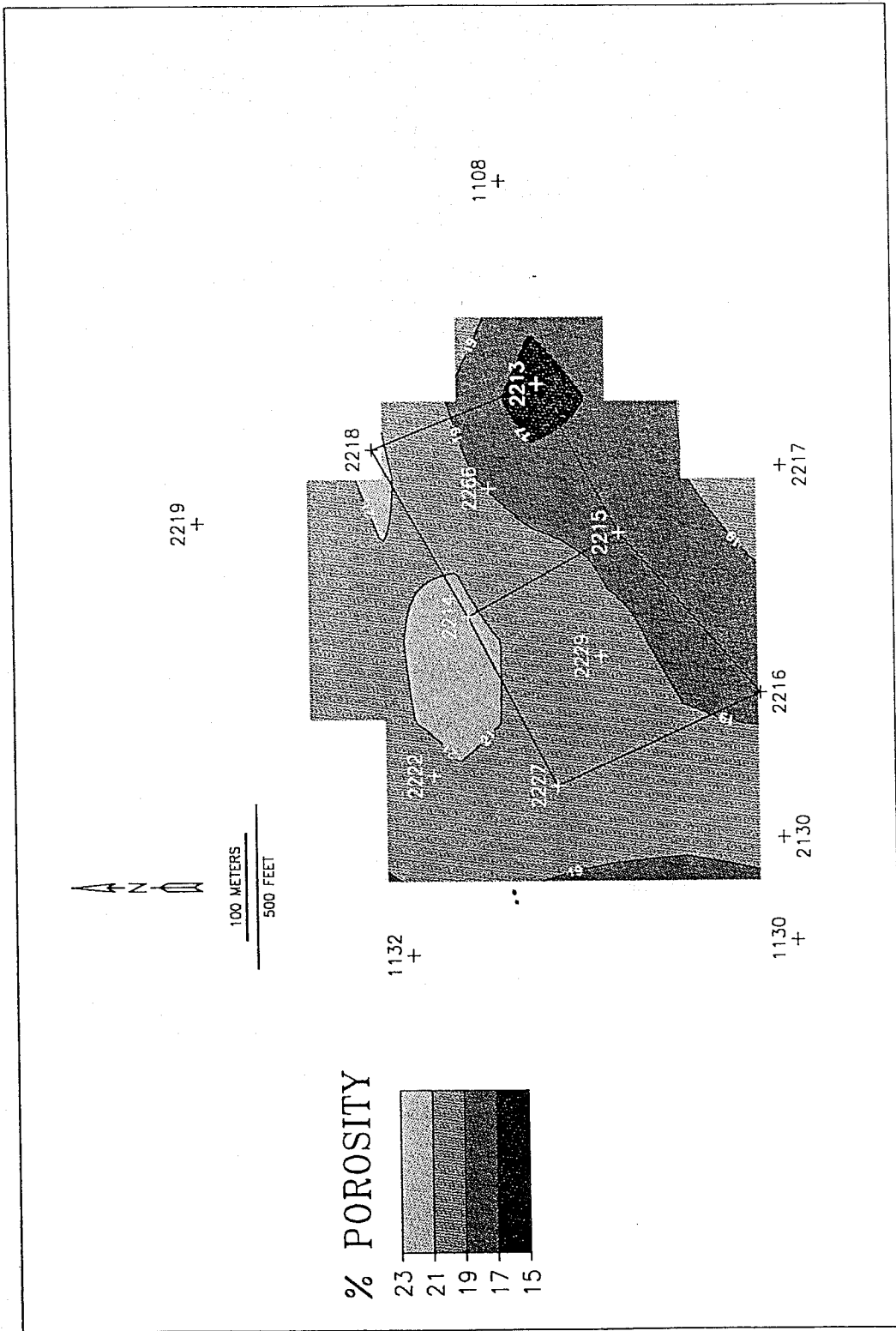


Figure 79. Subsurface porosity map for the southern waterflood study area, Granny Creek field. Stratigraphic horizon represented is a plane intersecting the midpoint of the fine-grained member of the Big Injun sandstone in each well. Well 2214 at this interval contains an isolated high (> 21%) porosity zone; wells 2216, 2215, and 2213 are connected by high (17%-19%) porosity zone. Contour interval = 2%.

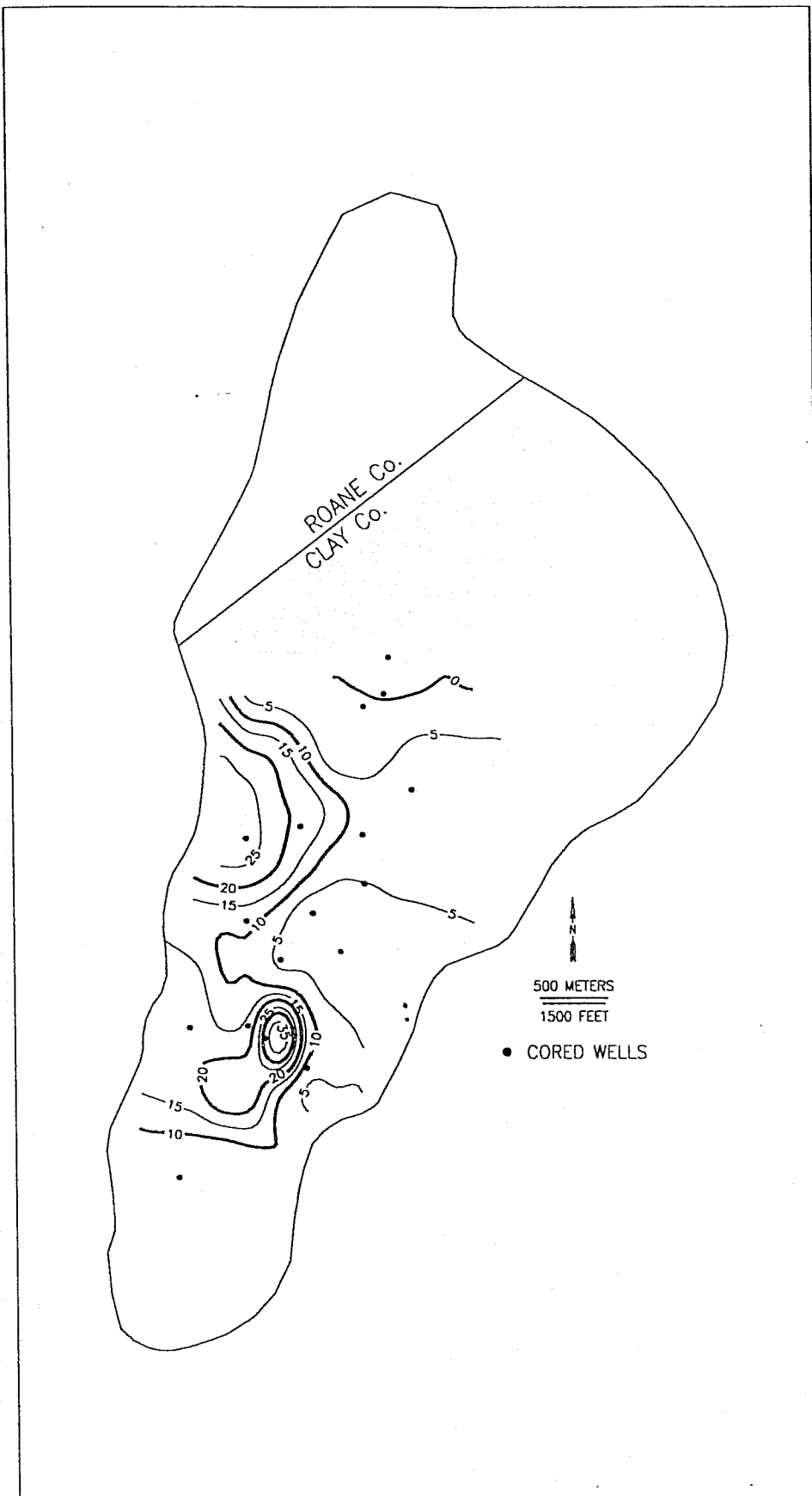


Figure 80. Variation of core permeability for Zone A within the Big Injun Formation, Granny Creek field, West Virginia.

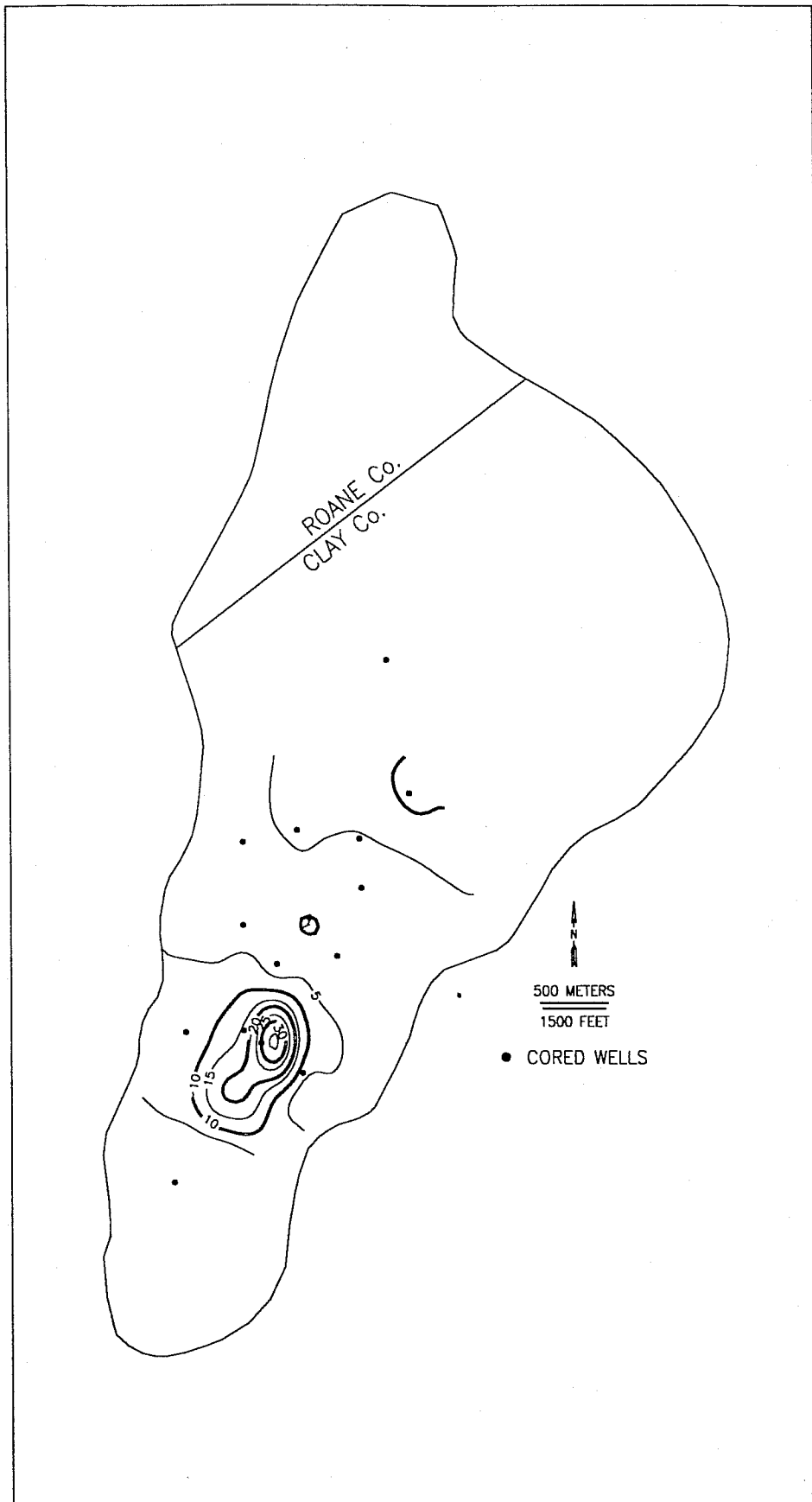


Figure 81. Variation of core permeability for Zone B within the Big Injun Formation, Granny Creek field, West Virginia.

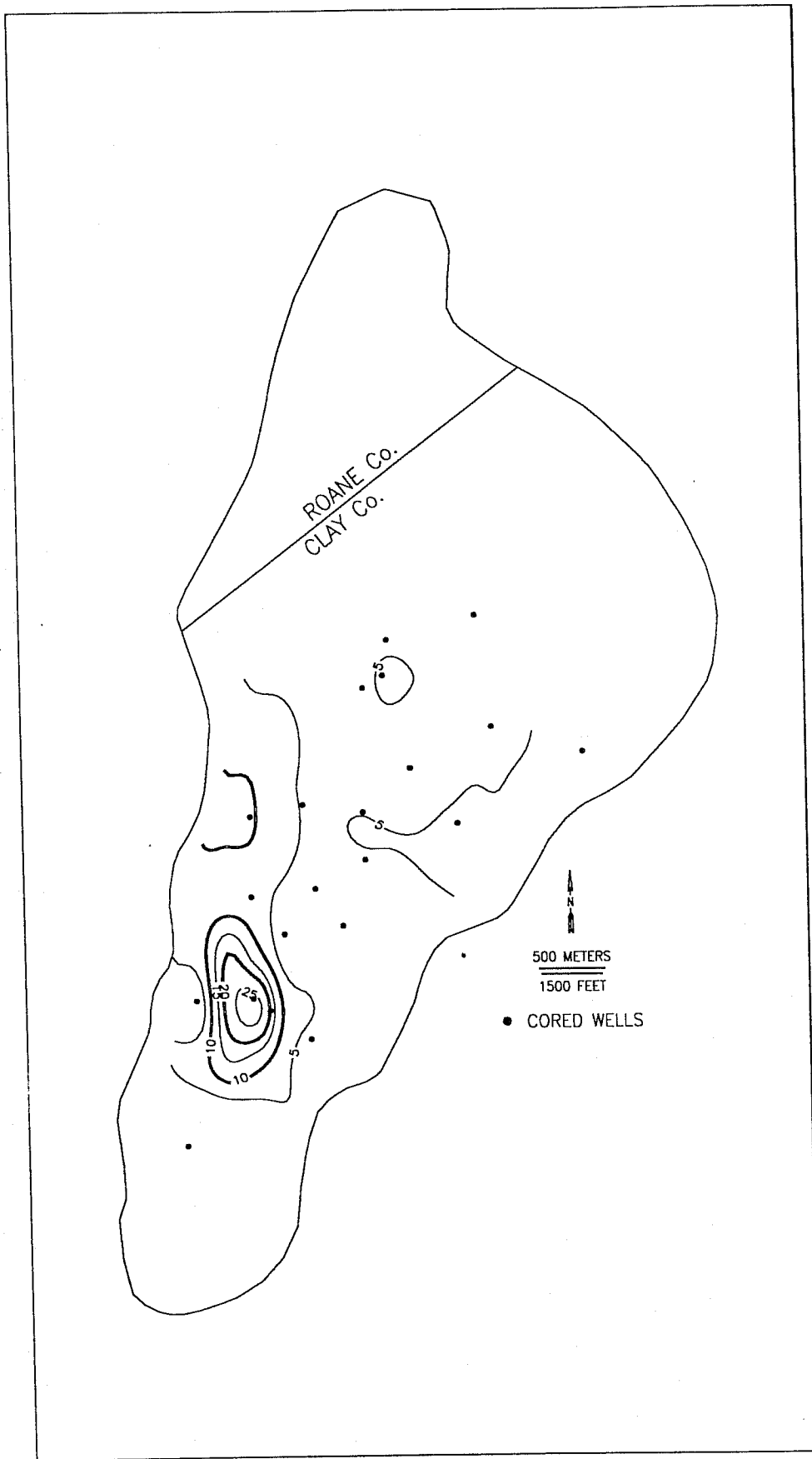


Figure 82. Variation of core permeability for Zone C within the Big Injun Formation, Granny Creek field, West Virginia.

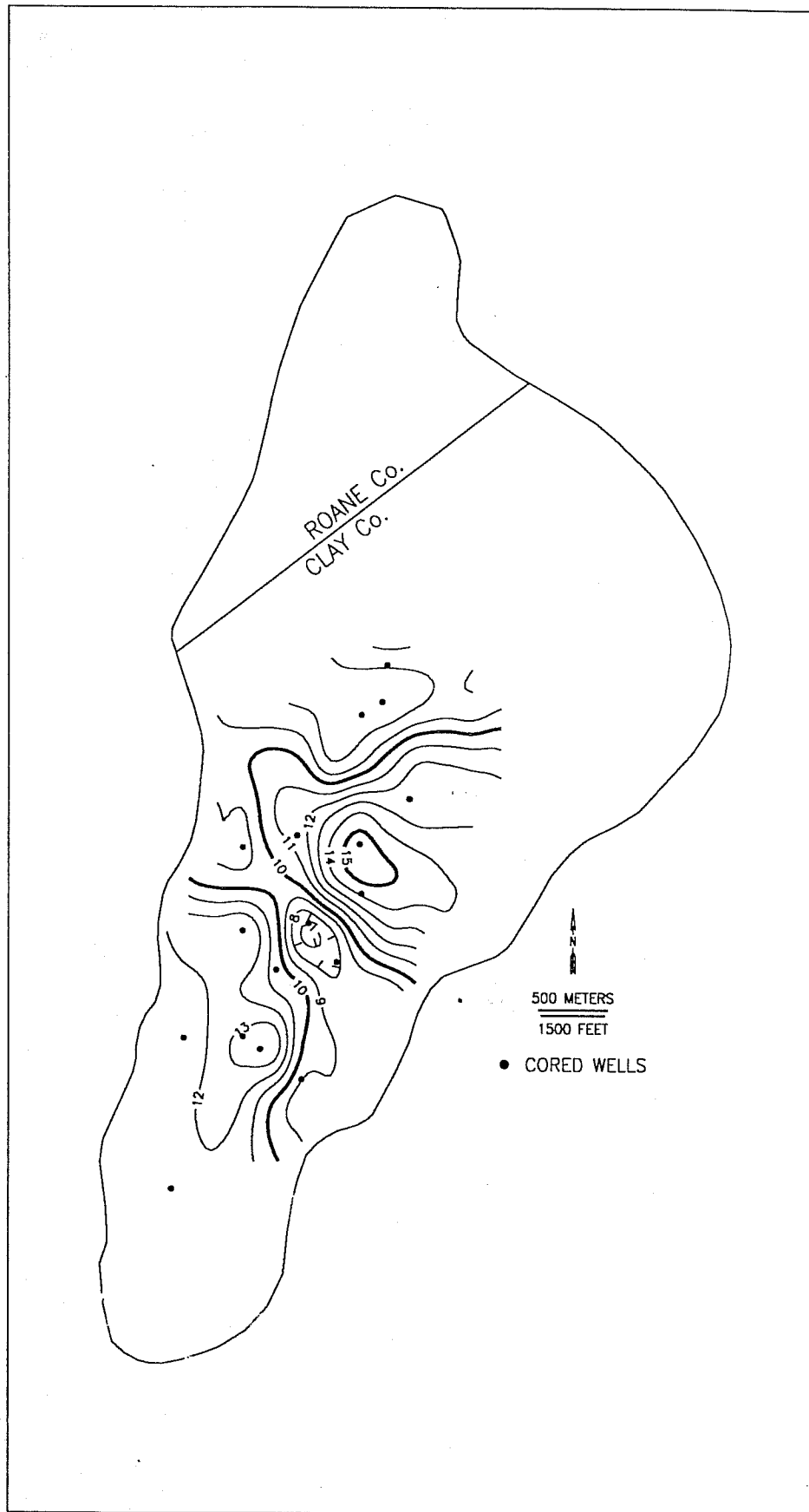


Figure 83. Variation of core porosity for Zone A within the Big Injun Formation, Granny Creek field, West Virginia.

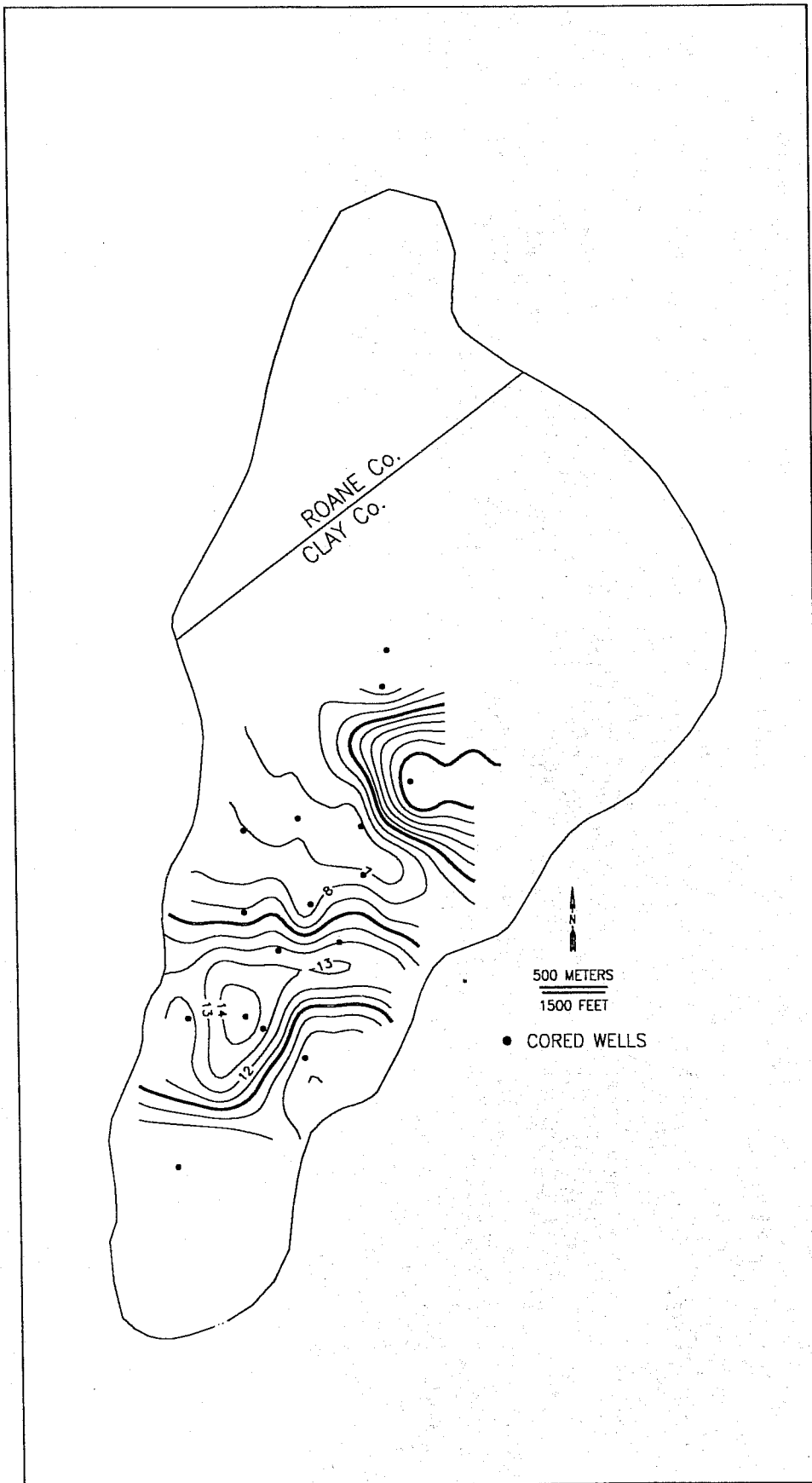


Figure 84. Variation of core porosity for Zone B within the Big Injun Formation, Granny Creek field, West Virginia.

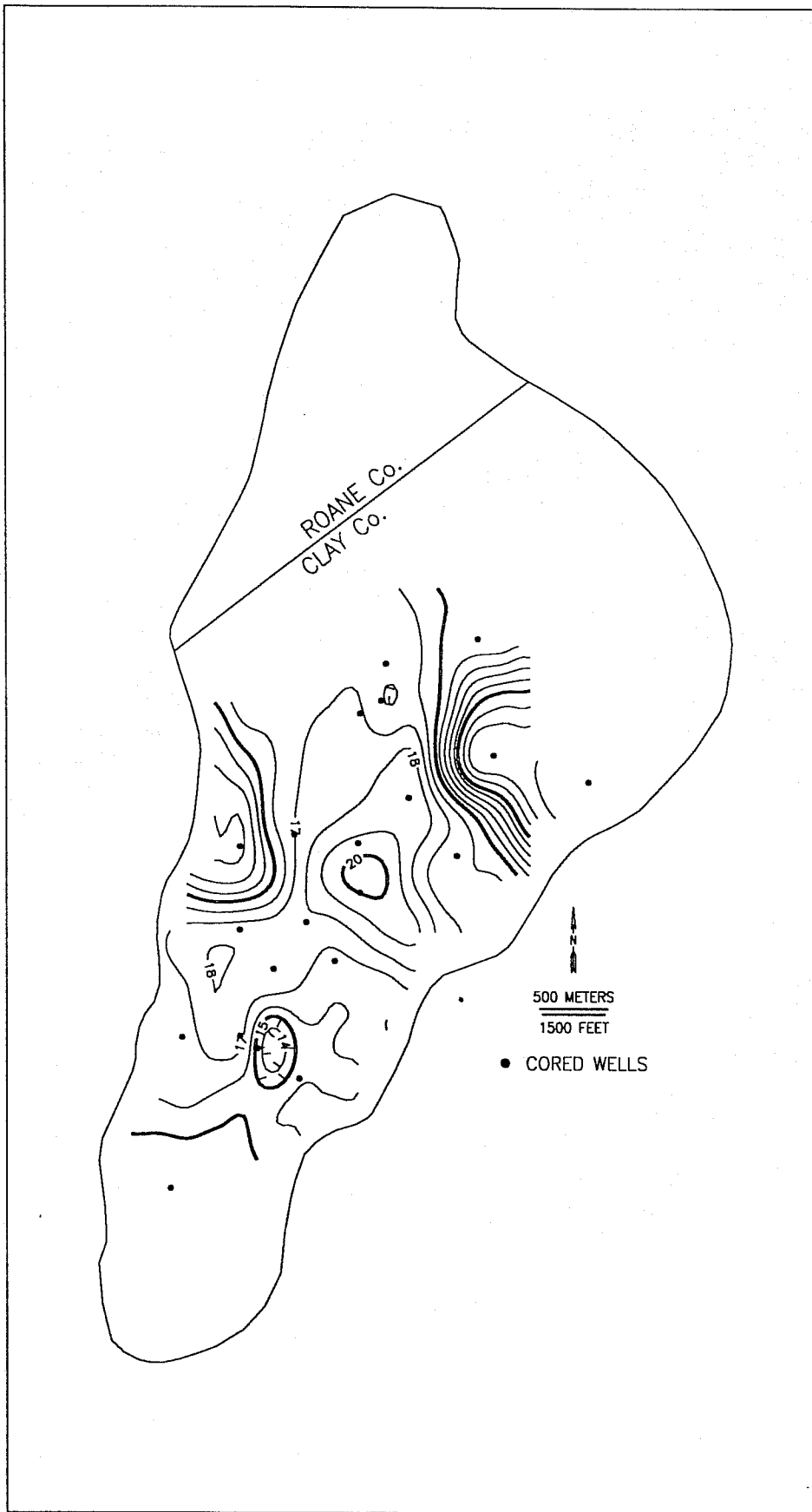


Figure 85. Variation of core porosity for Zone C within the Big Injun Formation, Granny Creek field, West Virginia.

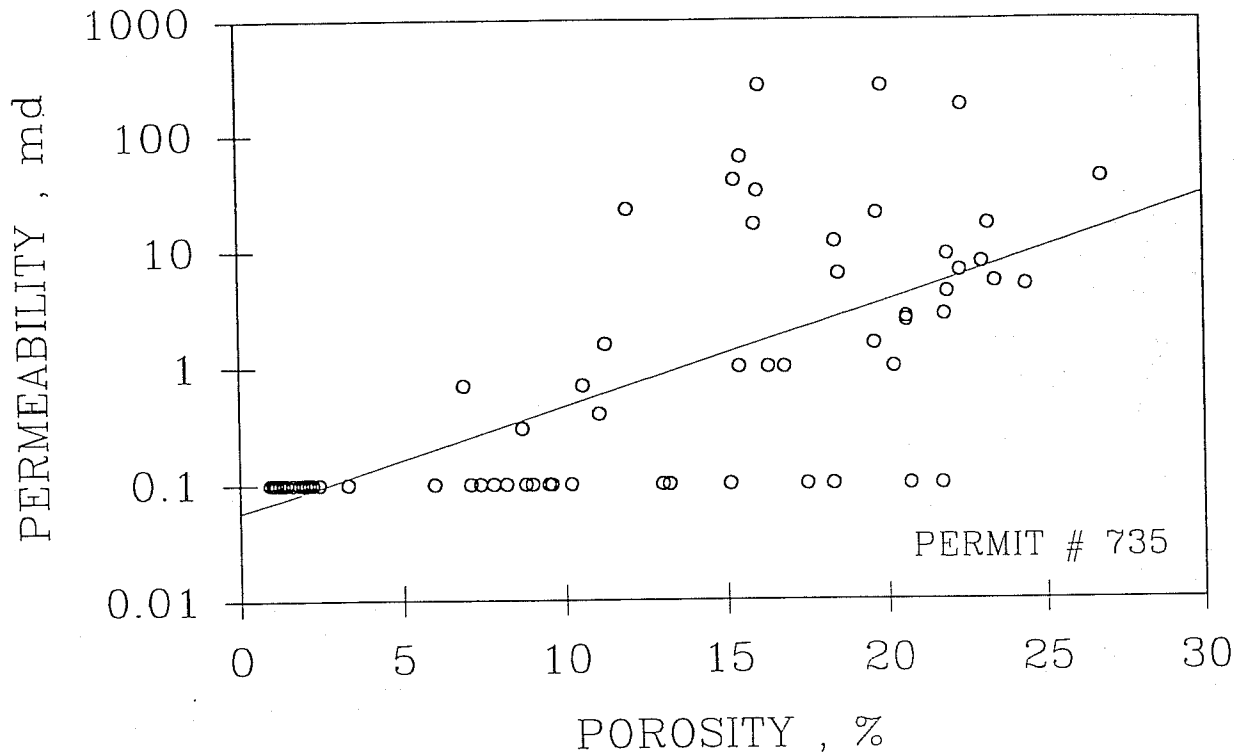


Figure 86. Core permeability-positivity correlation for all points from the Big Injun Formation at Well No: 735, Granny Creek field, West Virginia.

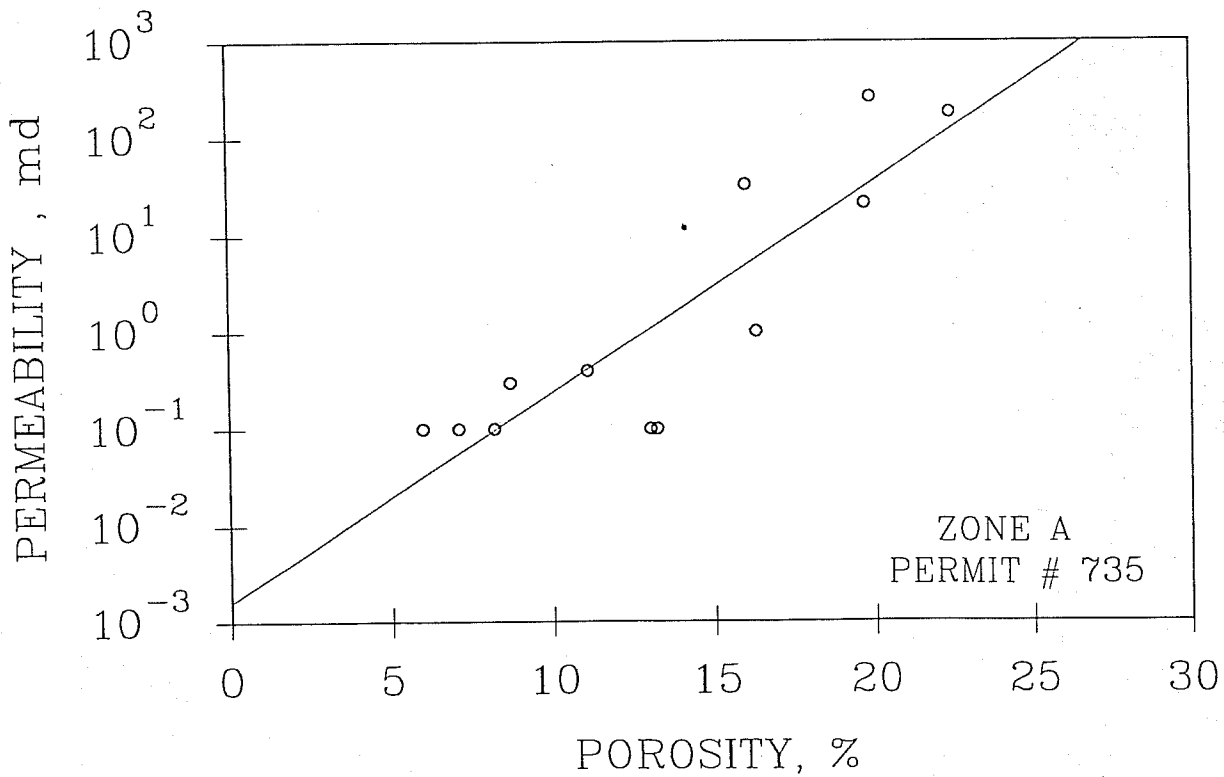


Figure 87. Core permeability-positivity correlation for all points from zone A within the Big Injun Formation at Well No: 735, Granny Creek field, West Virginia.

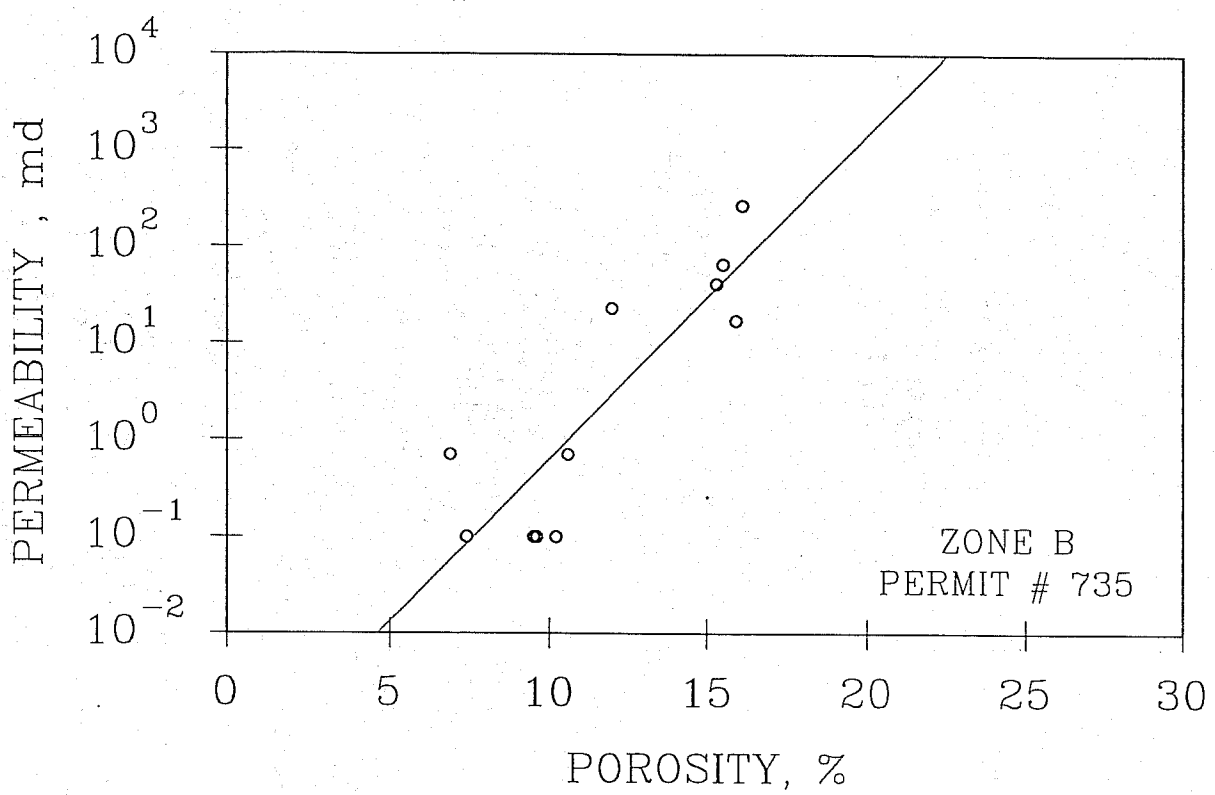


Figure 88. Core permeability-positivity correlation for all points from zone B within the Big Injun Formation at Well No: 735, Granny Creek field, West Virginia.

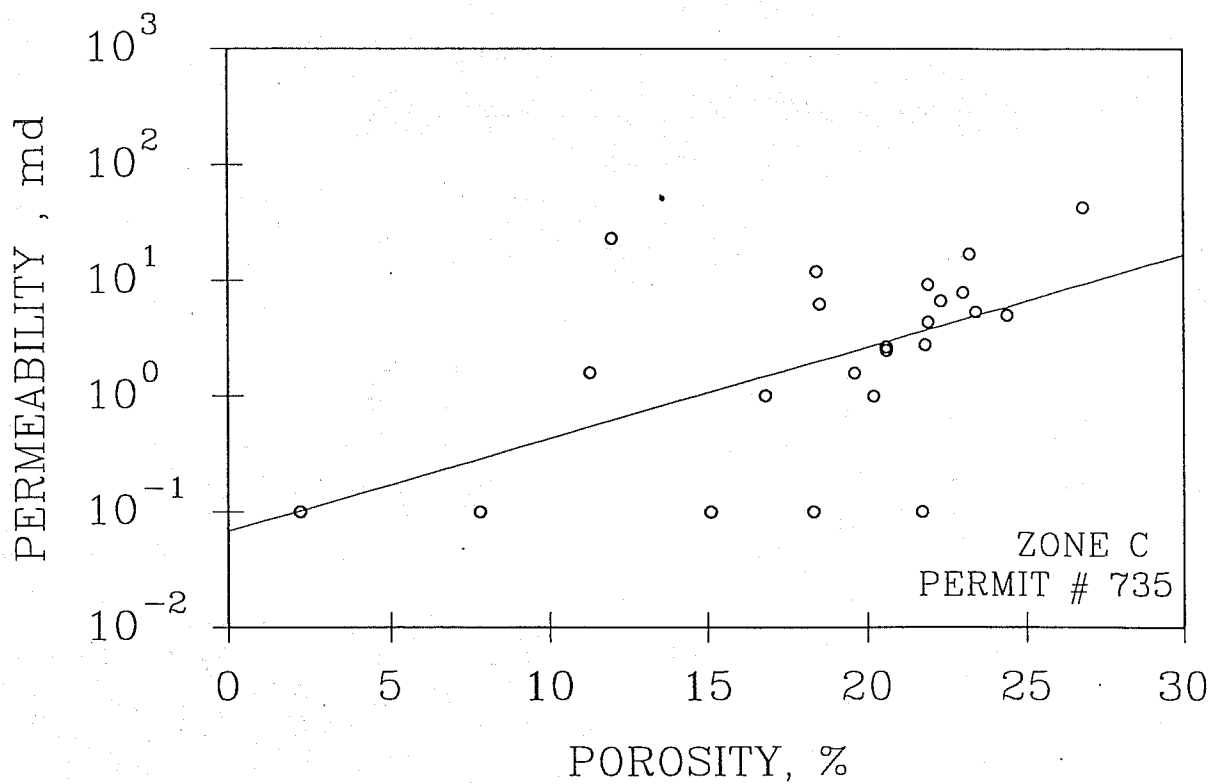


Figure 89. Core permeability-positivity correlation for all points from zone C within the Big Injun Formation at Well No: 735, Granny Creek field, West Virginia.

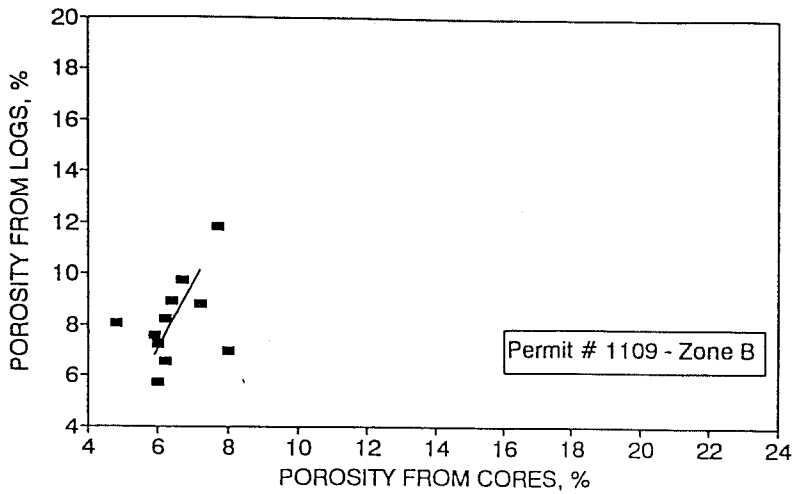


Figure 90. Variation of porosity from log calculations with porosity from core measurements for Zone B within Big Injun Formation at Well No: 1109, Granny Creek field, West Virginia.

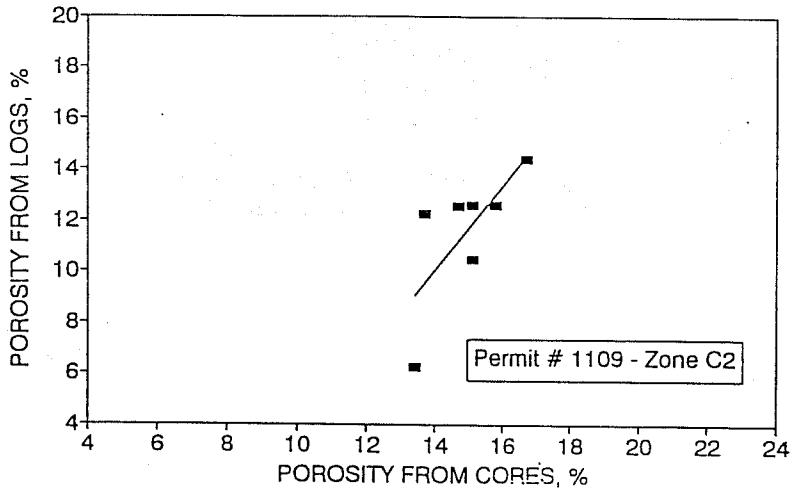


Figure 91. Variation of porosity from log calculations with porosity from core measurements for Zone C3 within Big Injun Formation at Well No: 1109, Granny Creek field, West Virginia.

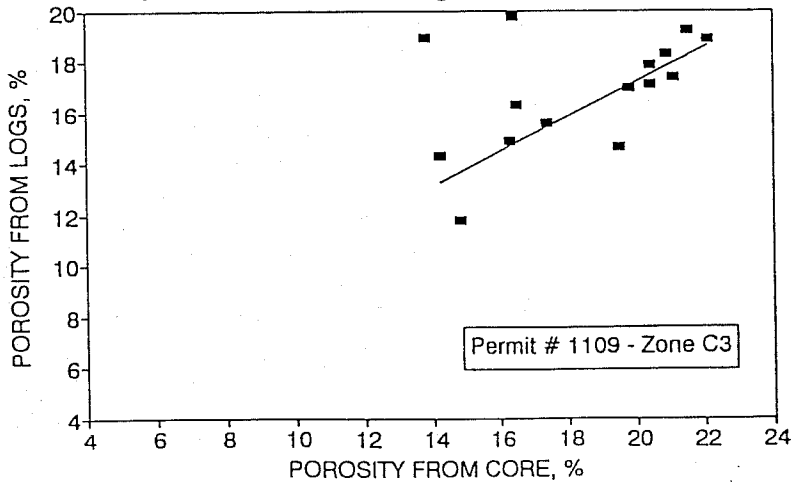


Figure 92. Variation of porosity from log calculations with porosity from core measurements for Zone C2 within Big Injun Formation at Well No: 1109, Granny Creek field, West Virginia.

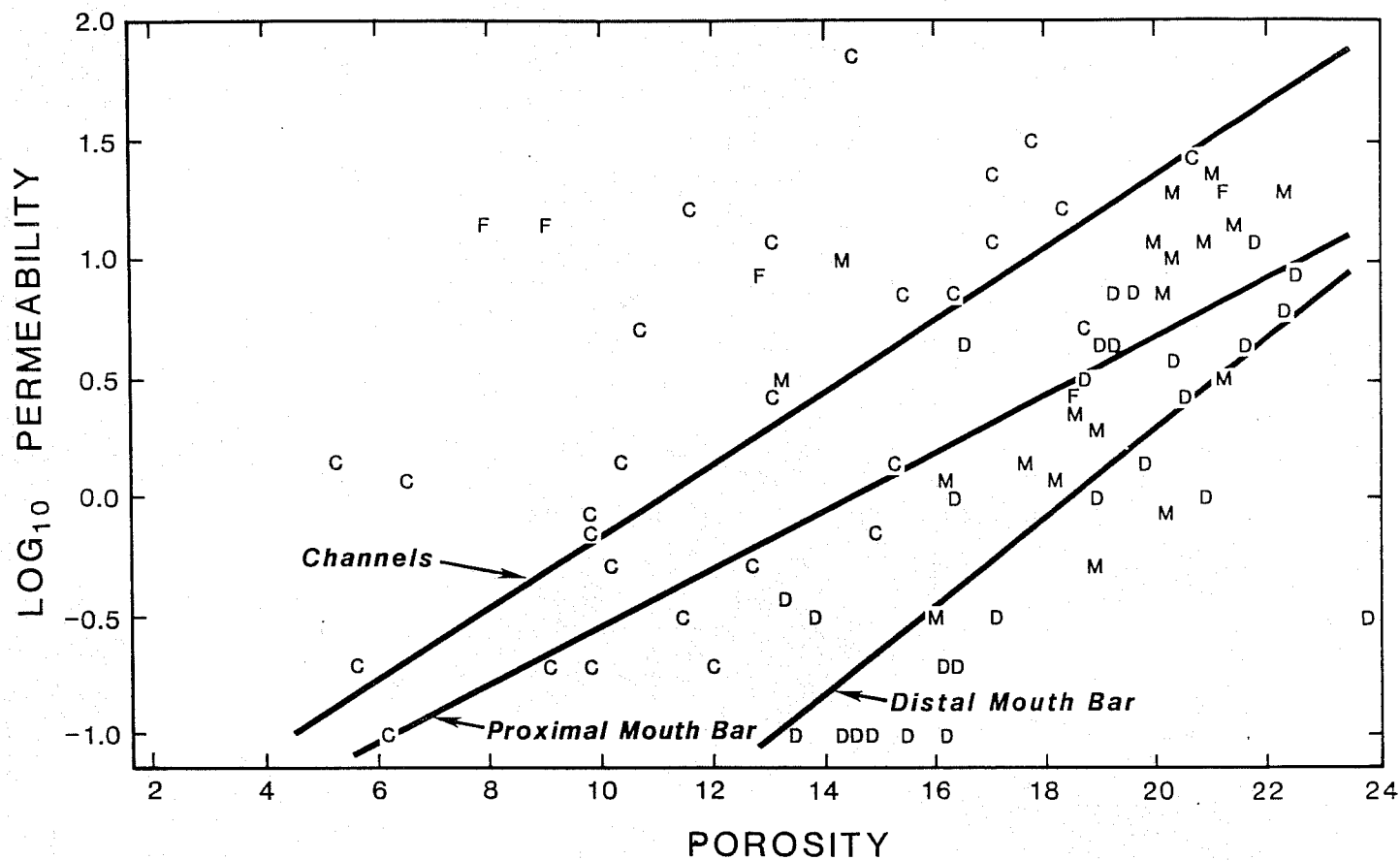


Figure 93. Relationship between porosity and permeability determined from core samples. C = minor bed load channels; D = distal mouth bars; M = marine-influenced proximal mouth bars; F = fluvial-influenced proximal mouth bars.

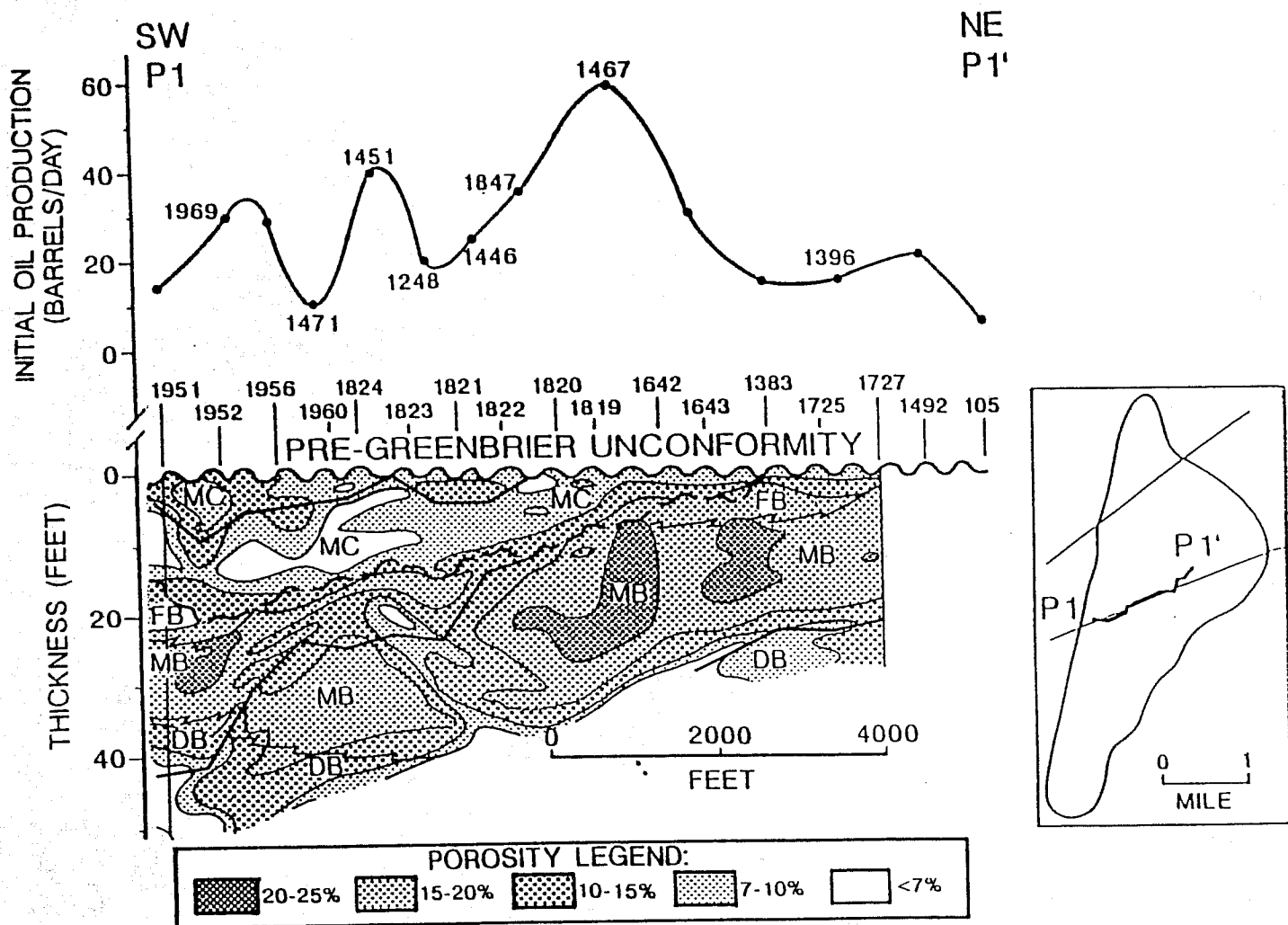


Figure 94. Log porosity facies superimposed on subfacies along profile P1-P1' in Granny Creek field. Initial oil production is plotted above the cross section. Numbered points represent wells located near the line of section; unnumbered points are wells shown in the cross section.

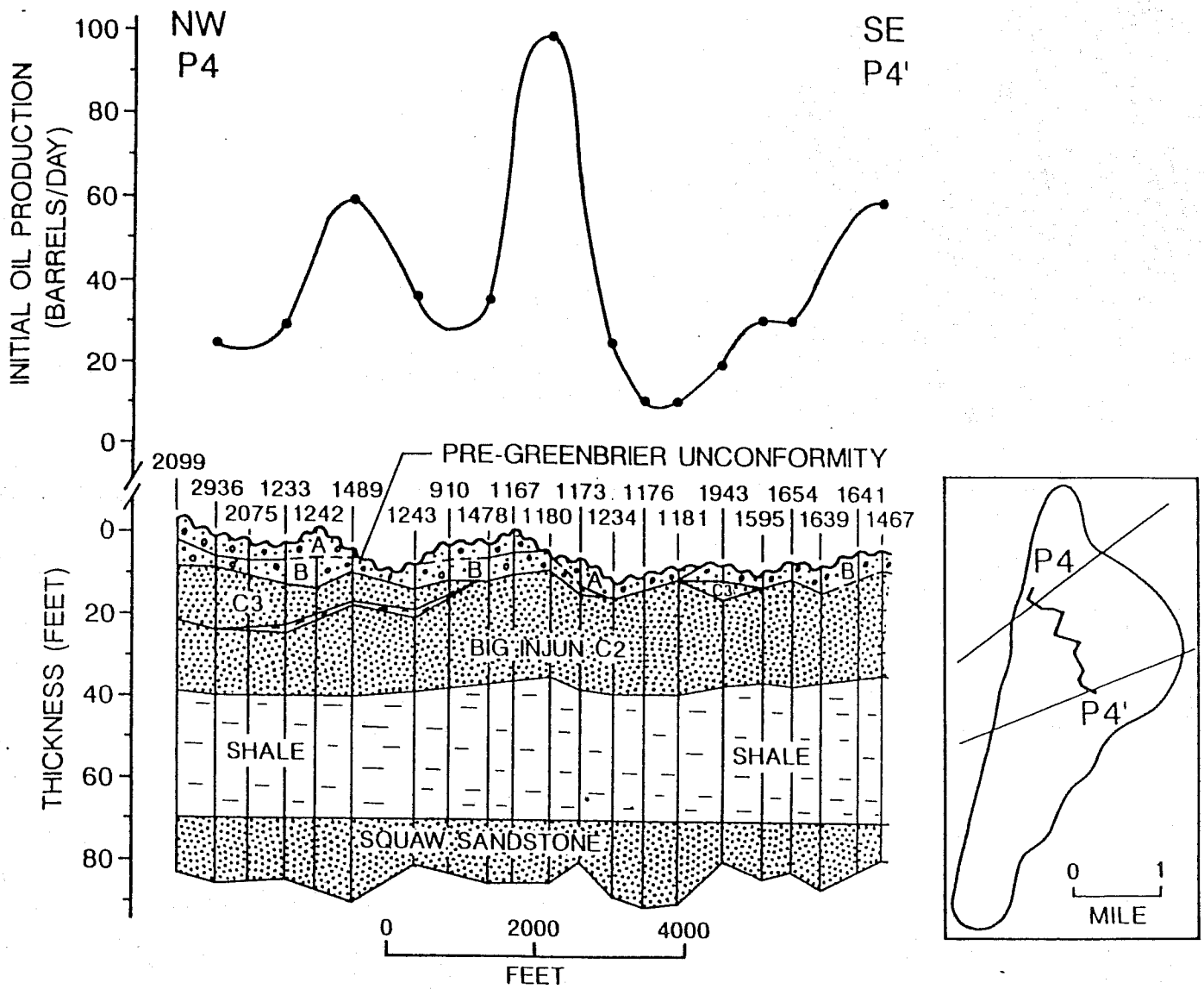


Figure 95. Stratigraphic cross section P4-P4' located parallel and near the pinch out margin of the B member in the Granny Creek field. Initial oil production is plotted above the cross section. Wells that were used are indicated by black dots.

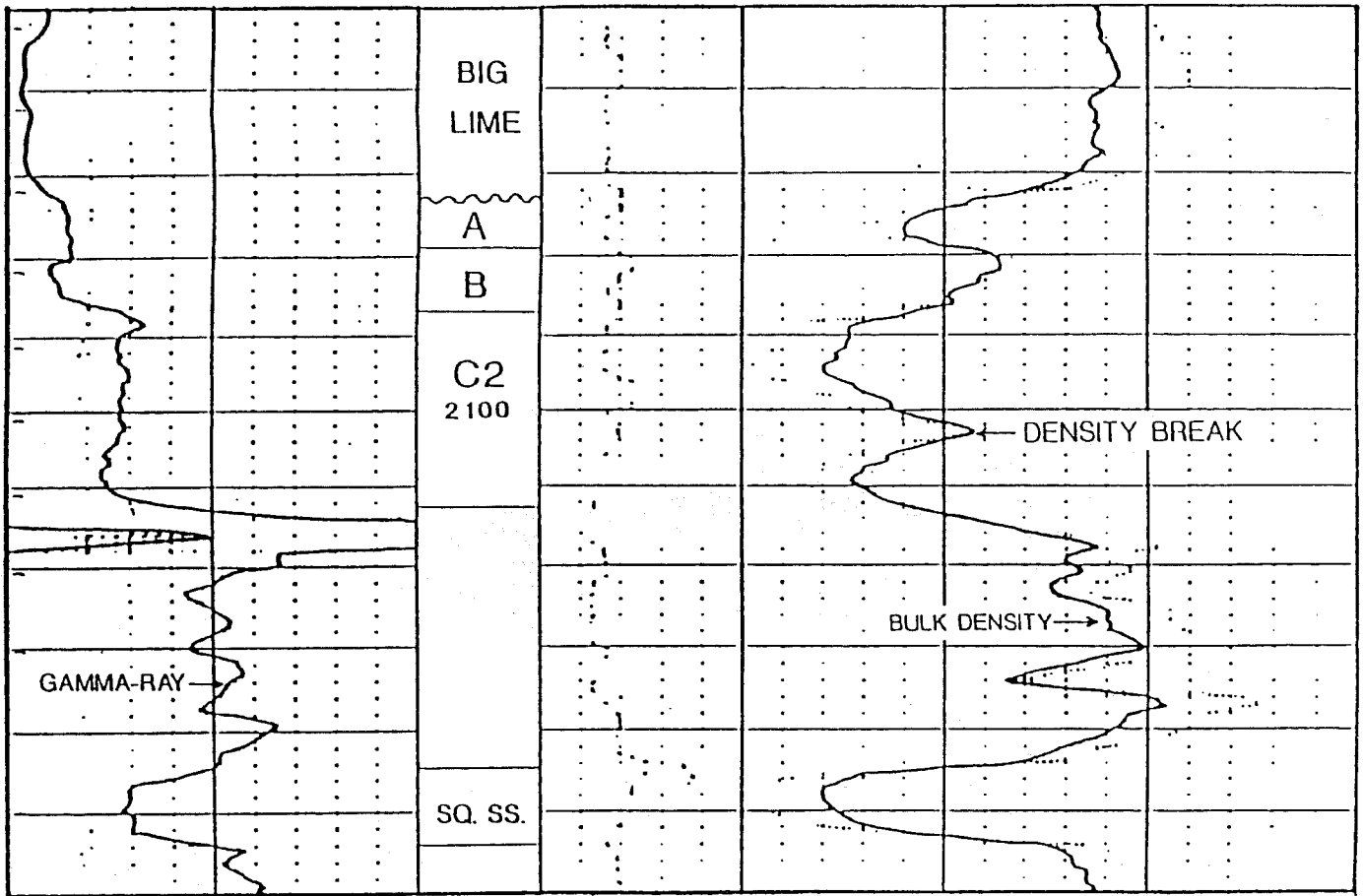


Figure 96. A non-depositional "density break" does not correspond with a gamma-ray deflection, thereby occurring within C2 tongue of Big Injun sandstone suggesting a post-depositional origin. Well Clay 2231, Granny Creek field.

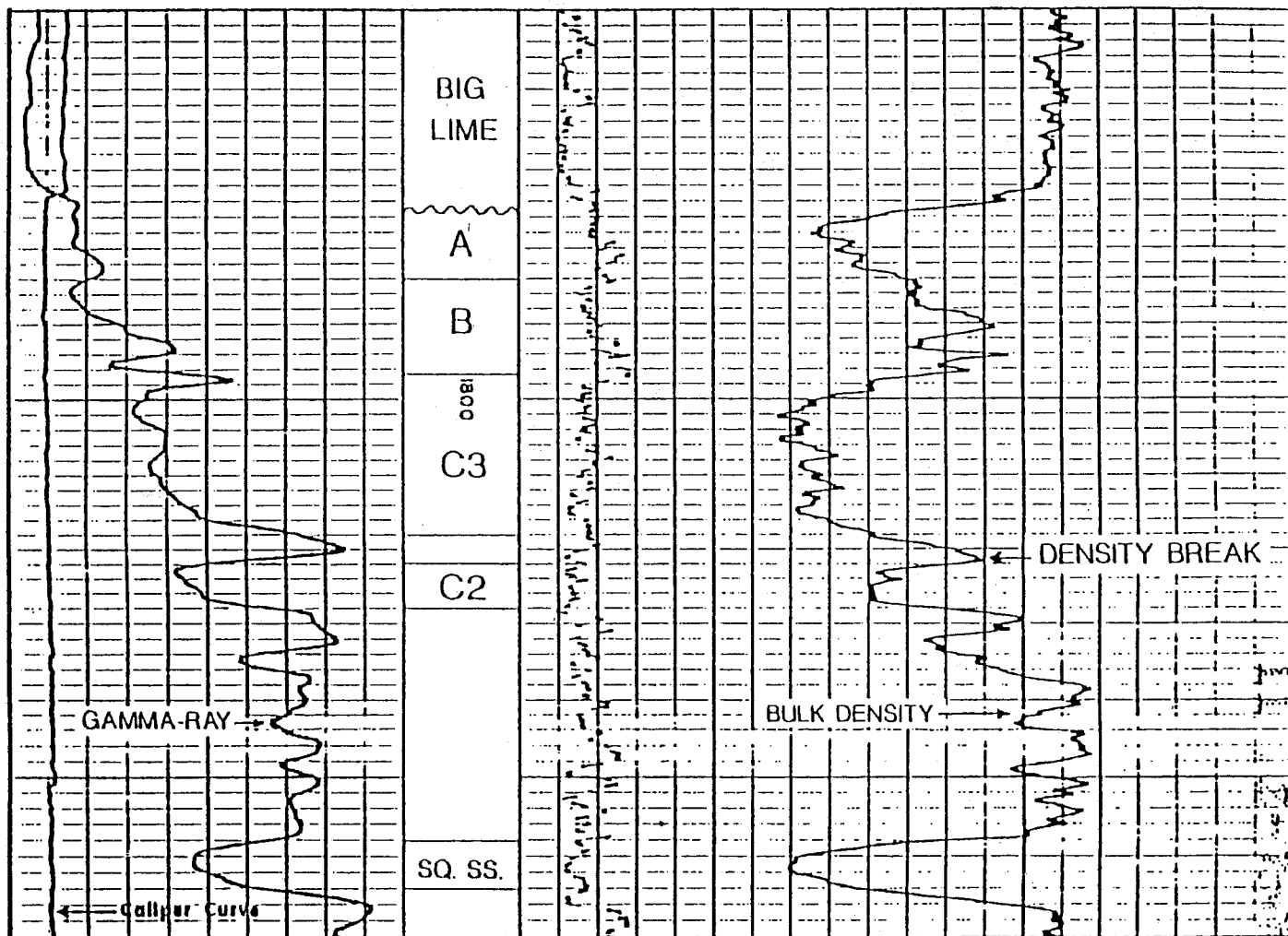


Figure 97. Depositional "density break" at boundary between C2 and C3 tongues of Big Injun sandstones correlates with gamma-ray deflection. Bulk densities are relatively low for A and C members (and tongues C3, C2) but high for B member of Pocono Big Injun. Well Clay 2231, Granny Creek field.

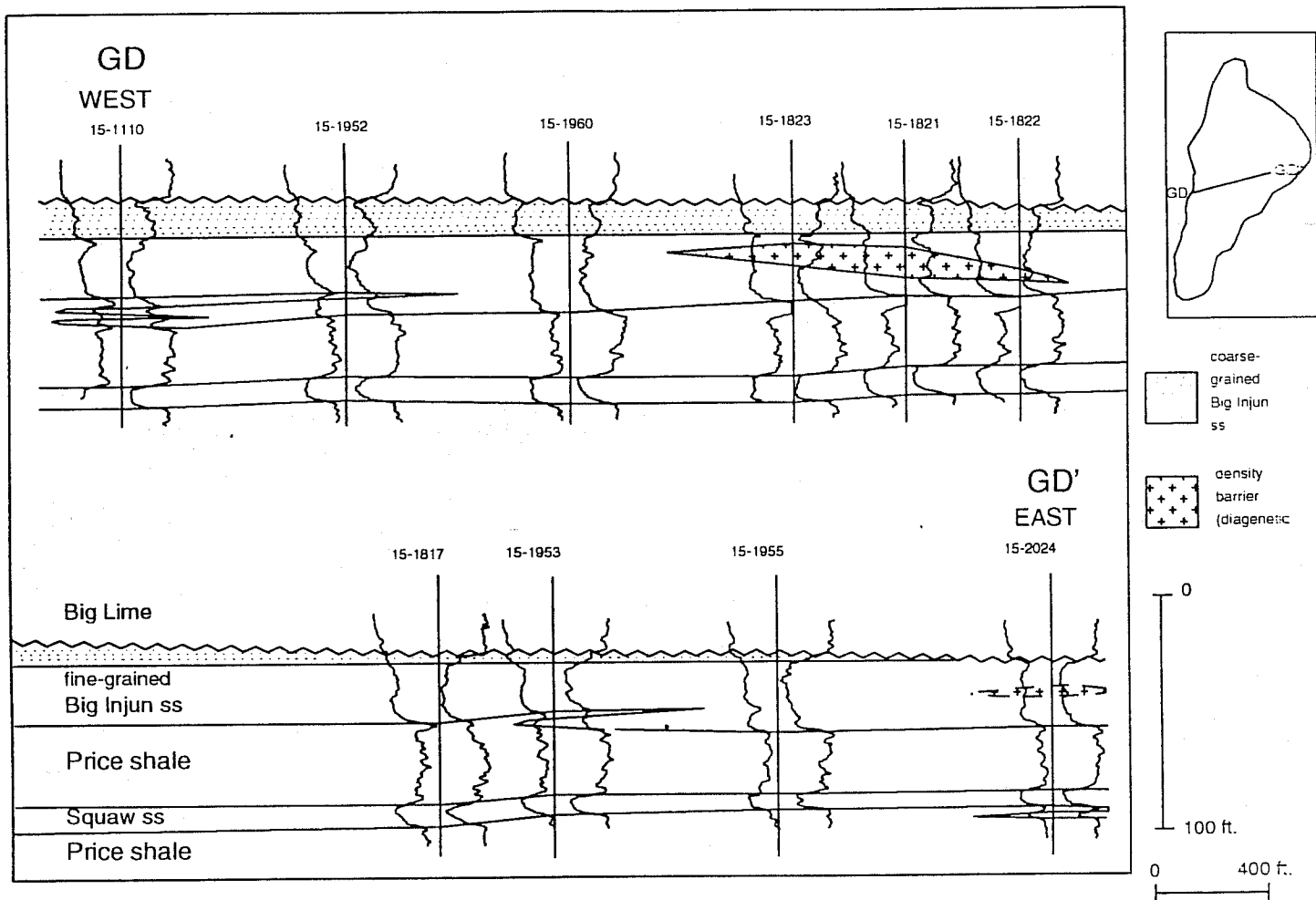


Figure 98. An east-northeast cross-section through the central part of Granny Creek. This cross-section shows the interfingering of the shale and sandstone and inclined and horizontal density barriers. The southern part of density barrier number 7 in Figure 100 is inclined.

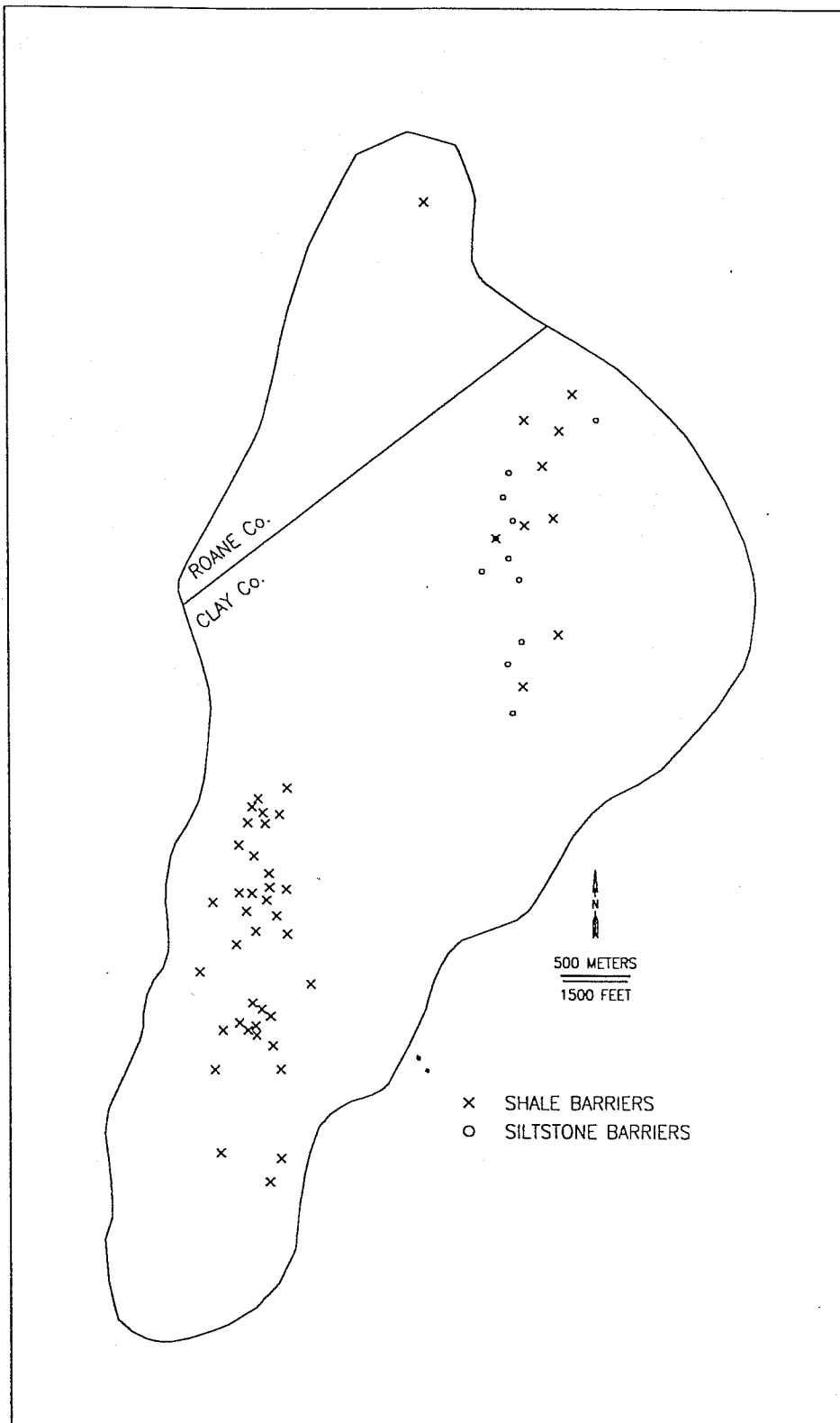


Figure 99. A map of Granny Creek showing the lateral extent of the shale and siltstone. "X"'s indicate wells with shale barriers; circles indicate wells with siltstone barriers.

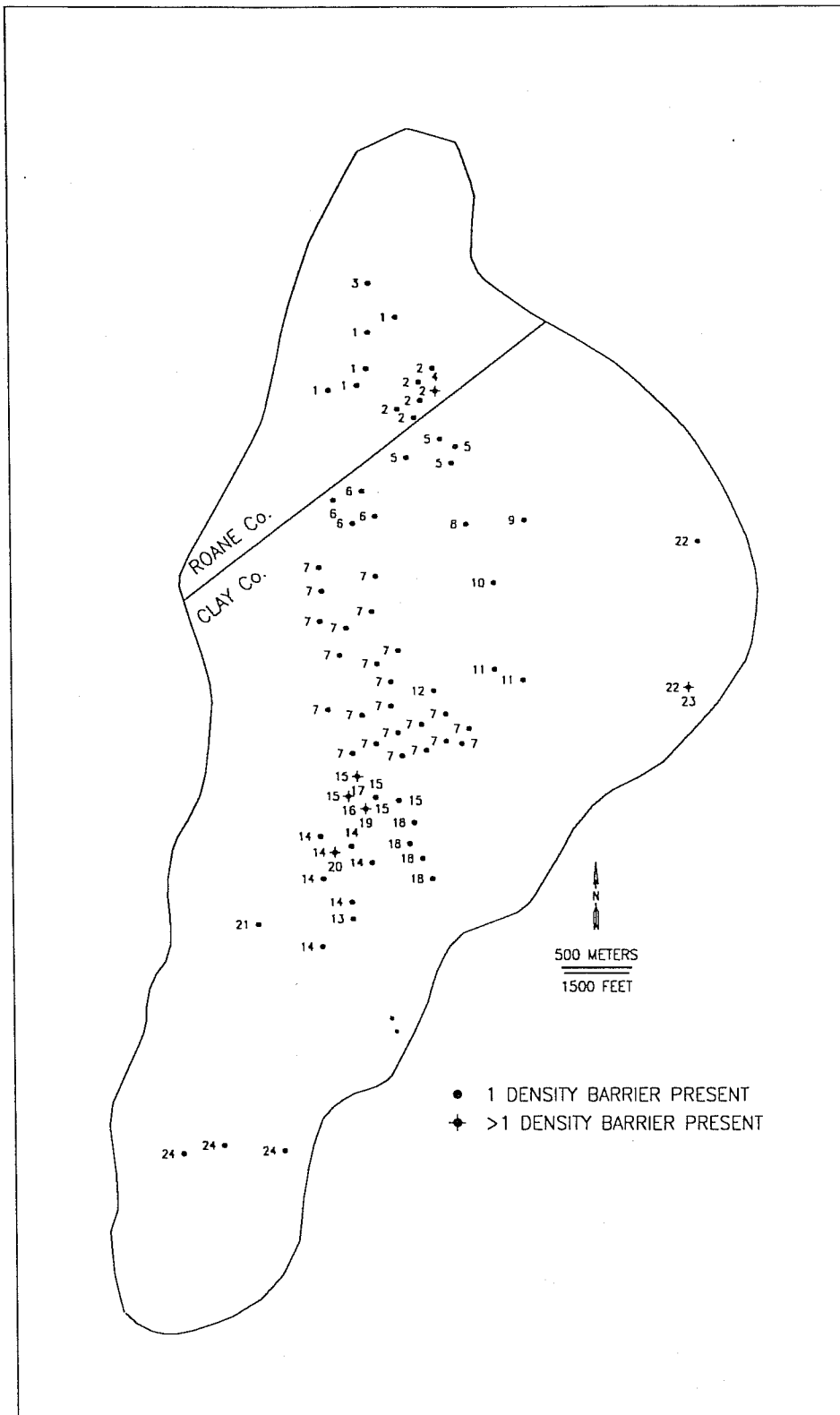


Figure 100. A map of Granny Creek showing lateral extent of the density barriers. Filled circles and "+"s indicate wells with density barriers. The number next to the well location identifies density barriers that may correlate with each other.

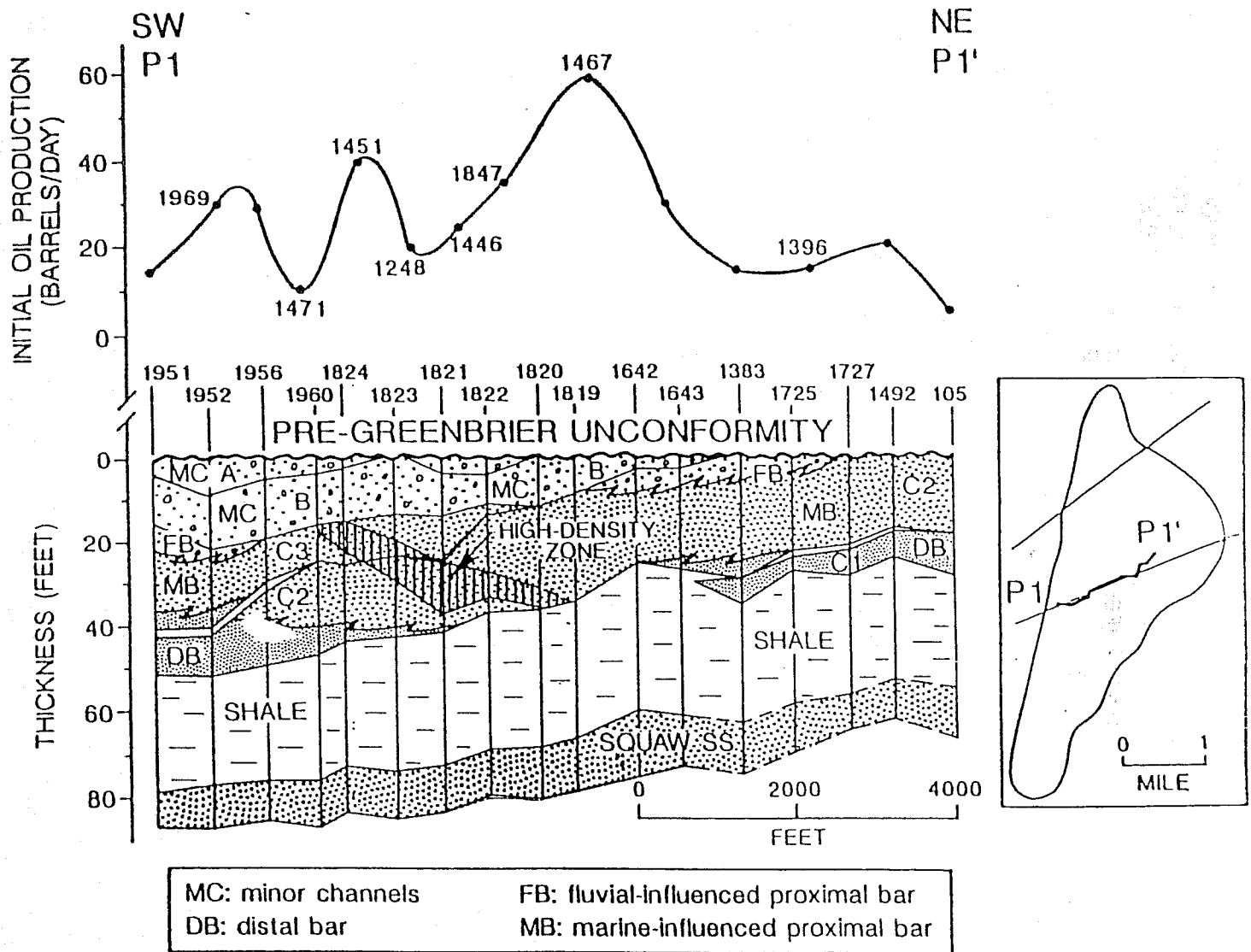


Figure 101. Initial oil production along stratigraphic cross section P1-P1' showing subfacies, high-density zone, relatively impermeable thin beds at boundary of tongues, and presence/ absence of capping B member (potential seal over pay zone in C member). Initial oil production is plotted above section. Numbered points represent wells located near the line of section; unnumbered points are wells shown in the cross section.

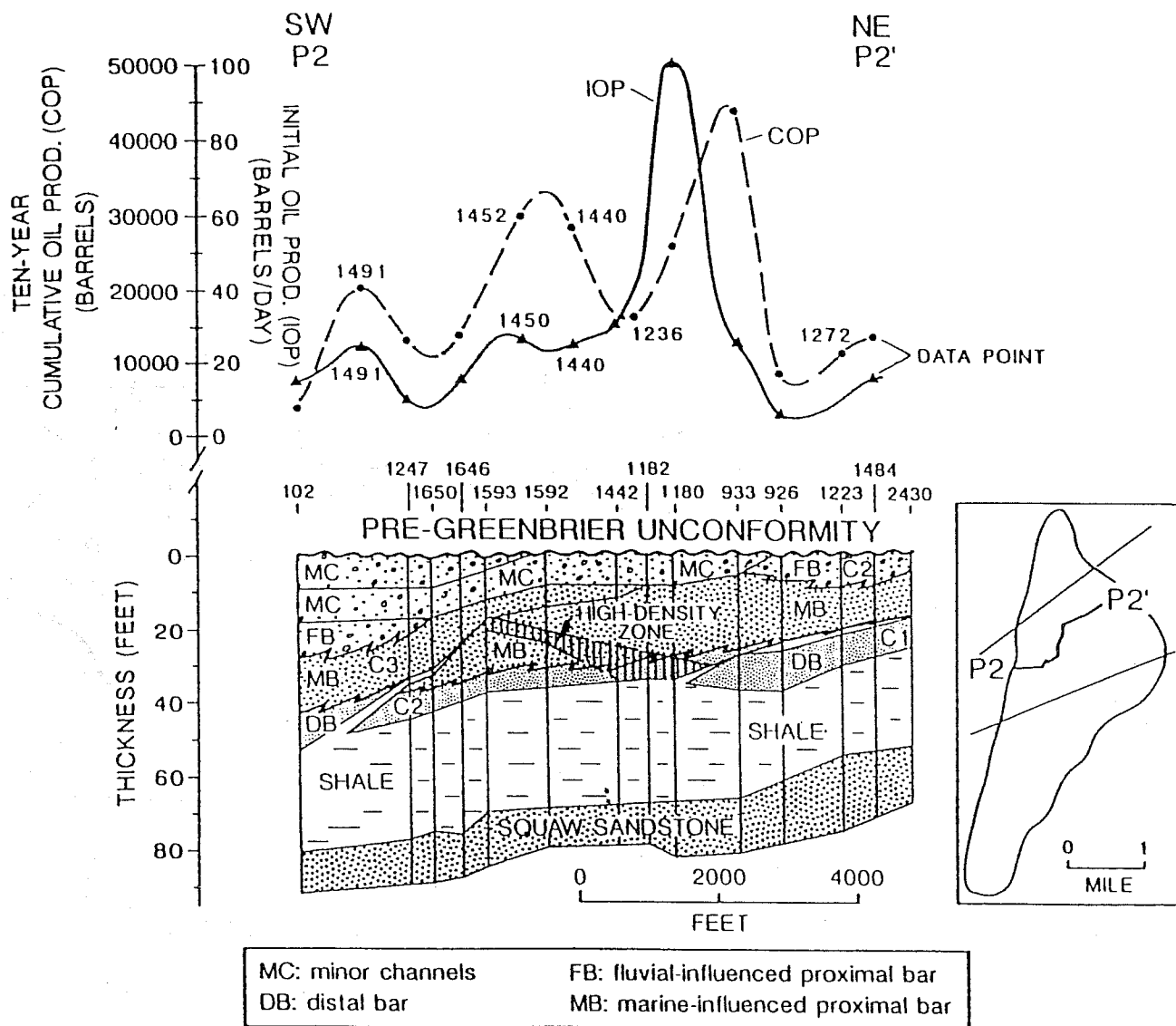


Figure 102. Comparison of oil production (initial and cumulative flow) along stratigraphic cross-section P2-P2' showing relationship between permeable proximal mouth-bar facies and probable partial barriers to fluid flow. Tongue boundaries and high density zone are potential partial barriers interpreted from reduced log porosity.

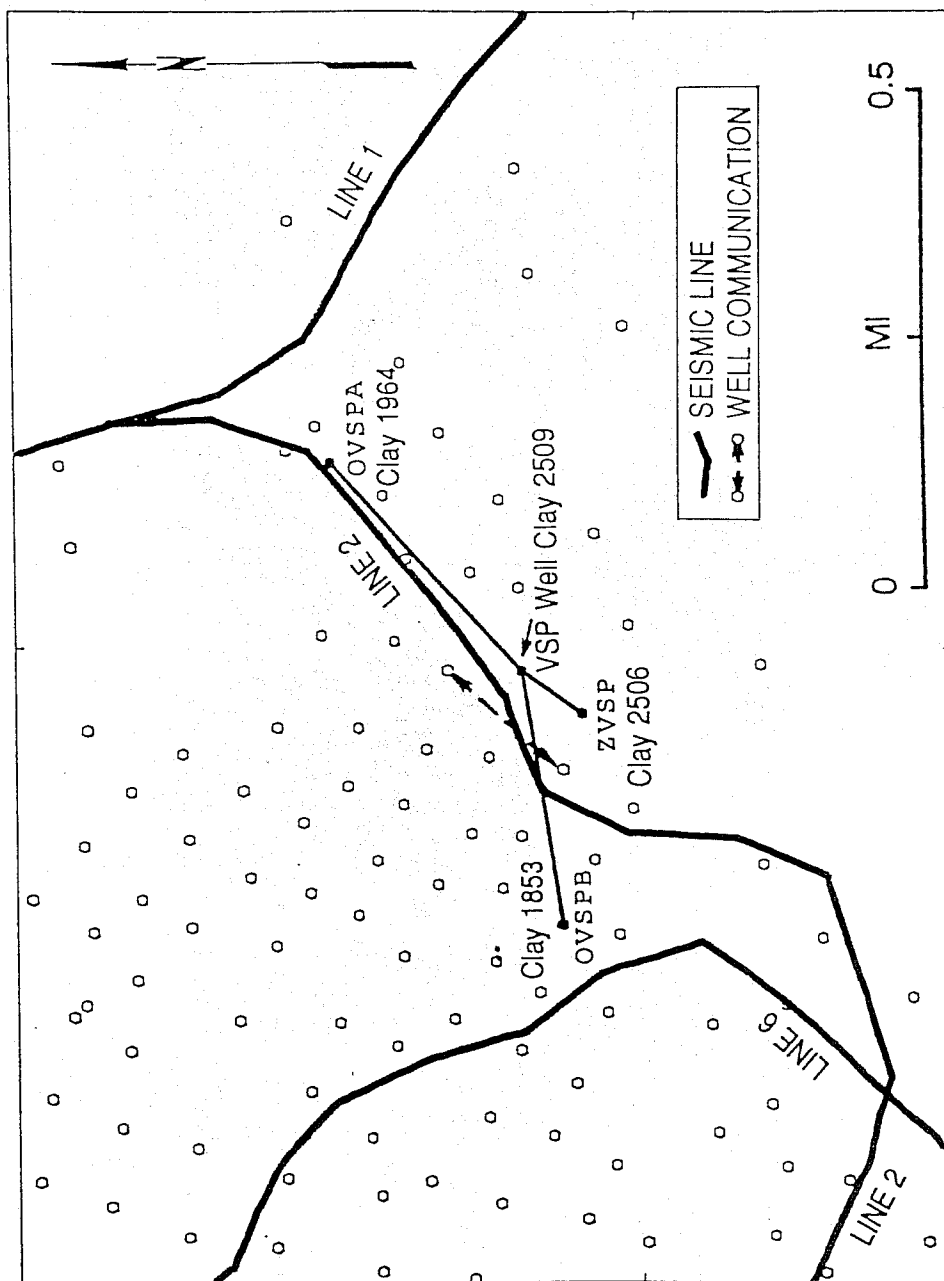


Figure 103. The location of the three VSP offsets shot in CNR's Parker no. 21981 well are shown along with the location (dashed line) of two wells between which communication problems were encountered by Columbia Natural Resources, Inc.

VSP
1395 ft OFFSET
S82°W

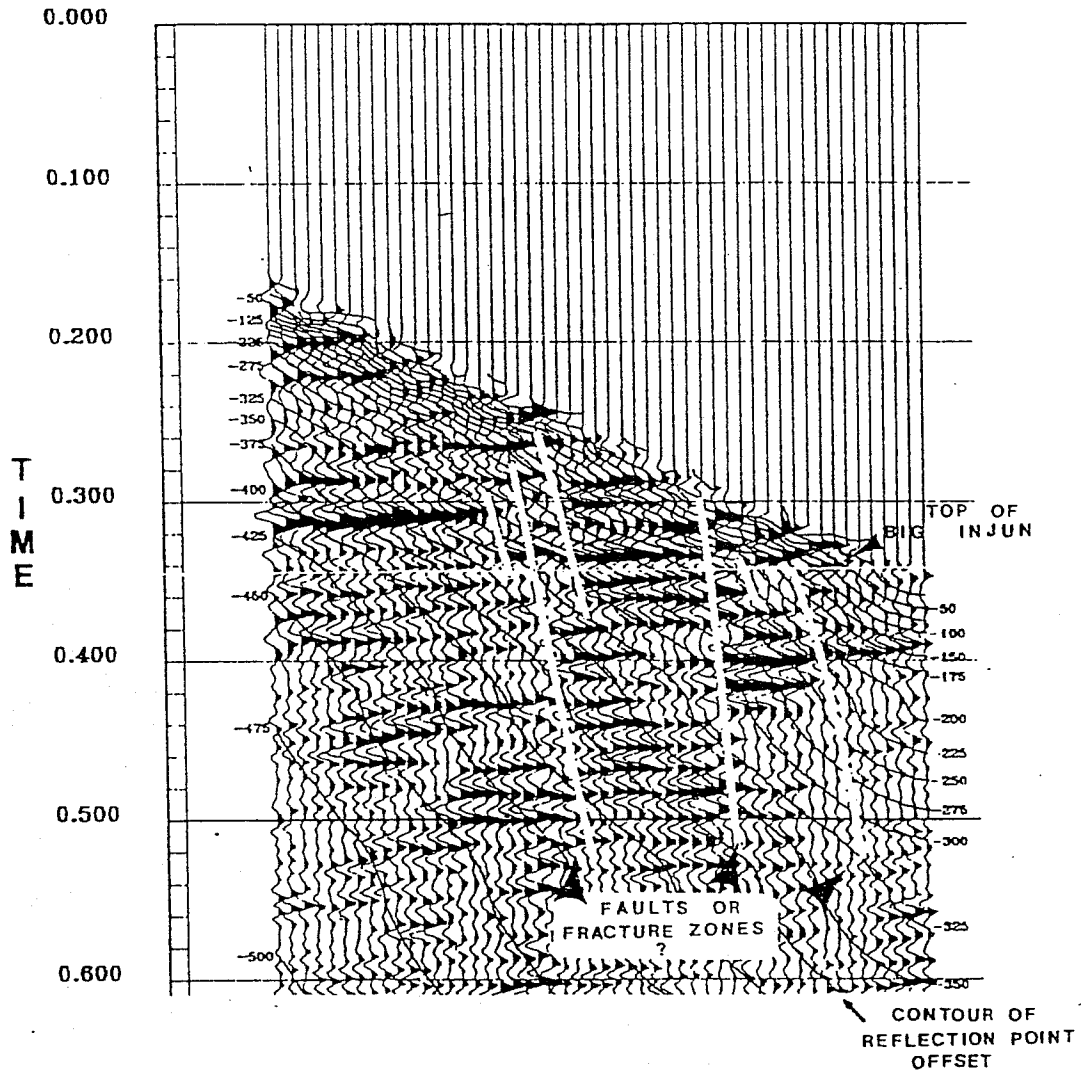


Figure 104. The western offset VSP is shown after moveout correction and waveshape deconvolution. Possible faults or fracture zones have been interpreted.

VSP
1600 ft OFFSET
N 48.5°E

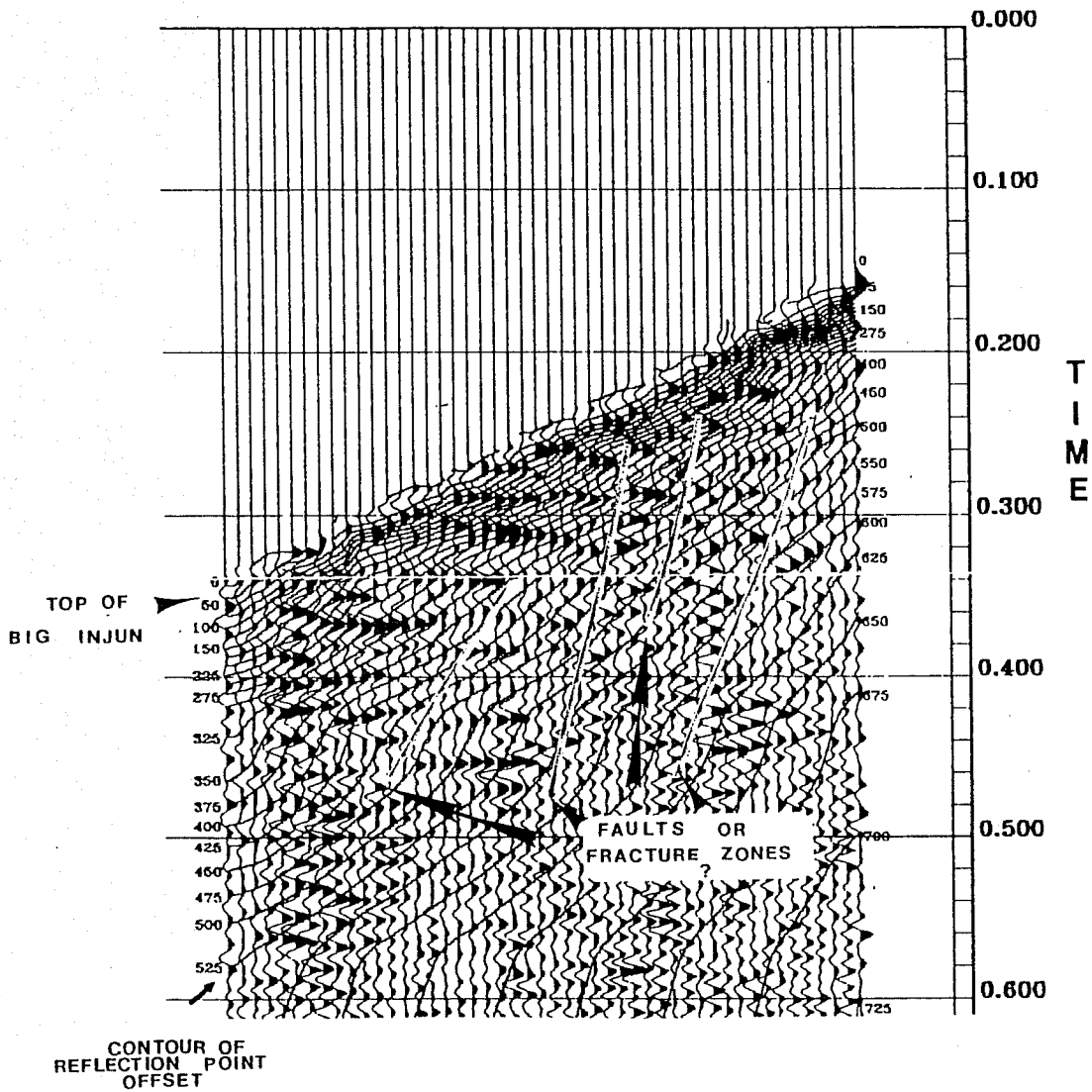


Figure 105. The northeastern VSP offset is shown after movement correction and waveshape deconvolution. Possible faults and fracture zones have been interpreted.

LINE 2

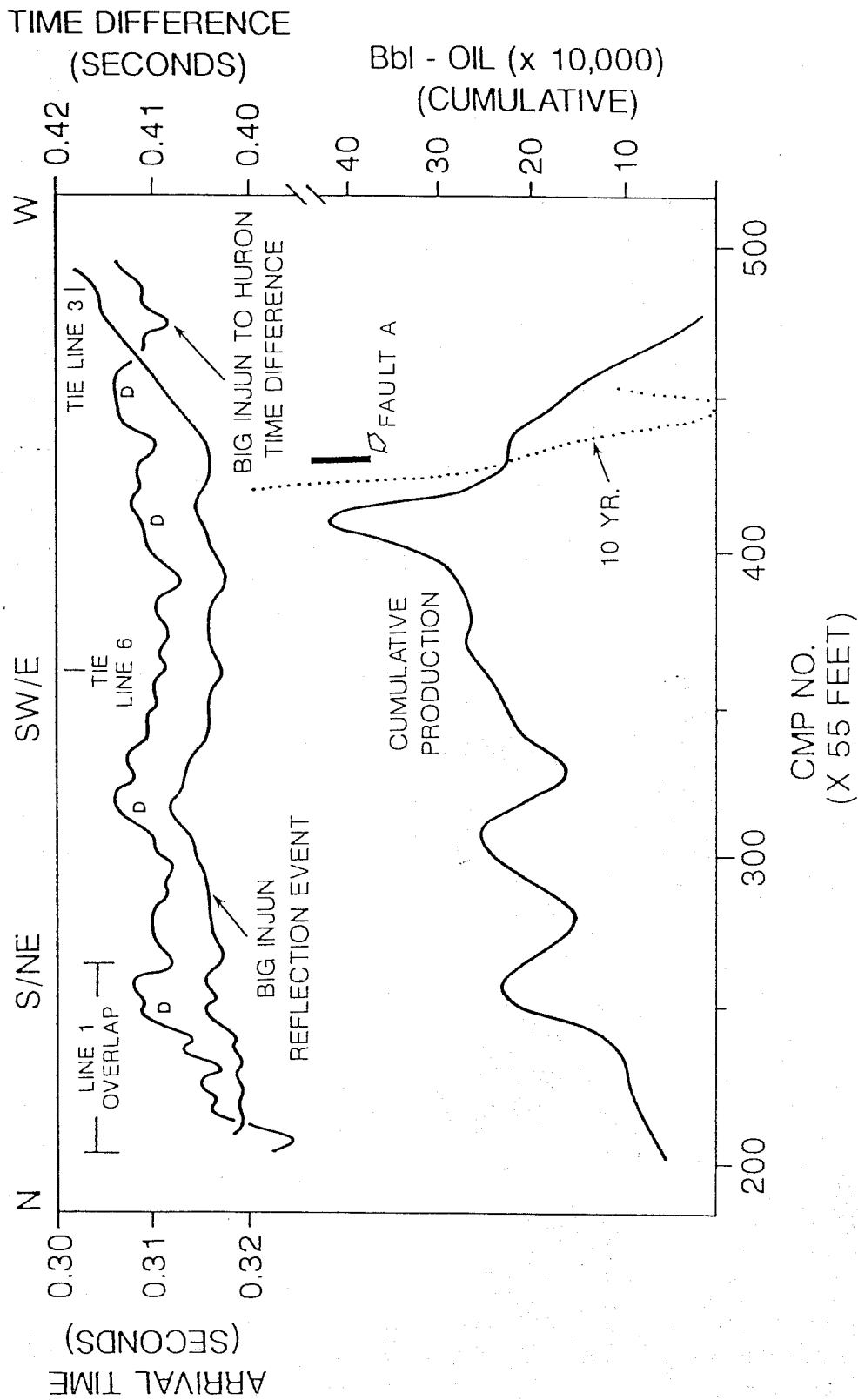


Figure 106. Arrival times of the Big Injun reflection event are compared to the traveltime difference between the Big Injun and Huron reflection events along Line 2. Traveltime differences increase upwards in this plot. Primary production and ten year cumulative (dotted) are plotted across the bottom for comparison. Areas marked D represent local thickening within the syncline.

LINE 6

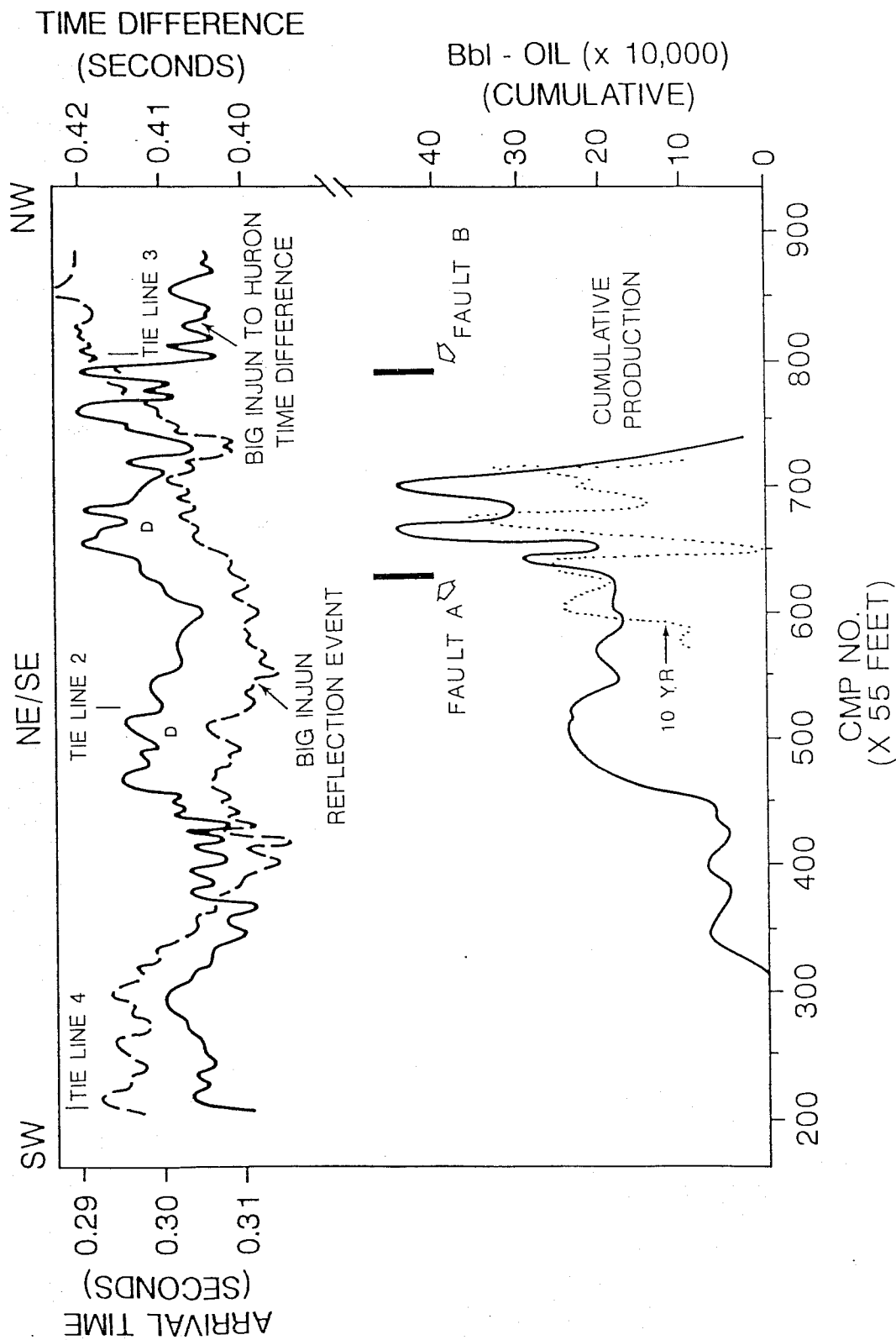


Figure 107. Arrival times of the Big Injun reflection event are compared to the traveltime difference between the Big Injun and Huron reflection events along Line 6. Traveltime differences increase upwards in this plot. Primary production and ten year cumulative (dotted) are plotted across the bottom for comparison. Areas marked D represent local thickening within the syncline.

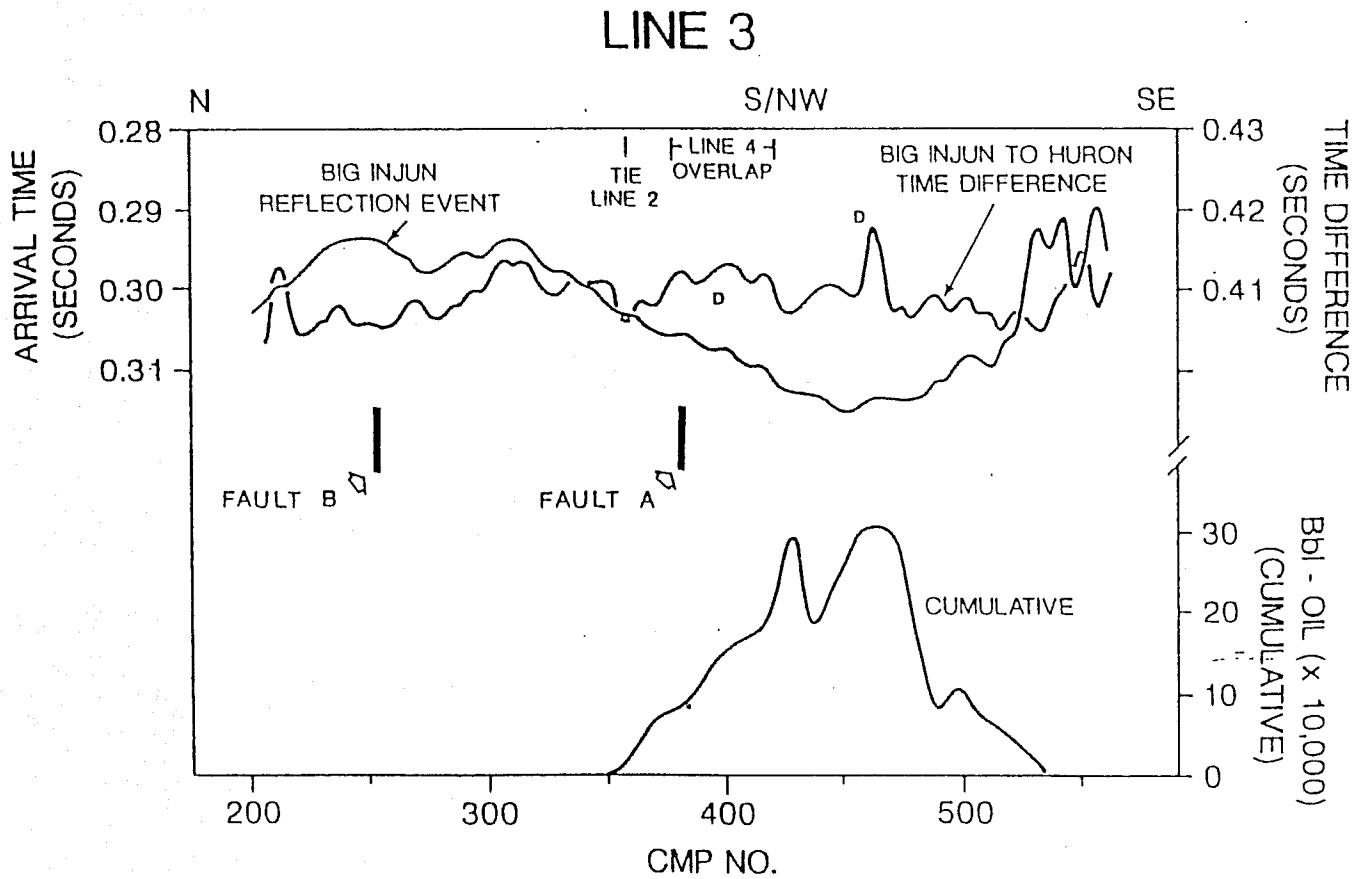


Figure 108. Arrival times of the Big Injun reflection event are compared to the traveltime difference between the Big Injun and Huron reflection events along Line 3. Traveltime differences increase upwards in this plot. Primary production and ten year cumulative (dotted) are plotted across the bottom for comparison. Areas marked D represent local thickening within the syncline.

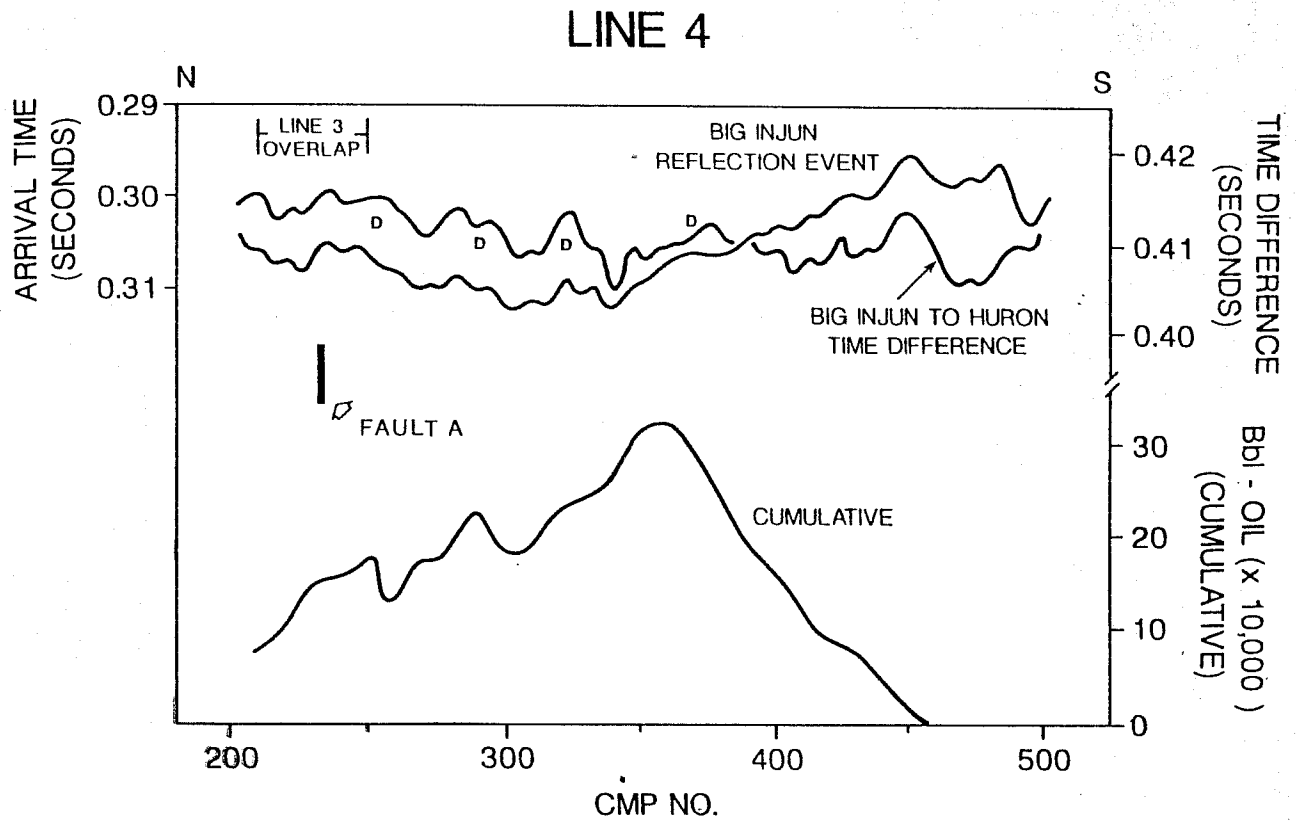


Figure 109. Arrival times of the Big Injun reflection event are compared to the traveltime difference between the Big Injun and Huron reflection events along Line 4. Traveltime differences increase upwards in this plot. Primary production and ten year cumulative (dotted) are plotted across the bottom for comparison. Areas marked D represent local thickening within the syncline.

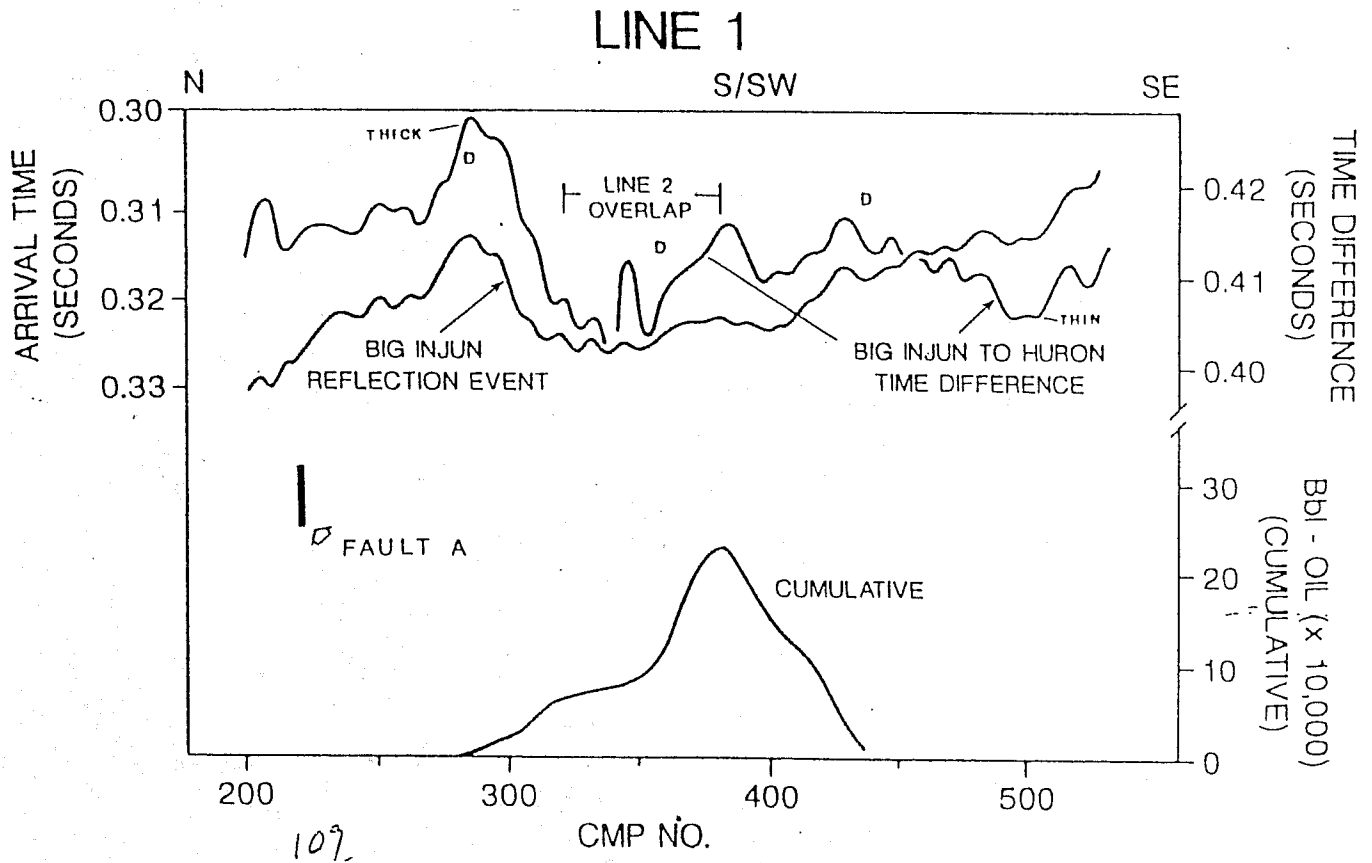


Figure 110. Arrival times of the Big Injun reflection event are compared to the traveltime difference between the Big Injun and Huron reflection events along Line 1. Traveltime differences increase upwards in this plot. Primary production and ten year cumulative (dotted) are plotted across the bottom for comparison. Areas marked D represent local thickening within the syncline.

STRUCTURE	UNIT	GENERAL TREND
THIEF ZONES	BIG INJUN/BIG LIME	NE
NATURAL FRACTURES	(SURFACE)	COMPLEX
NATURAL FRACTURES	DEVONIAN SHALE	NE
COAL CLEATS	(SURFACE)	E-W
INSITU STRESS	(BIG LIME)	E-W
FAULTS	BASEMENT	NE
SMALL THRUSTS	(SURFACE)	NE
SMALL FOLDS	(SURFACE)	NE
SMALL FOLDS	(BIG LIME)	NE/N-S

Table 1. Preliminary compilation of general trends of structure in the Granny Creek field area.

Table 4. MEASURED PERMEABILITY VALUES OF WELLS 1110, 1133, AND 1134 FROM GRANNY CREEK FIELD, WEST VIRGINIA.

PERMIT No.	DEPTH	PERMEABILITY (md)	
1110	1886' 8"	28.14	
	1894' 11"	1.05	
	1894' 11"	0.25 *	
	1898' 11"	0.45	
	1901' 9"	0.36	
	1902' 6"	31.56	
	1908'	10.69	
	1908'	1.38 *	
	1912' 6"	22.68	
	1928' 2"	1.09	
	1133	2083' 6"	7.02
		2086' 3"	3.68
		2086' 3"	0.38 *
2089' 10"		0.76	
2089' 10"		0.11 *	
2096' 6"		10.53	
2105' 9"		5.94	
2111' 7"		0.96	
2115'		0.31	
2115'		0.23 *	
1134		2191'	0.22
		2195'	8.55
		2198' 6"	30.96
	2198' 6"	14.82 *	
	2201' 11"	2.30	
	2201' 11"	0.61 *	
	2209' 9"	1.01	
	2209' 9"	0.60 *	
	2214' 6"	5.52	
	2221' 6"	2.22	

* Permeability measured in vertical direction.

Table 5. WATER SATURATION PERCENT.

County*	Permit Number	Zone A	Zone B	Zone C3	Zone C2	Zone C1
15	735	-	-	-	-	-
15	774	-	-	-	-	90.68
15	775	-	-	-	-	-
15	788	-	-	-	-	-
15	852	60.89	30.95	46.71	-	-
15	853	-	-	-	-	-
15	868	50.35	33.42	37.44	65.46	-
15	903	-	-	-	-	-
15	910	-	35.91	-	33.28	-
15	1059	53.3	83.45	71.21	69.64	-
15	1060	-	-	-	-	34.44
15	1107	37.9	29.4	-	40.57	-
15	1108	-	31.9	-	36.01	99.58
15	1109	44.5	30.32	35.57	66.53	-
15	1110	24.75	26.15	31.93	83.86	-
15	1126	24.71	39.17	33.94	60.04	-
15	1128	-	-	-	-	-
15	1130	34.21	32.39	47.29	49.41	-
15	1132	-	-	-	-	-
15	1134	-	35.67	-	38.39	36.55
15	1167	-	-	-	-	-
15	1176	-	-	-	-	-
15	1184	-	-	-	-	-
15	1185	-	-	-	-	-
15	1224	-	-	-	-	-
15	1225	-	-	-	-	-
15	1242	-	-	-	-	-
15	1243	-	-	-	-	-
15	1591	-	-	-	-	-
15	1592	-	-	-	-	-
15	1596	-	-	-	-	-
15	1598	-	37.38	33.47	36.52	-
15	1601	-	-	-	-	-
15	1621	-	-	-	-	-
15	1626	-	-	-	-	-
15	1630	-	-	-	-	-
15	1639	-	-	-	-	-
15	1649	-	-	-	-	-
15	1726	-	-	-	-	-
15	1783	-	-	-	-	-
15	1933	-	-	-	-	-
15	1936	-	-	-	-	-
15	1941	-	-	-	-	-
15	1942	-	-	-	-	-
15	1951	-	-	-	-	-
15	1953	-	-	-	-	-
15	2001	-	-	-	-	-
15	2002	-	-	-	-	-
15	2133	-	-	-	-	-
15	2136	-	-	-	-	-
15	2150	-	-	-	-	-
15	2214	34.04	19.08	-	21.96	-
15	2215	-	-	-	-	-
15	2216	-	-	-	-	-
15	2222	-	-	-	-	-
15	2227	-	-	-	-	-
15	2229	-	-	-	-	-
15	2253	27.06	38.87	27.04	35.04	-
15	2297	-	-	-	-	-
15	2298	-	-	-	36.3	63.23
15	2301	-	-	-	-	-
15	2428	-	-	-	-	-
15	2430	-	-	-	34.15	98.91
15	2472	-	-	-	-	-
87	2102	-	-	-	-	-
87	2410	-	0.45	0.24	0.27	-
87	2411	-	-	-	-	-
87	2848	-	-	-	-	-
87	3415	-	-	-	-	-

Table 5. cont. POROSITY PERCENT

County	Permit Number	Zone A	Zone B	Zone C3	Zone C2	Zone C1
15	735	15.27	13.4	23.99	8.7	-
15	774	-	-	-	-	6.08
15	775	-	-	-	-	11.74
15	788	-	-	-	-	15.13
15	852	8.75	9.75	18.74	-	-
15	853	9.61	9.11	16.44	-	-
15	868	9.25	8.29	19.51	12.78	-
15	903	17.63	-	21.23	-	-
15	910	-	14.11	-	15.88	-
15	1059	9.13	3.5	12.41	7.22	-
15	1060	-	-	-	-	17.44
15	1107	11.78	9.49	-	15.18	-
15	1108	-	12.2	-	19.18	5.71
15	1109	10.8	7.76	17.04	12.07	-
15	1110	12.81	8.6	18.69	7.3	-
15	1126	14.58	8.03	17.16	12.3	-
15	1128	-	5.46	13.7	12.25	-
15	1130	12.06	8.81	13.27	15.41	-
15	1132	13.45	7.33	12.06	16.35	-
15	1134	-	6.49	-	14.15	16.28
15	1167	11.97	9.49	-	18.94	-
15	1176	13.41	-	-	18.2	-
15	1184	9.75	10.21	-	18.62	-
15	1185	13.91	-	-	20.1	-
15	1224	-	-	-	15.69	3.29
15	1225	-	-	-	16.33	-
15	1242	7.38	7.28	14.93	14.03	-
15	1243	-	9.09	15.22	18.2	-
15	1591	8.71	7.73	18.28	13.46	-
15	1592	-	7.49	16.71	-	-
15	1596	-	9.65	18.96	14.25	-
15	1598	-	7.19	13.94	18.1	-
15	1601	-	10.41	-	18.83	-
15	1621	-	9.12	14.99	14.64	-
15	1626	-	12.62	16.12	18.35	-
15	1630	-	11.73	-	16.88	-
15	1639	-	9.44	-	16.41	-
15	1649	7.57	3.56	11.53	8.04	-
15	1726	-	-	-	18.81	8.22
15	1783	-	-	-	15.96	10.82
15	1933	15.36	12.01	17.52	10.26	-
15	1936	14.61	9.12	18.85	11.07	-
15	1941	16.18	13.54	18.06	7.84	-
15	1942	14.59	10.53	16.17	6.76	-
15	1951	12.8	10.63	17.68	7.79	-
15	1953	-	9.77	-	15.98	8.44
15	2001	8.49	8.48	12.37	11.81	-
15	2002	11.09	10.24	13.82	13.97	-
15	2133	-	11.01	16.89	19.02	-
15	2136	11.36	10.88	15.75	10.86	-
15	2150	11.76	9.23	16.33	17.96	-
15	2214	11.39	10.17	-	19.8	-
15	2215	8.55	11.18	-	17.92	-
15	2216	13.97	9.23	-	14.14	-
15	2222	8.36	9.33	-	16.69	-
15	2227	10.63	7.72	-	18.92	-
15	2229	-	9.73	-	16.87	-
15	2253	9.33	7.87	19.92	16.64	-
15	2297	-	-	-	19.64	14.62
15	2298	-	-	-	15.73	10.83
15	2301	-	8.8	17.68	12.49	-
15	2428	11.97	-	-	18.64	-
15	2430	-	-	-	17.23	5.5
15	2472	-	-	-	19.35	6.05
87	2102	14.44	-	20.68	16.5	-
87	2410	-	5.71	20.61	20.48	-
87	2411	-	-	-	16.68	-
87	2848	-	-	-	19.42	-
87	3415	-	-	-	2.48	-

*15 = Clay, 87 = Roane

COARSE-GRAINED BIG INJUN SANDSTONE

	B MEMBER (POSSIBLE SEAL) PRESENT				B MEMBER (POSSIBLE SEAL) ABSENT	
	FINE-GRAINED BIG INJUN MEMBER (PAY ZONE)				Variable C Member Subfacies	
	Thick PMB Pinch Out	Thick PMB No Pinch Out	Thin PMB Pinch Out	FPB Pinch Out		
P1 - P1' Wells	1643 1819 1820 1952 1819 - 1642	1821 1822 1823 1951	1824	1646 1650 1960	105 1383 1492 1721 1725	
P2 - P2' Wells	933 1180 1182 1491	1440 1442 1450 1592	1247	1646 1650	926 1223 1484 2430	
P4 - P4' Wells	1167 1173 1180 1242 1478 1595 1639 1641 1654 1943 2936					
Average IOP P1 - P1'	N = 6 38 b/d	N = 4 24 b/d	N = 1 20 b/d	N = 1 10 b/d	N = 4 13 b/d	N = 16
Average IOP P1 - P1'	N = 3 51 b/d	N = 5 23 b/d	N = 1 10 b/d	N = 2 12 b/d	N = 4 14 b/d	N = 15
Average IOP P1 - P1'	N = 13 50 b/d				N = 3 12 b/d	N = 16
Average IOP For 3 Cross Sections	N = 22 46 b/d	N = 9 24 b/d	N = 2 15 b/d	N = 3 11 b/d	N = 11 13 b/d	

TABLE 6: Initial oil production is affected by pre-Greenbrier unconformity according to cross sections P1 - P1', P2 - P2', P4 - P4', as well as thickness of marine proximal mouth bar "pinching out" against B member seal. PMB = marine proximal mouth bar, FPB = fluvial proximal mouth bar, N = number of wells, b/d = barrels per day.

